2005

Support mechanism of rammed aggregate piers

Ha Thuc Van Pham
Iowa State University

Support mechanism of rammed aggregate piers

by

Ha Thuc Van Pham

A dissertation submitted to the graduate faculty

in partial fulfillment of the requirements for the degree of

DOCTOR OF PHILOSOPHY

Major: Civil Engineering (Geotechnical Engineering)

Program of Study Committee:
David J. White, Major Professor
Vernon R. Schaefer
Radhey S. Sharma
Charles T. Jahren
Igor A. Beresnev

Iowa State University

Ames, Iowa

2005

Graduate College
Iowa State University

This is to certify that the doctoral dissertation of

Ha Thuc Van Pham

has met the dissertation requirements of Iowa State University

Signature was redacted for privacy.

Major Professor

Signature was redacted for privacy.

For the Major Program

TABLE OF CONTENTS

LIST OF FIGURES

CHAPTER 2: INFLUENCE OF LATERAL STRESS ON SOIL BEHAVIOR

CHAPTER 3: BEHAVIOR OF ISOLATED RAMMED AGGREGATE PIERS FROM A FINITE ELEMENT ANALYSIS

CHAPTER 4: SUPPORT MECHANISM OF RAMMED AGGREGATE PIERS. I. FIELD PERFORMANCES

CHAPTER 5: SUPPORT MECHANISM OF RAMMED AGGREGATE PIERS. II. NUMERICAL ANALYSES

LIST OF TABLES

CHAPTER 2: INFLUENCE OF LATERAL STRESS ON SOIL BEHAVIOR

CHAPTER 3: BEHAVIOR OF ISOLATED RAMMED AGGREGATE PIERS FROM A FINITE ELEMENT ANALYSIS

CHAPTER 4: SUPPORT MECHANISM OF RAMMED AGGREGATE PIERS. I. FIELD PERFORMANCES

CHAPTER 5: SUPPORT MECHANISM OF RAMMED AGGREGATE PIERS. II. NUMERICAL ANALYSES

CHAPTER 1: GENERAL INTRODUCTION

OVERVIEW

Construction over highly compressible soils can create excessive settlement and bearing capacity problems. To overcome these difficulties, deep foundation elements such as driven piles or drilled shafts have been traditionally used to transfer the surcharge loads exerted by the superstructures to a more competent layer at greater depths. Although deep foundation methods have proven to be effective in most cases, these methods are relatively expensive when constructed over large areas and may also cause unwanted delay during construction.

As alternatives to deep foundation methods, ground improvement technologies have been widely used to improve the load-carrying capacity and the stiffness of the shallow soil layers located immediately underneath the superstructures. According to Mitchell (1981), basic concepts of ground improvement such as drainage, densification, cementation, reinforcement, drying, and heating were developed hundreds or even thousands of years ago. Although the basic principles of ground improvement are unchanged since the early days, the practices have been changing with time owning to the development of new materials, machineries, and technologies. Over the past 70 years, soil improvement technologies have mainly focused on the development of vibratory methods for densification of cohesionless soils, injection and grouting materials and procedures, and new concepts of soil reinforcement (Mitchell 1981).

Among other soil reinforcement technologies, rammed aggregate pier systems have been emerging rapidly during the last two decades to become one of the most popular methods for stiffening and stabilizing soft soils in the United States. *Rammed Aggregate Pier*™ (also known as *Geopier*® *Soil Reinforcement*) technology was developed in the early 1980s to provide an economical alternative to deep foundations and traditional methods of soil improvement, such as over-excavation and replacement. Since the inception, rammed aggregate piers have been used to support a wide range of structures including column footings, highway embankments, heavily-loaded slabs, slopes, retaining walls, and industrial storage tanks (Lawton and Fox 1994, White and Suleiman 2004, Minks *et al.* 2001, Wissmann *et al.* 2002, Wong *et al.* 2002, Wissmann *et al.* 2001). Typical applications of rammed aggregate pier systems include settlement control, bearing capacity improvement, slope stabilization, uplift capacity enhancement, and liquefaction mitigation. Construction procedures for a rammed aggregate pier are well described in the literature (Lawton and Fox, 1994, Lawton et al. 1994). The standard construction procedure includes backfilling and ramming of successive thin layers of base-course aggregate is a pre-bored cavity using a beveled tamper connected to low amplitude, high frequency hydraulic hammer. The aggregate is compacted by impact energy rather than the vibrating energy. As a result of ramming, the backfilling aggregate is pushed laterally along the shaft and vertically at the bottom of the cavity thereby pre-stressing and pre-straining the matrix soil adjacent to the cavity wall (Fox and Cowell 1998).

Although successful performances of rammed aggregate pier systems have been well documented (Lawton and Fox 1994, Lawton et al. 1994, White et al. 2002), insights into the load-transfer mechanism of the piers and the pier-soil interaction have yet to be elucidated.

Since rammed aggregate piers are relatively short and generally not intended to penetrate to a competent layer, the rammed aggregate pier system is essentially a floating system in which the surcharge load will have to be dissipated mostly through the pier-soil interfacial friction. The additional lateral stress induced from pier installation not only provides more confinement around the pier, which subsequently improves the interfacial friction, but also may alter the behavior of the matrix soil itself. To gain insight into the complex pier-soil interaction and the impact of the pier installation on soil behaviors, several research projects were conducted, using both experimental and numerical approaches. The results obtained from these research projects have established the elements for this dissertation.

OBJECTIVES AND SCOPE

The primary objectives of this research were: (1) to investigate the influence of induced lateral stress on the mechanical behavior of soils based on the results from stress path control tests; (2) to investigate the load-transfer mechanism and the interaction between isolated rammed aggregate piers and the matrix soil through the use of a finite element model; (3) to evaluate the current method for estimating settlement and bearing capacity of footings supported by rammed aggregate piers; (4) to evaluate the use of an axisymmetric finite element model to study the behavior of pier groups in supporting rigid column footings, and (5) to establish a new modulus-based method for estimating pier-supported footing settlements.

A laboratory testing program which includes four series of stress path control tests was implemented for the first research objective. Soil specimens remolded from western Iowa loess were subjected to four controlled stress paths with varied drainage conditions.

Fundamental geotechnical tests including soil indices, compaction, one-dimensional consolidation, and unconfined compression tests were also performed.

Two square reinforced concrete footings supported by two groups of rammed aggregate piers and three isolated rammed aggregate piers were constructed in Neola, Iowa. The footings width was 2.29 and the thickness was 0.46 m. All piers in the pier groups were 0.76 m in diameter and installed at two depths of 2.79 m and 5.10 m. Two piers in each group were instrumented with a tell-tale reference plate. Three isolated piers of 0.76 m diameter were installed near the trial pier-supported footings at 2.79 m, 3.0 m, and 5.10 m. All isolated piers were equipped with tell-tale reference plates and covered with a 0.46 m thick concrete cap.

Prior to the construction of the footings and isolated piers, comprehensive *in-situ* and laboratory testing programs were implemented. *In-situ* tests included the cone penetration test with pore water pressure measurement (CPT), the pressuremeter test (PMT), and the flat dilatometer test (DMT). Laboratory tests conducted on undisturbed soil samples collected from the construction site included soil indices, one-dimensional consolidation, consolidated undrained (UU) compression, and the consolidated drained (CD) tests. Samples of the aggregate used to construct the rammed aggregate piers were also collected from the construction site for laboratory tests. Tests conducted on re-compacted aggregate samples included gradation, compaction, and CD compression tests.

Full scale load tests were conducted on the trial footings and also on the isolated piers. Instrumentation includes total stress cells and inclinometer casing. Readings from stress cells and inclinometers were taken simultaneously with the performance of the load tests.

Results from the load tests and instrumentation work were used to validate the finite element model and evaluate the current design method for estimating bearing capacity and settlement of footings supported by rammed aggregate piers.

Finally, an axisymmetric finite element model was developed using the computer program Plaxis (version 8.2) for the modeling of isolated rammed aggregate piers and pier groups. Model parameters were estimated from the laboratory and the *in-situ* tests mentioned above. An advanced elasto-plastic constitutive model was selected for the analysis. The pier installation process was modeled as an expanding cavity in which boundary conditions were estimated from field measurements.

ORGANIZATION OF THE DISSERTATION

The dissertation is presented as a compilation of four papers submitted to scholarly geotechnical engineering journals. Each paper appears as a dissertation chapter which includes references to literature reviewed, research data, and significant findings, with suggestions for further studies. Following the main body of the dissertation is a general conclusion that summarizes significant research findings from each paper and provides additional recommendations for future research.

The first paper presents an experimental study performed to investigate the influence of induced lateral stress on shear strength, vertical stiffness, and preconsolidation pressure of the reconstituted Iowa loess. Four series of stress path control tests were conducted in which soil specimens remolded from western Iowa loess, were consolidated under increased lateral stress before being loaded vertically in either drained or undrained fashion.

The second paper describes a numerical analysis using an axisymmetric, finite element model to study the behavior of isolated rammed aggregate piers subjected to compressive load. The load transfer mechanism along pier shaft and pier-soil interactions is particularly investigated in this paper. Constitutive parameters of the materials involved in the numerical analysis were determined from in-situ and laboratory tests. The finite element model was validated by comparing the numerical results with the data obtained from full-scale, instrumented load tests.

The third paper presents results from full-scale, instrumented load tests conducted on two trial square pier-supported footings and three isolated rammed aggregate piers. Group effects are investigated by comparing the behavior of an individual pier within the pier group and an isolated pier from the same diameter and length. Evaluation of the current design methods for computing bearing capacity of pier-supported footing is carried out by comparing the calculated parameters with the measured values.

The fourth paper presents a numerical study on the support mechanism of rammed aggregate pier groups. The numerical study focuses on the group behavior of rammed aggregate piers and the vertical stress distribution underneath the footings. A modulus-based method developed based on the homogenization approach combined with the finite element stress distribution for estimating footing settlement is also presented in this paper.

The appendix consists of five sections. Appendix A presents tabulated data obtained from all stress path control tests. Appendix B provides tabulated data obtained from the full-scale load tests and instrumentation. Appendix C presents the computations of the bearing capacity and settlement of the trial pier-supported footings using the current design procedure.

Appendix D describes the principles of the hardening-soil constitutive model. Appendix E presents the axial strain distributions along the shaft of the isolated rammed aggregate piers studied in Chapter 3.

REFERENCES

1. Fox, N.S., and Cowell, M.J. (1998). *Geopier™ Foundation and Soil Reinforcement Manual*. Geopier Foundation Company, Inc., Blacksburg, VA, USA.
2. Lawton, E.C., and Fox, N.S. (1994). "Settlement of structures supported on marginal or inadequate soils stiffened with short aggregate piers." *Proceedings of Vertical and Horizontal Deformations of Foundations and Embankments, Geotechnical Special Publication No. 40*, ASCE, College Station, TX, 2, 962-974.
3. Lawton, E.C., Fox, N.S., and Handy, R.L. (1994). "Control of settlement and uplift of structures using short aggregate piers." *Proceedings of In-situ. Deep Soil Improvement, Geotechnical Special Publication No. 45*, ASCE, Atlanta, GA, 121-132.
4. Minks, A.G., Wissmann, K.J., Caskey, J.M., and Pando, M.A. (2001). "Distribution of stresses and settlements below floor slabs supported by rammed aggregate piers." Proceedings of the 54th Canadian Geotechnical Conference, Calgary, Canada, September 16-19.
5. Mitchell, J.K. (1981). "Soil improvement: State-of-the-art." *Proceedings of the 10th International Conference on Soil Mechanics and Foundation Engineering*, Stockholm, Sweden, 4, 509-565.

6. White, D. J., Wissmann, K. J., Barnes, A., and Gaul, A. (2002). "Embankment support: a comparison of stone column and rammed aggregate pier soil reinforcement". *Proceedings of the 55th Canadian Geotechnical Conference*, Niagara Falls, Ontario, Canada.

7. White, D.J., Gaul, A.J., and Hoevelkamp, K. (2003). *Highway applications for rammed aggregate pier in Iowa soils*. Final report, Iowa DOT TR-443.

8. Wissmann, K.J., Williamson, T., Jean, C., and Ringholz, R. (2001). "Use of Geopier soil reinforcing elements to support a large aboveground tank facility in Texas." *Proceedings of the 2001 Annual Operating Conference*, Independent Liquid Terminals Association, Houston, TX, 1-8.

9. Wissmann, K.J., FitzPatrick, B.T., White, D.J., and Lien, B.H. (2002). "Improving global stability and controlling settlement with Geopier soil reinforcing elements." Proceedings of the 4th International Conference on Ground Improvement Techniques, Kuala Lampur, Malaysia, 753-760.

10. Wong D.O., FitzPatrick, B.T., and Wissmann, K.J. (2004). "Stabilization of retaining walls and embankments using rammed aggregate piers™." *Proceedings of Geo-Trans 2004, Geotechnical Special Publication No. 126*, ASCE, Los Angeles, CA, 1866-1875.

CHAPTER 2: INFLUENCE OF LATERAL STRESS ON SOIL BEHAVIOR

A paper submitted to the Journal of Geotechnical and Geoenvironmental Engineering

David J. White[1] and Ha T.V. Pham[2]

ABSTRACT

The development of high lateral stresses in the adjacent soil during the driving of displacement piles plays an important and well-known role in the development of pile skin friction. Less well understood is the influence of lateral stress fields, whether natural or man-induced, on vertical compressibility. This paper reports an evaluation of stress path-controlled axisymmetric (triaxial) tests performed to measure changes in soil behavior under varying lateral stress conditions. Soil specimens remolded from western Iowa loess (ML) were first consolidated under lateral stresses ranging from at rest (K_o) to passive (K_p), and then loaded vertically. Drained and undrained loading conditions are reported. Results show that lateral stress increases the interpreted vertical preconsolidation pressure and deviator stress at failure, and substantially reduces compressibility. These behavioral changes are believed to result from permanent changes in soil fabric and from inter-particle friction reversals. Interpreted vertical preconsolidation stress (p'_{cv}) values from e–log(p'_v) relationships indicate that p'_{cv} is not dependent solely on past maximum vertical effective stress, and might be better defined as the vertical stress required to induce a change in soil fabric which lateral stress has played a key role in developing. By considering the influence

[1] Assistant Professor, Department of Civil, Construction and Environmental Engineering, Iowa State University of Science and Technology, Ames, IA 50011-3232, USA, djwhite@iastate.edu
[2] Graduate Research Assistant, Department of Civil, Construction and Environmental Engineering, Iowa State University of Science and Technology, Ames, IA 50011-3232, USA, htvpham@iastate.edu

of lateral stress on soil behavior, better predictions of settlement could be made for structures supported by soil subjected to high in-situ lateral stress fields.

INTRODUCTION

The development of high lateral stresses in the adjacent soil during the driving of displacement piles plays an important and well-known role in the development of pile skin friction. Less well understood is the influence of lateral stress fields, whether natural or man-induced, on vertical compressibility. Examples of these include the influence of lateral stress of natural soil subject to swelling from moisture variations and the influence of lateral stress on soils subject to induced pressures such as those induced by the installation of displacement piles. Identifying and measuring these complex lateral stress zones should provide new insights into soil behavior and is particularly important for applications where loads are supported by composite soil-pile systems (e.g., embankment fills over pile-reinforced foundation, floor slab, raft foundation, etc.). Recent in-situ lateral stress measurements in soil surrounding rammed aggregate piers reveal complex systems of concentric passive, plastic and elastic stress zones (Fig. 2.1) (see Handy and White 2005a; 2005b).

As early as 1932, Casagrande suggested from field observations of pile driving that soil is completely remolded to a distance equal to the pile radius, and that there is a loss of soil structure to a distance of three radii (Casagrande 1932). Other researchers have confirmed this finding (Cummings *et al.* 1948, Orrje and Broms 1967), showing that undrained shear strength decreases as far as two to four pile diameters from the pile surface, with some remolding occurring as far as six to twelve pile diameters away. Conversely,

increases in undrained shear strength with time have also been reported in soil surrounding driven piles (Seed and Reese 1955, Eide *et al.* 1961; Flaate 1972, Randolph *et al.* 1979). Others report indirect evidence of high lateral stress development, in some cases as high as the passive limit based on back-calculated values from pile pull-out tests (e.g. Ireland 1957, Mansur and Hunter 1970, Tavenas 1971). These early studies led to applications of cavity expansion theory in soils to predict pile shaft friction, end bearing capacity, uplift capacity, radial consolidation, and lateral capacity (Soderberg 1972; Wood and Wroth 1977; Cook and Price 1978; Randolph *et al.* 1979; Kirby and Esrig 1979; Randolph and Houlsby 1984; Fleming *et al.* 1985). More recently, back-calculations of induced lateral stress in the vicinity of rammed aggregate piers from uplift load tests have also shown lateral stress levels approaching the passive limit (Caskey 2001). Measurements reported by Chen and Kulhawy (2001) indicate that pressure-injected footing installations in cohesionless soils induce soil compaction zones extending outward as far as four pier diameters. Visual evidence of lateral stress development (i.e. radial cracks) from a displacement pile can be seen in Fig. 2.2.

It has been observed from K_o Stepped Blade tests that plastic stress zones at the upper portion of the piers overlap to create a continuum of high lateral stresses in the matrix soil between groups of rammed aggregate piers (Handy and White 2005a, 2005b). Figure 2.3 shows radial and tangential stress levels near the Rankine's passive limit for soil confined by a group of short aggregate piers installed in alluvial clay (see White *et al.* 2003). This finding supports the concept that axisymmetric testing methods (i.e. equal radial and tangential stresses) can be used to simulate stress states for soil confined in a group of closely spaced displacement piles.

This paper describes results from a laboratory study to measure the influence of lateral pre-stressing on shear strength, stiffness, and preconsolidation pressure. Four series of stress path-controlled tests were conducted on remolded loess in which soil specimens were consolidated under induced lateral stress conditions before being loaded vertically.

CONCEPTUAL APPROACH

The framework for the test plan reported in this paper is based on a hypothesis introduced by Handy (2001) that describes a possible role of induced lateral stress on the consolidation characteristics of soils. A key point of the discussion is illustrated in Fig. 2.4. Vector *AB* represents the initial stress path of a normally consolidated soil. The consolidation envelope that coincides with vector *AB* defines two ranges of deformation: a near-linear elastic deformation zone and the virgin compression zone. If the vertical stress is assumed to be constant, then the lateral stress induced by the installation of a displacement pile yields the stress path *BC*. At the ultimate condition, the induced lateral stress can be as high as the Rankine's passive limit, which is defined by the extension of the failure envelope. The foundation load subsequently applied to the soil is illustrated by the stress path *CD*. After the soil is laterally stressed, the vertical stress must be greatly increased (e.g. from V_1 to V_2) to induce consolidation. In other words, if the applied vertical stress were lower than V_2, then the deformation experienced by the soil would be in the near-linear elastic region. For a normally consolidated soil and assuming $K_o = 1 - \sin\phi$ (Jaky 1944), the ratio V_2/V_1 can be expressed by the reinforcement factor, K_r, as:

$$K_r = \frac{K_p}{K_o} = \frac{1+\sin\phi}{(1-\sin\phi)^2} \qquad [2.1]$$

Thus, for a friction angle, ϕ, equal to 30 degrees, V_2 can increase up to six times V_1 before initiating consolidation settlement (Handy 2001).

Under axisymmetric (i.e. triaxial) loading conditions, the mean effective stress (p'_f), the deviatoric stress (q_f), and the specific volume (v_f), of soil at the critical state are related by the following equations (Schofield and Wroth, 1968):

$$q_f = (\sigma'_1 - \sigma'_3)_f = Mp'_f = M\left(\frac{\sigma'_1 + \sigma'_2 + \sigma'_3}{3}\right)_f \quad [2.2]$$

$$v_f = 1 + e_f = \Gamma - \lambda \ln p'_f = \Gamma - \lambda\left(\frac{\sigma'_1 + \sigma'_2 + \sigma'_3}{3}\right)_f, \quad [2.3]$$

$$M_c = \frac{q_f}{p'_f} = \frac{6\sin\phi'}{3 - \sin\phi'} \quad [2.4]$$

where M_c is the slope of the failure envelope (FE) in compression space of the p'-q diagram; σ'_1, σ'_2, and σ'_3 are the principal effective stresses; Γ is the specific volume (at p' = 1 kPa); λ is the slope of the isotropic normal consolidation line; and ϕ' is the friction angle.

Before failure, a soil must yield at a stress state that is characterized by the initial yield surface. This model assumes that soil behaves elastically at stress states within the initial yield surface, and elasto-plastically at stress states on the initial yield surface. Soil anisotropy and the preconsolidation mean effective stress control the shape and size of the initial yield surface (Wong and Mitchell 1975; Graham and Houlsby 1983; and Houlsby and Sharma 1999).

PROPERTIES OF THE TEST MATERIAL

Soil collected for this study was obtained from the Loess Hills region of southwestern Iowa. Peorian loess in this area forms a massive surface deposit which mantles older (pre-Wisconsin) loesses and glacial deposits, and is believed to be eolian in origin (Davidson and Handy 1952). The loess in this region is predominantly silt. Grain size analysis indicates about 98% fines (≤75 μm) with 11% clay-size particles (≤ 2 μm). The liquid limit and plasticity index are 28% and 6%, respectively, which classifies the material as ML. Specific gravity is 2.70. Based on standard Proctor compaction tests (ASTM-D698 2002), the optimum water content is 17.5% and the maximum dry density is 1.70 g/cm^3.

Remolded specimens for triaxial testing were prepared using an impact compaction device 50 mm diameter by 100 mm length. (Details of the compaction apparatus are described by O'Flaherty *et al.* 1963.) In lieu of one layer of compaction, each sample was compacted in two 50 mm thick layers to improve vertical uniformity. Compaction energy was adjusted by varying the hammer drop height so that the initial dry density of all samples was uniform (i.e. γ_d = 1.62 ± 0.01 g/cm^3, or about 95% compaction). Samples were compacted on the wet side of optimum (20%) to reduce the potential for collapse during the back pressure saturation process. The degree of saturation after compaction was about 81%. Table 2.1 summarizes the initial void ratios after compaction.

TEST APPARATUS AND PROCEDURE

Tests were carried out using a stress path triaxial system similar to that originally developed by Bishop and Wesley (1975). The system is a semi-automatic, computer-controlled feedback apparatus in which cell, back, and axial pressures are independently

controlled by bladder-air-water pressure assemblies. Strain-controlled compression is conducted using a constant rate of strain pump. An extension device is fitted to the top of the specimen cap through which vacuum pressure is introduced. With the introduction of vacuum pressure at the top of the specimen, extension conditions in which lateral stress is higher than vertical stress (i.e. $K > 1$) are possible. All samples were back pressure saturated with de-aired water using incremental back pressure steps of 35 kPa until Skempton's pore pressure parameter, $B \geq 0.96$. Lateral filter paper was used to enhance the drainage rate during the backpressure saturation and consolidation phases. During backpressure saturation, the difference between cell pressure and back pressure was maintained at 1.0 kPa. At the end of back pressure saturation, a minimum back pressure of at least 210 kPa was maintained for the remainder of the test to maintain saturation. Following saturation, all samples were isotropically consolidated at a mean effective stress of 250 kPa and then allowed to swell back to an effective stress of 1.0 kPa. In this manner all specimens were made to a void ratio of about 0.66 (see Table 2.1). The samples were pre-consolidated at the same pressure to create uniform stress histories. Following the back pressure saturation and isotropic consolidation phases, four different stress path-controlled test series, denoted as *CU*, *LCU-*K_{iso}, *LCU-*K_o, and *LCD*, were performed.

The *CU* test series consists of conventional consolidated undrained triaxial tests. Eight samples were isotropically consolidated at eight different confining pressures (σ'_c): 25, 50, 75, 100, 125, 150, 175, and 200 kPa. After consolidation, the samples were vertically loaded in an undrained condition at a constant strain rate of 0.635%/min. Total stress and excess pore water pressure as a function of axial strain were recorded during the tests. Final

void ratios were back-calculated from the oven-dried weight of the sample after completing the tests.

The *LCU-K_{iso}* test series was performed as follows: (1) K_o-consolidate at σ'_v equal to 50 kPa and σ'_c equal to 25 kPa (i.e., K_o = 0.5); (2) while maintaining constant vertical stress (σ'_v = 50 kPa, $\Delta\sigma'_v$ = 0), increase confining pressure to K = 1, 1.5, 2, 2.5, or 3, and allow sample to consolidate; (3) following lateral consolidation, increase vertical stress, σ'_v, until K = 1.0 (isotropic stress condition) and consolidate again; and (4) close drainage lines and load vertically to failure at a constant strain rate of 0.635%/min while monitoring changes in excess pore water pressure.

The *LCU-K_o* test series was essentially the same as *LCU-K_{iso}*, except that the K value in step (3) is reduced to 0.5 by increasing the vertical stress.

The *LCD* test series also included the first two steps described for *LCU-K_{iso}*. However, after consolidation at various K values, the samples were vertically loaded in increments by increasing stress in a drained condition with the confining stress unchanged. The loading procedure used in this step is essentially a stress control process in which the samples were allowed to consolidate for each vertical stress increment until the failure load was reached. A summary of load steps for all test series is presented in Table 2.1.

INITIAL YIELD SURFACE AND SHEAR STRENGTH PARAMETERS

To establish baseline shear strength parameter values and the yield envelope location, results from the *CU* tests are presented in Fig. 2.5 and 2.6. The slope (M_c) of the failure envelope in the *q-p'* plot is 1.33, which corresponds to an effective stress friction angle of 33

degrees. Figure 2.6a, which shows the deviator stress versus axial strain, indicates that the soil behaves as a strain-hardening material. During axial undrained loading, excess pore water pressure measurements (Fig. 2.6b) indicate dilatation for confining stress values lower than about 75 kPa (i.e. $OCR = 4$), and compression for confining stress is higher than about 100 kPa (i.e. $OCR < 3$). The deviator stress at the maximum strain ($\varepsilon_1 = 20\%$) is used to plot the failure envelopes in all tests.

Yield point locations used to define the yield surface in Fig. 2.5a were determined graphically from the stress-strain curves in Fig. 2.6a. The yield point locations were determined at the transition from stiff to less stiff response ($\varepsilon_1 \leq 1.0$) (see Wood 1990). The shape of the yield surface is similar to results from Houlsby and Sharma (1999) for anisotropically consolidated soils. The axial strain at which yielding occurred ranged from 0.3 to 1.0% in all tests.

Figure 2.5b shows the isotropic triaxial consolidation test results from which the preconsolidation mean pressure (p'_c) is estimated to be about 300 kPa, which is higher than the maximum isotropic consolidation stress applied to all samples (i.e. $p' = 250$ kPa). Figure 2.5b also shows that the isotropic normal consolidation line (*ISO-NCL*) and the failure envelope in the e–p' plot are not parallel. Been and Jefferies (1985) observe similar results, and attribute this behavior to decreased dilatancy with increased confining stress. The interpreted isotropic compression index (C_c) and the recompression index (C_r) are 0.258 and 0.023, respectively.

INFLUENCE OF LATERAL STRESS ON SOIL BEHAVIOR

Yield Surface Migration

The yield surface in q–p' space (Fig. 2.5a) indicates the stress state that separates an elastic response from an elasto-plastic response. The size and shape of the yield surface depend on soil anisotropy and the preconsolidation mean stress (p'_c). For comparison to the *CU* test series, Figures 2.7 through Fig. 2.12 show the q–p' plots and yield surfaces for test series *LCU-*K_{iso}, *LCU-*K_o, and *LCD*, respectively. In all figures, the effective stress path is shown by solid lines and represents the stress-controlled consolidation increments. The dashed lines represent the effective stress paths during strain-controlled, undrained vertical loading (*CU*, *LCU-*K_{iso}, and *LCU-*K_o) or stress-controlled, drained (*LCD*) vertical loading. The initial lateral consolidation stages (i.e. simulation of induced lateral stress) for all test series are shown by the downward-trending stress paths in the extension zone.

All samples in the *LCU-*K_{iso} test series were initially K_o – consolidated at $K = 0.5$ and subsequently consolidated at $K = 1.0$, 1.5, 2.0, 2.5, or 3.0 by maintaining vertical stress at 50 kPa and increasing the confining stress. Following consolidation, all specimens were loaded back to $K = 1.0$ by increasing the vertical stress. Once at volumetric equilibrium, the specimens were loaded vertically with the drainage lines closed. The test results shown on Fig. 2.6 indicate similar compression yield envelope locations for test series *CU* and *LCU-*K_{iso}.

In contrast to the *CU* and *LCU-*K_{iso} tests shown in Figs. 2.5a and 2.7a, measurements from test series *LCU-*K_o show that the yield surface shifts upward to higher deviator stress values (Fig. 2.9a). The only difference between *LCU-*K_{iso} and *LCU-*K_o test procedures is that

the samples were consolidated back to a K_o-consolidation stress state following consolidation at $K = 1.0$. By first consolidating under high lateral stress conditions and then increasing the vertical stress and consolidating further, this stress path simulates lateral consolidation from pile installation followed by consolidation under a vertical footing load. As shown in Fig. 2.9a, new yield points were shifted upward without increasing the mean preconsolidation pressure, p'_c, and without applying a stress state beyond the initial yield envelope. This behavior suggests that the soil may be reinforced from a permanent change in soil fabric.

Figure 2.9b shows that the void ratio decreased during the lateral consolidation phases as predicted by Handy (2001). During the loading and consolidation period from the end of the lateral consolidation to the K_o stress state (i.e. pre-shear stress state), changes in void ratio are almost zero. The authors interpret the data as consolidation beginning only when the vertical stress is sufficient to overcome inter-particle shear stresses developed during lateral consolidation. (These phenomena and micro-scale changes in soil fabric are being investigated in a separate study using scanning electron microscopy and x-ray computed tomography techniques.)

Test series *LCD* (Fig. 2.11 and 2.12) show results similar to *LCU-K_o*, in that the yield envelope is expanded to higher deviator stress levels than in the *CU* tests. For test series *LCD*, lateral consolidation was followed by stress-controlled vertical consolidation increments. Figure 2.11b shows little consolidation up to the compression yield envelope after the lateral consolidation phase.

Preconsolidation Pressure

Measuring and interpreting the load history of soil in terms of void ratio versus the logarithm of the vertical effective stress (e-log(p'_v)) is a widely used design procedure in geotechnical engineering. Conventional procedures provide the following interpretation (Terzaghi 1943): (1) Preconsolidation pressure can be interpreted as the past maximum vertical effective stress; and (2) A soil state to the right of the normal consolidation line is impossible. Based on the test results described in this paper, however, there is evidence to question these interpretations.

Figure 2.13 presents a plot showing the conventional e-log(p'_v) relationship for the *LCD* test results. Recall that during the lateral consolidation phases, the vertical stress was held constant at 50 kPa. Following lateral consolidation, vertical stress was increased in increments allowing for consolidation at each step. The test results show that the process of lateral consolidation increases the interpreted vertical preconsolidation effective stress and that by consolidating soil under high lateral stresses it is possible to obtain data points that plot to the right of the isotropic consolidation envelope. These findings suggest that the interpreted vertical preconsolidation stress values from e–log(p'_v) relationships are not dependent solely on past maximum vertical effective stress. The vertical preconsolidation pressure (p'_{cv}) might be better defined as the vertical stress required to induce a change in soil fabric which lateral stress has played a role in developing. In this case the interpreted p'_{cv} increases up to 1.7 times the value determined from the isotropic triaxial consolidation test.

Figure 2.14 shows the same data set as Fig. 2.13, but using the e–log(p') relationship, where p' is the mean effective stress. Results indicate that, as expected, the void ratio

decreases during lateral consolidation, and that the void ratio decreases at a reduced rate as the applied vertical stress exceeds the stress corresponding with stress reversal (preconsolidation mean pressure, p'_c). The data plots to the left of the original isotropic virgin curve, which results in a lower preconsolidation mean stress compared with the original preconsolidation value (p'_{co} = 300 kPa). This is not unexpected, since the loading conditions are anisotropic.

Secant Modulus and Compression Index

Figures 2.6a through Fig. 2.12a show the stress-strain curves for all test series. As expected, stiffness increases with increased confining stress. Figure 2.15 shows that the E_{50} secant modulus values (based on 50 percent of the failure deviator stress) increase with mean consolidation pressure for each test series. The E_{50} secant modulus values for the *LCU-*K_{iso} and *LCU-*K_o tests are up to 1.6 and 6 times the E_{50} secant modulus values for the *CU* tests. The E_{50} secant modulus values of about 90 MPa for the *LCU-*K_o tests are as high as densely compacted aggregate (White *et al.* 2003). Secant modulus values for *LCD* are not shown because the stress-strain curves indicate an almost perfectly elastic-plastic behavior (Fig. 2.12a). For these tests at low strain levels, it appears that the stress-strain curves slightly rebounded as K decreased during vertical drained loading, giving an infinitely high modulus. Stored energy in the form of inter-particle shear stresses and rotation of soil particles after full friction reversals may account for this behavior.

Figure 2.16 shows that for test series *LCD*, the compression index (C_c) is reduced up to 390 times, and the swell index (C_r) is reduced up to about 35 times relative to the isotropic consolidation test results. The *LCD* test results show that the soil exhibits the stiffest

response for $K = 1.0$. At $K = 3.0$, C_c is reduced only 60 times and C_r is reduced about 8 times — possibly because the specimens were loaded outside of the initial extension yield surface.

Shear Strength Parameter Values

Figure 2.7a shows that for test series *LCU-*K_{iso}, the effective stress friction angle increased from 33 degrees (*CU*) to 35 degrees. In this case, the lateral consolidation sequence shows only a slight increase in deviator stress at failure. Handy's (2001) hypothesis that lateral stress can extend the zone of near-linear elastic behavior is supported by comparing the deviator stress values that intersect the initial yield envelopes for the K = 0.5 and K = 3.0 stress paths, 55 kPa and 145 kPa, respectively. In this case, the vertical effective stress component is increased about five times before exhibiting elasto-plastic behavior. Likewise, vertical stress is increased about six times before reaching the deviator stress at failure. (This value is similar to that predicted by Eq. 2.1.)

Figure 2.9a shows that the effective stress friction angle increased from 33 degrees (*CU*) to about 40 degrees for *LCU-*K_o. This significant increase in shear strength suggests that particle rearrangements play an important role in the behavior of soils after they are laterally consolidated, and that the behavior of soils depends not only on their stress histories, but also on their strain histories (Houlsby and Sharma, 1999).

Figure 2.11a shows the *LCD* test series results. Vertical compression loading was terminated when significant sample bulging was observed, which in some cases was prior to reaching the failure deviator stress. This test series was a stress-controlled and drained process. The deviator stress at failure was significantly higher than all other test series. Although similar to the *CU* test results in that the calculated friction angle is 33.0 degrees,

the increase in deviator stress at failure is explained by an increase in the cohesion intercept (about 270 kPa). The development of a cohesion term is further evidence of significant changes in the soil fabric. Compared to the *CU* test series, the deviator stress at failure increases up to 5 times at $K = 3.0$.

PRACTICAL SIGNIFICANCE

Traditionally soil behavior has been studied in terms of vertical pre-stressing, which occurs when a soil has been subject to pressures exerted by glaciers, construction traffic or when overburden pressure has been removed above the top of a soil deposit (i.e. erosion or excavation). The paradigm is that past applications of vertical stress overconsolidate soil deposits, making them both stronger (changing the shape of the Mohr-Coulomb failure envelop) and stiffer (changing the compressibility of the soil from virgin response to recompression response on the e-log(p'_v) curve). By subjecting a soil sample to consolidation testing, then C_c, C_r and p'_{cv} can be predicted. But if the soil was laterally overconsolidated, a different response is observed. Like a vertically overconsolidated soil, two distinct e-log(p'_v) curves are observed: one for recompression and one for virgin response. But, relative to the vertically overconsolidated soil there are two differences: the slope of the recompression curve is flatter and the value of the preconsolidation pressure is higher. The authors think that this is related to the orientation of soil particles and inter-particle shear stresses.

So when is it useful and how does it make a difference?

1. Predicting the response of a laterally overconsolidated soil using vertical consolidation approaches and correlations produces conservative results (i.e.

predicting C_c from Atterberg limits and then using $C_r = C_c/8$, would be conservative)

2. Including effects of lateral overconsolidation is advantageous because of its positive effects on soil behavior (increasing shear strength and reducing compressibility).

Where do laterally consolidated soils occur?

1. Natural soil deposits with relatively high *PI* that are subjected to swelling (i.e. overconsolidated expansive clay);
2. Next to the base of retaining walls (passive side) or behind pre-stressed braced excavation;
3. Soil subjected to compaction (deep dynamic compaction and roller type impact compaction); and
4. Laterally overconsolidated soil next to displacement pile and ground improvement systems such as rammed aggregate piers where soil compressibility is considered in design.

SUMMARY AND CONCLUSION

An experimental study was conducted to investigate the influence of lateral stress on the behavior of soil. Results from this study show that lateral stress significantly influences shear strength and compressibility. Behavioral changes are believed by the authors to result from permanent changes in soil fabric and from inter-particle friction reversals. Major findings from this research include the following:

1. The process of lateral consolidation prior to vertical loading delays consolidation by increasing the apparent preconsolidation pressure. A new definition is presented for interpreting preconsolidation stress from e-log(p'_v) relationships as *the stress required to induce a change in soil fabric, for which lateral stress and inter-particle shear stresses have a significant influence*. As the result of the increase in preconsolidation pressure, it is possible to go to the right of the isotropic consolidation envelope. For the laterally consolidated specimens, both compression index C_c and recompression index C_r were greatly reduced, rendering the soil much stiffer after lateral consolidation.

2. The effective stress friction angle of the soil increased from 33 degrees (*CU*) to 40 degrees (*LCU-K_o*). This is a significant increase, and suggests that friction reversals and strain history play important roles in the behavior of soils. The deviator stress at failure obtained from *LCD* tests is significantly higher than all other tests. Similar to the *CU* test results, the back-calculated friction angle from *LCD* tests was 33 degrees; however, cohesion of about 270 kPa was observed. The development of cohesion is believed to result from over-consolidation of the sample (soil fabric change) and, again, because the friction between soil particles was fully reversed.

3. Secant modulus values for *LCU-K_{iso}* showed increases up to 1.6 times the *CU* test values. Stress-strain curves from *LCU-K_o* produced secant modulus values up to 6 times higher than those from *CU* test results. Stress-strain curves from the *LCD* test series indicate an almost perfectly elastic-plastic behavior with an extremely

high secant modulus. It is believed by the authors that stored energy in the form of inter-particle shear stresses and the rotation of soil particles after full friction reversals account for this behavior.

ACKNOWLEDGEMENT

This research was funded by Geopier Foundation Company, Inc. and Iowa State University of Science and Technology. The support of these agencies is gratefully acknowledged. Helpful review comments were provided by Dr. Vernon R. Schaefer, Dr. Kord J. Wissmann and Dr. Richard L. Handy.

NOTATION

The followiing symbols are used in this paper:

B	=	Skempton's pore pressure parameter
C_c	=	compression index
C_r	=	swelling index
e	=	void ratio
e_f	=	void ratio at failure
ϕ'	=	effective stress friction angle
Γ	=	specific volume at p' = 1 kPa
K	=	ratio of lateral effective stress to vertical effective stress
K_o	=	coefficient of earth pressure at rest
K_p	=	coefficient of passive earth pressure
λ	=	slope of the isotropic normal consolidation line
M_c	=	slope of the failure envelope in compression space

M_e = slope of the failure envelope in extension space

OCR = over-consolidation ratio

p'_c = preconsolidation mean effective stress

p' = mean effective stress = $\frac{1}{3}(\sigma'_1 + \sigma'_2 + \sigma'_3)$

q = deviator stress = $(\sigma'_1 - \sigma'_3)$

p'_f = effective mean stress at failure

q_f = deviator stress at failure

$\sigma'_1, \sigma'_2, \sigma'_3$ = effective principal stresses

σ'_r = radial effective stress

σ'_θ = tangential effective stress

σ'_v = vertical effective stress

p'_{vc} = preconsolidation vertical effective stress

v_f = specific volume at failure

REFERENCES

1. ASTM-D698 (2002). "Test method for laboratory compaction characteristics of soils using standard effort." *Annual book of ASTM standards*, ASTM International.

2. Been, K., and Jefferies, M.G. (1985). "A state parameter for sands." *Geotechnique*, 35(2), 99-112.

3. Bishop, A.W., and Wesley, L.D. (1975). "A hydraulic triaxial apparatus for controlled stress path testing." *Geotechnique*, 25(4), 657-670.

4. Casagrande, A. (1932). "The structure of clay in its importance in foundation engineering." *Contributions to Soil Mechanics*, Boston Society of Civil Engineers, Boston, 72-112.

5. Caskey, J.M. (2001). *Uplift Capacity of Rammed Aggregate Pier Soil Reinforcing Elements*. M.Sc. Thesis, University of Memphis, Memphis, TN, USA.

6. Chen, J., and Kulhawy, F. (2001). "Compaction Effects Induced in Cohesionless Soils by Installation of Pressure-Injected Footings." *Proceedings of Foundations and Ground Improvement, Geotechnical Special Publication No. 113*, ASCE, Blacksburg, VA, 113-230.

7. Cooke, R.W., and Price, M.J. (1978). "Strains and displacements around friction piles." *Proceedings of the 8th International Conference on Soil Mechanics and Foundation Engineering*, ISSMGE, Moscow, Russia, 3(9), 52-60.

8. Cummings, M., Kerkhoff, G.O., and Peck, R.B. (1948). "Effect of driving piles into soft clay." *Transactions of ASCE*, 115, 275-350.

9. Davidson, D.T., and Handy, R.L. (1952) "Property variation in the Peorian (Wisconsin) loess of southwestern Iowa." *Proceedings of Iowa Academy of Science*, 59, 248-265.

10. Eide, O., Hutchinson, J.N. and Landva, A. (1961). "Short and long term test loading of a friction pile in clay." *Proceedings of the 5th International Conference on Soil Mechanics and Foundation Engineering*, ISSMGE, Paris, France, 45-54.

11. Flaate, K. (1972). "Effects of pile driving in clays." *Canadian Geotechnical Journal*, 9, 81-88.

12. Fleming, W.G.K., Weltman, A.J. Randolph, M.F., and Elson, W.K. (1985). *Piling Engineering*. John Wiley and Sons.

13. Graham, J., and Houlsby, G.T. (1983). "Anisotropic elasticity of a natural clay." *Geotechnique*, 33(2), 165-180.

14. Handy, R.L. (2001). "Does lateral really influence settlement?" *Journal of Geotechnical and Geoenvironmental Engineering*, ASCE, 127(7), 623-626.

15. Handy, R.L., and White, D.J. (2005a). "Stress zones near displacement pier I: Plastic and Liquefied Behavior." *Journal of Geotechnical and Geoenvironmental Engineering*, ASCE (*accepted for publication*).

16. Handy, R.L., and White, D.J. (2005b). "Stress zones near displacement pier II: Radial Cracking and Wedging." *Journal of Geotechnical and Geoenvironmental Engineering*, ASCE (*accepted for publication*).

17. Houlsby, G.T., and Sharma, R.S. (1999). "A conceptual model for the yielding and consolidation of clays." *Geotechnique*, 49(4), 491-501.

18. Ireland, H.O. (1957). "Pulling tests on piles in sand." *Proceedings of the 4th International Conference on Soil Mechanics and Foundation Engineering*, ISSMGE, London, UK, 2, 43-45.

19. Jaky, J. (1944). "The coefficient of earth pressure at rest." *Journal of the Hungarian Society of Engineers and Architects*, 7, 355-358.

20. Kirby, R.C., and Esrig, M.I. (1979). "Further development of a general effective stress method for prediction of axial capacity for driven piles in clay." *Proceedings of Recent Development in the Design and Construction of Piles*, ICE, 335-344.

21. Mansur, C.I., and Hunter, A.H. (1970). "Pile tests – Arkansas river project." *Journal of the Soil Mechanics and Foundation Division*, ASCE, 96(SM5), 1545-1582.

22. O'Flaherty, C.A., Edgar, C.E., and Davidson, D.T. (1963). *The Iowa compaction apparatus: a small sample apparatus for use in obtaining density and strength measurements of soils and soil-additives.* Special report prepared for the 42nd Annual Meeting of the Highway Research Board, NAS-NCR, Washington D.C., Project No. HR-83 of the Iowa Highway Research Board.

23. Orrje, O., and Broms, B.B. (1967). "Effects of pile driving on soil properties." *Proceedings of ASCE*, 55(SM5), Part I, 59-73.

24. Randolph, M.F., Carter, J.P., and Wroth, C.P. (1979). "Driven piles in clay – the effects of installation and subsequent consolidation." *Geotechnique*, 29(4), 361-393.

25. Randolph, M.F., and Houlsby, G.T. (1984). "The limiting pressure on a circular pile loaded laterally in cohesive soil." *Geotechnique*, 34(4), 613-623.

26. Schofield, A.N., and Wroth, C.P. (1968). *Critical State Soil Mechanics*. New York: McGraw-Hill.

27. Seed, H.B, and Reese, L.C. (1955). "The action of soft clay along friction piles." *Transactions of ASCE*, 122, 731-754.

28. Soderberg, L.O. (1972). "Consolidation theory applied to foundation pile time effects." *Geotechnique*, 12, 217-225.

29. Tavenas, F.A. (1971). "Load test results on friction piles in sand." *Canadian Geotechnical Journal*, 8(7), 7-22.

30. Terzaghi, K. (1943). *Theoretical Soil Mechanics*. New York, Wiley.

31. White, D. J., Suleiman, M.T., Pham, H.T., and Bigelow, J. (2002). *Constitutive Equations for Aggregates Used in Geopier Foundation Construction.* Final Report, Iowa State University, Ames, IA, USA.

32. White, D.J., Gaul, A.J., and Hoevelkamp, K. (2003). *Highway Applications for Rammed Aggregate Piers in Iowa Soils*. Final Report, Iowa DOT Project TR-443, CTRE Project 00-60.

33. Wong, P.K.K., and Mitchell, R.J. (1975). "Yielding and plastic flow of sensitive cemented clay." *Geotechnique*, 25(4), 763-782.

34. Wood, D.M. (1990). *Soil Behavior and Critical State Soil Mechanics*. Cambridge University Press.

35. Wood, D.M., and Wroth, C.P. (1977). "Some laboratory experiments related to the results of pressuremeter tests." *Geotechnique*, 27(2), 181-201.

Table 2.1. Summary of four series of stress path control tests

Series	Description	Sample	e_0	e_1	e_2	e_3	p' (kPa)	K_{max}
CU	Isotropically consolidated, undrained compression (CU) tests	S1-25	0.661	0.657	0.650	0.650	25	1.0
		S1-50	0.663	0.659	0.639	0.639	50	1.0
		S1-75	0.662	0.661	0.628	0.628	75	1.0
		S1-100	0.659	0.656	0.615	0.615	100	1.0
		S1-125	0.658	0.663	0.610	0.610	125	1.0
		S1-150	0.660	0.661	0.604	0.604	150	1.0
		S1-175	0.659	0.660	0.595	0.595	175	1.0
		S1-200	0.661	0.658	0.589	0.589	200	1.0
LCU-K_{iso}	Anisotropically consolidated, undrained compression tests	S2-K10	0.661	0.663	0.642	0.642	50	1.0
		S2-K15	0.665	0.660	0.635	0.635	75	1.5
		S2-K20	0.665	0.656	0.623	0.623	100	2.0
		S2-K25	0.660	0.659	0.614	0.614	125	2.5
		S2-K30	0.663	0.661	0.605	0.605	150	3.0
LCU-K_o	Anisotropically consolidated, undrained compression tests	S3-K10	0.667	0.663	0.646	0.646	67	1.0
		S3-K15	0.658	0.658	0.636	0.636	100	1.5
		S3-K20	0.658	0.657	0.636	0.636	133	2.0
		S3-K25	0.661	0.661	0.627	0.627	167	2.5
		S3-K30	0.665	0.660	0.617	0.617	200	3.0
LCD	Anisotropically consolidated, drained compression tests	S4-K10	0.664	0.659	0.683	0.679	133	1.0
		S4-K15	0.641	0.657	0.649	0.644	175	1.5
		S4-K20	0.664	0.662	0.641	0.630	200	2.0
		S4-K25	0.657	0.663	0.609	0.596	233	2.5
		S4-K30	0.666	0.660	0.606	0.582	275	3.0

Note: *e_0, e_1, e_2, e_3 = void ratio after compaction, after isotropic consolidation at 250 kPa and swell back to 1 kPa, after lateral consolidation, and end of test, repectively.*
p' = mean effective stress before shear
K_{max} = maximum K value during consolidation

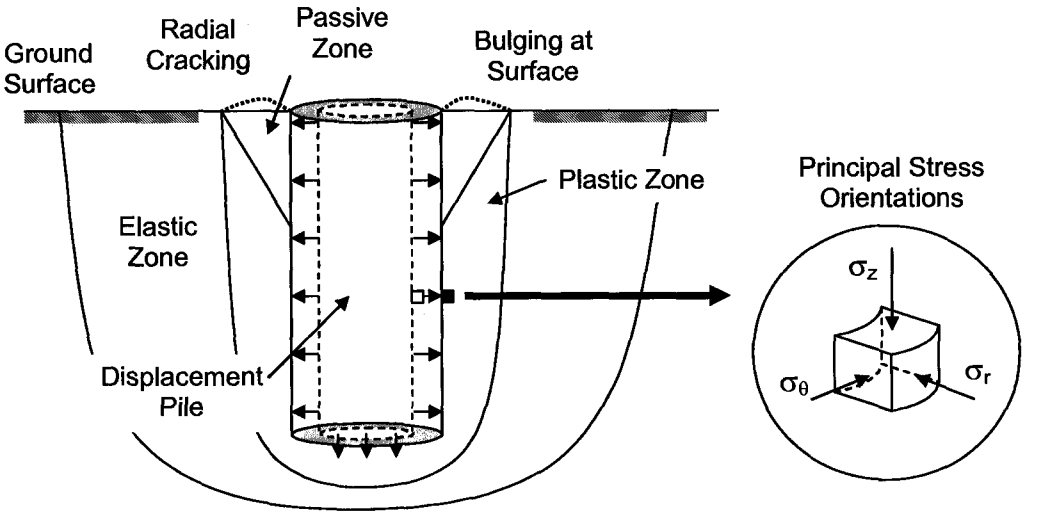

Figure 2.1. Principal stresses at soil element adjacent to rammed aggregate pier. (σ_z, σ_r, and σ_θ indicate the vertical stress, radial stress and tangential stresses, respectively.)

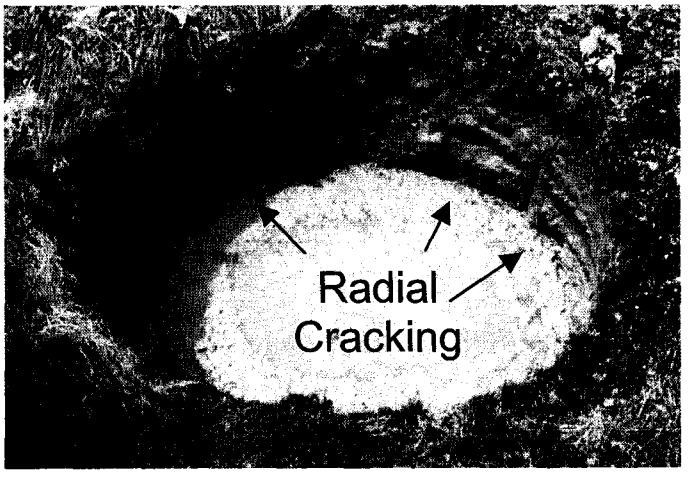

Figure 2.2. (Color) Evidence of radial cracking at ground surface of displacement pile

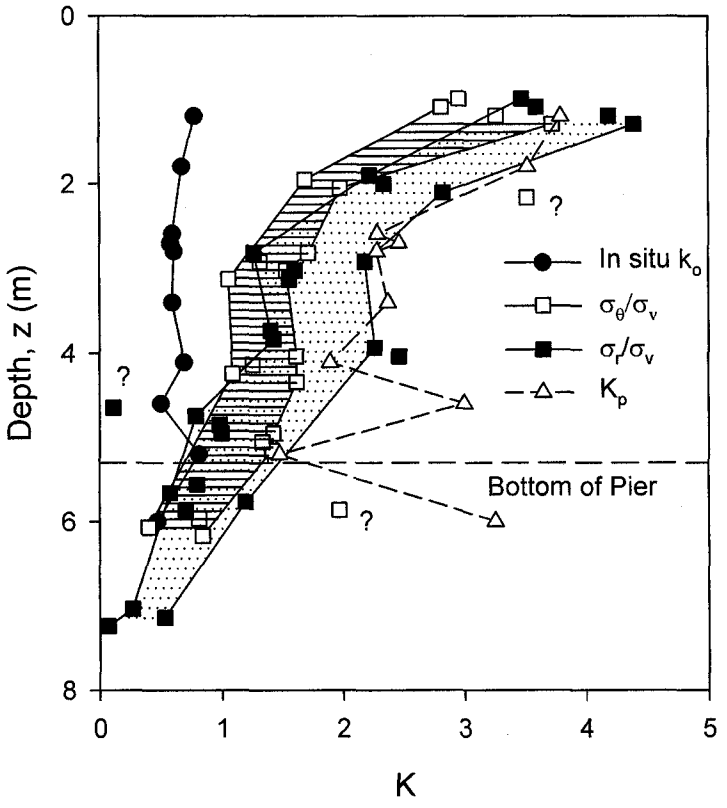

Figure 2.3. In-situ radial and tangential soil stress measurements within group of closely spaced rammed aggregate piers (White et al. 2003). Data indicates range of measurements from K_o Stepped Blade tests oriented to measure stress in radial and tangential direction (perpendicular to each other). K_o and K_p were estimated from effective stress shear strength parameters.

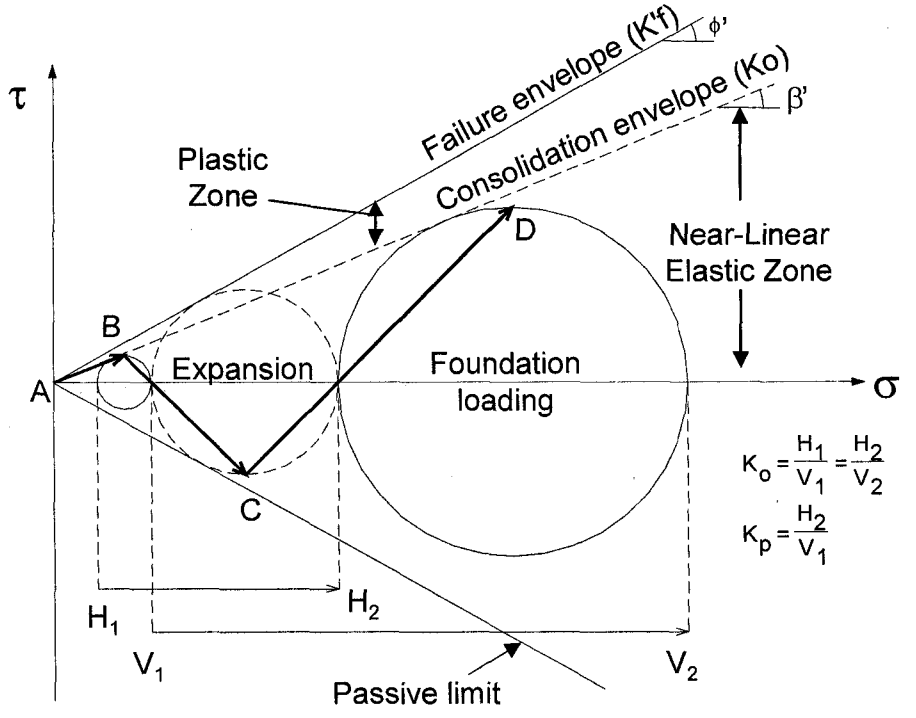

Figure 2.4. Typical stress paths encountered around displacement pile (after Handy 2001)

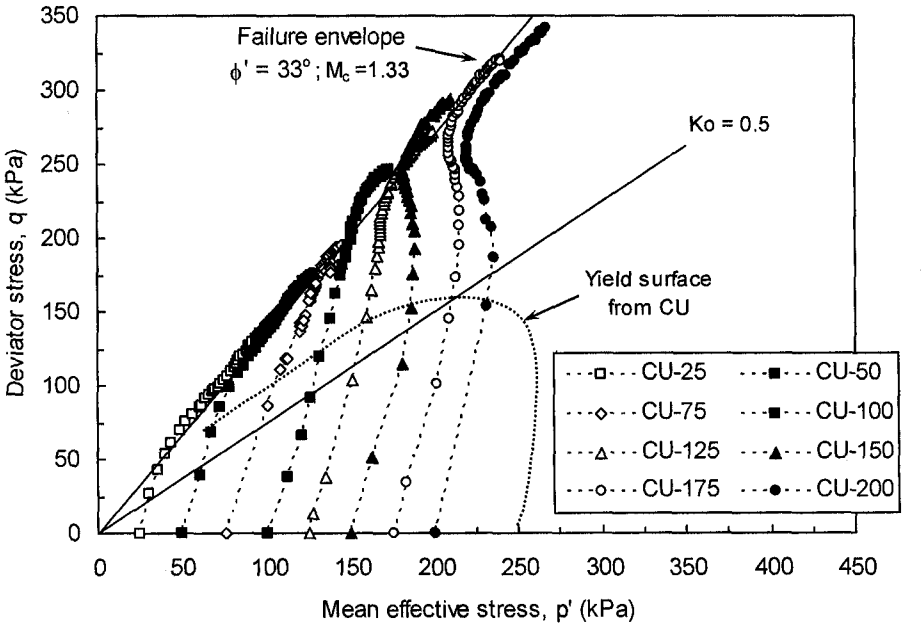

(a)

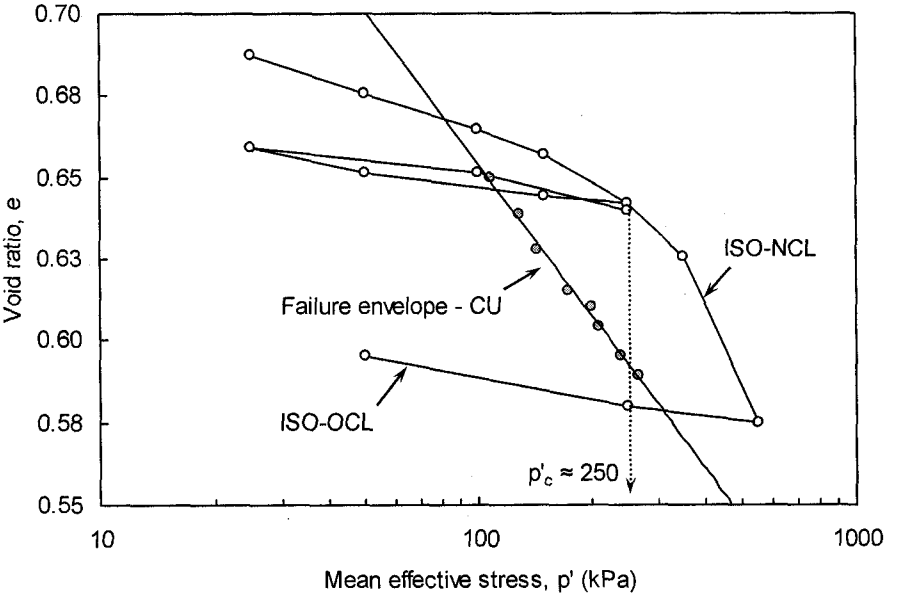

(b)

Figure 2.5. (a) Effective stress paths from *CU* test series and (b) Isotropic normal consolidation line (*ISO-NCL*) from isotropic triaxial consolidation test

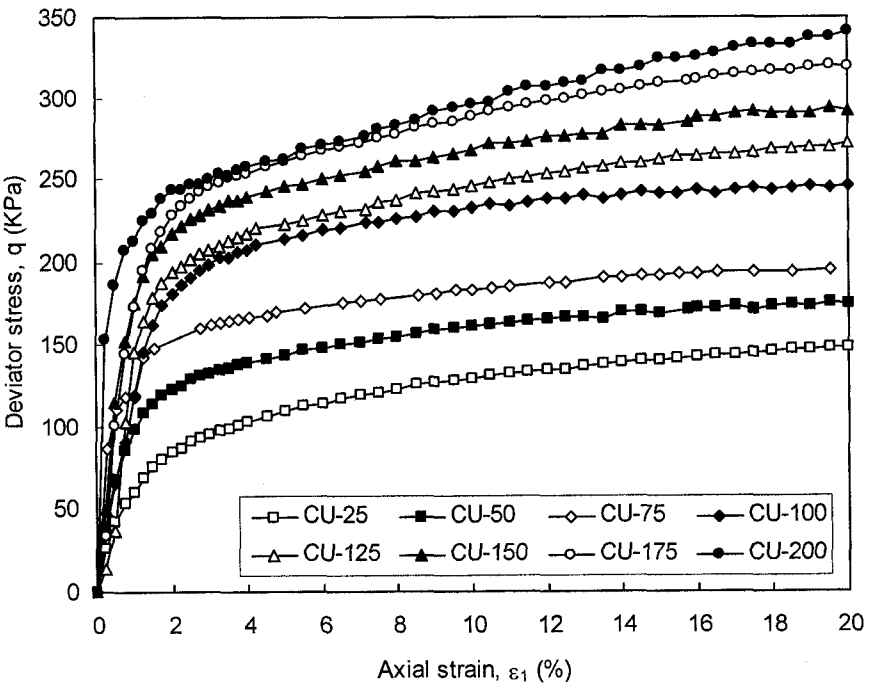

(a)

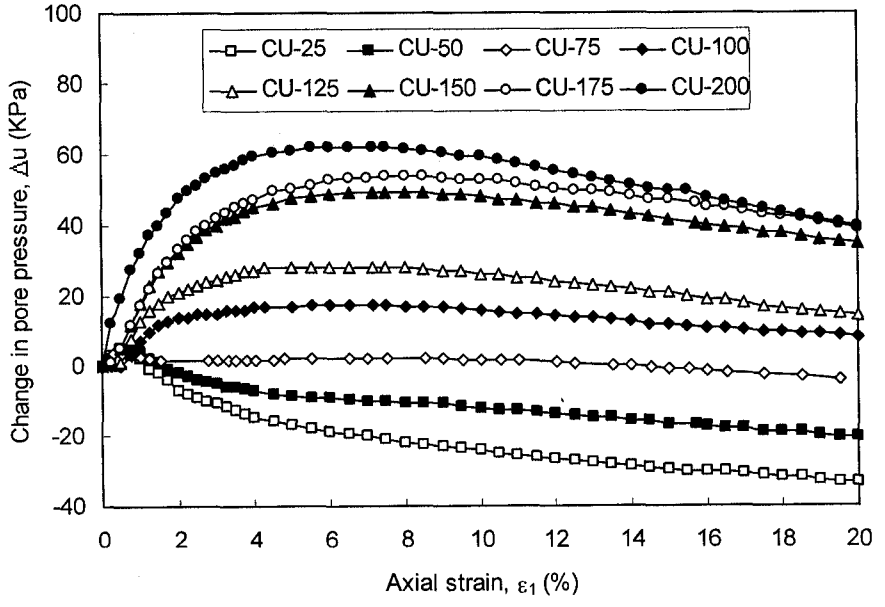

(b)

Figure 2.6. (a) Stress-strain relationships and (b) Pore pressure variation in *CU* test series

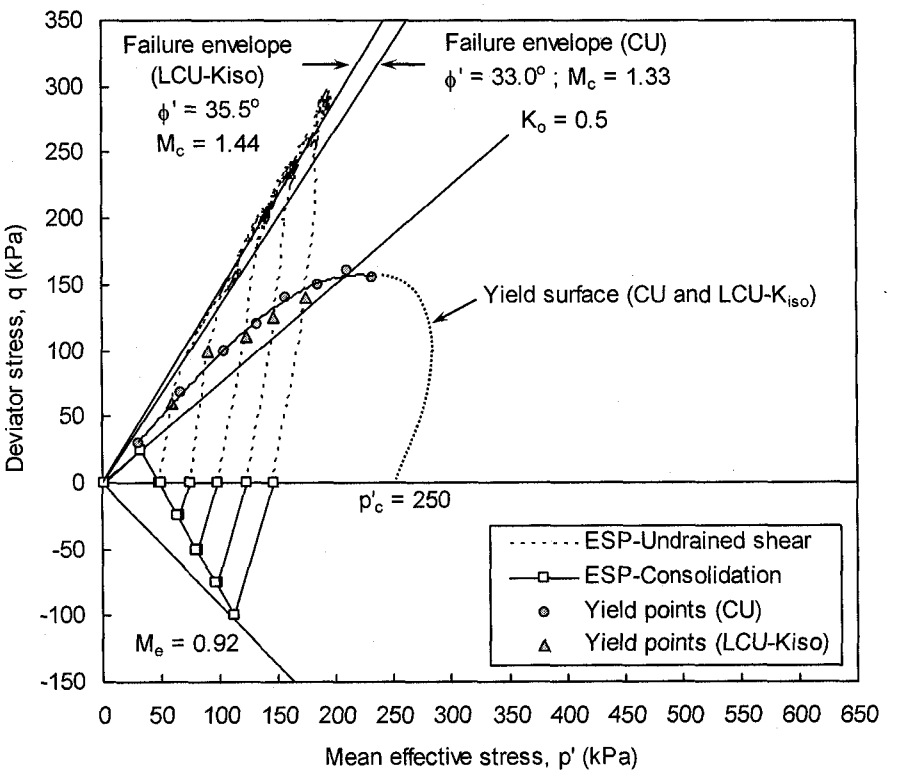

(a)

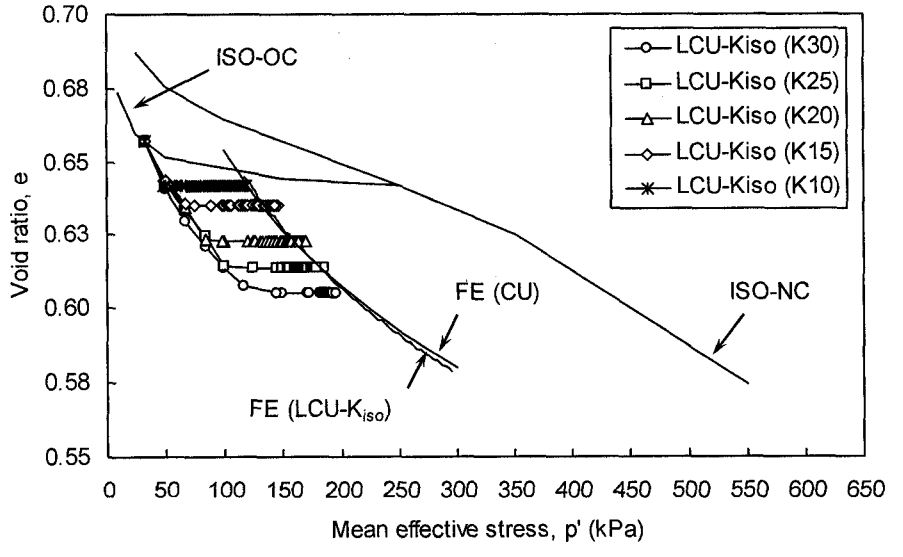

(b)

Figure 2.7. Failure envelope and yield locus in (a) *q-p'* plane; and (b) *e-p'* plane obtained from *LCU-K_{iso}* test series

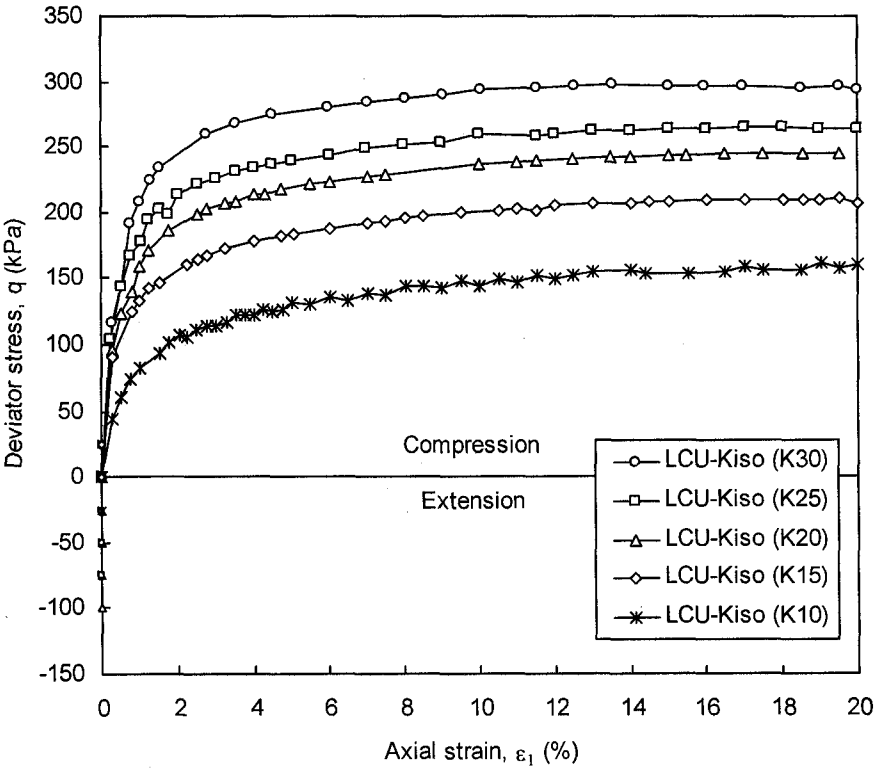

(c)

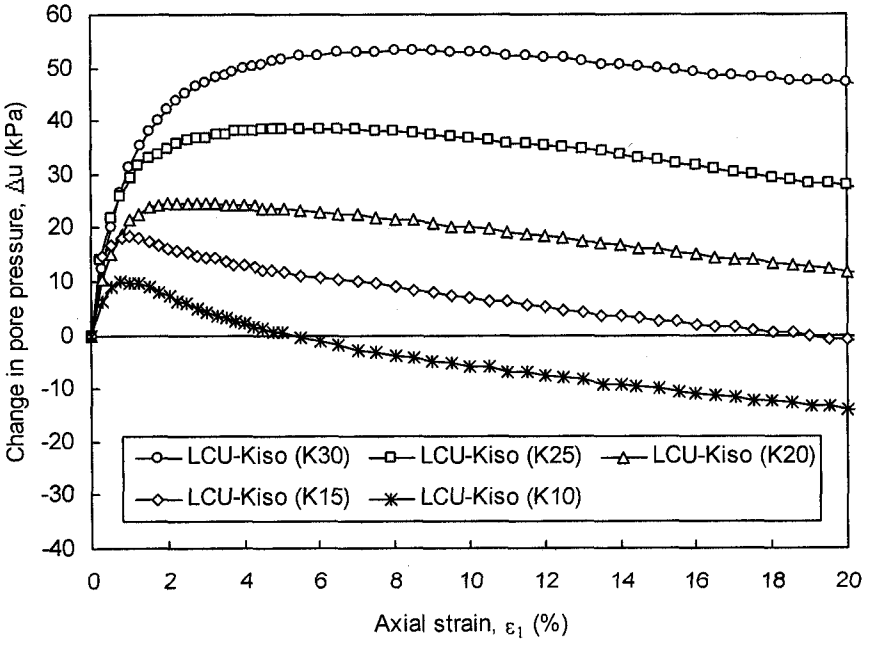

(d)

Figure 2.8. (a) Stress-strain relationship and (a) Pore water pressure variation obtained from *LCU-K_{iso}* test series

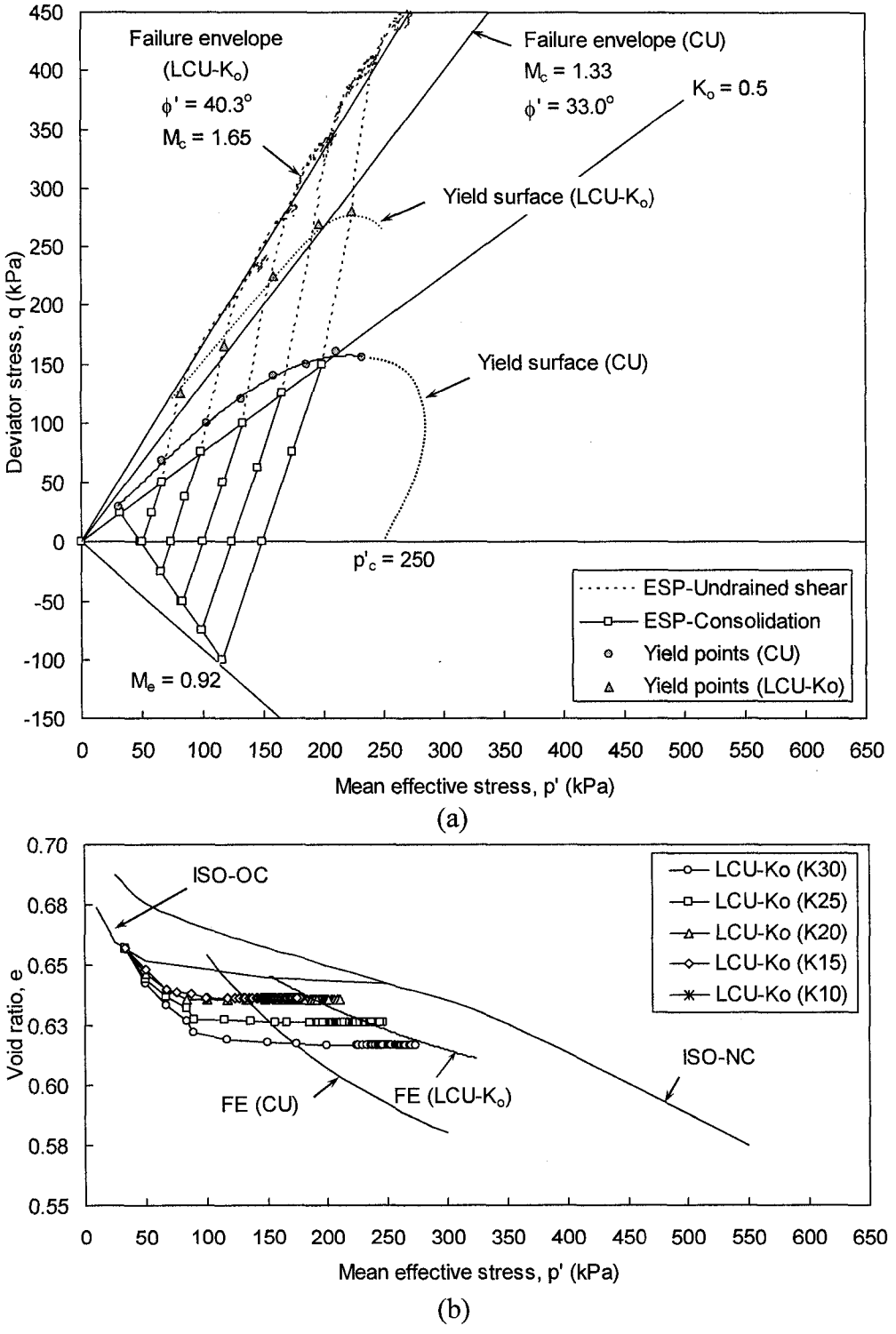

Figure 2.9. Failure envelope and yield locus in (a) *q-p'* plane; and (b) *e-p'* plane obtained from *LCU-K$_o$* test series

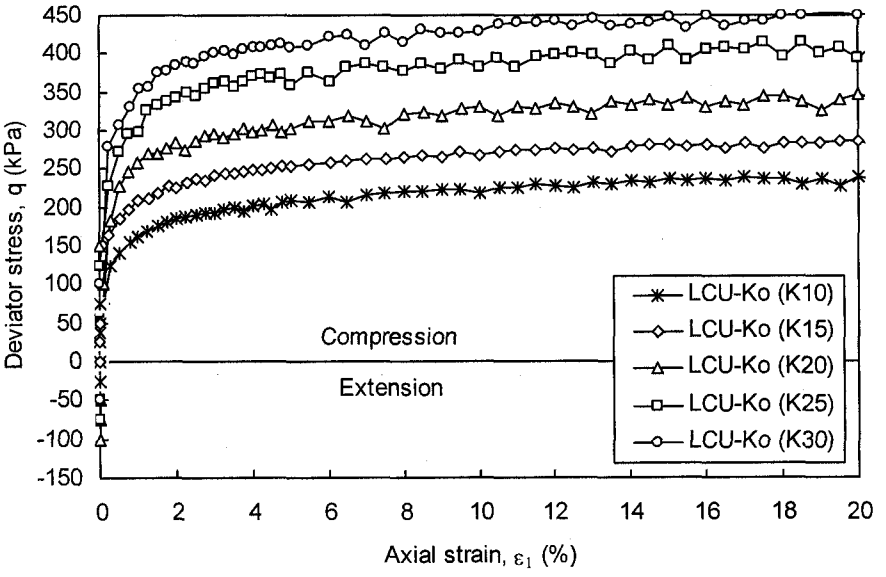

(c)

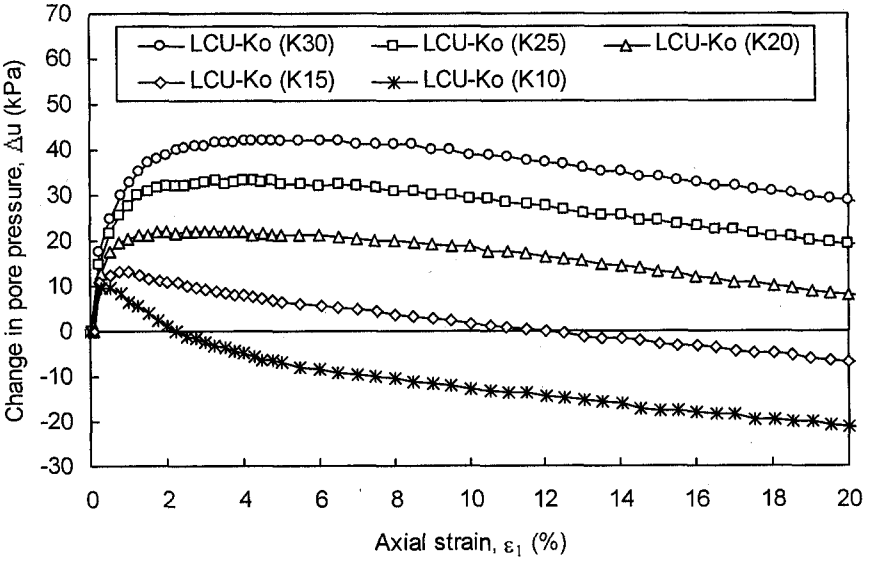

(d)

Figure 2.10. (a) Stress-strain relationship; and (b) Pore water pressure variation obtained from *LCU-K_o* test series

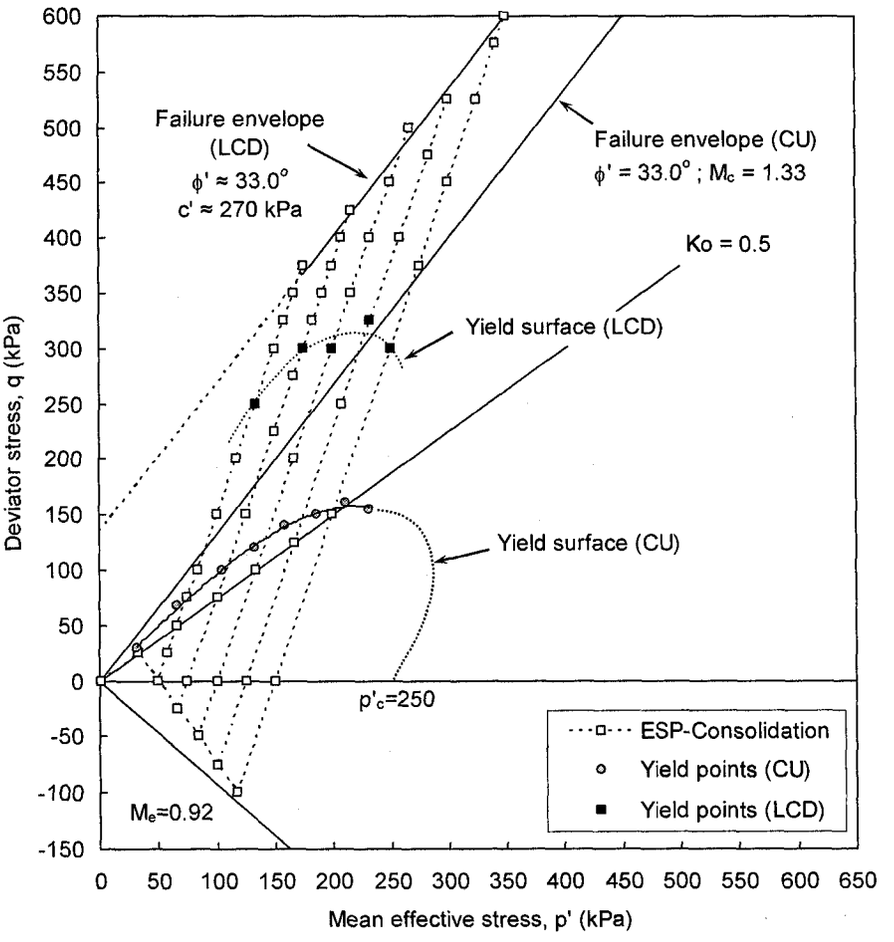

(a)

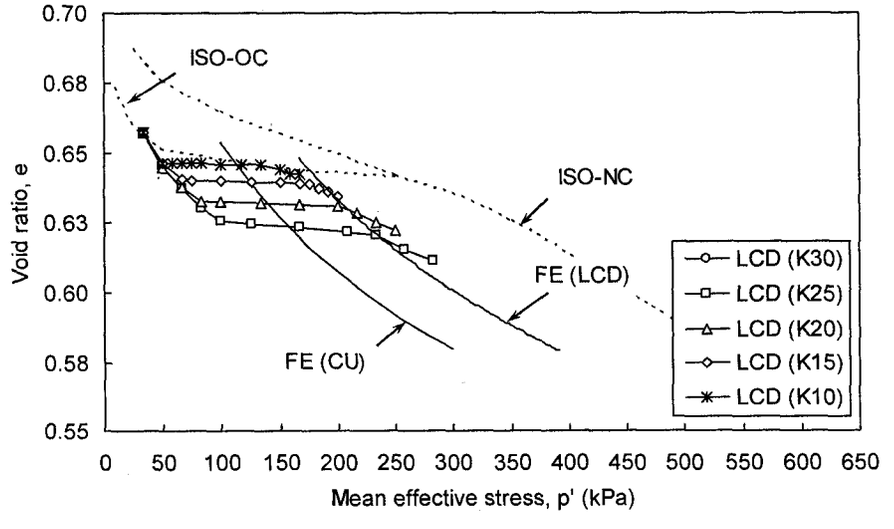

(b)

Figure 2.11. Failure envelope and yield locus in (a) *q-p'* plane; and (b) *e-p'* plane obtained from *LCD* test series

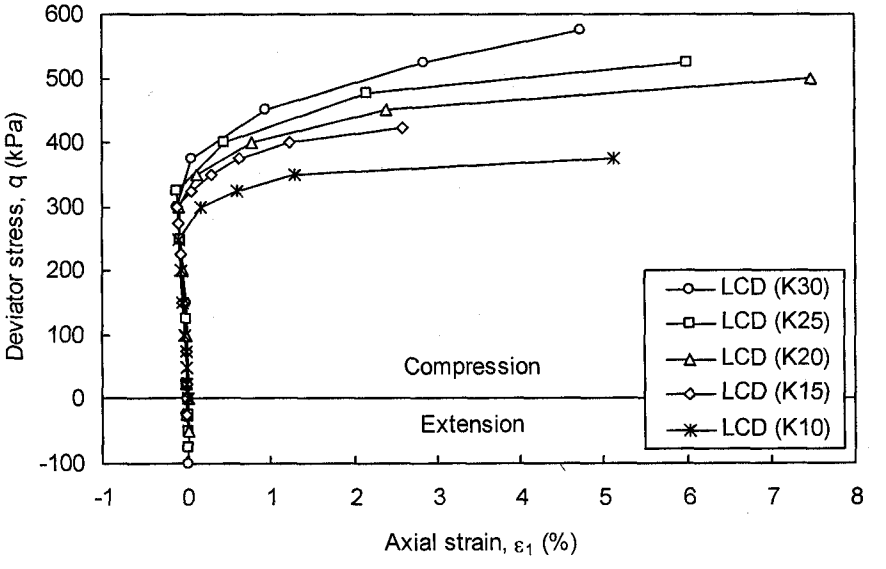

(c)

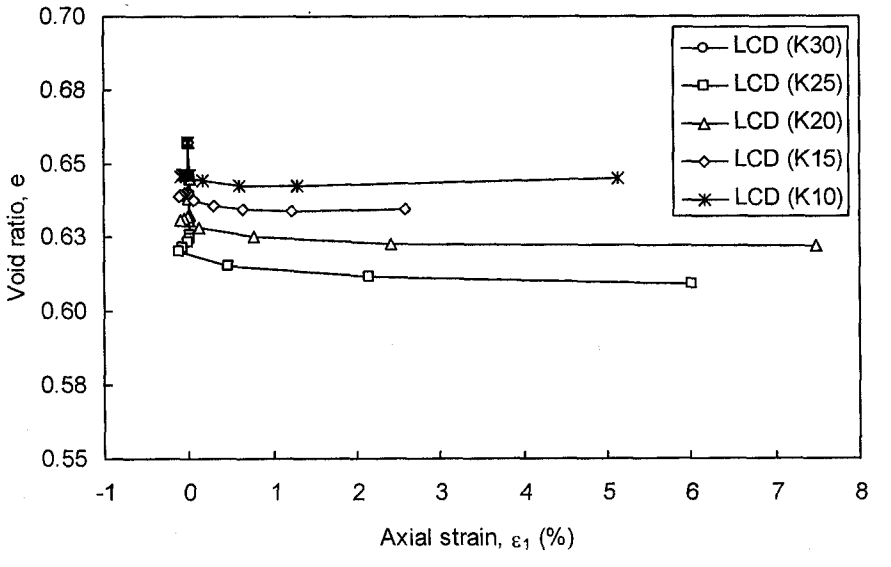

(d)

Figure 2.12. (a) Stress-strain relationship; and (b) Pore water pressure variation obtained from *LCD* test series

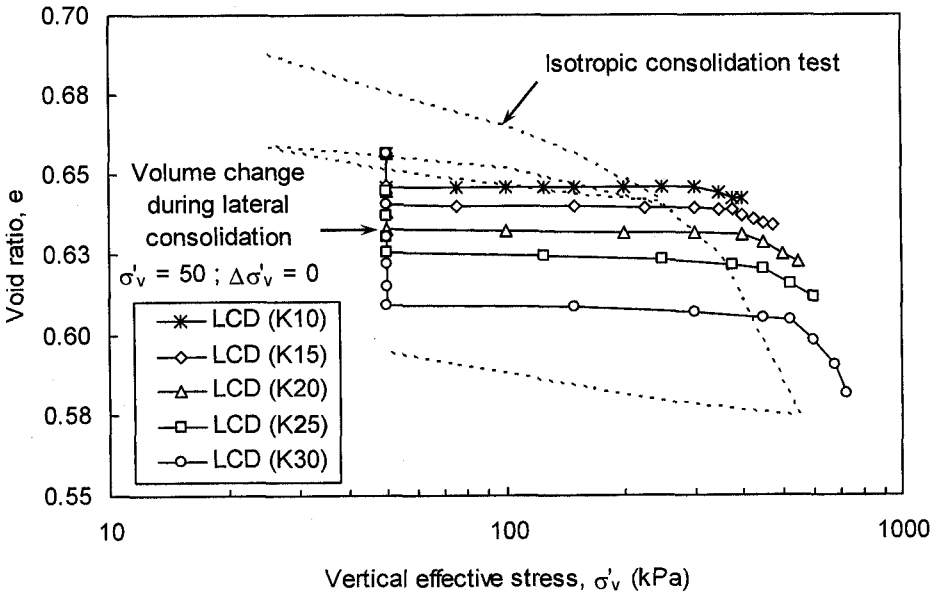

Figure 2.13. Volume change during *LCD* series — e-log(p'_v)

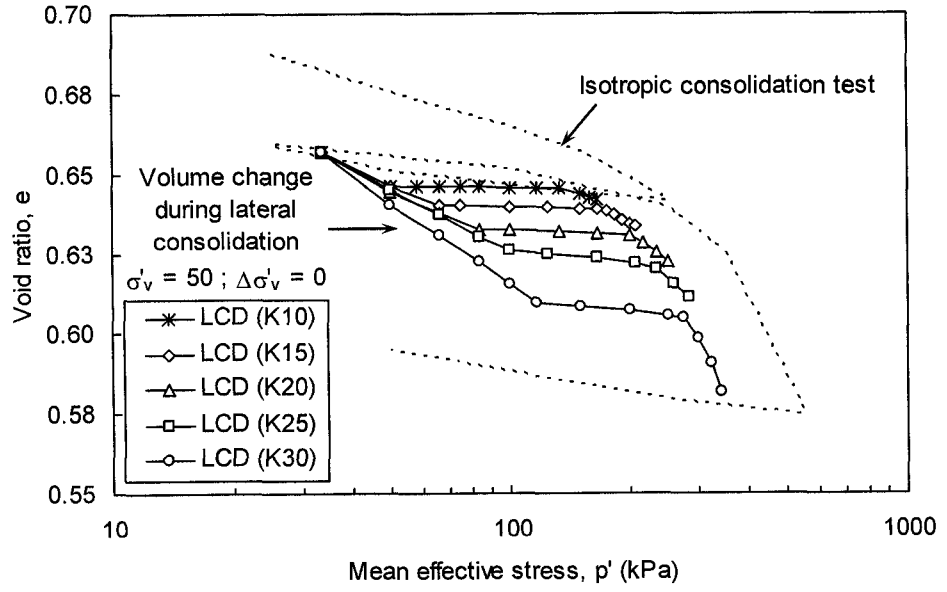

Figure 2.14. Volume change during *LCD* series — e-log(p')

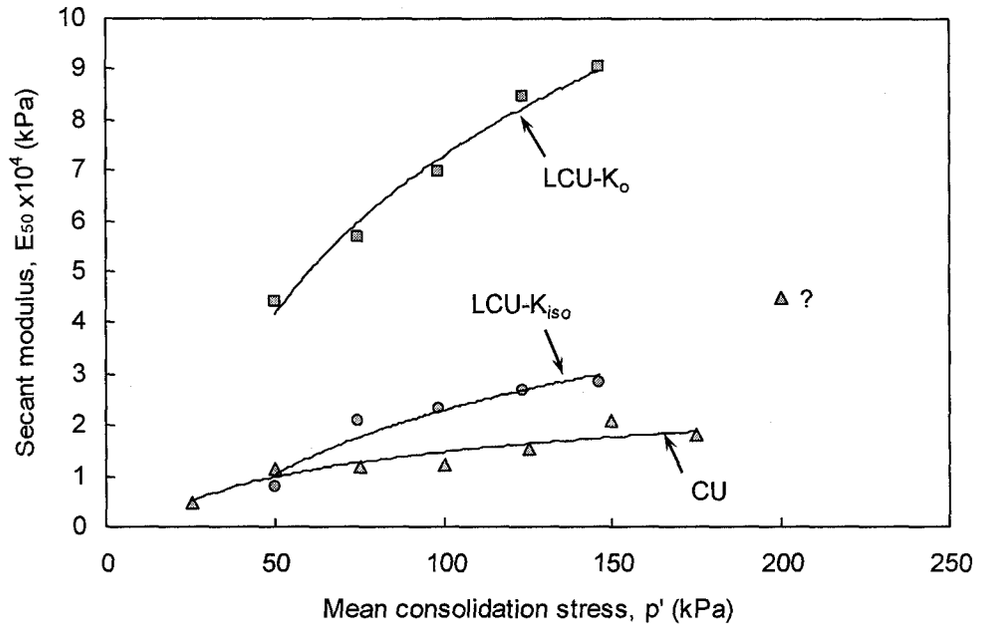

Figure 2.15. Undrained secant modulus of the soil in *LCU-K_{iso}* and *LCU-K_o* series

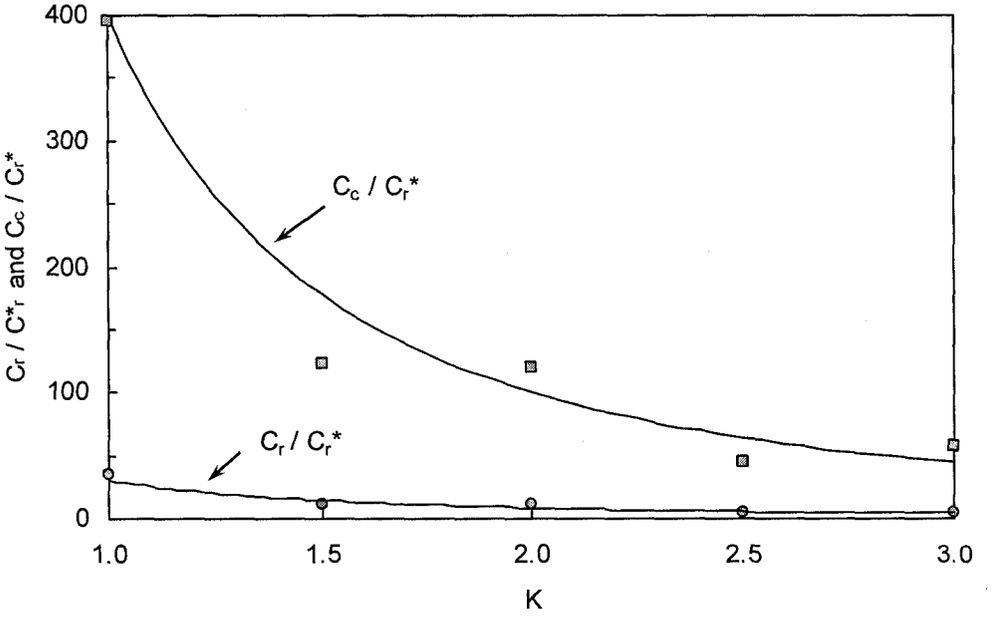

Figure 2.16. Vertical stiffness of soil as function of K obtained from *LCD* test series where C^*_r indicates recompression index determined from isotropic triaxial consolidation test.

CHAPTER 3: BEHAVIOR OF ISOLATED RAMMED AGGREGATE PIERS FROM A FINITE ELEMENT ANALYSIS

A paper submitted to the International Journal of Geomechanics

Ha T.V. Pham[1], David J. White[2], and Kord J. Wissmann[3]

ABSTRACT

This paper provides new insights into the complex composite interactions between isolated rammed aggregate piers and the surrounding matrix soil when the piers are subject to vertical loads. Isolated rammed aggregate piers were studied using an axisymmetric, elasto-plastic, finite element model calibrated with field measurements. To better understand the influence of stress development in the matrix soil from pier construction, which forces aggregate downward and outward into the borehole wall, the finite element model simulated the expansion of a pre-bored cavity in the radial direction and downward at the base of the cavity. Constitutive modeling parameters were determined from in-situ and laboratory measurements. Validation of the finite element model was performed by comparing the numerical predictions with the results of full-scale, instrumented load tests. Numerical results show that pre-stressing the matrix soil during pier construction is a key factor in controlling the pier load-settlement behavior, and that bulging deformation near the top of the

[1] Graduate Research Assistant, Department of Civil, Construction and Environmental Engineering, Iowa State University of Science and Technology, Ames, IA 50011-3232, USA. htvpham@iastate.edu
[2] Assistant Professor, Department of Civil, Construction and Environmental Engineering, Iowa State University of Science and Technology, Ames, IA 50011-3232, USA. djwhite@iastate.edu
[3] President and Chief Engineer, Geopier Foundation Company, Inc., 1997 South Main Street, Suite 703, Blacksburg, VA 24060, kwissmann@geopiers.com

pier mobilizes shear stresses at the pier-soil contact resulting in rapid load dissipation with depth along the pier.

INTRODUCTION

Rammed aggregate piers are constructed by compacting base-course aggregate in a pre-bored cavity using a beveled tamper connected to a high energy hydraulic rammer. Recently, rammed aggregate piers have been used widely in the United States to support shallow foundations on soft soils for commercial building support, large fuel storage tanks, and a wide range of projects for transportation infrastructure such as box culverts, embankments, and mechanically stabilized earth walls (Lawton and Fox 1994, Wissmann *et al.* 2002, White *et al.* 2003). Current engineering practice for settlement prediction of structures supported by rammed aggregate piers considers two distinctive zones in the soil — the upper zone, which is partly altered by the intrusion of the piers and the lower zone, which contains the unaltered soil below the pier (Wissmann *et al.* 2000). Calculating the settlement of these two zones requires a knowledge of the composite pier-soil stiffness of the upper zone, the vertical stress distribution, and the modulus of the lower zone. These variables depend on a number of factors including the stiffness of the pier material and the matrix soil, the pier mechanical deformation behavior (i.e. bulging or punching), the induced stress regime due to pier installation, and the load transfer mechanism along the pier.

Behaviors of granular piles have been previously studied using both analytical and numerical approaches (Hughes and Withers 1974, Hughes et al. 1975, Balaam and Poulos 1978, Mitchell and Huber 1985, Lee and Pande 1998, Kirsch and Sondermann 2001). While most consideration has been given to the bearing capacity and the load-displacement

characteristics of granular piles (Barskdale and Bachus 1983), limited knowledge regarding the interactions between granular pile and the matrix soil has been gained. Although insights into the pile-soil interaction in terms of the development of interfacial stresses have been described previously for driven concrete piles (Randolph *et al.* 1979, Cooke *et al.* 1979, Potts and Martins 1982, Jardine and Potts 1988, Reul 2004), these analyses are only adequate for relatively stiff piles in which bulging deformation is negligible.

Numerical analyses using the finite element (FE) method presented in this paper aims to provide new insights into the complex interaction between isolated rammed aggregate piers of two different lengths and the matrix soil in which the stress-dependent properties of the compacted aggregate (i.e., stiffness and dilatancy) are considered. The induced stress regime around the pier element results from the pier installation process unique to this construction technique and was simulated by monotonically expanding a pre-bored cavity radially into the matrix soil and downward at the base. The cavity expansion FE modeling was facilitated using displacement-controlled boundary conditions determined from field measurements. This modeling approach corresponds to the strain path method introduced by Baligh (1985). The FE models were calibrated by comparing the modeling predictions with full-scale, instrumented load test results. The pier-soil interaction was investigated by studying the development of the interfacial stresses in the matrix soil due to pier installation and loading, the deformation characteristic of the pier, and the load transfer mechanism within the pier and along the pier-soil contact.

PIER INSTRUMENTATION AND TESTING

Figure 3.1a shows the equipment for installing rammed aggregate piers. The installation process involves ramming successive thin layers of base-course aggregate in a drilled cavity using a beveled tamper (Lawton and Fox 1994). The first layer is typically 0.3 to 0.6 m thick consisting of open-graded aggregate. Well-graded, base-course aggregate is typically used in subsequent layers of nominal 0.3 m thickness. Typical diameters of the drilled cavity are 0.61, 0.76, and 0.92 m, with the 0.76 m diameter most prevalent. As a result of the high compaction energy and the shape of the beveled tamper head, each layer of aggregate is forced radially into the surrounding soil creating an undulatory pier shaft (Fig. 3.1b)

The performance of three isolated rammed aggregate piers installed at a test site in Neola, Iowa (USA) was used to validate the FE models developed in this study. These test piers with drilling diameter of 0.76 m were installed with the construction procedure described above. All piers were capped with a 0.45-m thick, cast-in-place concrete cap. Test pier P_1 was installed to a depth of 3.0 m from the ground surface. This pier was instrumented with four 23 cm diameter total stress cells located at 0.66, 1.32, 1.50 and 2.26 m measured from the ground surface. Because the stress cell installed at 1.32 m was damaged during pier installation, measurements for this cell are not presented herein. Figure 3.2 shows the setup of the stress cells along P_1. A tell-tale reference plate was also installed near the bottom of P_1 (tell-tale depth = 2.7 m). The tell-tale plate consisted of a rectangular steel plate attached to two opposing threaded steel bars that were extended to the top of the pier in protective PVC sleeves. Test piers P_2 and P_3 were installed to depths of 2.74 m and 5.05 m, respectively. Both piers were equipped with tell-tale reference plates (tell-tale depth = 2.44 m and 4.75 m,

respectively) but had no total stress cells. Load tests performed on all test piers were carried out in accordance with ASTM-D1143 (1994). The loads were applied in a "drained" fashion such that the rate of the pier vertical movement under a given load increment must approach an asymptote maximum before the subsequent load increment was applied.

CONSTITUTIVE MODEL FOR SOILS AND AGGREGATE

A cap model known as the hardening-soil model (Schanz *et al.* 1999) was used to characterize the behavior of the soils and the aggregate in this study. The hardening-soil model is essentially an elasto-plastic model developed based on isotropic plastic theory combined with hardening rules (Potts and Zdravkovic 1999). The failure state of the material is defined in accordance with the Mohr-Coulomb failure criterion. The shape and location of the deviatoric shear yield surface depends upon the stress state (p', q) and plastic shear strains whereas the size of the compression cap is mainly controlled by the isotropic preconsolidation pressure, p'_c, and the at-rest coefficient of lateral earth pressure, K_o. The material behaves elastically when the stress state is within the yield surface and elasto-plastically when the stress state is on the yield surface. The nonassociated flow rule (Rowe 1962) is applied for the deviatoric shear yielding whereas the associated flow rule is used to describe yielding on the compression cap.

Constitutive parameters of the hardening-soil model can be readily determined from consolidated-drained (CD) triaxial and oedometer tests. Fundamental model parameters include the confining stress-dependent secant modulus for the primary deviatoric loading (E_{50}), the confining stress-dependent modulus for the primary isotropic compression (E_{oed}), the confining stress-dependent elastic unloading/reloading parameters (E_{ur}, ν_{ur}), and the

effective shear strength parameters (c', ϕ', ψ). The amount of stress dependency for all moduli is given by the power m. Details on how to determine the constitutive model parameters from CD and oedometer tests are described in Schanz *et al.* (1999).

MODEL DESCRIPTIONS AND PROCEDURE

An axisymmetric model was developed in this study using the computer program Plaxis (version 8.2). The model consisted of a single pier installed in a two-layer matrix soil profile. The initial diameter of the cavity was 0.76 m with varying depth of 2.74, 3.0, and 5.05 m. The concrete in the pier cap was modeled as a linear elastic, non-porous material. Interface elements with strength reduction ratio of 1.0 (i.e., perfectly rough condition) were introduced along the cap-soil contact. Thin solid continuum elements were used along the pier-soil contact in lieu of interface elements. An unstructured FE mesh was generated within the physical domain of the model which contains first-order, 15-node triangular elements.

The matrix soil profile consisted of a one m thick desiccated crust layer overlying 13 m of soft alluvial clay. The physical boundary of the model was extended to 10 m measured radially from the center of the pier. Full fixity was applied along the bottom and the right-side boundaries of the model whereas vertical rollers were introduced along the symmetrical axis. The initial stress condition was generated using the K_o approach where element shear stresses are assumed to be zero. For the lower alluvial clay layer, $K_o = 1\text{-}\sin\phi'$ (Jaky 1944) was assumed whereas $K_o = 1.0$ was assigned to the upper desiccated crust layer.

The magnitude of downward displacement at the bottom of the pier cavity and diametric cavity expansion are functions the soil type, aggregate type and the applied

compaction effort. At the referenced test site, a prescribed downward displacement corresponding to about 8 cm was measured from the change in elevation of a reference mark on the beveled tamper before and after ramming, and the radius of the cavity increased about 4 cm measured near the top of the pier after ramming. To simulate the long-term stress condition after pier installation, cavity expansion was modeled as a "drained" process using effective stress parameter values. The step-by-step modeling procedure is described as follows:

1. Expand the cylindrical cavity by applying incremental outward displacement along the shaft (4 cm) and downward displacement at the bottom of the cavity (8 cm);
2. Back-fill the cavity with compacted aggregate and a concrete cap to create the pier; and
3. Apply incremental vertical stress on top of the pier until failure is observed.

DETERMINATION OF CONSTITUTIVE PARAMETERS

Soil properties used in this numerical analysis were derived from both in-situ and laboratory tests conducted on samples collected adjacent to the test piers. Cone penetration test (CPT) soundings were carried out to obtain subsurface information. According to the CPT data (Fig. 3.3), the site stratigraphy consists of a one m thick layer of stiff desiccated clay overlying about 13 m of soft alluvial clay (CL), overlying stiff glacial till and then weathered shale bedrock. Correlations from the CPT measurements (see Kulhawy and Mayne 1990) indicate an average friction angle of about 22 degrees for the alluvial clay layer, which is of primary interest in this study. The undrained shear strength (s_u) of the alluvial

clay was estimated from CPT results to be about 17 kPa. The groundwater table was observed at approximately two m below the ground surface during pier installation and testing.

Laboratory tests conducted to determine soil parameter values for the analysis included consolidated-drained (CD) triaxial tests and oedometer tests. Undisturbed samples for CD triaxial tests were extracted at 4.2 m from the ground surface and were tested at confining pressures of 25.5, 41, and 60 kPa. Effective cohesion and friction angle values are 2 kPa and 24 degrees, respectively. The soil exhibits a contractive, strain-hardening behavior under the deviatoric loading condition (Figs. 3.4a and 3.4b). Figure 3.4a shows good agreement between the stress-strain relationships of the soil obtained from CD tests and the hardening-soil model formulations. Oedometer tests performed on two undisturbed samples collected at 3.74 m and 4.04 m measured from the ground surface indicate that the alluvial clay is normally consolidated with the average initial void ratio of 1.0 and a compression index, C_c, of 0.28. Because no laboratory samples from the desiccated layer were collected for analysis, the properties of this layer were estimated from CPT data. Table 3.1 summarizes the constitutive model parameters for the matrix soils.

Constitutive model parameter values for the compacted aggregate were derived from CD tests conducted under varying confining pressures. Aggregate samples of crushed limestone (classified as GP) obtained from the test site were compacted in a 102 mm diameter by 204 mm high steel split mold to produce specimens for the CD tests. Details of the sample preparation are given by White *et al.* (2002a). Figures 3.4c and 3.4d show the stress-strain-volume behavior of the compacted aggregate obtained from CD tests. The

aggregate exhibits a strain-softening behavior under deviatoric loading. An average dilatancy angle of 12 degrees was used for the analysis (Fig. 3.4d). It is shown that the hardening-soil model can only capture the elastic response and either the peak or the post-peak shear strengths of the aggregate. The lack of capability to describe the post-peak softening behavior of the hardening-soil model is not surprising since the yield surface of the hardening-soil model is always below the failure envelop. The FE analysis conducted in this study uses post-peak shear strength parameters to model the aggregate. A summary of the modeling parameters for the compacted aggregate is provided in Table 3.1.

MODEL VERIFICATION

For rammed aggregate piers installed in homogeneous soft soil, pier bulging and tip movement are two typical deformation mechanisms (Wissmann *et al.* 2001). The development of stresses at the bottom of the pier and tip movement usually occurs when the pier length is less than two to three times the diameter. When the pier length is greater than three times the diameter, bulging deformation often prevails (see White and Suleiman 2004). For rammed aggregate piers instrumented with a tell-tale reference plate, the deformation mode can be observed. Bulging deformation occurs when the load-displacement curve obtained at the tell-tale location is approximately linear. On the contrary, the development of tip stresses can be recognized when there exists an inflection point on the tell-tale load-displacement curve.

Figure 3.5 shows the load-displacement curves of three test piers obtained from both FE analyses and full-scale load tests. Based on the displacements recorded at the tell-tale reference plates, at high applied loads, P_1 and P_3 show bulging deformation whereas P_2

develops tip stresses (Fig. 3.5b). As can be seen in Fig. 3.5, the load-displacement curve of P_3 is well captured by the FE model. The design loads (i.e. point of increased curvature) of the three test piers calculated from the FE analyses range from 280 to 330 kN. This range of design load value agrees well with the data obtained from the load tests on P_1 and P_3. Based on the load test performed on P_2, the design load is about 200 kN, which is less than the calculated FEM value. Although the FE model overestimated the design load for P_2, the model is capable of capturing the deformation mode of this pier (i.e. movement of the pier tip). The top displacement of P_1, calculated by the FE model, is almost coincident with the load test data until the applied load approaches 350 kN. As the applied load exceeds 350 kN, the FE model predicts greater settlement than shown by the load test data. Moreover, relatively large displacements calculated at the tell-tale location of P_1 (Fig. 3.5b) suggest the development of tip stresses rather than bulging deformation shown by the data. One reason for this lack of agreement may be that the installation of four stress cells altered the behavior of this pier (White *et al.* 2003). The unexpected stiff response of P_1 at the end of the test also reinforces this assumption. Another explanation for differences between the measured and calculated values is that the FE analysis used post-peak shear strength parameter values for the aggregate instead of using peak shear strength parameters.

Figure 3.6 shows the variation of the axial stress along P_1 with applied load. The stresses calculated by the FE model are in good agreement with the measured stresses, particularly in light of difficulties that are inherent with total stress measurement (Dunniclif 1993). This agreement lends credibility to the further interpretation of the numerical results.

STRESSES IN THE MATRIX SOIL

Pier Installation

In axisymmetric analysis, there exist four non-zero stress components — radial stress (σ'_r), vertical stress (σ'_z), tangential stress (σ'_θ), and the shear stress in the z-r plane (τ_{rz}) (Fig. 3.7). Figure 3.7 shows the calculated variation in σ'_z, σ'_z, σ'_θ, and τ_{zr} with radial distance from the edge of pier P_3 at an arbitrary depth of 1.5 m after pier installation and before pier loading, where σ_i is the initial stress prior to cavity expansion. Adjacent to the pier, radial stress σ'_r is greater than σ'_{ri} by a factor of 4.5. The decay of σ'_r with radial distance is approximately logarithmic to a distance of about 20 times the initial pier radius. The calculated tangential stress, σ'_θ, adjacent to the pier is greater than $\sigma'_{\theta i}$ by a factor of 2. The calculated vertical stress, σ'_z, adjacent to the pier slightly increases to about 1.2 times the initial value. The calculated σ'_θ also decreases rapidly with radial distance whereas σ'_z shows an initial drop before returning to the pre-installation value at a distance of about 11 times the pier radius. The trends of σ'_r, σ'_z, and σ'_θ with radial distance are similar to those reported in Randolph *et al.* (1979) for driven concrete piles in normally consolidated clays.

Results from the numerical modeling also indicate the generation of shear stress, τ_{zr}, along the pier-soil contact after pier installation. The generation of τ_{zr} is a consequence of cavity expansion and downward displacement applied at the bottom of the cavity. Moreover, the interfacial shear stress, τ_{zr}, generated (i.e. the change in shear stress from the initial condition) from pier construction is found to be oriented downward along the pier shaft and decreases rapidly from 13 kPa at the pier edge to zero at a distance of about three times the pier radius.

Pier Loading

The variations of interfacial stress components adjacent to P_2 and P_3 during the pier loading are presented in Fig. 3.8 for the same soil element shown in Fig. 3.7. For pier settlement less than about 18 mm, σ'_z and τ_{zr} increase while σ'_r decreases. When pier settlement increase over 18 mm, σ'_r adjacent to P_3 increases which is indicative of bulging. As bulging occurs, the interfacial shear stress, τ_{zr}, increases. The calculated σ'_r adjacent to P_2 slightly increases with pier settlement greater than 18 mm, but to a lesser extent as compared to that encountered in P_3. The increase from negative to positive values in τ_{zr}, which occurs for both piers, indicates a reversal of the interfacial shear stresses during pier loading, which brings about a rotation in the principal stress orientation (Potts and Martin 1982, Lawton *et al.* 1994).

STRESS DISTRIBUTIONS FOR RAMMED AGGREGATE PIERS

The vertical load applied to the top of an isolated rammed aggregate pier is resisted by two components—shaft resistance along the pier-soil contact and tip resistance developed at the pier base. Initially, the applied vertical compressive load is carried mainly by shear resistance at the pier-soil interface. For short aggregate piers (less than 3 pier diameters), high applied loads can result in full mobilization of shear resistance at the pier-soil contact and cause build-up of tip stresses. This loading condition can lead to pier tip deformation in design calculations. For longer piers, the applied compressive load usually dissipates before reaching the pier tip due to shaft resistance and pier bulging. Bulging is expected to occur in the upper part of the pier and limits development of uniform mobilization of shaft resistance.

An objective of the finite element analysis was to investigate stress distributions for isolated short and long piers starting with the post-installation stress conditions.

Pier Vertical Stress Distribution

Figure 3.9 shows the distribution of vertical stress with depth through the pier shaft under a range of vertical loads. The results show that rammed aggregate piers rapidly transfer load to the matrix soil with a large portion of the load transfer occurring in the upper 1.5 m of the pier. In terms of vertical stress transfer, about 75 percent of the stress for P_2 and almost 100 percent for P_3 is dissipated before reaching the bottom of the pier for the range of applied loads.

Interfacial Shear Stress Distributions

Figure 3.10 shows the distribution of pier-soil interfacial shear stresses for P_2 and P_3 during pier loading. Both piers initially show highly mobilized shear stresses at the upper portion (depth = 0.5 m) of the piers for applied loads less than the design loads (P_2 = 200 kN and P_3 = 270 kN). As the applied compressive load increases, the distribution of interfacial shear stress is affected by bulging deformation, which promotes shaft resistance at the pier-soil contact at a depth of about 1.0 m. As applied compressive loads exceed 280 kN, increased mobilization of shaft resistance is achieved in P_2 which results in a more uniform distribution of the interfacial shear stress along the pier-soil contact (Fig. 3.10a). Conversely, P_3 shows increased bulging with increased compressive loads, which promotes the interfacial shear stress at the bulging depth rather than distributing the load down the pier. This behavior is in contrast to rigid concrete piles, where virtually no bulging occurs and the

distribution of the interfacial shear can be fairly uniform with depth (Poulos and Mattes 1969).

LOAD TRANSFER MECHANISM

Influence of Residual Installation Stress

As described previously, the unique pier construction process pre-mobilizes tip resistance and shaft friction (i.e. develops residual stresses). These residual stresses develop an upward resultant force acting on the pier prior to pier vertical loading. Fig. 3.11 shows calculated load-deflection responses (top and bottom of pier) for piers P_2 and P_3 under the full range of vertical load conditions. For both piers the construction process results in pre-mobilization of shear stress in the matrix soils and development of tip stresses (left portion of Fig. 3.11). As the applied vertical load is increased, the pre-mobilized shear stresses must be overcome to induce significant settlements. Initially, the vertical load is resisted by the shear stresses that develop along the pier-soil interface. As the applied compressive load increases, the shaft resistance becomes fully mobilized first near the top of the pier and then propagates down the shaft as the applied load increases. In this paper the resultant force shown in Fig. 3.11 is the sum of the load carried at the pier bottom plus the load carried by the pier shaft. The displacement at which the interface shear resistance is fully mobilized herein referred to as the pier critical displacement.

As shown in Fig. 3.11, the critical displacement of P_2 is about 18 mm (top of pier) which corresponds to an applied vertical load of 280 kN. From Fig. 3.5, it can be seen that this load falls in the range of the design load based on the load-displacement curve. As the displacement exceeds 14 mm, interfacial shear stress in P_2 plateaus giving rise to increased

tip stress and plunging deformation. The critical displacement for P_3 is much higher at about 110 mm (top of pier). This displacement corresponds to an applied load of about 580 kN, which is much higher than the design load (see Fig. 3.5). This behavior suggests that the pier is long enough that shear deformation (bulging) must take place within the pier, rather than in the soil at the tip of the pier.

Parametric Study

This section presents a parametric study carried out to further investigate the influence of residual stresses on the load-displacement characteristics of rammed aggregate piers. The investigation was accomplished by performing analyses in which the bottom bulb displacement was eliminated from the pier construction process (RAP-NB) and also in which both the bottom bulb displacement and radial cavity expansion displacements were eliminated (RAP-NS).

Figure 3.12 shows the load-displacement curves of P_2 and P_3 in the parametric study. Both P_2 and P_3 show poor agreement with full-scale test results when the induced radial stress regime is neglected (RAP-NS). The reason is partly that the radial stress induced from pier installation acts analogously to confining stress in a triaxial test — the higher the radial stress the higher the pier strength and stiffness. Furthermore, the pier installation process pre-mobilizes shear stresses in the matrix soil that resist applied compressive loads (Fig. 3.11). Also shown in Fig. 3.12 is the effect of neglecting the bottom bulb construction (RAP-NB) on the load-displacement behavior of rammed aggregate piers. The construction of the bottom bulb is simulated in this study by applying downward displacements at the bottom of the cavity during pier installation. The prescribed downward displacement at the base of the

cavity results in an upward reaction (pre-stressing) at the tip of the pier prior to pier loading, thus mobilizing the pier tip resistance prior to application of the compressive load. It is observed that the construction of the bottom bulb has a more pronounced influence on P_2 compared to P_3. This is because P_2, which is the shorter pier, relies more on the tip stress than P_3 to resist the applied compressive loads.

SUMMARY AND CONCLUSION

Axisymmetric finite element analyses were performed to investigate the response of rammed aggregate piers to axial loading. The pier installation process was modeled by expanding a cylindrical cavity radially into the matrix soil and downward at the base. Analysis parameter values were selected from the results of in-situ and laboratory tests performed to characterize the matrix soil and pier materials. The FE model was calibrated by comparing the numerical predictions with the results of full-scale, instrumented load tests performed on three isolated rammed aggregate piers. Major conclusions drawn from this study are summarized as follows:

1. The results of the analyses show that the model successfully captured the load-deflection behavior and stress transfer mechanics of both short and long piers when compared with field instrumentation data. Good correspondence between the field data and the results of the numerical simulations were achieved only when the pier hole was radially and axially expanded to simulate the stress field generated by the expansion of constructed piers. These results suggest that the expansion of the pier cavity is an important mechanism in the behavior of rammed aggregate piers.

2. The expansion of the pier cavity increases the radial stress in the matrix soils surrounding the pier and rotates the principal stresses by introducing interfacial shear stress that is oriented downward along the pier-soil contact. During pier loading, the interfacial shear stress reverses which causes a second rotation of the principal stress orientation.

3. The increase in radial stress due to pier installation provides a marked increase in confinement around the piers which significantly stiffens the pier during pier loading. Construction of the bottom bulb provides a more pronounced influence on the load-displacement behavior of the shorter pier (P_2) compared to the longer pier (P_3).

4. Most of the applied compressive load is dissipated within the range where bulging deformation occurs. The distribution of the interface shear stress along the piers is highly non-uniform and more complex compared to that reported on isolated concrete piles. The interfacial shear stress becomes relatively uniform in P_2 once the design load is exceeded. Continuing to increase the compressive load on P_3 tends to promote build-up of interfacial shear stresses at bulging depth rather than distributing to the lower part of the pier.

5. The installation of rammed aggregate piers pre-stresses the matrix soil and creates a pre-mobilized uplift resultant force acting on the pier prior to pier loading. During subsequent pier loading, the applied vertical compressive stress is initially resisted by the shaft resistance that develops along the pier-soil contact. As the compressive load increases, the shaft resistance becomes fully mobilized first at

the top of the pier and then propagates down the shaft of the pier. The displacement at which the shaft resistance is fully mobilized is referred to as the critical displacement. The compressive load corresponding to the critical displacement is about the same as the ultimate load estimated for P_2 but is significantly higher than the ultimate load estimated for P_3. This behavior suggests that failure must take place within P_3 rather than in the soil underneath the pier.

ACKNOWLEDGEMENT

This research was sponsored by the Iowa DOT under contract TR-443, Geopier Foundation Company, Inc. and Iowa State University of Science and Technology. The support of these agencies is greatly acknowledged. Ken Hoevelkamp, Aaron Gaul and Dr. Muhannad Suleiman assisted with conducting the load tests and Peterson Contractors, Inc. installed the test piers.

NOTATION

c'	=	effective stress cohesion
C_c	=	compression index
D	=	pier diameter
e_{min}	=	minimum void ratio
e_{max}	=	maximum void ratio
e_{ini}	=	initial void ratio
E_{ur}^{ref}	=	reference unloading/reloading modulus corresponding to p^{ref}

E_{50}^{ref} = reference secant modulus corresponding to p^{ref}

E_{oed}^{ref} = reference modulus corresponding to p^{ref}

ϕ' = effective stress friction angle

γ = wet density

K_o = *at-rest* coefficient of lateral earth pressure

m = power for stress-level dependency

ν_{ur} = unloading-reloading Poisson's ratio

p' = mean effective stress

p^{ref} = reference confining stress

q = deviator stress

R_f = failure ratio

s_u = undrained shear strength

$\sigma_1^{'}$ = major principal effective stress

$\sigma_3^{'}$ = minor principal effective stress

$\sigma_{\theta i}^{'}$ = initial tangential stress

$\sigma_{ri}^{'}$ = initial radial effective stress

$\sigma_{zi}^{'}$ = initial vertical effective stress

$\sigma_{\theta}^{'}$ = tangential effective stress

$\sigma_r^{'}$ = radial effective stress

$\sigma_z^{'}$ = vertical effective stress

$\sigma_{tension}$ = tension cut-off stress

τ_{rz} = shear stress in *z-r* plan

ψ = dilatancy angle

REFERENCES

1. ASTM-D1143 (1994). "Test method for bearing capacity of soil for static load and spread footings." *Annual book of ASTM standards*, ASTM International.
2. Balaam, N.P., and Poulos, H.G. (1978). "Methods of analysis of single stone columns." *Proceedings of the Symposium on Soil Reinforcing and Stabilizing Techniques*, Australia, 497-512.
3. Baligh, M.M. (1985). "Strain path method." *Journal of Geotechnical Engineering*, ASCE, 11(9), 1108-1136.
4. Barksdale, R.D., and Bachus, R.C. (1983). *Design and construction of stone columns.* Report No. FHWA/RD-83/026, National Technical Information Service, Springfield, VA.
5. Cooke, R.W., Price, G., and Tarr, K. (1979). "Jacked piles in London Clay: a study of load transfer and settlement under working conditions." *Geotechnique*, 29(2), 113-147.
6. Dunniclif, J. (1993). *Geotechnical instrumentation for monitoring field performance.* John Wiley and Sons, Inc.
7. Hughes, J.M.O., and Withers, N.J. (1974). "Reinforcing of soft cohesive soils with stone columns." *Ground Engineering*, 7(3), 42-49.

8. Hughes, J.M.O., Withers, N.J., and Greenwood, D.A. (1975). "A field trial of the reinforcing effect of a stone column in soil." *Geotechnique*, 25(1), 31-44.

9. Jaky, J. (1944). "The coefficient of earth pressure at rest." *Journal of the Hungarian Society of Engineers and Architects*, 7, 355-358.

10. Jardine, K.J., and Potts, D.M. (1988). "Hutton tension leg platform foundations: prediction of driven pile behaviour." *Geotechnique*, 38(2), 231-252.

11. Kirsch, F., and Sondermann, W. (2001). "Ground improvement and its numerical analysis." *Proceedings of the 15th International Conference on Soil Mechanics and Foundation Engineering*, ISSMGE, Istanbul, Turkey, 1775-1778.

12. Kulhawy, F.H., and Mayne, P.W. (1990). *Manual on estimating soil properties for foundation design.* EL-6800 Electric Power Research Institute, Paolo Alto, California.

13. Lawton, E.C., and Fox, N.S. (1994). "Settlement of structures supported on marginal or inadequate soils stiffened with short aggregate piers." *Proceedings of Vertical and Horizontal Deformations of Foundations and Embankments, Geotechnical Special Publication No. 40*, ASCE, College Station, TX, 2, 962-974.

14. Lee, J.S., and Pande, G.N. (1998). "Analysis of stone-column reinforced foundations." *International Journal for Numerical and Analytical Methods in Geomechanics*, 22, 1001-1020.

15. Mitchell, J.K., and Huber, T.R. (1985). "Performance of stone column foundation." *Journal of Geotechnical Engineering*, ASCE, 111(2), 205-223.

16. Potts, D.M., and Martins, J.P. (1982). "The shaft resistance of axially loaded piles in clay." *Geotechnique*, 32(4), 369-386.

17. Potts, D.M., and Zdravkovic, L. (1999). *Finite element analysis in geotechnical engineering: Volume I – Theory*. Telford Publishing, London.

18. Poulos, H.G., and Mattes, N.S. (1969). "The behaviour of axially-loaded end-bearing piles." *Geotechnique*, 19, 285-300.

19. Randolph, M.F., Carter, J.P., and Wroth, C.P. (1979). "Driven piles in clay – the effect of installation and subsequent consolidation." *Geotechnique*, 29(4), 361-393.

20. Reul, O. (2004). "Numerical study of the bearing behavior of piled rafts." *International Journal of Geomechanics*, ASCE, 4(2), 59-68.

21. Rowe, P.W. (1962). "The stress-dilatancy relation for static equilibrium of an assembly of particles in contact." *Proceedings of Royal Society of London, Series A: Mathematical and Physical Sciences*, 269(1339), 500-527.

22. Schanz, T., Vermeer, P.A., and Bonnier, P.G. (1999). "Formulation and verification of the hardening-soil model." *Proceedings of Beyond 2000 in Computational Geotechnics*, Balkema, Rotterdam, 281-290.

23. White, D.J., Gaul, A.J., and Hoevelkamp, K. (2003). *Highway applications for rammed aggregate pier in Iowa soils*. Final report, Iowa DOT TR-443.

24. White, D.J., Suleiman, M.T., Pham, H.T., and Bigelow, J. (2002). *Constitutive equations for aggregates used in Geopier® foundation construction.* Final Report, Iowa State University, Ames, IA, USA.

25. White, D.J. and Suleiman, M.T. (2004). "Design of short aggregate piers to support highway embankments." *Journal of the Transportation Research Board*, Transportation Research Record, Number 1868, 103-112.

26. Wissmann, K.J., Fox, N.S., and Martin, J.P. (2000). "Rammed aggregate piers defeat 75-foot long driven piles." *Proceedings of Performance Confirmation of Constructed Geotechnical Facilities, Geotechnical Special Publication No. 94*, ASCE, Amherst, MA, 198-210.

27. Wissmann, K.J., Moser, K., Pando, M. (2001). "Reducing settlement risks in residual piedmont soil using rammed aggregate pier elements." *Proceedings of Foundations and Ground Improvement, Geotechnical Special Publication No. 113*, Blacksburg, VA, 943-957.

28. Wissmann, K.J., FitzPatrick, B.T., White, D.J., and Lien, B.H. (2002). "Improving global stability and controlling settlement with Geopier soil reinforcing elements". *Proceedings of the 4th International Conference on Ground Improvement Techniques*, Kualar Lampur, Malaysia, 753-760.

Table 3.1. Constitutive model parameters for soils and aggregate

Parameter	Aggregate	Alluvial clay	Desiccated soil
Effective stress friction angle, ϕ' (degrees)	47	24	35
Effective stress cohesion, c' (kPa)	4	2	2
Dilatancy angle, ψ (degrees)	12	0	0
Average wet density, γ (kg/m^3)	2100	1924	1924
Deviatoric reference modulus, E_{50}^{ref} (kPa)	61000	3000	9000
Compression reference modulus, E_{oed}^{ref} (kPa)	61000[a]	1500	4500
Unloading/reloading modulus, E_{ur}^{ref} (kPa)	1220000[b]	9000[b]	27000[b]
Power for stress-level dependency, m	0.48	1	1
Unloading/reloading Poisson's ratio, ν_{ur}	0.2	0.2	0.2
Reference stress, p^{ref}, kPa	34.5	25.5	25.5
Failure ratio, R_f	0.88	0.96	0.96
K_o for normal consolidation, K_o^{NC}	0.27	0.59	0.43
Initial void ratio, e_{ini}	0.33	1	1
Minimum void ratio (contraction), e_{min}	0.329	-	-
Maximum void ratio (dilation), e_{max}	0.393	-	-
Tensile cut-off, $\sigma_{tension}$	0	0	0

[a] *Assume:* $E_{oed}^{ref} = E_{50}^{ref}$ [b] *Assume:* $E_{ur}^{ref} = 3x\,E_{50}^{ref}$

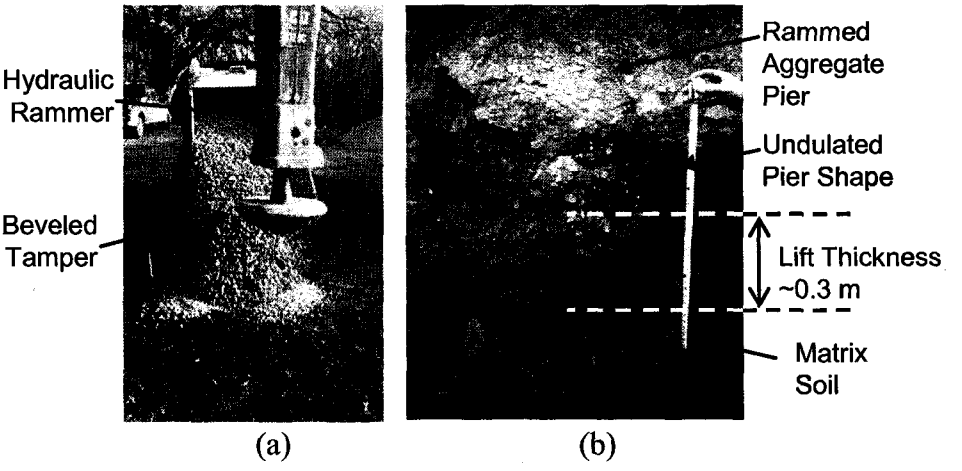

Figure 3.1. (Color) (a) Beveled tamper and hydraulic rammer used during pier construction and (b) partially excavated pier

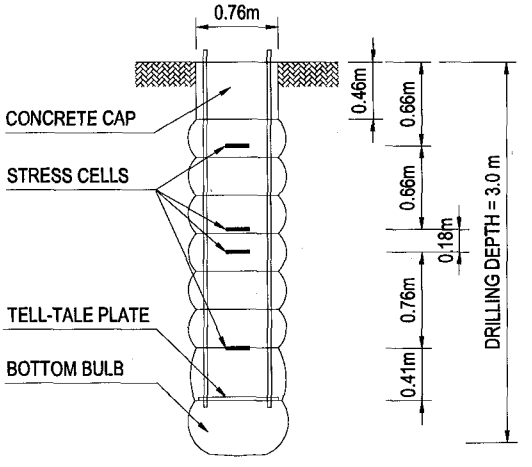

Figure 3.2. Instrumentation for test pier P_1 (L = 3.0 m)

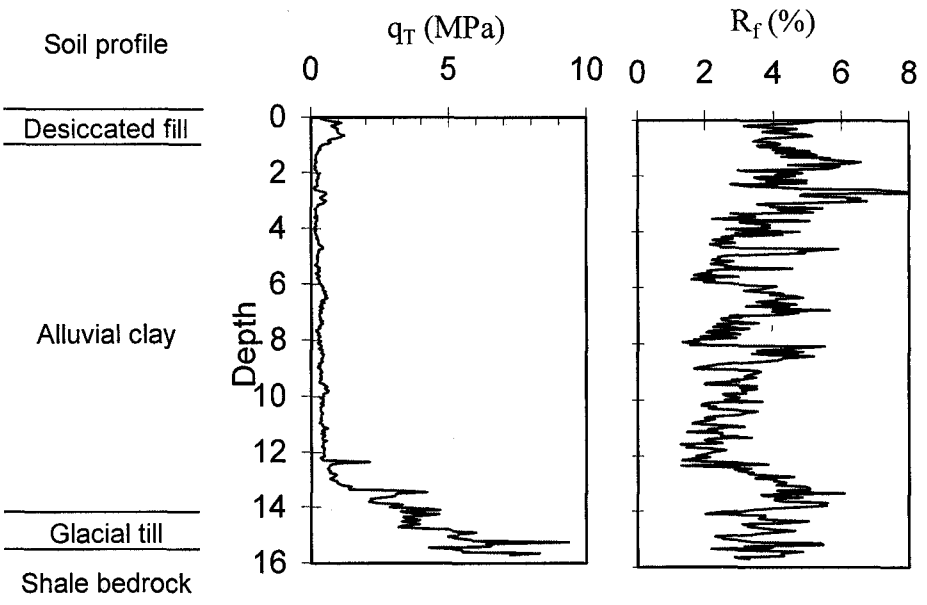

Figure 3.3. Soil profile and CPT results at the test site

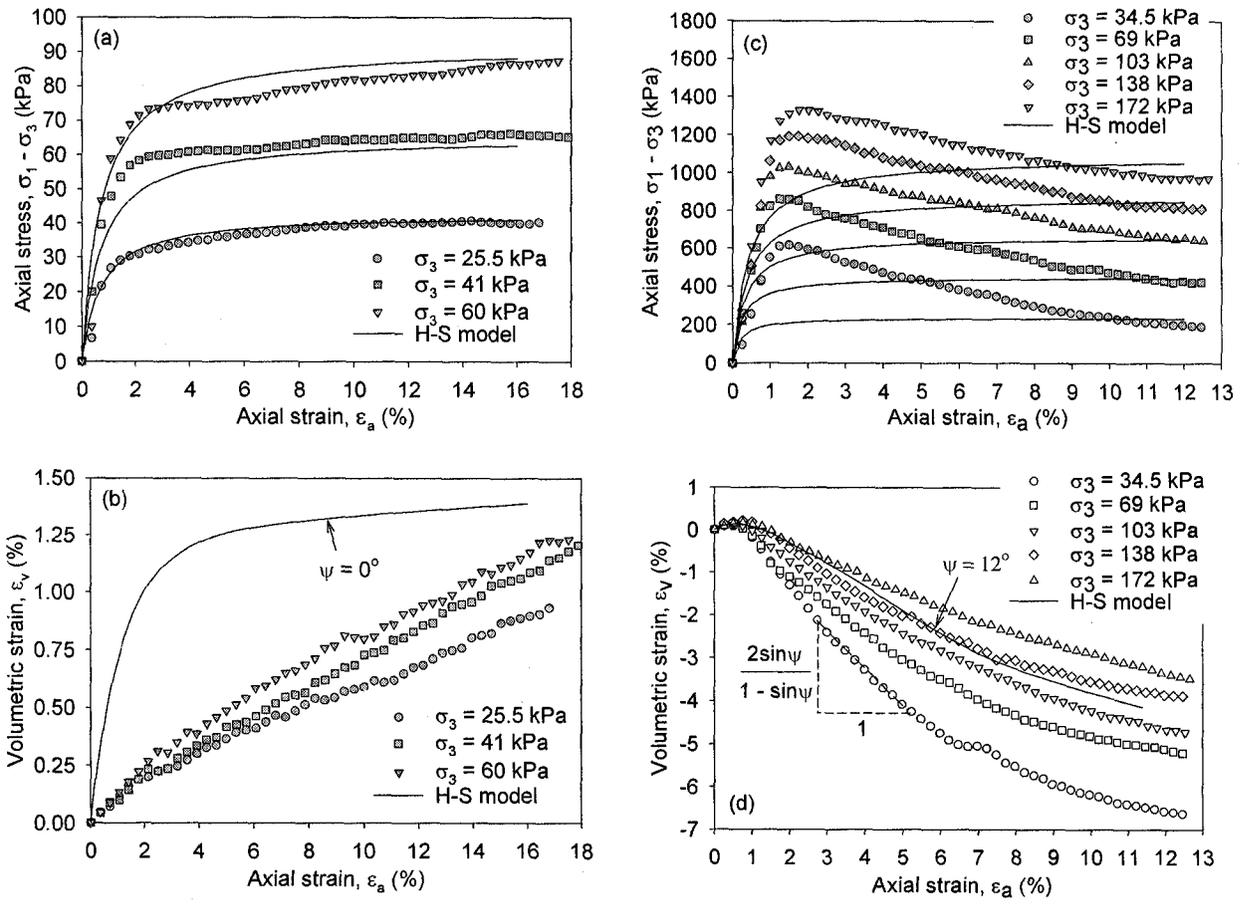

Figure 3.4. Characterization of the alluvial clay and the aggregate in CD triaxial tests

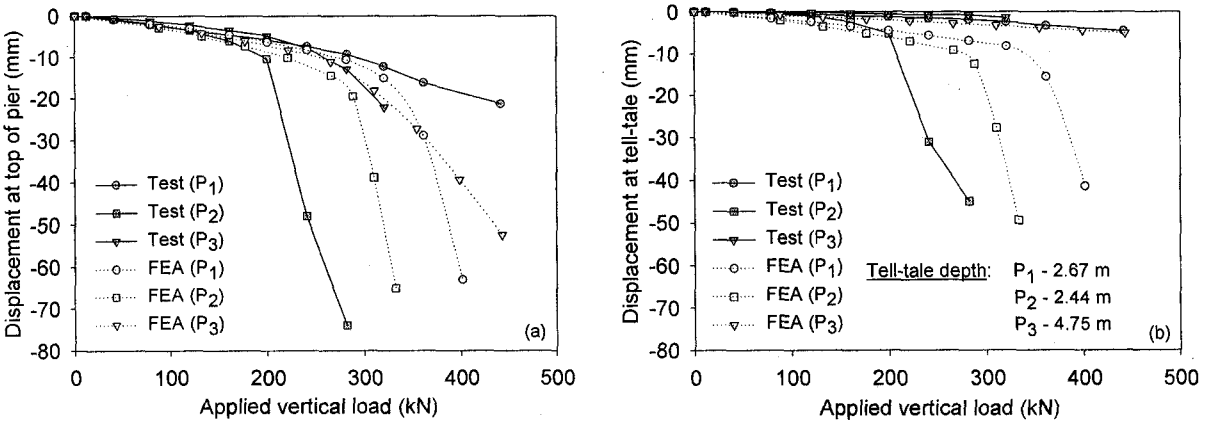

Figure 3.5. Load-displacement curves of three test piers: (a) at top of the pier and (b) at tell-tale elevation (P_1 = 3.0 m; P_2 = 2.74 m; P_3 = 5.05 m)

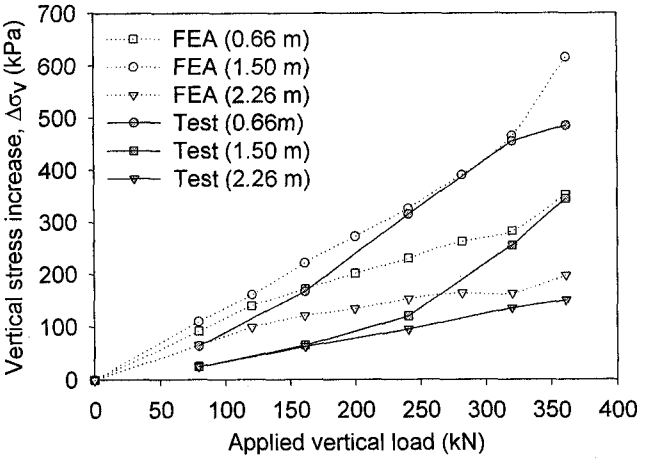

Figure 3.6. Vertical stress increase along P_1 (L = 3.0 m) as a function of applied load

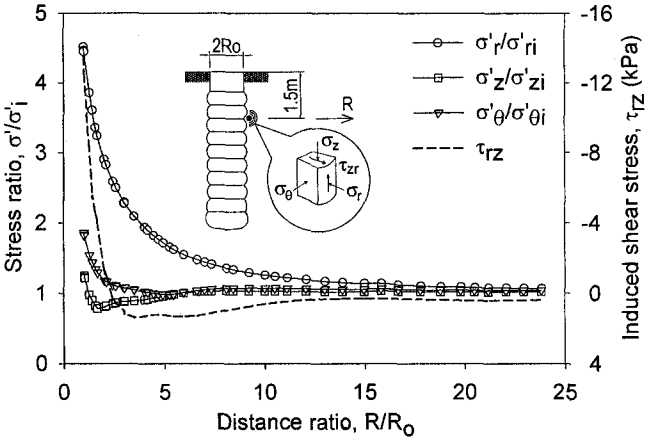

Figure 3.7. Calculated radial distribution of stresses after the installation of P_3 (L = 5.05 m)

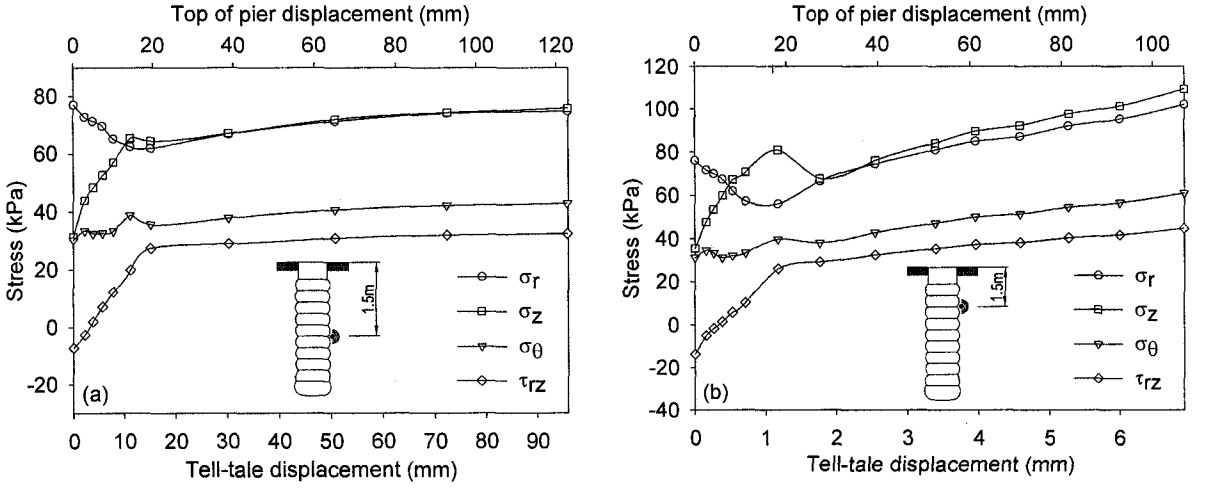

Figure 3.8. Calculated variation of interfacial stresses during pier loading: (a) P_2 (L = 2.74m) and (b) P_3 (L = 5.05 m)

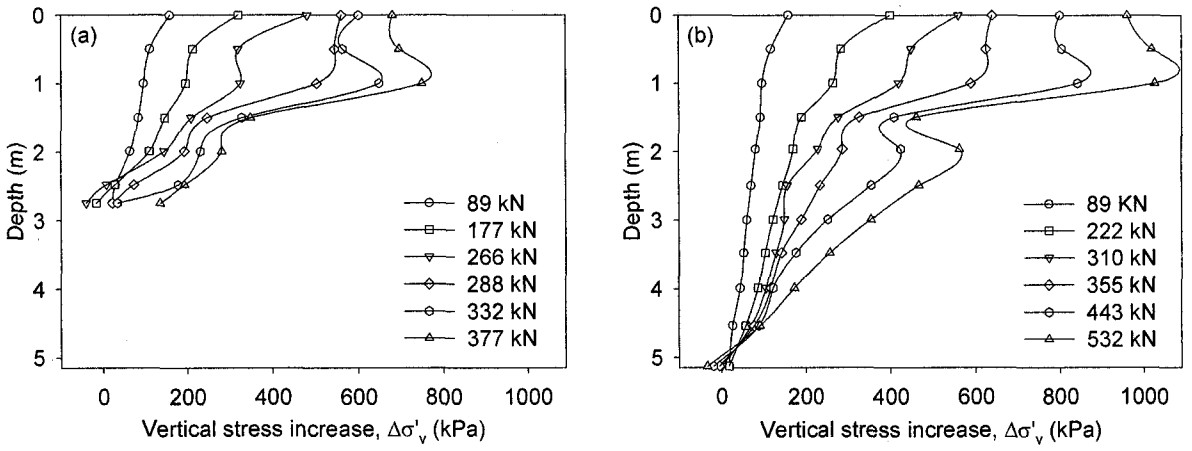

Figure 3.9. Calculated vertical stress increase: (a) along P_2 (L=2.74 m); and (b) along P_3 (L=5.05 m). Depth was measured from the bottom of the footing.

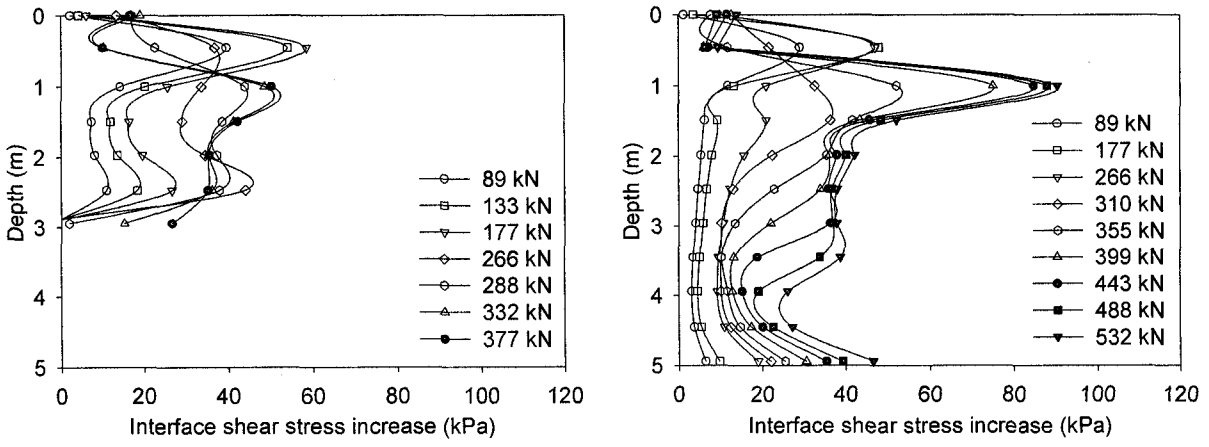

Figure 3.10. Calculated interfacial shear stress increase: (a) along P_2 (L = 2.74 m) and (b) along P_3 (L = 5.05 m). Depth was measured from the bottom of the footing.

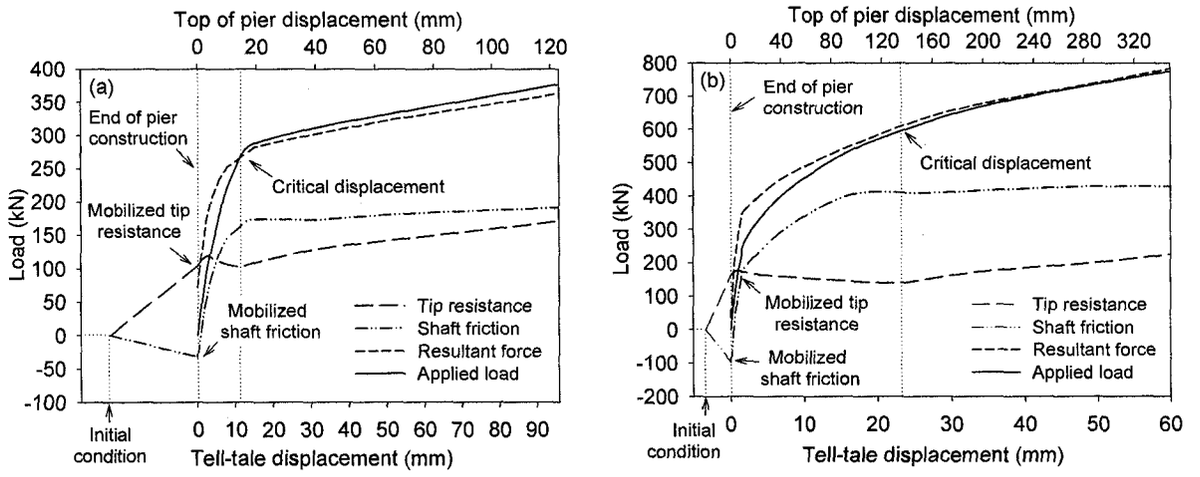

Figure 3.11. Calculated load transfer as a function of applied load: (a) P_2 (L = 2.74 m) and (b) P_3 (L = 5.05 m)

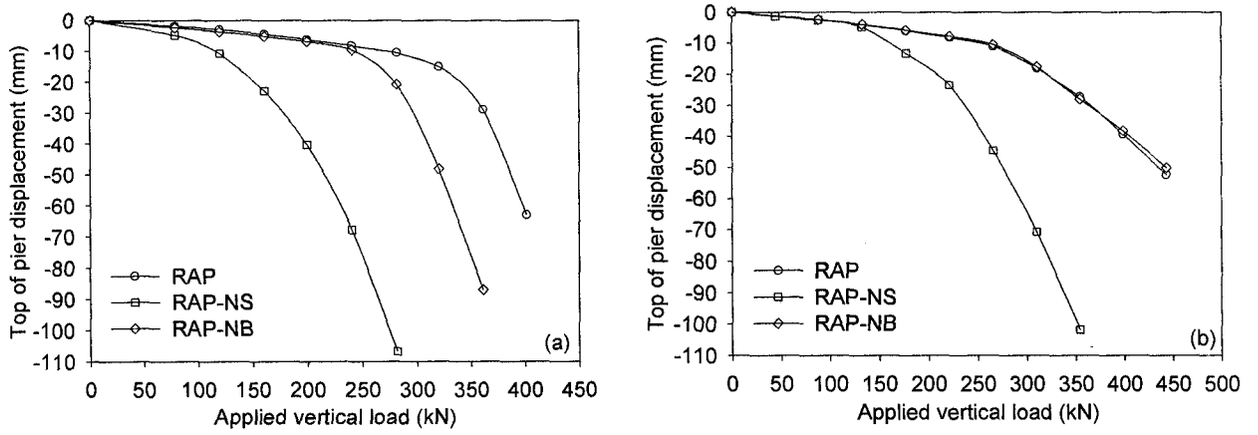

Figure 3.12. Calculated load-displacement curves: (a) P_2 – top of pier displacement; (b) P_2 – tell-tale displacement; (c) P_3 – top of pier displacement; and (d) P_3 – tell-tale displacement (P_2 – L = 2.74 m ; P_3 – L = 5.05 m)

CHAPTER 4: SUPPORT MECHANISM OF RAMMED AGGREGATE PIERS. I. FIELD PERFORMANCES

A paper to be submitted to the Journal of Geotechnical and Geoenvironmental Engineering

David J. White[1], Ha T.V. Pham[2], and Kenneth K. Hoevelkamp[3]

ABSTRACT

This paper is the first of a two-part series describing an investigation of the mechanical behavior of rammed aggregate piers in supporting rigid column footings. The first paper presents the results obtained from five full-scale, instrumented load tests performed on two rigid footings supported by rammed aggregate pier groups and three isolated rammed aggregate piers of the same diameter. The footings and rammed aggregate piers were constructed in a test site that consists of uniform soft clay overlain by a thin layer of desiccated fill. Comprehensive *in-situ* and laboratory tests were conducted prior to pier installation to characterize the geotechnical conditions of the test site. Interpretations of the test results focused on load-deformation behaviors of the isolated piers and pier groups, group efficiency, stress concentration of on pier top, and stress transfer mechanism along the shaft of the piers. Current design methods for calculating bearing capacity of rammed aggregate pier-supported footings were evaluated by comparing the calculated values with field measurements.

[1] Assistant Professor, Department of Civil, Construction and Environmental Engineering, Iowa State University of Science and Technology, Ames, IA 50011-3232, USA, djwhite@iastate.edu
[2] Graduate Research Assistant, Department of Civil, Construction and Environmental Engineering, Iowa State University of Science and Technology, Ames, IA 50011-3232, USA, htvpham@iastate.edu
[3] Associate Project Engineer, Geopier Foundation Company – West, 94 Montara Drive, Aliso Viejo, CA 92656, USA, kenh@geopier.com

INTRODUCTION

Over the last two decades, rammed aggregate piers have been effectively used as a cost-effective solution to mitigate intolerable settlement and improve the bearing capacity of soft soils underneath column footings (Lawton and Fox 1994, Lawton *et al.* 1994, Wissmann *et al.* 2001). Rammed aggregate piers are constructed by back-filling and compacting successive thin layers (~ 0.3 m) of base-course aggregate in pre-bored cavities using a specially designed, beveled tamper (Fox and Cowell 1998). During pier installation, the compaction effort for the first back-filling layer of aggregate (~ 0.3 to 0.6 m) is routinely increased to create a bottom bulb that provides a firm base on which the remainder of the pier is constructed. The densely compacted aggregate in the borehole significantly increases the composite modulus of subgrade reaction within the pier-reinforced zone (Lawton and Fox 1994, Lawton *et al.* 1994). Moreover, as a result of compaction, the aggregate in the cavity is expanded laterally along the shaft and downward at the bottom of the cavity thereby pre-stressing and pre-straining the matrix soil around the pier (Fox and Cowell 1998, Handy and White 2005a,b, Pham *et al.* 2005).

This paper is the first of a two-part series describing an investigation of the mechanism of rammed aggregate piers in supporting rigid column footings. Part I of this series presents the results of five full-scale, instrumented load tests conducted on two trial footings supported by rammed aggregate piers and three isolated piers of the same diameter. Part II of this series describes a numerical study in which the field performances of the pier-supported footings and isolated rammed aggregate piers presented in Part I are simulated by a finite element model.

CONSTRUCTION OF TRIAL FOOTINGS AND ISOLATED PIERS

Two square reinforced concrete footings (denoted as G_1 and G_2) were constructed at a test site in Neola, Iowa. Each footing was supported by a group of four 0.76 m diameter rammed aggregate piers installed in a square pattern with the center-to-center spacing of 1.07 m. The width of the footings was 2.29 m and the thickness was 0.46 m. The average installation depths for rammed aggregate piers in G_1 and G_2 were 2.79 m and 5.10 m, respectively. The area replacement ratio (R_a), which is defined as the ratio of the total area of the piers in the footing over the footing area, is about 0.35. The finished pier head elevation was 0.46 m below grade. After pier installation, the soil mass above the pier head elevation was carefully removed and the footings were built by casting the concrete directly over the steel reinforcements placed on top of the pier-soil area. Three isolated rammed aggregate piers (denoted as P_1, P_2, and P_3), were also installed at the same site with P_1 and P_2 having the same length and diameter as those of the piers in G_1 and G_2, respectively. The isolated pier P_3, which also had the same diameter as that of P_1 and P_2, was installed at 3.0 m from grade. The isolated piers were capped with 0.46 m thick concrete caps. The construction sequence for the trial pier-supported footings is illustrated in Fig. 4.1.

INSTRUMENTATION

The instrumentation used in this study included 230 mm diameter total stress cells, tell-tale reference plates, and inclinometer casings. Eight stress cells were installed in G_1 such that four cells were placed within two opposing piers at different depths, one cell was placed on top of a pier in the group, and three cells were placed on top of the matrix soil right beneath the footing. An inclinometer casing was installed adjacent to G_1 to the depth of 10 m

from grade to monitor the lateral displacement in the matrix soil during pier installation and pier loading. Tell-tale reference plates were installed near the bottom (i.e., on top of the bottom bulb) of two opposing piers in each pier group. The tell-tale reference plate, which is used to measure the deflection at the base of the pier, consists of a rectangular steel plate attached to two threaded steel bars that are extended to the top of the footing. The steel bars are protected by PVC sleeves to reduce contact friction. Figure 4.2a shows the schematic of the instrumentations attached to G_1.

Figure 4.2b shows the instrumentations used in P_3. Four stress cells were installed along the shaft of P_3 at various depths. Two inclinometer casings denoted as I_1 and I_2 were installed at 0.165 m and 0.38 m respectively from the edge of P_3 to the depth of about 9.5 m from grade. Tell-tale reference plates were installed in all isolated piers.

MATERIAL FOR RAMMED AGGREGATE PIER CONSTRUCTION

The rammed aggregate piers in this study were constructed using a base-course, crushed limestone classified as GP with about 3% of weight passing No. 200 sieve. Laboratory tests performed on the aggregate samples collected from the test site included sieve analysis, density, void ratio, and consolidated drained (CD) triaxial tests. The CD triaxial tests were conducted at five confining stresses (σ_3 = 35, 69, 103, 138, 172 kPa) on aggregate samples re-compacted in a 101.6 mm diameter by 203.2 mm high steel split mold. Details of the remolding process are presented in White *et al.* (2002). The compacted aggregate shows a strain-softening behavior with dilatation under deviatoric loading condition. Effective shear strength parameters (c', ϕ') of the compacted aggregate are 4 kPa and 47°, respectively. The average dilatancy angle (ψ) is approximately 12°. The elastic

modulus, E_s, for the compacted aggregate is about 85 MPa, which was estimated from CD test results based on the in-situ stress condition. Details of the constitutive behaviors of the compacted aggregate in CD tests are described in Pham *et al.* (2005). A summary of the engineering properties of the aggregate is presented in Table 4.1.

SITE INVESTIGATION

A comprehensive testing program including *in-situ* and laboratory tests was conducted to assess the geotechnical conditions of the test site. *In-situ* tests were carried out prior to the construction of the piers to obtain the geotechnical profile and provide additional information for bearing capacity and settlement computations. *In-situ* tests performed at the test site included the cone penetration test with pore water pressure measurement (CPT), the pressuremeter test (PMT), the flat dilatometer test (DMT), and the Iowa borehole shear test (BST).

A summary of the CPT is shown in Fig. 4.3. Test results indicate a 13 m thick layer of soft alluvial clay (CL) overlying glacial till and weathered shale bedrock. The alluvial clay appears to be fairly uniform and is overlain by a thin layer of desiccated fill (ML) with the average thickness of about 1.0 m. Correlations from the CPT results (see Kulhawy and Mayne 1990) indicate an average friction angle of about 22° for the alluvial clay layer and 35° for the desiccated fill. The average friction angle of the alluvial clay obtained from BST (Lutenegger *et al.* 1978) was about 23°, which agrees favorably with the value estimated from CPT data. The undrained shear strength (s_u), which was estimated from CPT data using the relationship proposed by Robertson and Campanella (1983), was about 30 kPa for the alluvial clay and 150 kPa for the desiccated fill. The ground water table was observed at

about 2 m below grade. The *in-situ* pore water pressure regime was found to be at static condition within the first ten meters of the profile. At greater depths, *in-situ* pore water pressures were slightly higher than the static values.

Figure 4.4 compares the elastic modulus and the undrained shear strength of the soils obtained CPT, DMT, and PMT results. The procedure developed by Briaud (1989) was used to reduce the data from PMT. For DMT data, the procedure proposed by Marchetti (1980) is adopted. As shown in Fig. 4.4, results obtained from PMT and DMT data were fairly consistent with those estimated from CPT data. The average modulus values of the alluvial clay and the desiccated fill were approximately 3.5 MPa and 8 MPa, respectively. Based on DMT data, the coefficient of lateral earth pressure (K_o) was about 0.59 for the alluvial clay and 1.0 for the desiccated fill.

Laboratory tests conducted in this study included unit weight, soil classification, water content, void ratio, one-dimensional consolidation, unconsolidated undrained (UU) triaxial compression, and consolidated drained (CD) triaxial compression tests. Undisturbed soil samples used for the one-dimensional consolidation, UU triaxial, and CD triaxial tests were collected from the alluvial clay layer at various depths using the standard 79 mm diameter Shelby tube. Figure 4.5 shows the distribution with depth of natural moisture content, Atterberg's limits, and void ratio measured from the Shelby tube samples. Average liquid limit and plasticity index values are 44% and 16%, respectively. *In-situ* moisture content, which slightly decreases with depth from 42% to 32%, results in an average liquidity index of about 0.8. Hydrometer analysis shows that the alluvial clay is composed of about 74% silt-size and 26% clay-size particles. The material is classified as CL according to USCS which is also consistent with the CPT results.

The CD triaxial compression tests were conducted at three confining stresses of 21, 41, and 62 kPa. The alluvial clay exhibited a strain-hardening behavior with the effective cohesion (c') and the friction angle (ϕ') of 2 kPa and 24°, respectively. The undrained shear strength (s_u) and the undrained modulus (E_u) of the alluvial clay, estimated from UU test results, were approximately 30 kPa and 2.5 MPa, respectively. Result from one-dimensional consolidation tests indicated that the alluvial clay was slightly overconsolidated with the compression index (C_c) of about 0.13. In overall, good agreements between *in-situ* and laboratory test results have been achieved. Engineering properties of the alluvial clay and the desiccated fill are summarized in Table 4.1.

LOAD TEST PERFORMANCE

The compressive load tests conducted on the trial footings were facilitated by the use of four 100-ton hydraulic jacks placed on the surface of the footing right above the center of the four supporting piers. The reaction system consists of two identical I-beam loading frames connected to sixteen helical anchors screwed to the weathered shale layer through four secondary beams (Fig. 4.1e and 4.1f). The loading frame was designed based on the capacity of the hydraulic jacks. Four circular steel plates with the diameter of 760 mm and the thickness of 2.5 mm were placed underneath each hydraulic jack to distribute the concentrated loads to a larger area. A similar setup was used for the load tests on isolated piers except that only one 100-ton hydraulic jack was used for each pier. All tests were conducted in a stress-controlled manner in which the displacement under a certain load level was allowed to approach the maximum asymptote before a higher load level was applied. The tests were terminated when the compressive load could not be maintained constantly.

During the load tests, displacements at the top of the footings and at the tell-tale plates were recorded. The final set of data used to produce load-displacement curves was computed as the average displacements recorded at the considered elevation. Readings from stress cells and the inclinometer casing were taken simultaneously with the performance of the load tests.

TEST RESULTS

Load-Settlement Behaviors

Different modes of deformation can be observed in granular piles subjected to compressive load depending on the soil condition and pile length (Barksdale and Bachus 1983). Typical modes of deformation for rammed aggregate piers installed in homogeneous soft soil include bulging and tip movement (Wissmann *et al.* 2001). In general, tip movement typically occurs when the pier length is less than about three times the diameter. For greater pier lengths, bulging is prevalent (Barksdale and Bachus 1983, White and Suleiman 2005). When a rammed aggregate pier is equipped with a tell-tale plate, the deformation mode of the pier can be recognized based on the shape of the tell-tale load-settlement curve. Bulging occurs when the tell-tale load-settlement curve is approximately linear. On the contrary, tip movement can be recognized when there exists an inflection point on the tell-tale load-settlement curve (Pham *et al.* 2005).

Figure 4.6 shows the load-settlement curves of the isolated piers and the pier groups obtained from the load tests. Based on the shape of the tell-tale load-settlement curves, it can be seen that P_1 and G_1 develop tip movement whereas P_2 and G_2 develop bulging deformation during the tests. The length/diameter ratio for P_1 and G_1 is 3.0 whereas this ratio for P_2 and

G_2 is about 6.0. The inflection point on the tell-tale load-settlement curve can be observed when the compressive loads are equal to 240 kN for P_1 and 1060 kN for G_1. Beyond these load levels, full mobilization of shaft friction may be achieved and any further increment in the applied compressive load will be fully transmitted to the tip of the pier. During the tests, P_2 exhibited a stiffer load-bearing response compared to P_1. However, the difference is not significant when the applied compressive load is within the working range (< 200 kN). For two pier groups, the load-settlement curves of G_1 and G_2 are coincident when the applied compressive load is less than 800 kN. As the compressive load exceeds 800 kN, G_2 shows a stiffer load-bearing response when compared to G_1.

Ultimate Bearing Capacity Estimated from Load-Settlement Curves

The ultimate bearing capacity of the isolated piers and pier groups in this study can be estimated based on the ultimate pier load determined from load-settlement curves (Bowles 1996, p. 996). In this study, the ultimate load on the load-settlement curve is taken as the load that corresponds to the top settlement of 25 mm (see Fig. 4.6). It should be noted that this settlement value is also considered to be the allowable settlement for the design of footings supported by rammed aggregate piers (Fox and Cowell 1998). Vesic (1975) recommended that the ultimate pier load be defined where the slope of the load-settlement curve reaches a minimum. Using the Vesic (1975) approach for the load-settlements curves shown in Fig. 4.6 results in ultimate pier loads that are close to those determined from 25-mm approach. Another graphical method used in this study to determine the ultimate pier load is the double tangent method (Lawton and Warner 2004). When using the double tangent method, the ultimate pier load is defined as the load at which the tangents of the upper and the lower parts of the load-settlement curve intersect. Values of the ultimate pier

load, the ultimate bearing capacity, and the corresponding top settlement are presented in Table 4.2. The ultimate bearing capacity is calculated as the ultimate pier load divided by the corresponding area. For an isolated pier, the corresponding area is the cross-sectional area of the pier whereas the corresponding area for a pier group is the area of the footing. It is indicated in Table 4.2 that the ultimate pier load determined by the 25-mm method is always higher than or at least equal to that estimated by the double tangent method. Moreover, the ultimate pier loads of P_2 and G_2 increases about 20% when compared to those of P_1 and G_1.

Group Efficiency

In practice, the design load is commonly taken at the end of the linear portion of the load-settlement curve. Following this procedure, the design loads of P_1 and P_2 are about 200 kN and 255 kN, respectively (see Fig. 4.6a). For the pier groups, the design loads are approximately 820 kN for G_1 and 1000 kN for G_2 (see Fig. 4.6b). Since there are four piers in each group, the group efficiency of both G_1 and G_2 is equal to 1.0 at the design load level. The group efficiency estimated from field measurements by Lawton and Warner (2004) on rammed aggregate piers with the length/diameter ratio of 4.0 is about 0.9. Barksdale and Bachus (1983) reported that the group efficiency of granular piles installed in cohesive soils ranged from 0.8 to 1.0.

The group efficiency in terms of settlement for both pier groups is presented in Fig. 4.7. The settlement of an isolated pier divided by the settlement of a pier group is plotted against the applied compressive load. For compressive loads lower than 150 kN per pier, the group efficiency in terms of settlement of both G_1 and G_2 is about 1.0. As the compressive load increases over 150 kN per pier, the group efficiency in terms of settlement increases

rapidly in G_1 to about 4.7 by the end of the test, however; practically maintains around 1.0 in G_2.

Stress Concentration Ratio

Fig. 4.8 shows the stress concentration ratio obtained from the stress cell data in G_1. The stress concentration ratio is calculated as the ratio of the contact stress on top of the pier divided by the contact stress on top of the matrix soil. The stress concentration ratio increases with increasing compressive load from about 3.8 at 424 kN to about 5.5 at 1000 kN. As the compressive load increases over 1100 kN, the stress concentration ratio slightly decreases. Similar trends were also reported by Lawton and Warner (2004) based on field measurements. Typical value of stress concentration ratio for granular piles ranges from 2 to 5 (Goughnour et al. 1979, Barksdale and Bachus 1983). Based on field measurements, Lawton and Warner (2004) reported that stress concentration ratio for rammed aggregate piers can be as high as 16. Since rammed aggregate piers are not intended to penetrate to a hard layer, the maximum value of stress concentration ratio may depend on the type of soil located at the pier tip.

Stiffness Modulus

Settlement of a rigid footing supported by a group of rammed aggregate piers can be estimated as the ratio of the stress concentrated on top of an individual pier in the pier group divided by the stiffness modulus of the pier (Lawton and Fox 1994, Wissmann *et al.* 2001). In design practice, the stiffness modulus of an individual pier in the pier group is routinely obtained from *on-site* modulus load test performed on an isolated pier of the same length and diameter.

According to Lawton and Fox (1994), the stress concentrated on top of an individual pier of a pier group (q_g) can be calculated based on the spring analogy as follows:

$$q_g = \frac{qR_s}{R_a(R_s - 1) + 1} \qquad [4.1]$$

where q is the footing stress, R_s is the stress concentration ratio, and R_a is the area replacement ratio. Using the information presented in Fig. 4.8, the stress concentration ratio of an individual pier in G_1 can be taken as 5. Since the stress concentration ratio in G_2 was not measured, two values of 5 and 10 are assumed. Figure 4.9 compares the stiffness modulus values of the isolated piers (P_1 and P_2) calculated from the load-settlement data with those of the individual piers in the pier groups (G_1 and G_2). The stiffness modulus of the individual piers in the pier groups is calculated using q_g values determined from Eq. 4.1. As shown in Fig. 4.9, the stiffness modulus decreases rapidly with settlement especially when the settlement is less than 10 mm. As the settlement exceeds 10 mm, the stiffness modulus gradually approaches a minimum asymptote. At settlements less than 25 mm, the stiffness modulus of the isolated piers is slightly higher than that of the individual piers in the pier groups. However, when the settlement is larger than 25 mm, the stiffness modulus values for all piers are practically the same. The stress concentration ratio is found to have a minor effect on the stiffness modulus values. Finally, it is indicated that using the stiffness modulus of an isolated pier to calculate settlement of a pier group results in a conservative value of settlement.

Lateral Displacement in the Matrix Soil

Lateral displacement profile in the matrix soil adjacent to rammed aggregate piers can be depicted from the deformed shape of the inclinometer casings installed adjacent to G_1 and

P_3. To set up a benchmark for the subsequent measurements, initial readings were taken from all inclinometers prior to pier installation. For the inclinometer adjacent to G_1, subsequent measurements were taken immediately after pier installation and also at three load levels of 424, 836, and 1248 kN during pier loading. For two inclinometers adjacent to P_3, subsequent readings were also taken after pier installation and at four loads of 110, 182, 257, and 363 kN.

Figure 4.10a shows the lateral movement in the matrix soil adjacent to G_1 and P_3 immediately after pier installation. The installation of P_3 creates a large movement (~ 8 mm) in the matrix soil where the bottom bulb is formed. The maximum value of lateral displacement obtained near the bottom bulb is equivalent to about 10% of the pier diameter. Large difference in the lateral displacements obtained from I_1 and I_2 indicates that the lateral movement in the matrix soil decreases fairly rapidly with radial distance. Moreover, it can be seen that the installation of G_1 displaces the matrix soil to a lesser extent when compared to P_3.

Lateral displacement profiles of all inclinometers during pier loading are shown in Fig. 4.10b to 4.10d. The lateral displacement values shown in Fig. 4.10b to 4.10d are incremental and are calculated as the difference between the absolute lateral displacement and the displacement measured after pier installation. Maximum lateral displacements of 0.5, 2.5 and 6.6 mm are observed from the inclinometer installed adjacent to G_1 at compressive loads of 424 kN, 836 kN and 1248 kN, respectively (Fig. 4.10b). The zone of lateral movement in the matrix soil near G_1 extends to about 6.0 m from grade which is approximately equal to about 2.5 times the shaft length of the piers. Larger displacements observed at the bottom of pier elevation confirm the fact that the piers in G_1 develop tip

movement under compressive loads. Increase in the lateral displacement encountered at the depth from 1.0 to 2.0 m from grade indicates that the piers in G_1 may also slightly bulge during the load test.

The lateral displacement profile of the matrix soil adjacent to P_3 (Fig. 4.10c and 4.10d) indicates that P_3 develops bulging deformation when subjected to compressive load. Maximum lateral displacement is recorded within the alluvial clay which implies that bulging occurs in this layer rather than in the desiccated fill. The bulging depth shown in Fig. 4.10c and 4.10d is about 1.6 m from grade. If the pier is simplified as a triaxial sample then the depth to bulging can be approximated as:

$$z_b = z_o + 0.5 d_{shaft} \tan(45 + \frac{\phi}{2}) \qquad [4.2]$$

where z_b is the bulging depth measured from grade, z_o is the depth at which bulging starts to occur, D is the diameter of the pier shaft, and ϕ' is the effective friction angle of the pier material. Using Eq. 4.2 and assuming that bulging takes place within the alluvial clay layer (z_o = 1 m) give a value of 1.96 m for bulging depth which agrees fairly well with the measured value.

Vertical Stress Distributions

The vertical stress distributions along the shaft of P_3 and G_1 are presented in Fig. 4.11. The vertical stress increase at a given load is calculated as the difference between the absolute vertical stress and the vertical stress at the post-construction stage. The distribution of vertical stress increase in P_3 and G_1 appear to be nonlinear and dissipate more rapidly with depth within the first meter of the pier shaft where bulging occurs (see Fig. 4.10). As shown in Fig. 4.11a, the vertical stress increase at the footing-bottom elevation (0.46 m) is higher

than that at top of the footing (grade elevation) due to the concentration of vertical stress on pier top. At 240 kN, the vertical stress increase in P_3 at the depth of 2.3 m (~ $3d_{shaft}$) is about 25% of the induced vertical stress at the footing-bottom elevation. For the pier group (G_1), this percentage is about 40% at the depth of 1.8 m (~$2.4d_{shaft}$). The average rate of vertical stress dissipation in P_3 is approximately 60 kPa/m, which is about two times as high as the dissipation rate estimated in G_1. Moreover, the dissipation rate of the vertical load increases with the increasing compressive load.

BEARING CAPACITY CALCULATIONS

The bearing capacity calculation procedure for footings supported by rammed aggregate piers was described by Lawton and Warner (2004). In general, the ultimate bearing capacity of the pier-supported footing is defined as the minimum pressure among those estimated from four possible modes of failure as follows:

i) bulging of an individual pier in the pier group;

ii) shearing below the tip of an individual pier in the pier group;

iii) shearing within the pier-reinforced zone; and

iv) shearing below the pier-reinforced zone.

The last two failure mechanisms shown above are only applicable for pier groups but not for isolated piers. Table 4.3 summarizes the calculated bearing capacity values for both isolated piers and pier groups in this study. The calculations are made based on the procedure described in Lawton and Warner (2004). Also shown in Table 4.3 is the bearing capacity values determined from load-settlement curves. The determined bearing capacity values are presented in Table 4.3 as a range of values corresponding to different graphical

methods used for estimation. Details of the bearing capacity calculations are presented in Pham (2005).

Numerical results shown in Table 4.3 indicate that the controlling failure mechanism for G_1 and P_1 is shearing below individual pier. This finding is consistent with the observed load-settlement behavior at the tell-tale plate (see Fig. 4.7). For a given failure mechanism, the bearing capacity values of the G_1 and P_1, calculated using fully drained parameters (c', ϕ'), are generally higher than the bearing capacity values calculated using undrained parameters (s_u). Compared to the bearing capacity values estimated from load-settlement curves, the calculated bearing capacity values are overestimated. As shown in Table 4.3, the controlling failure mechanism of G_2 and P_2 is bulging deformation. This finding is also consistent with the observation from load-settlement curves (Fig. 4.7). For both G_1 and G_2, the bearing capacity values calculated based on shearing within and below the pier-reinforced zone are always higher than those computed from bulging and shearing below pier tip. This finding suggests that the later two failure mechanisms shown in Table 4.3 seldom control the bearing capacity failure.

SUMMARY AND CONCLUSION

Full-scale, instrumented load tests were performed on two trial square footings supported by two groups of four rammed aggregate piers of different lengths. To highlight the group effects, three isolated piers of the same diameter and length with those in the groups were also constructed and tested at the same site. Interpretations of the test results focus on the load-deformation behaviors of the piers, load transfer along pier shaft, stress distribution in underneath the footing, and the group effects. Current design methods for

estimating ultimate bearing capacity of pier-supported footing were evaluated based on the test results. Major findings from this study include the following:

1. Under compressive loads, the shorter pier group (G_1) developed tip movement whereas the longer pier group (G_2) developed bulging deformation. The mode of deformation could be well recognized from the load-settlement curves obtained from tell-tale reference plates. The mode of pier deformation can also be identified by monitoring the lateral displacement in the adjacent soil using inclinometers. For G_1, the zone of lateral movement in the matrix soil below pier tip was extended to about 1.5 times the shaft length of the piers.
2. The group efficiency of both G_1 and G_2 was about 1.0 at the design load level. The stress concentration ratio was found to increase with the applied compressive load. Vertical compressive stress was found to dissipate more rapidly along the shaft of an isolated pier when compared to an individual pier of the pier group.
3. The predicted bearing capacity failure mechanism for P_1 and G_2 was shearing below the tip. For P_2 and G_2, the predicted failure mechanism was bulging deformation. These predicted failure mechanisms agreed favorably with the observed failure mechanisms from load-settlement curves. The bearing capacity values calculated using the current design method were higher than the values estimated from load-settlement curves. Shearing within and below the pier-reinforced zone were found to seldom control the bearing capacity failure.

ACKNOWLEDGEMENT

This research was sponsored by the Iowa DOT under contract TR-443, Geopier Foundation Company, Inc. and Iowa State University of Science and Technology. The support of these agencies is greatly acknowledged. Mr. Aaron Gaul and Dr. Muhannad Suleiman assisted with conducting the load tests and Peterson Contractors, Inc. installed the test piers.

REFERENCES

1. Barksdale, R.D., and Bachus, R.C. (1983). *Design and construction of stone columns.* Report No. FHWA/RD-83/026, National Technical Information Service, Springfield, VA.
2. Bowles, J.E. (1996). *Foundation analysis and design.* 5th Edition, McGraw-Hill Companies, Inc.
3. Briaud, J-L. (1989). The pressuremeter test for highway applications. Report No. FHWA-IP-89-008, Federal Highway Admistration, Washington D.C., USA.
4. Fox, N.S., and Cowell, M.J. (1998). *Geopier™ Foundation and Soil Reinforcement Manual.* Geopier Foundation Company, Inc., Blacksburg, VA, USA.
5. Goughnour, R.R., and Bayuk, A.A. (1979). "A field study of long-term settlements of loads supported by stone columns in soft ground." *International Conference on Soil Reinforcement: Reinforced Earth and Other Techniques*, Paris, 1, 279-286.
6. Handy, R.L., and White, D.J. (2005a). "Stress zones near displacement piers: I. Plastic and liquefied behavior." *Journal of Geotechnical and Geoenvironmental Engineering, ASCE (accepted for publication).*

7. Handy, R.L., and White, D.J. (2005b). "Stress zones near displacement piers: II. Radial cracking and wedging." *Journal of Geotechnical and Geoenvironmental Engineering*, ASCE (*accepted for publication*).

8. Jaky, J. (1944). "The coefficient of earth pressure at rest." *Journal of the Hungarian Society of Engineers and Architects*, 7, 355-358.

9. Kulhawy, F.H., and Mayne, P.W. (1990). *Manual on estimating soil properties for foundation design*. EL-6800 Electric Power Research Institute, Paolo Alto, CA, USA.

10. Lawton, E.C., and Fox, N.S. (1994). "Settlement of structures supported on marginal or inadequate soils stiffened with short aggregate piers." *Proceedings of Vertical and Horizontal Deformations of Foundations and Embankments, Geotechnical Special Publication No. 40*, ASCE, College Station, TX, 2, 962-974.

11. Lawton, E.C., and Warner, B.J. (2004). *Performance of a group of Geopier elements loaded in compression compared to single Geopier elements and unreinforced soil.* Final Report, Report No. UUCVEEN 04-12, University of Utah, Salt Lake City, UT, USA.

12. Lawton, E.C., Fox, N.S., and Handy, R.L. (1994). "Control of settlement and uplift of structures using short aggregate piers." *Proceedings of In-situ Deep Soil Improvement, Geotechnical Special Publication No. 45*, ASCE, Atlanta, GA, 121-132.

13. Lutenegger, A.J., Handy, R.L., and Remmes, B.D. (1978). "Bore hole shear test for stiff soil." *Journal of Geotechnical Engineering Division*, ASCE, 104(11), 1403-1407.

14. Marchetti, S. (1980). "In-situ tests by flat dilatometer." *Journal of Geotechnical Engineering Division*, ASCE, 106(GT3), 299-321.

15. Pham, H.T.V. (2005). *Support mechanism of rammed aggregate piers*. Ph.D. dissertation, Iowa State University, Ames, IA, USA.

16. Pham, H.T.V., White, D.J., and Wissmann, K.J. (2005). "Behavior of isolated rammed aggregate piers from a finite element analysis." *International Journal of Geomechanics*, ASCE (*under review*).

17. Robertson, P.K., and Campanella, R.G. (1986). *Guidelines for use, interpretation, and application of the CPT and CPTU*. 3rd Eds., Hogentogler and Co., Inc.

18. Vesic, A.S. (1975). "Bearing capacity of shallow foundation." *Section 3 in Foundation Engineering Handbook*, Edited by Winterkorn, H.F., and Fang, H-Y, 121-147.

19. White, D.J. and Suleiman, M.T. (2005). "Design of short aggregate piers to support highway embankments." *Journal of the Transportation Research Board*, Transportation Research Record, No. 1868, 103-112.

20. White, D.J., Gaul, A.J., and Hoevelkamp, K. (2003). *Highway applications for rammed aggregate pier in Iowa soils*. Final report, Iowa DOT TR-443.

21. White, D.J., Suleiman, M.T., Pham, H.T., and Bigelow, J. (2002). *Constitutive equations for aggregates used in Geopier® foundation construction*. Final Report, Iowa State University, Ames, IA, USA.

22. Wissmann, K.J., Moser, K., Pando, M. (2001). "Reducing settlement risks in residual piedmont soil using rammed aggregate pier elements." *Proceedings of Foundations and Ground Improvement, Geotechnical Special Publication No. 113*, ASCE, Blacksburg, VA, 943-957.

NOTATION

c'	=	effective stress cohesion
C_c	=	compression index
d_{shaft}	=	pier nominal diameter
E_s	=	elastic modulus
E_u	=	undrained modulus
k_g	=	modulus of subgrade reaction of the pier
K_o	=	*at-rest* coefficient of lateral earth pressure
q	=	induced pressure at the footing bottom
q_g	=	stress concentrated on top of the pier element
R_a	=	area replacement ratio
R_s	=	stress concentration ratio
s_u	=	undrained shear strength
z_b	=	bulging depth
z_o	=	depth at which bulging starts
ϕ'	=	effective stress friction angle
γ	=	wet density
σ_3	=	confining stress
ψ	=	dilatancy angle
w_n	=	natural moisture content

Table 4.1. Mechanical properties of the compacted aggregate and the alluvial clay

No	USCS Classification	Soil properties								
		γ (kN/m^3)	w_n (%)	c' (kPa)	ϕ' (deg)	ψ (deg)	s_u (kPa)	K_o (-)	C_c (-)	E_s (MPa)
1	GP	20.6	6	4	47	12	-	-	-	85
2	CL	18.9	36	2	24	0	30	0.6	0.1	3.5
3	ML	18.9	36	2	35	0	150	1.0	-	8.0

Table 4.2. Ultimate bearing capacity measured from load tests

Test	Parameter	Method of Analysis	
		Double Tangent	25-mm
P_1	Settlement at ultimate load (mm)	11	25
	Ultimate pier load (kN)	200	240
	Ultimate bearing capacity (MPa)	0.440	0.530
P_2	Settlement at ultimate load (mm)	9	25
	Ultimate pier load (kN)	250	290
	Ultimate bearing capacity (MPa)	0.550	0.640
G_1	Settlement at ultimate load (mm)	18	25
	Ultimate pier load (kN)	920	1060
	Ultimate bearing capacity (MPa)	0.175	0.202
G_2	Settlement at ultimate load (mm)	25	25
	Ultimate pier load (kN)	1240	1240
	Ultimate bearing capacity (MPa)	0.236	0.236

Table 4.3. Calculated ultimate bearing capacity of isolated piers and pier groups

Failure mechanism	Drainage	P_1 (MPa)	P_2 (MPa)	G_1 $n_s = 5$ (MPa)	G_2 $n_s = 10$ (MPa)
Bulging	Undrained	1.32	1.32	0.62	0.54
Shearing below the Tip of Individual Pier	Undrained	1.01	1.36	0.47	0.56
	Drained	1.02 (T) 1.36 (M) 1.76 (H) 1.80 (V)	2.04 (T) 3.39 (M) 3.86 (H) 3.95 (V)	0.48 (T) 0.64 (M) 0.84 (H) 0.85 (V)	0.85 (T) 1.41 (M) 1.61 (H) 1.65 (V)
Shearing within Pier-Reinforced Zone	Drained	—	—	9.65 (T) 15.05 (M) 6.77 (H) 8.69 (V)	
Shearing below Pier-Reinforced Zone	Undrained	—	—	1.08	2.70
	Drained	—	—	2.54 (T) 3.02 (M) 3.23 (H) 3.50 (V)	8.44 (T) 10.26 (M) 9.17 (H) 10.93 (V)
Measurements	Partly drained	0.44 to 0.53	0.55 to 0.64	0.18 to 0.20	0.24 to 0.24

Note: T – Terzaghi's factors, M – Meyerhof's factors, H – Hansen's factors, V – Vesic's factors

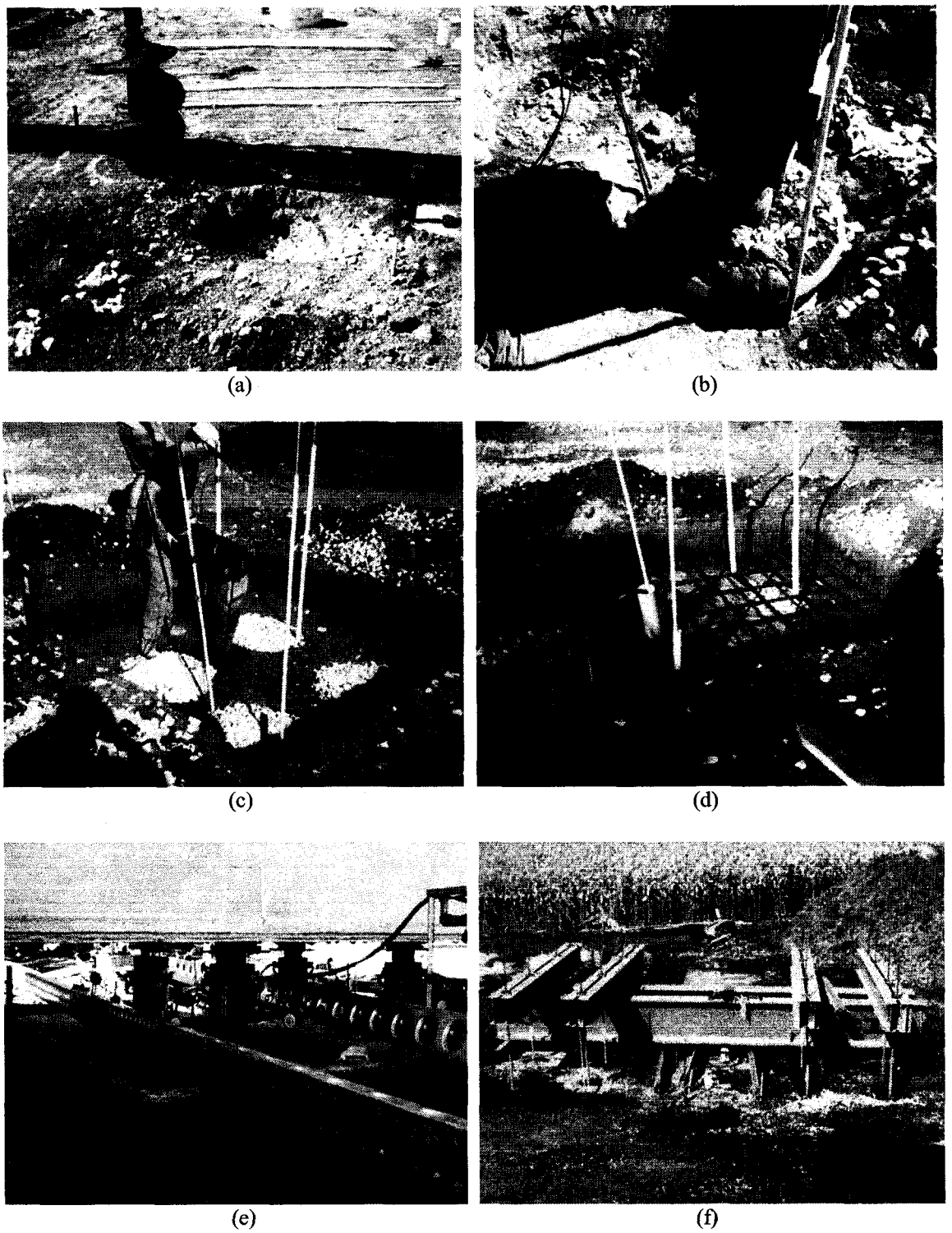

Figure 4.1. (color) Photos illustrating (a) drilling cavity, (b) aggregate compaction, (c) surface preparation for footing, (d) instrumentation and steel reinforcement, (e) four-jack load test setup, (f) load test frame with helical anchors

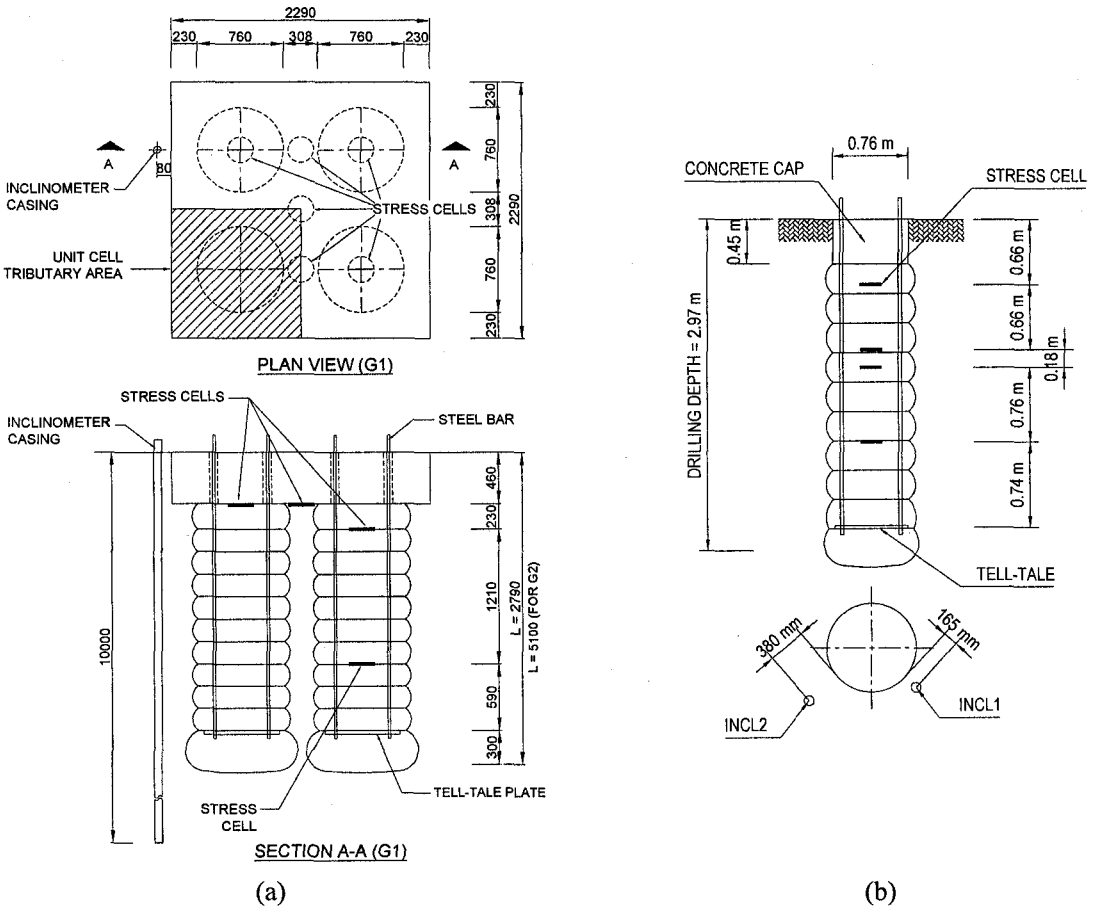

Figure 4.2. Instrumentation on (a) G_1 and (b) P_3

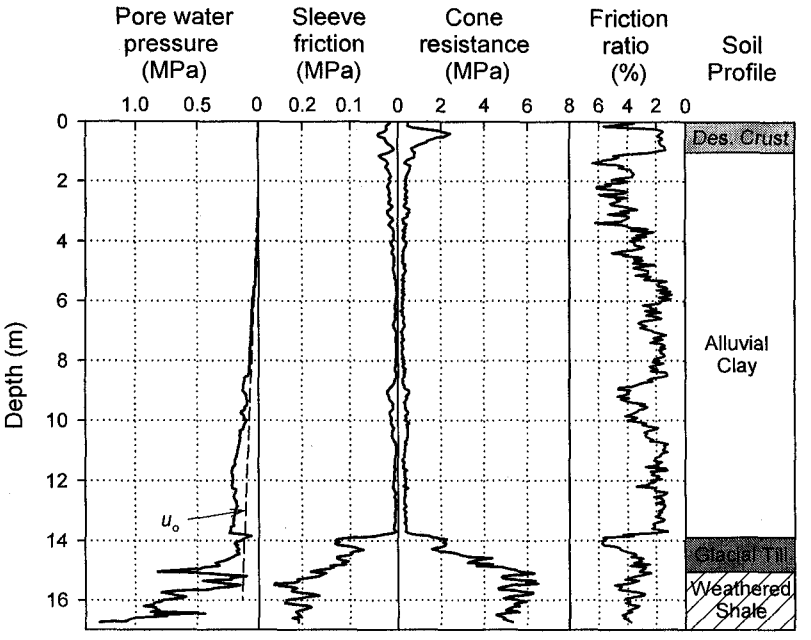

Figure 4.3. Summary of CPT results

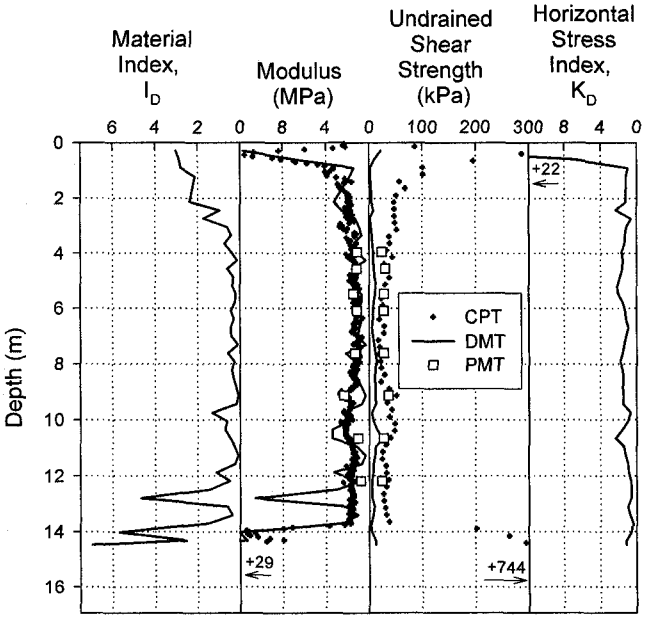

Figure 4.4. DMT results with modulus and shear strength comparisons to CPT and PMT

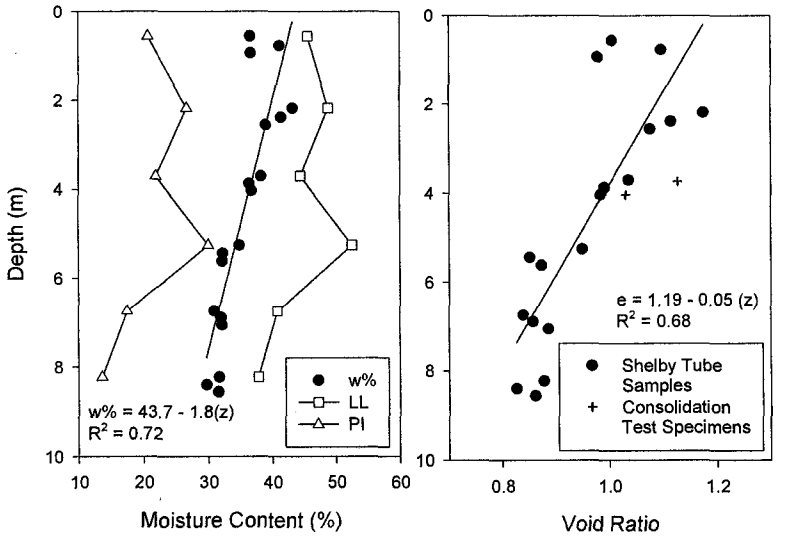

Figure 4.5. In-situ moisture content, Atterberg limits, and void ratio profiles

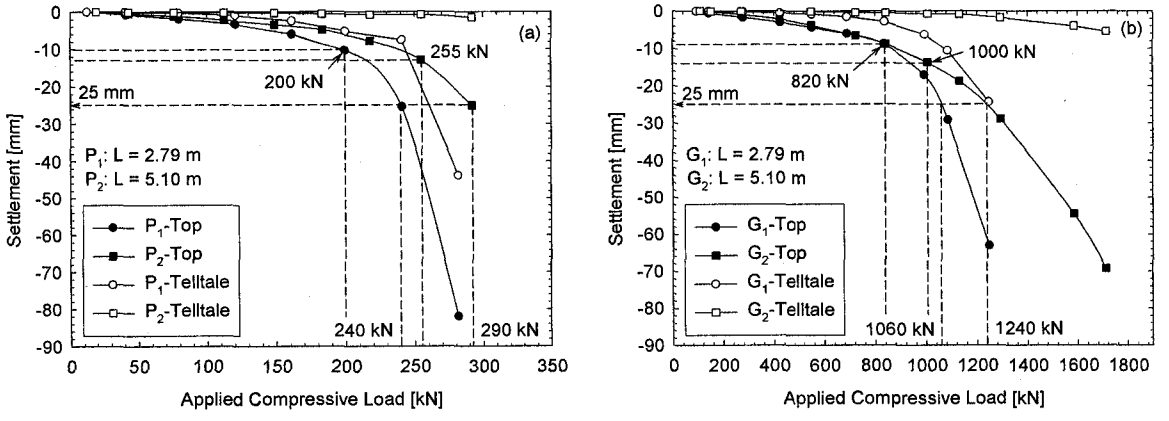

Figure 4.6. Measured load-settlement curves of: (a) P_1 and P_2; (b) G_1 and G_2

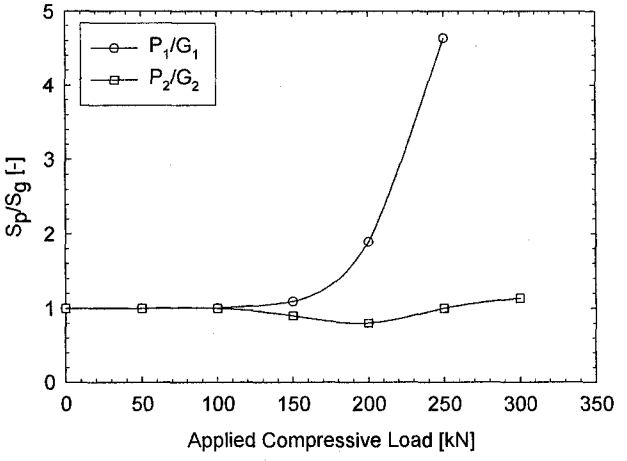

Figure 4.7. Group efficiency in terms of settlement: isolated pier vs. pier group

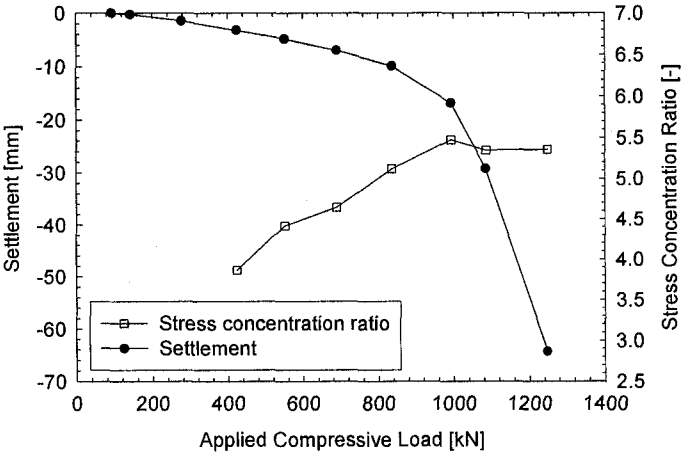

Figure 4.8. Stress concentration ratio as function of compressive load

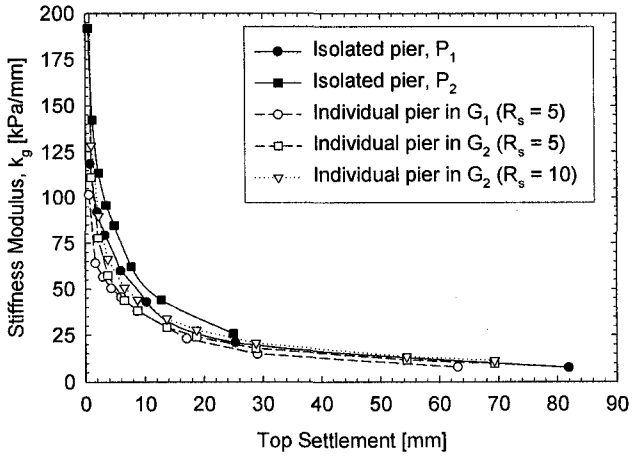

Figure 4.9. Modulus of subgrade reaction of isolated pier, pier-supported footing, and an individual pier in pier group

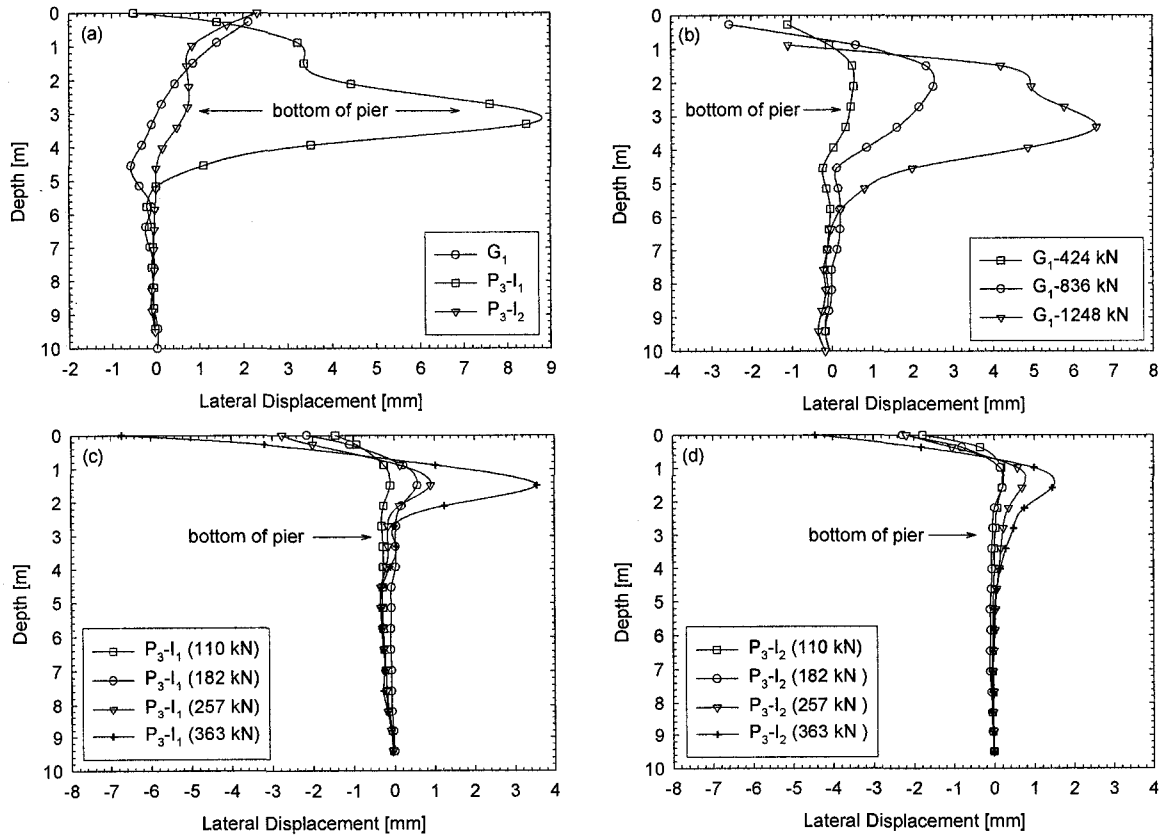

Figure 4.10. Lateral displacement in the matrix soil: (a) after installation; (b) adjacent to G_1; (c) adjacent to P_3 (I_1); and (d) adjacent to P3 (I_2)

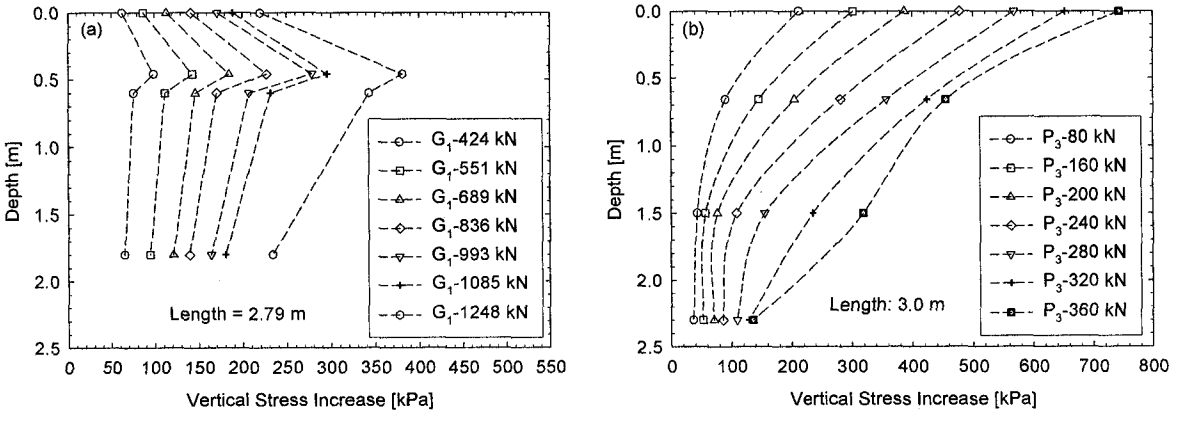

Figure 4.11. Measurements of vertical stress increase along pier shaft: (a) G_1; and (b) P_3

CHAPTER 5: SUPPORT MECHANISM OF RAMMED AGGREGATE PIERS. II. NUMERICAL ANALYSES

A paper to be submitted to Journal of Geotechnical and Geoenvironmental Engineering

Ha T.V. Pham[1] and David J. White[2]

ABSTRACT

This paper is the second of a two-part series describing an investigation of the mechanical behavior of rammed aggregate piers in supporting rigid square footings. In this paper, the performances of two trial pier-supported footings and three isolated rammed aggregate piers during compressive load tests were simulated by an axisymmetric finite element model and compared experimental data. A hardening-soil constitutive model with parameters estimated from in-situ and laboratory tests was used to characterize the constitutive behaviors of the pier material and the matrix soil. Pier groups were modeled as unit cells with the tributary area determined from the center-to-center spacing. Cavity expansion modeling was used to simulate the pier installation process. Verifications of the numerical model were carried out by comparing the numerical results with the data obtained from full-scale, instrumented load tests. Interpretation of the numerical results focused on load-deformation behavior, group effect, stress concentration ratio, and the development of stresses in the matrix soil. In addition, the distribution of vertical stress underneath the pier-supported footings is characterized. A modulus-based approach used to estimate the settlement of the pier-supported footing is also presented. (*177 words*)

[1] Graduate Research Assistant, Department of Civil, Construction and Environmental Engineering, Iowa State University of Science and Technology, Ames, IA 50011-3232, USA. htvpham@iastate.edu
[2] Assistant Professor, Department of Civil, Construction and Environmental Engineering, Iowa State University of Science and Technology, Ames, IA 50011-3232, USA. djwhite@iastate.edu

INTRODUCTION

The use of rammed aggregate piers to reduce excessive settlement of column footings constructed over soft soils has been well documented (Lawton and Fox 1994, Lawton et al. 1994). It was reported by Lawton and Fox (1994) that settlements observed at a number of structures stabilized by rammed aggregate piers were generally less than those predicted using conventional geotechnical procedures for settlement analysis. Similar observations were later reported by Lawton *et al.* (1994) and Handy *et al.* (1999). The discrepancy between the predicted and the actual settlement is believed to be a result of (1) the conservatism of the stiffness-based approach used to calculate the upper-zone settlement in which the pier length is neglected; (2) the omission of the increase in confinement in the pier-reinforced zone achieved from pier installation, (3) the inadequacy of the assumption regarding the stress distribution underneath the pier-supported footing, and (4) the omission of the pier-soil-pier interactions within the pier group.

Part I of this two-part series described the experimental results of two full-scale trial pier-supported footings and three isolated rammed aggregate piers when subjected to compressive loads. Part II of this series herein presents a numerical study in which the pier-supported footings and isolated rammed aggregate piers are simulated through the use of an axisymmetric finite element (FE) model. The construction-induced stress regime in the pier-reinforced zone is regenerated by considering the pier installation as a cavity expansion process (Pham *et al.* 2005). Constitutive modeling parameters of the compacted aggregate and the matrix soils were estimated from the results of *in-situ* and laboratory tests. In this study, a pier-supported footing is modeled as a unit cell. The stress distributions in the upper and the lower zone are characterized based on numerical results. A simplified hybrid

solution based on the homogenization approach combined with FE stress distributions for calculating the elastic settlements of rammed aggregate pier systems is also presented in this paper.

NUMERICAL MODELING

Constitutive Model

The hardening-soil model developed by Schanz *et al.* (1999) was used to describe the constitutive behaviors of the matrix soils and the aggregate in this study. The hardening-soil model is essentially a non-linear, elasto-plastic model in which the yield surface in the principal stress space consists of a hardening hexagonal yield surface enclosed by a hardening cap. Failure of the material is defined in accordance with the Mohr-Coulomb criterion. Non-associated flow rule is used to determine plastic strains on the yield surface whereas associated flow rule is used to characterize the plastic straining on the cap. Constitutive model parameters of the hardening-soil model can be readily determined from CD triaxial and one-dimensional consolidation tests (Schanz *et al.* 1999). Constitutive model parameters of the desiccated fill layer were assumed based on the data from *in-situ* tests (see Part I). Table 5.1 summarizes the values of the constitutive parameters used for the matrix soils and the aggregate. Details of the constitutive behaviors of the compacted aggregate and the matrix soils are presented in Pham *et al.* (2005).

Descriptions of the FE Model

The finite element method has been widely used to model foundations supported by granular piles (Aboshi *et al.* 1979, Balaam and Brooker 1981, Mitchell and Hubner 1985, Lee and Pande 1998, Kirsch and Sondermann 2001). In this study, an axisymmetric FE

model was developed using the computer program Plaxis (version 8.2). The pier-supported footings were modeled as a unit cell which consists of a pier element supporting a circular footing. The tributary area of the unit cell was assumed to be one fourth of the trial footing area. Details of the unit cell concept were described by Barksdale and Bachus (1983). Calculation of the tributary area based on pier spacing was suggested by Balaam and Brooker (1981). This same model was used to study the response of isolated piers except that the diameter of the unit cell footing was equal to the pier diameter. Dimensions of the unit cell and the isolated pier in the models are shown in Fig. 5.1a.

Figure 5.1b shows the dimensions of the FE model used in this study. The model consisted of a pier installed in a 2-layer matrix soil profile. The matrix soil profile consisted of a 1.0 m thick desiccated crust layer overlying 13.0 m of soft alluvial clay. The physical boundary of the model was extended to 10.0 m measured radially from the center of the pier. The concrete in the footing was modeled as a linear elastic, non-porous material. Full fixity was provided along the bottom of the model. The vertical boundaries of the model were locked in the horizontal direction. An unstructured FE mesh that consists of 15-node, linear triangular elements was used. A fully drained condition was assumed for both pier installation and pier loading processes. A static pore water pressure profile was generated based on the location of the water table which was set at 2.0 m from the ground surface. Measurements taken from piezometers installed at about 0.3 m from a pier edge at this site revealed that the excess pore water pressures fully dissipated within 30 seconds after stopping the ramming operations (White *et al.* 2003). Time dependent soil behaviors around rammed aggregate piers are being investigated in a separate study.

Interface elements with strength reduction ratio of 0.1 were introduced along the footing-soil vertical interface to reflect the relatively poor contact between the footing and the soil. Thin solid continuum elements having effective shear strength parameters the same as those of the matrix soil were used along the pier-soil contact in lieu of interface elements (see Potts and Zdravkovic 1999).

Modeling Procedure

The initial condition was assumed to be at the end of the cavity drilling. Initial stresses were generated using the K_o-procedure in which the effective vertical stress was calculated as the buoyant weight of the soil and the effective horizontal stress, which includes both radial and tangential stresses, was defined as the product of the effective vertical stress and a pre-defined K_o value. For the alluvial clay layer, K_o = 1-sinϕ' (Jaky 1944) was assumed whereas K_o = 1.0 was assigned to the desiccated crust layer. The initial shear stress was assumed to be zero.

The pier installation process was modeled by applying outward uniform displacement along the shaft and downward uniform displacement at the bottom of the cavity. The strain-controlled cavity expansion process was terminated when the cavity strains along the shaft and at the bottom of the cavity were respectively equal to 5% and 10% of the nominal diameter of the cavity (Pham *et al.* 2005). The expanded cavity was then filled with compacted aggregate and the concrete footing was placed on top of the pier-soil system. The stress-controlled load tests were simulated by applying incremental uniform pressure on the top of the footing.

MODEL VERIFICATIONS

Load-Deformation Behaviors

As previously described in Part I, two pier-supported footings (denoted as G_1 and G_2) and three isolated rammed aggregate piers (denoted as P_1, P_2, and P_3) were constructed and tested in the same site. Verifications of the finite element model developed in this study are made by comparing the FE results with those measured from the full-scale, instrumented load tests conducted on the pier-supported footings and the isolated piers. Figure 5.2 compares the load-settlement curves obtained from FE analyses with the measured curves from the full-scale load tests. The load values used to produce the load-settlement curves for G_1 and G_2 are calculated as one fourth of the total applied load on the footing. In design practice, the design load is commonly taken at the end of the elastic portion of the load-settlement curve. Following this procedure, the design loads of G_1 and G_2, as indicated in Fig. 5.2, are about 840 kN and 880 kN, respectively. Taking into account the seating loads applied at the beginning of the tests, the compressive loads that are actually induce settlement (ΔF_{design}) are 746 kN and 770 kN for G_1 and G_2, respectively (see Fig. 5.2). As indicated in Fig. 5.2, the calculated load-settlement results agree well with the measurements until the compressive load reaches the design level. As the applied load exceeds the design load level, FE analyses slightly underestimate the settlement except for P_1 where the predicted load-settlement curve indicates a stiffer response compared to the measured curve. Better agreement between the calculated and the measured load-settlement curve can be obtained by using true interface elements with reduced stiffness and shear strength. However, the authors of this paper believe that if the properties of the interface elements are not measured then adjusting the stiffness and shear strength of the interface elements to have a better match between the

measured and the predicted load-settlement curve would be more or less a curve-fitting exercise. Finally, the load-settlement responses in both G_1 and G_2 are quite similar to those of the isolated piers with the same length and diameter.

Figure 5.3 shows the lateral movement profile in the matrix soil adjacent to G_1 obtained from inclinometer measurements and FE analyses. In general, the shape of the lateral displacement profile is well captured by FE analyses. Maximum lateral displacements predicted by FE analyses are 1.6 and 4.2 mm at compressive loads of 836 kN and 1248 kN, respectively. Compared to the measured displacement values of 2.5 and 6.6 mm, the calculated displacements are slightly smaller but the trends are similar.

Vertical Stress Distributions

Distributions of the vertical stress increase along the shaft of the isolated pier (P_3) and pier group (G_1) obtained from FE analyses and stress cell measurements are presented in Fig. 5.4. As indicated in Fig. 5.4a, good agreement between the measured and the calculated stresses in P_3 is attained. Comparison of the measured and the calculated stresses in G_1 (Fig. 5.4b) also shows a good agreement especially when considering the difficulties in accurately measuring total stress in the field (Dunniclif 1993).

Contact Stresses and Stress Concentration Ratio

Figure 5.5 compares the total stress cell measurements and the predicted contact stresses on top of the pier (q_g) and on top of the matrix soil (q_m) for G_1. Good agreement is achieved between the measured and the calculated q_m. However, FE analyses slightly overestimate q_g as compared to the measured values. The stress concentration ratio (n_s) calculated from FE results ranges from 2 to 10 when the compressive load increases from 143 kN to 1085 kN. Moreover, FE analyses indicates that n_s increases with the compressive

load up to a peak value at the compressive load of 1085 kN before dropping to a somewhat constant value as the compressive load increases further. This behavior, however, is not observed in the measured data. One reason for this lack of agreement may be that the capacity of the stress cell on the pier is exceeded and the measured n_s at the compressive load of 1085 kN shown in Fig. 5.5b may correspond to the capacity of the stress cell rather than the actual stress. Based on field measurements, Lawton and Warner (2004) reported that n_s of a rammed aggregate pier-supported rigid footing dropped dramatically after the ultimate pier load is exceeded. Similar trending in n_s was also presented in Kirsch and Sondermann (2001) based on a scaled model test. Also shown in Fig. 5.5 are q_g, q_m, and n_s calculated from FE analyses for G_2. It is indicated that when the applied compressive load is lower than about 800 kN, calculated q_g and q_m for both G_1 and G_2 are quite similar. The variation of n_s calculated for G_2 also shows the same trending compared to G_1 except that a peak value of about 11 is achieved at the compressive load of 1584 kN.

COMPARISON BETWEEN ISOLATED PIER AND UNIT CELL MODELS

Although rammed aggregate piers are commonly installed in groups, the settlement analysis of a pier group is essentially based on the behavior of an isolated pier (Fox and Cowell 1998). In this section, the response of a pier group modeled as a unit cell to a given compressive load is compared with the response of an isolated pier subjected to the same load magnitude.

Figures 5.6 compares the behaviors of G_1 and P_1 based on a number of parameters including pier axial load distribution, vertical stress in the matrix soil, interfacial shear stress, lateral effective stress in the matrix soil, lateral movement in the matrix soil, and shear strain

at the pier-soil contact. Three compressive loads of 120, 250, and 300 kN were selected for comparison. These loads are considered to be analogous to a working load, the yielding load, and a post-yielding load. As shown in Fig. 5.6a, pier axial load distributions along P_1 and G_1 are almost coincident when the applied compressive load is less than or equal to 250 kN. This is because at these load levels, the differences in lateral effective stress (Fig. 5.6d) and interfacial shear strain (Fig. 5.6f) are not significant between G_1 and P_1. When the applied compressive load is equal to 300 kN, the difference in both lateral effective stress and interfacial shear strains between P_1 and G_1 becomes considerable. As a result, the axial pier load dissipates more rapidly in G_1 compared to P_1 (Fig. 5.6a). Further interpretation of the numerical results reveals that the influence depth of the footing in G_1 is about 1.0 m from grade (Fig. 5.6b). Below this depth, the distributions of all investigated parameters except the lateral movement and the interfacial shear strain are quite similar between G_1 and P_1. Moreover, the increased lateral stress in G_1 due to the footing-induced vertical stress also prevents the lateral movement in the matrix soil as shown in Fig. 5.6e. At the working load level (120 kN), the difference in the responses of G_1 and P_1 is insignificant.

Figure 5.8 shows the comparison between P_2 and G_2. Similar to P_1 and G_1, three compressive loads of 120, 250, and 350 kN are selected for comparison. The influence depth of the footing in G_2, as shown in Fig. 5.7b, is also at about 1.0 m from grade. Within this depth, the vertical stress in the matrix soil (Fig. 5.7b), the lateral effective stress (Fig. 5.7c), and the interfacial shear stress (Fig. 5.7d) adjacent to G_2 are higher than those adjacent to P_2. At greater depths, all stresses are essentially the same in both cases. Compared to P_1 and G_1, the difference in all parameters between P_2 and G_2 is generally less significant. As a result, distributions of the axial pier load along G_2 and P_2 are quite similar even at the compressive

load that exceeds the design level (350 kN). Unlike P_1 and G_1, the interfacial shear strain in P_2 and G_2 concentrates at the upper part of the pier which indicates bulging deformation.

STRESS PATH IN THE MATRIX SOIL

To gain further insight into the pier-soil interactions, effective stress paths (following Lambe 1967) obtained from two soil elements adjacent to the unit cells (G_1 and G_2) and the isolated piers (P_1 and P_2) are shown in Fig. 5.8. These soil elements are located at 0.75 m and 1.5 m from grade (0.29 m and 1.04 m from footing bottom). Failure envelops determined based on the friction angle of the alluvium clay (K_{f1}) and the top crust (K_{f2}) are established in both compression and extension spaces. Stress states in both soil elements during cavity expansion are found to be on the extension failure envelops which indicated a Rankine passive stress condition. The application of compressive load on top of the pier during load tests increases the vertical stress in the soil elements and causes the stress paths to go upward into the compression space (i.e., above the p' axis). Once the Rankine active stress condition is reached, the stress path in the soil element located at 1.50 m continues to move upward along the failure envelope. Contrarily, the stress path in the soil element at 0.75 m declines along the failure envelope. This stress path trending corresponds to an unloading process. Since the depth of influence of the unit cell footing is about 1.0 m from grade, the stress paths of the soil element at the depth of 1.50 m are almost coincident between the unit cell and the isolated pier. For the soil element at 0.75 m, before reaching the Rankine active stress condition, the stress path obtained from the unit cell is located to the right of stress path obtained from the isolated pier. This is because the vertical stress

exerted from the unit cell footing increases the mean stress in the adjacent soil compared to the isolated pier.

In an axisymmetric analysis, there are four non-zero stress components — radial stress (σ'_r), vertical stress (σ'_z), tangential stress (σ'_θ), and the shear stress in the *z-r* plane (τ_{rz}). Since other shear stresses ($\tau_{z\theta}$ and $\tau_{\theta r}$) are zero, the tangential stress, σ'_θ, is always one of the principal stresses. Depending on the loading condition, the tangential stress can either be the minor principal stress (σ'_3) or the intermediate principal stress (σ'_2). Principal stresses of two soil elements located at 0.75m and 1.50 m next to G_1 and G_2 are shown in Fig. 5.9 at different loading stages. Loading stages include the initial stress condition (Initial), increment steps of cavity expansion (CE), pier construction, and the application of vertical compressive loads. For the soil element at 1.50 m (Fig. 5.9a and 5.9b), the tangential stress in both G_1 and G_2 is always the minor principal stress. In other words, for a given major principal stress (σ'_1), the tangential stress controls the magnitude of the deviator shear stress. On the other hand, the tangential stress is not always minor principal stress in the soil element located at 0.75 m. As indicated in Fig. 5.9c and Fig. 5.9d, the magnitude of the deviator stress is only controlled by the tangential stress when the applied compressive load is higher than 278 kN. At lower loads, the minor principal stress in the *z-r* plan controls the magnitude of deviator shear stress.

STRESS DISTRIBUTION UNDERNEATH PIER-SUPPORTED FOOTINGS

Distributions of the vertical stress underneath footings supported by columnar systems are of practical importance. Knowledge of the stress distribution within the column-reinforced zone (i.e., upper zone) is necessary in estimating settlement and global stability

(Barksdale and Bachus 1983). Characterization of the vertical stress distribution underneath a strip footing supported by end-bearing compacted sand columns using plain-strain FE analysis was conducted by Aboshi *et al.* (1979). In this analysis, vertical stress contours in the sand column-reinforced zone were compared with the stress contours obtained from Boussinesq's solution for a homogenous, unreinforced soil. Following this approach, Barksdale and Bachus (1983) suggested a simplified method to estimate the vertical stress in the stone columns and the matrix soil by combining the Boussinesq's stress distribution with the stress concentration ratio.

For floating systems such as rammed aggregate piers, the distribution of vertical stress below the pier-reinforced zone (i.e., lower zone) is also needed for estimating the lower-zone settlement. Current design practice for analyzing rammed aggregate pier systems (Fox and Cowell 1998) assumes that the vertical stress increase underneath the pier-supported footing follows the Westergaard's solution and that the stress distribution in both the upper and the lower zone is not affected by pier installation. Although these assumptions can be used to reasonably approximate the vertical stress increase in the soil, a more superior method such as FE analysis is certainly preferable. In Fig. 5.10, the average vertical stress increase in G_1 and G_2 normalized by the applied footing pressure (q_o) is plotted against depth normalized by footing width (B). A hypothetical case which considers an unsupported footing is also analyzed using the Westergaard's and FE solutions. Vertical stress distributions predicted by these methods are compared with those determined by FE analyses when the footing is supported by G_1 and G_2. For the supported cases, the average vertical stress is determined with the assumption that the vertical stress increase, $\Delta\sigma_v$, across the

footing is uniform at a given depth and is determined as the weighted average of the vertical stresses on top of the pier and on the matrix soil as follows:

$$\Delta\sigma_v = \Delta q_g R_a + (1 - R_a)\Delta q_m \quad [5.1]$$

where Δq_g is the vertical stress increase on the pier, Δq_m is the vertical stress increase on the matrix soil, and R_a is the area replacement ratio. As can be seen in Fig. 5.10, for the unsupported footing, $\Delta\sigma_v$ predicted by the Westergaard's method is higher when compared to that obtained from FE analyses. If the settlement induced by $\Delta\sigma_v$ is assumed to be terminated at the the depth where $\Delta\sigma_v/q_o$ is 0.05 then the depths of zero settlement of G_1 and G_2 are equal to 1.5B and 2B, respectively. In other words, for a given footing width, the longer the pier, the deeper the vertical stress will be transmitted. As can be seen in Fig. 5.10, if the same assumption regarding the zero settlement depth is used for the Westergaard's method then the settlement will be terminated at 2.5B. The sole dependence of $\Delta\sigma_v/q_o$ on the footing width when following Westergaard's solution can potentially cause inaccuracy in estimating stresses underneath pier-supported footings.

CALCULATION OF SETTLEMENT USING MODULUS-BASED APPROACH

Figure 5.11 shows the distribution of vertical stress underneath G_1 and G_2 as a function of shaft length (H_{shaft}). As indicated in this figure, the distribution of $\Delta\sigma_v$ in the upper and the lower zone can be well characterized by two linear functions with the following form:

$$\frac{\Delta\sigma_v}{q_o} = a - b\frac{z - D_f}{H_{shaft}} \quad [5.2]$$

where values of a and b for the upper and the lower zone are shown in Fig. 5.11. If the upper zone is treated as a homogeneous composite block with a unique modulus value (E_{comp}) then the elastic modulus of the upper zone can also be estimated as:

$$E_{comp} = E_g R_a + (1 - R_a) E_m \qquad [5.3]$$

where E_{comp} is the average elastic modulus the pier-soil composite, E_g is the elastic modulus of the pier, and E_m is the elastic modulus of the matrix soil. Following the elastic theory, the settlement in the upper zone is calculated as:

$$S_{UZ} = \frac{\Delta\sigma_v H_{UZ}}{E_{comp}} \qquad [5.4]$$

where H_{UZ} is the thickness of the upper zone. Values of the E_g, E_s, and R_a are described in Part I of this series. Table 5.2 shows the settlements at the design loads (ΔF) of G_1 and G_2 estimated by the currently-used stiffness-based method, which is described in Part I of this series and the modulus-based method presented herein. In Table 5.2, E_{comp} is calculated using Eq. 5.2. The depths of zero settlement, where $\Delta\sigma_v/q_o$ is equal to 0.05, are indicated in Fig. 5.11 for G_1 and G_2. For evaluation purpose, the measured settlements of G_1 and G_2 at the design load are also shown in Table 5.1.

For G_1, comparison between the calculated and the measured settlement indicates that the stiffness-based method overestimates the total settlement by about 150%. As discussed in the preceding section, the inaccuracy in estimating $\Delta\sigma_v$ underneath the pier-supported footing of the Westergaard's method is the main reason that causes this discrepancy. Further investigation of Fig. 5.10 and 5.11 shows that $\Delta\sigma_v/q_o$ estimated by the Westergaard's method at the top of the lower zone of G_1 is about two times as high as that calculated by FE analyses. On the contrary, the stiffness-based method slightly underestimates the settlement

of G_2. This is because the depth to the bottom of the lower zone, when calculated using the Westergaard's method (2.5B), is actually less than the length of the piers in G_2. Accordingly, the total settlement of G_2 will be equal to S_{UZ} since there is no settlement in the lower zone. Compared to the stiffness-based method, the modulus-based method is superior since the length of the pier is considered in the analysis. The evidence is that the predicted settlements using the modulus-based method are closer to the measured values when compared to those calculated by the stiffness-based method. For practical purposes, parametric analyses will be needed in order to fully characterize the distribution of vertical stress underneath pier-supported footings.

SUMMARY AND CONCLUSION

Numerical analyses using the FE method were conducted to study the mechanical behaviors rammed aggregate piers in supporting rigid footings. Group effects were investigated by comparing the behaviors of an individual pier in the group with those of an isolated pier of the same length and diameter. The numerical model developed in this study utilized model parameters that were estimated from *in-situ* and laboratory tests. The FE model was verified by comparing the numerical results with those obtained from full scale compressive load tests with instrumentations. Conclusions drawn from this study are:

1. The FE model developed in this study successfully captured the mechanical behaviors of rammed aggregate piers used to support rigid footings. The load-settlement response of a pier group can be predicted from the modeling of an isolated pier of the same length and diameter. The stress concentration ratio was found to increase with the compressive load up to a peak level corresponding to

the yielding load. Continuing to increase the compressive load causes the stress concentration ratio to drop. This behavior was not observed in the field measurements.

2. Construction of the footing on top of the pier group increased the vertical stress in the matrix soil within the first meter from the footing bottom. As the vertical stress in the matrix soil increased, the lateral stress in the matrix soil also increased thus promoted the development of the interfacial shear stress. However, it was found that the improvement in the interfacial shears tress was not significant in this study. As a result, the behavior of the unit cell and the isolated pier are quite similar in terms of the distribution with depth of the axial pier load.
3. Rankine passive stress condition was obtained during pier installation. The application of compressive load on top of the pier during load tests increases the vertical stress in the soil elements and causes the stress paths to go upward towards the compression failure envelope. The tangential stress only became the intermediate principal in the soil element located at 0.75 m when the compressive load was less than 278 kN.
4. Using FE analyses, the vertical stress distribution underneath pier-supported footings can be characterized by a bi-linear function. Using the Westergaard's method can potentially result in an inaccurate stress distribution underneath pier-supported footings. Using the stiffness-based approach, the total settlement was significantly overestimated for G_1 and slightly underestimated for G_2. Compared to the settlements calculated by the stiffness-based, the predicted settlements using the modulus-based method were closer to the measured values.

ACKNOWLEDGEMENT

This research was sponsored by the Iowa DOT under contract TR-443, Geopier Foundation Company, Inc. and Iowa State University of Science and Technology. The support of these agencies is greatly acknowledged.

REFERENCES

1. Aboshi, H., Ichimoto, E., Enoki, M., and Harada, K. (1979). "The compozer: a method to improve characteristics of soft clays by inclusions of large diameter sand columns." *Proceedings of the International Conference on Soil Reinforcement: Reinforced Earth and Other Techniques*, Paris, 1, 211-216.
2. Balaam, N.P., and Brooker, J.R. (1981). "Analysis of rigid rafts supported by granular piles." *International Journal for Numerical and Analytical Methods in Geomechanics*, 5, 379-403.
3. Balaam, N.P., and Poulos, H.G. (1978). "Methods of analysis of single stone columns." *Proceedings of the Symposium on Soil Reinforcing and Stabilizing Techniques*, Australia, 497-512.
4. Barksdale, R.D., and Bachus, R.C. (1983). *Design and construction of stone columns.* Report No. FHWA/RD-83/026, National Technical Information Service, Springfield, VA.
5. Dunniclif, J. (1993). *Geotechnical instrumentation for monitoring field performance.* John Wiley and Sons, Inc.
6. Fox, N.S., and Cowell, M.J. (1998). *Geopier™ Foundation and Soil Reinforcement Manual.* Geopier Foundation Company, Inc., Blacksburg, VA, USA.

7. Handy, R.L., Fox, N.S., and Wissmann, K.J. (1999). "Short aggregate piers reinforce soils near tunnels." *Proceedings of Geo-Engineering for Underground Facilities, Geotechnical Special Publication No. 90*, ASCE, Urbana, IL, 1039-1047.

8. Kirsch, F., and Sondermann, W. (2001). "Ground improvement and its numerical analysis." Proceedings of the 15th International Conference on Soil Mechanics and Foundation Engineering, ISSMGE, Istanbul, Turkey, 1775-1778.

9. Lawton, E.C., and Fox, N.S. (1994). "Settlement of structures supported on marginal or inadequate soils stiffened with short aggregate piers." *Proceedings of Vertical and Horizontal Deformations of Foundations and Embankments, Geotechnical Special Publication No. 40*, ASCE, College Station, TX, 2, 962-974.

10. Lawton, E.C., and Warner, B.J. (2004). *Performance of a group of Geopier elements loaded in compression compared to single Geopier elements and unreinforced soil.* Final Report, Report No. UUCVEEN 04-12, University of Utah, Salt Lake City, UT, USA.

11. Lawton, E.C., Fox, N.S., and Handy, R.L. (1994). "Control of settlement and uplift structures using short aggregate piers." *Proceedings of In-Situ Deep Soil Improvement, Geotechnical Special Publication No. 45*, ASCE, Atlanta, GA, 121-132.

12. Lee, J.S., and Pande, G.N. (1998). "Analysis of stone-column reinforced foundations." *International Journal for Numerical and Analytical Methods in Geomechanics*, 22, 1001-1020.

13. Mitchell, J.K., and Huber, T.R. (1985). "Performance of stone column foundation." *Journal of Geotechnical Engineering*, ASCE, 111(2), 205-223.

14. Pham, H.T.V., White, D.J., and Wissmann, K.J. (2005). "Behavior of isolated rammed aggregate piers from a finite element analysis." *International Journal of Geomechanics*, ASCE, (*under review*)

15. Potts, D.M., and Zdravkovic, L. (1999). *Finite element analysis in geotechnical engineering: Volume I – Theory*. Telford Publishing, London.

16. Schanz, T., Vermeer, P.A., and Bonnier, P.G. (1999). "Formulation and verification of the hardening-soil model." *Proceedings of Beyond 2000 in Computational Geotechnics*, Balkema, Rotterdam, 281-290.

17. White, D.J., Gaul, A.J., and Hoevelkamp, K. (2003). *Highway applications for rammed aggregate pier in Iowa soils*. Final report, Iowa DOT TR-443.

NOTATION

σ_1' = major principal effective stress

σ_3' = minor principal effective stress

σ_r' = radial effective stress

E_{oed}^{ref} = reference modulus corresponding to p^{ref}

E_{50}^{ref} = reference secant modulus corresponding to p^{ref}

E_{ur}^{ref} = reference unloading/reloading modulus corresponding to p^{ref}

τ_{rz} = shear stress in *z-r* plan

σ_θ' = tangential effective stress

σ_z' = vertical effective stress

B = footing width

c' = effective stress cohesion

E_{comp} = elastic modulus of the pier-soil composite

E_g = elastic modulus of the pier element

e_{ini} = initial void ratio

E_m = elastic modulus of matrix soil

e_{max} = maximum void ratio

e_{min} = minimum void ratio

K_f = slope of the failure envelope in p-q space

K_o = *at-rest* coefficient of lateral earth pressure

m = power for stress-level dependency

n_s = stress concentration ratio

p' = mean effective stress

p^{ref} = reference confining stress

q_g = stress concentrated on top of the pier element

q_m = stress concentrated on top of matrix soil

q_o = induced pressure at the footing bottom

R_a = area replacement ratio

R_f = failure ratio

S_{UZ} = settlement of the upper zone

Δq_g = increase in the stress on top of the pier element

Δq_m = increase in the stress on top of matrix soil

$\Delta \sigma_v$ = vertical stress increase due to footing pressure

ϕ' = effective stress friction angle

γ = wet density

ν_{ur} = unloading-reloading Poisson's ratio

$\sigma_{tension}$ = tension cut-off stress

ψ = dilatancy angle

Table 5.1. Constitutive model parameters for the FE analysis

Parameter	Aggregate	Alluvial clay	Desiccated fill
Effective stress friction angle, ϕ' (degrees)	47	24	35
Effective stress cohesion, c' (kPa)	4	2	2
Dilatancy angle, ψ (degrees)	12	0	0
Average wet density, γ (kg/m^3)	2100	1924	1924
Deviatoric reference modulus, E_{50}^{ref} (kPa)	61000	3000	9000
Compression reference modulus, E_{oed}^{ref} (kPa)	61000[a]	1500	4500
Unloading/reloading modulus, E_{ur}^{ref} (kPa)	1220000[b]	9000[b]	27000[b]
Power for stress-level dependency, m	0.48	1	1
Unloading/reloading Poisson's ratio, ν_{ur}	0.2	0.2	0.2
Reference stress, p^{ref}, kPa	34.5	25.5	25.5
Failure ratio, R_f	0.88	0.96	0.96
K_o for normal consolidation, K_o^{NC}	0.27	0.59	0.43
Initial void ratio, e_{ini}	0.33	1.0	1.0
Minimum void ratio (contraction), e_{min}	0.329	-	-
Maximum void ratio (dilation), e_{max}	0.393	-	-
Tensile cut-off, $\sigma_{tension}$	0	0	0

[a] *Assume:* $E_{oed}^{ref} = E_{50}^{ref}$ [b] *Assume:* $E_{ur}^{ref} = 3x\,E_{50}^{ref}$

Table 5.2. Calculated settlements of G_1 and G_2 at design load level

Methods	G_1 (ΔF_{design} = 746 kN)						G_2 (ΔF_{design} = 770 kN)					
	Δq	E_{ave}	q_g	S_{UZ}	S_{LZ}	S_T	Δq	E_{ave}	q_g	S_{UZ}	S_{LZ}	S_T
	kPa	MPa	kN/ m^3	mm	mm	mm	kPa	MPa	kN/ m^3	mm	mm	mm
Stiffness-based method	291[a]	—	19	15	9	**24**	356[a]	—	44	8.1	0	**8.1**
Modulus-based method	142[b]	32	—	5.2	3.5	**8.7**	147[b]	32	—	10	0	**10**
Measured				—	—	**9.5**				—	—	**10**

[a] *Δq is denoted as q_g in Eq. 4.4 of Part I (G_1: R_s=4.7; G_2: R_s=10.4; R_a=0.35; $q=\Delta F_{design}/B^2$)*

[b] *$\Delta q = \Delta F_{design}/B^2$*

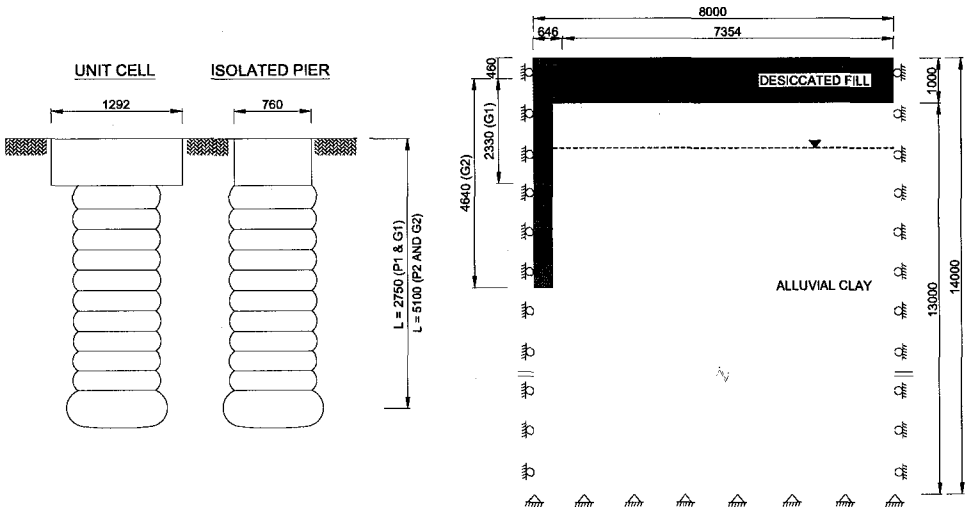

Figure 5.1. (a) Dimensions of the unit cell and isolated pier; (b) the structural model of a unit cell

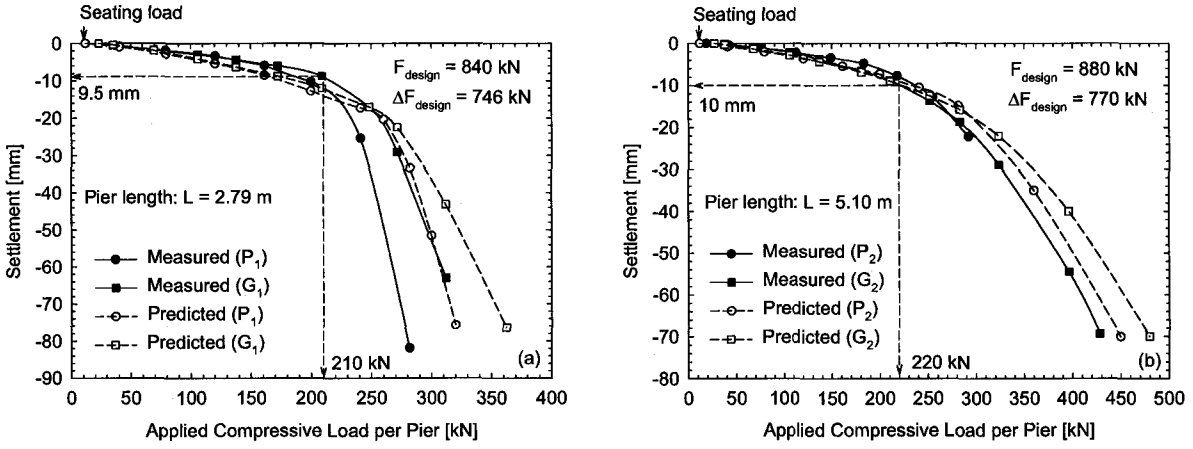

Figure 5.2. Measurements vs. predictions of the load-settlement curves of: (a) P_1 and G_1; and (b) P_2 and G_2

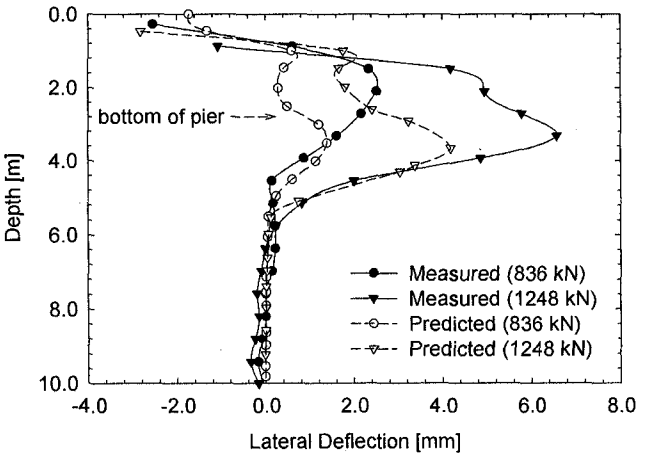

Figure 5.3. Measurements vs. predictions of lateral displacement in the matrix soil adjacent to G_1

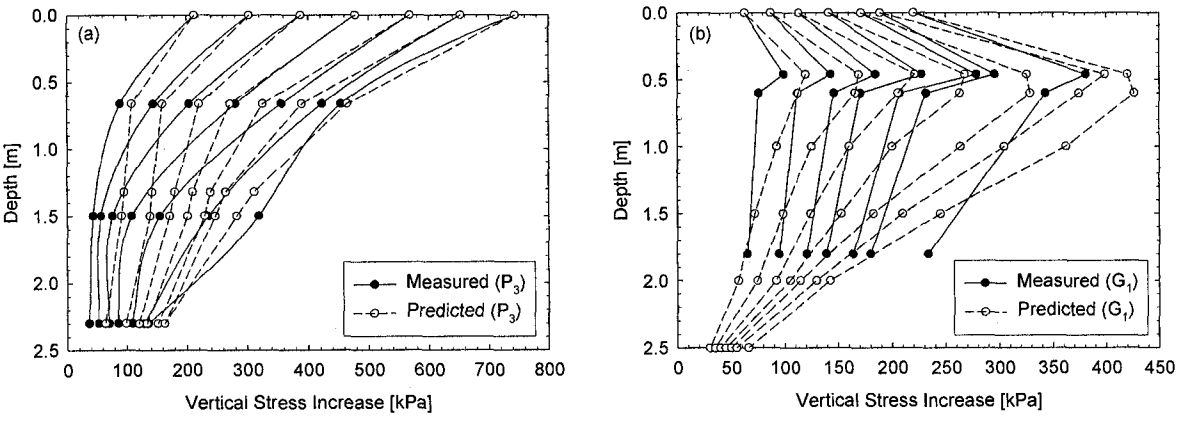

Figure 5.4. Measurements versus predictions of stress distribution along pier shaft: (a) isolated pier (P_3); and (b) pier group (G_1)

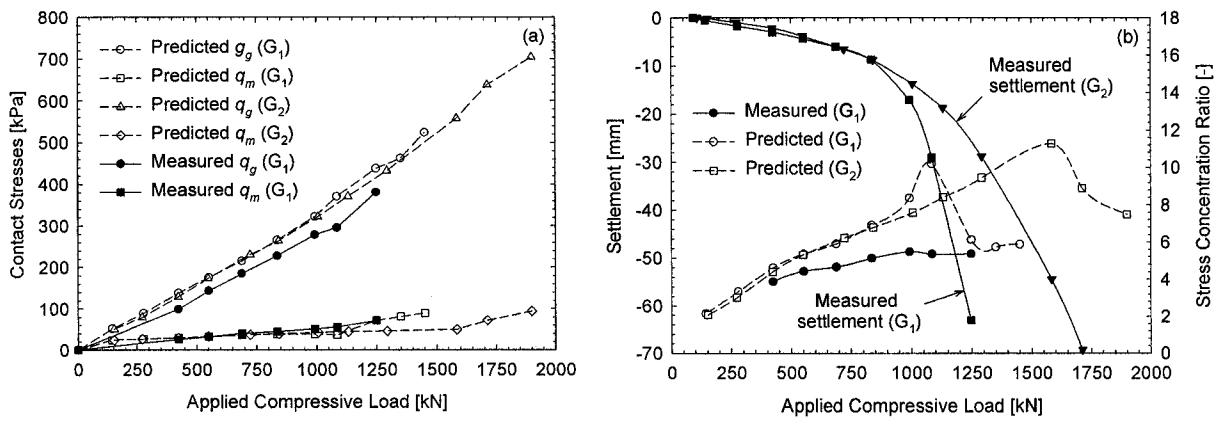

Figure 5.5. Measurements vs. predictions of contact stress and stress concentration ratio in G_1 and G_2

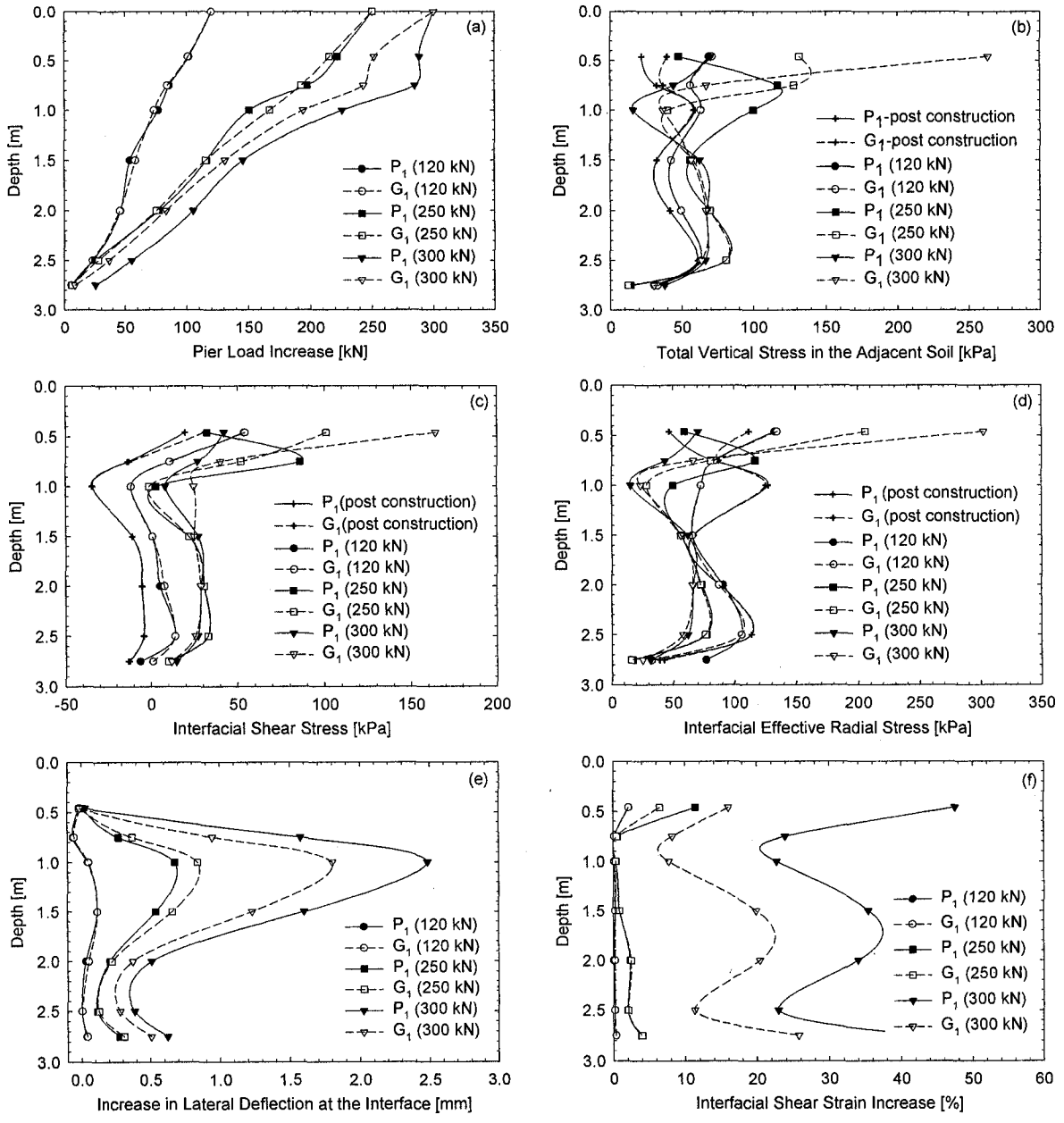

Figure 5.6. Comparison between G_1 and P_1: (a) pier axial load increase; (b) vertical total stress in the matrix soil; (c) interfacial shear stress; (d) Interfacial radial stress; (e) interfacial lateral deflection increase; and (f) interfacial shear strain increase

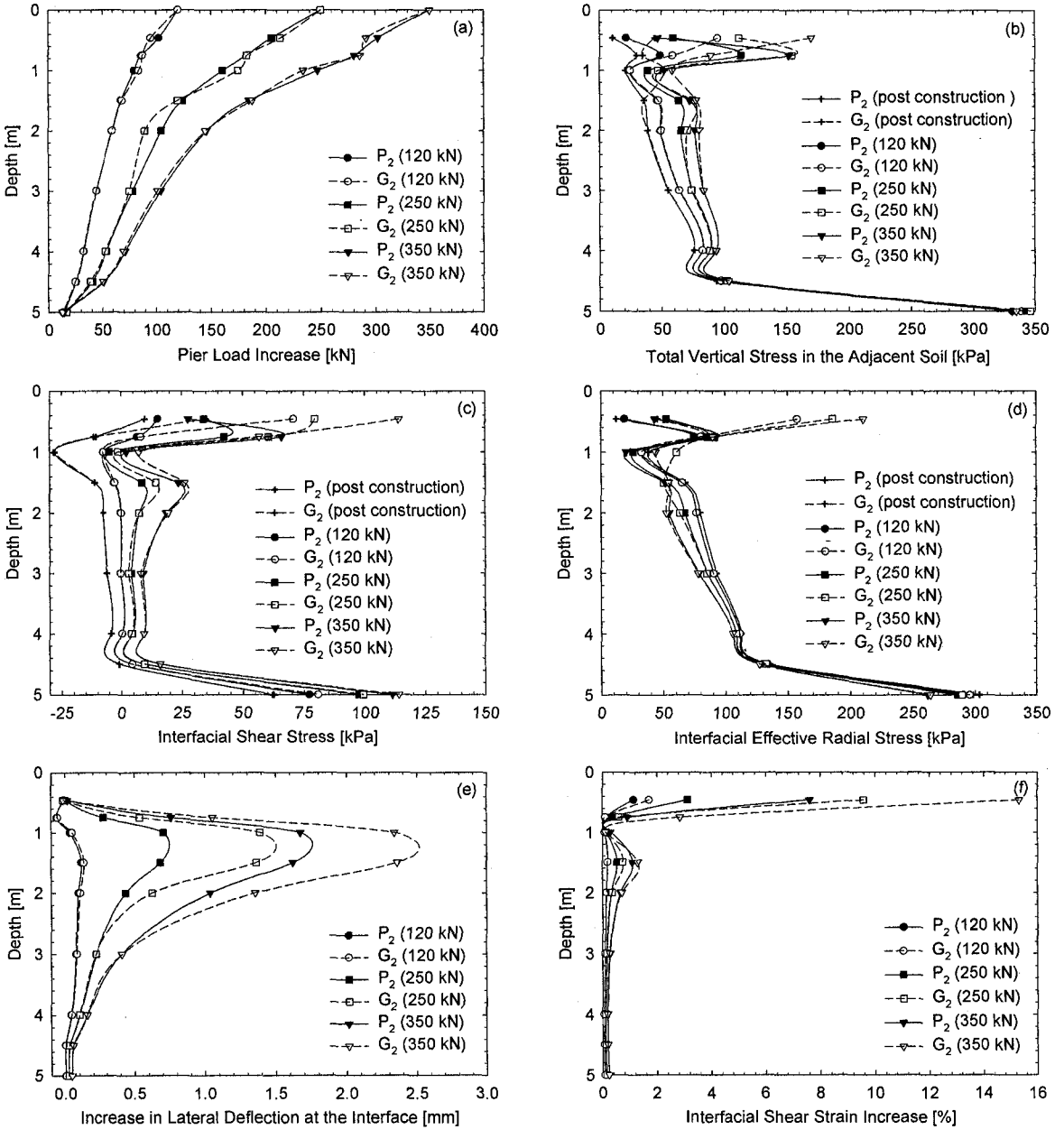

Figure 5.7. Comparison between G_2 and P_2: (a) pier axial load increase; (b) vertical total stress increase in the matrix soil; (c) interfacial shear stress; (d) Interfacial radial stress; (e) interfacial lateral deflection increase; and (f) interfacial shear strain increase

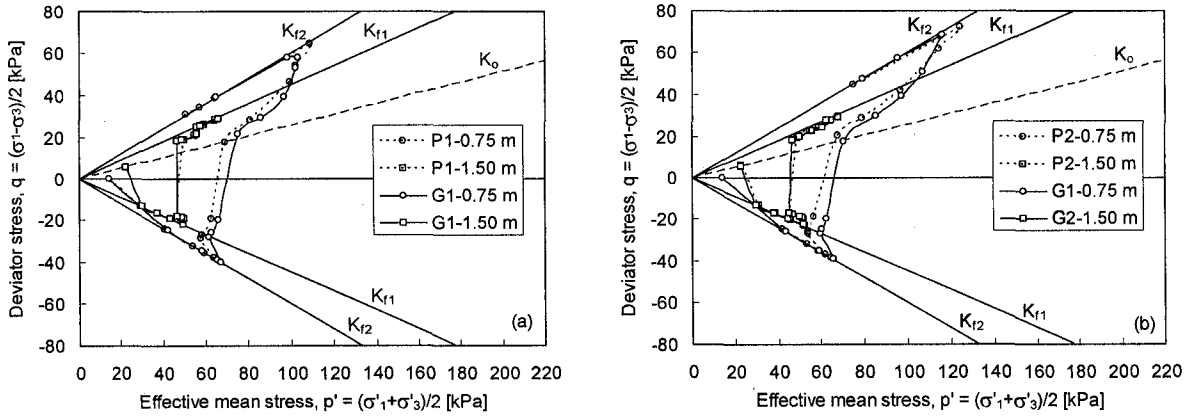

Figure 5.8. Stress paths in the matrix soil adjacent to pier groups and single piers

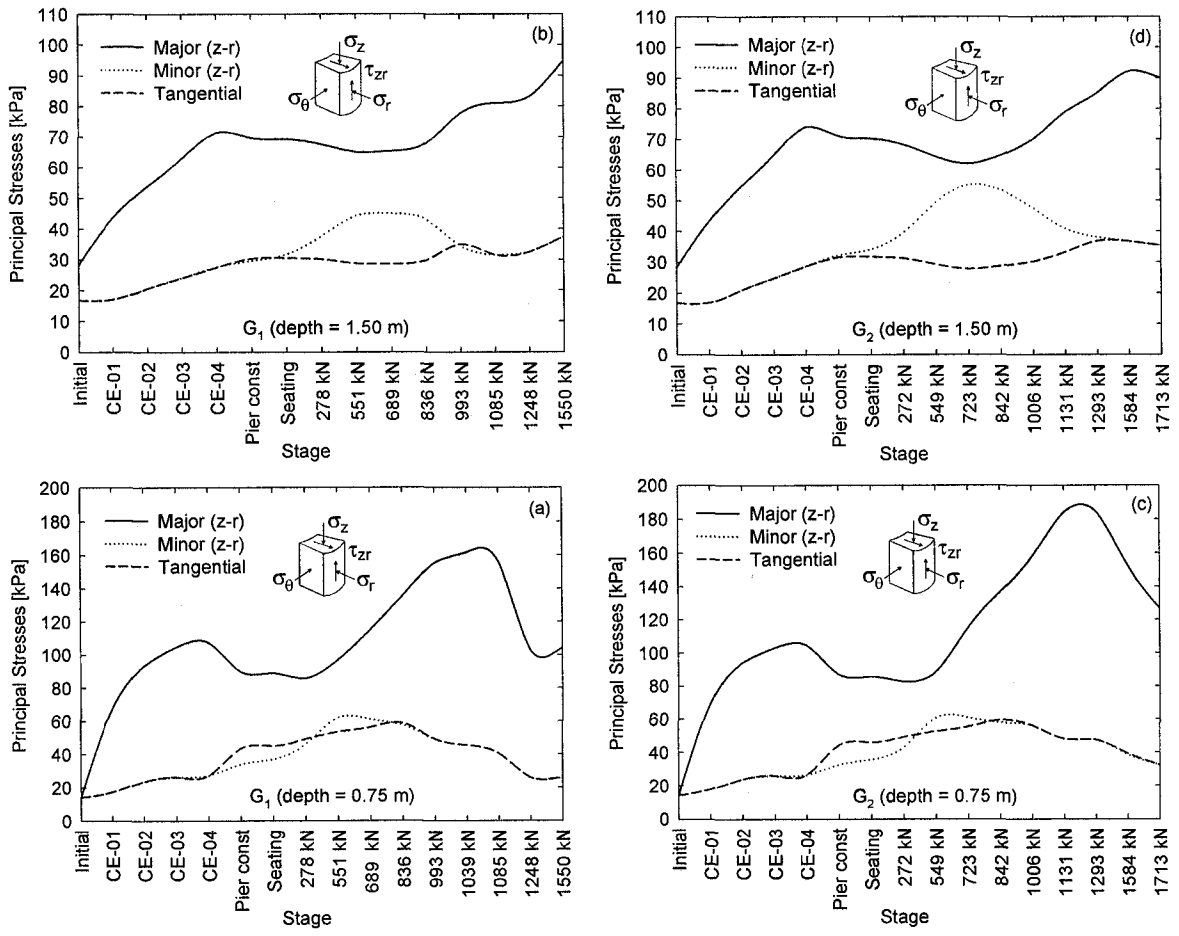

Figure 5.9. Principal stresses in two soil elements adjacent to G_1 and G_2

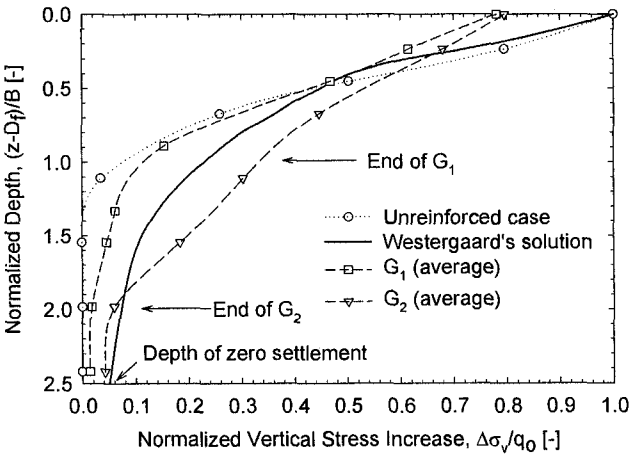

Figure 5.10. Distribution of $\Delta\sigma_v$ underneath the footing as a function of footing width

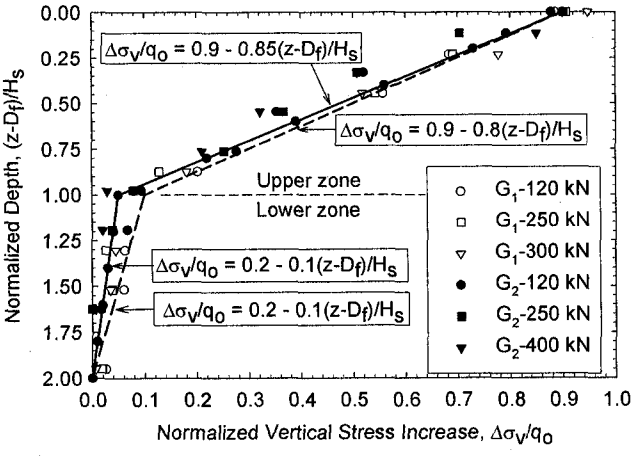

Figure 5.11. Distribution of $\Delta\sigma_v$ underneath the footings as a function of shaft length

CHAPTER 6: GENERAL CONCLUSIONS AND RECOMMENDATIONS FOR FURTHER STUDY

GENERAL CONCLUSIONS

The most important conclusions drawn from the four research studies presented in this dissertation are as follows:

1. The process of lateral consolidation prior to vertical loading delays consolidation by increasing the apparent preconsolidation pressure. As the result of the increase in preconsolidation pressure, it is possible to go to the right of the isotropic consolidation envelope. For the laterally consolidated specimens, both compression index C_c and recompression index C_r were greatly reduced, rendering the soil much stiffer after lateral consolidation.
2. The effective stress friction angle of the soil increased from 33 degrees (*CU*) to 40 degrees (*LCU-*K_o). The deviator stress at failure obtained from *LCD* tests is significantly higher than all other tests. The development of cohesion is believed to result from over-consolidation of the sample (soil fabric change) and, again, because the friction between soil particles was fully reversed.
3. Secant modulus values for *LCU-*K_{iso} showed increases up to 1.6 times the *CU* test values. Stress-strain curves from *LCU-*K_o produced secant modulus values up to 6 times higher than those from *CU* test results. Stress-strain curves from the *LCD* test series indicate an almost perfectly elastic-plastic behavior with an extremely high secant modulus. It is believed by the authors that stored energy in the form

of inter-particle shear stresses and the rotation of soil particles after full friction reversals account for this behavior.

4. The load-deflection behavior and stress transfer mechanics of both short and long piers can be well captured using the FE model developed in this study. Good correspondence between the field data and the results of the numerical simulations were achieved only when the pier hole was radially and axially expanded to simulate the stress field generated by the expansion of constructed piers. These results suggest that the expansion of the pier cavity is an important mechanism in the behavior of rammed aggregate piers.
5. The increase in radial stress due to pier installation provides a marked increase in confinement around the piers which significantly stiffens the pier during pier loading. Construction of the bottom bulb provides a more pronounced influence on the load-displacement behavior of the shorter pier (P_2) compared to the longer pier (P_3).
6. Most of the applied compressive load is dissipated within the range where bulging deformation occurs. The interfacial shear stress becomes relatively uniform in P_2 once the design load is exceeded. Continuing to increase the compressive load on P_3 tends to promote build-up of interfacial shear stresses at bulging depth rather than distributing to the lower part of the pier.
7. The installation of rammed aggregate piers pre-stresses the matrix soil and creates a pre-mobilized uplift resultant force acting on the pier prior to pier loading. During subsequent pier loading, the applied vertical compressive stress is initially resisted by the shaft resistance that develops along the pier-soil contact. As the

compressive load increases, the shaft resistance becomes fully mobilized first at the top of the pier and then propagates down the shaft of the pier.

8. The mode of deformation could be well recognized from the load-settlement curves obtained from tell-tale reference plates. At test site conditions, the mode of pier deformation depends on the length of the piers and can be identified by monitoring the lateral displacement in the adjacent soil using inclinometers.
9. The group efficiency for rammed aggregate piers can be reasonably taken as 1.0. The stress concentration ratio was found to increase with the applied compressive load. As the compressive load exceeded the yielding load, the stress concentration ratio dropped dramatically to a lower level. Vertical compressive stress was found to dissipate more rapidly along the shaft of an isolated pier when compared to an individual pier of the pier group.
10. The bearing capacity values calculated based on shearing below pier tip failure mechanism were close to the observed values. On the other hand, the bearing capacity values calculated based on bulging failure mechanism are slightly overestimated. Shearing within and below the pier-reinforced zone were found to seldom control the bearing capacity failure.
11. The mechanical behaviors of a group of rammed aggregate piers can be well captured by the unit cell FE model developed in this study. The load-settlement response of a pier group can be predicted from the modeling of an isolated pier of the same length and diameter.
12. Construction of the footing on top of the pier group increased the vertical stress in the matrix soil within the first meter from the footing bottom. As the vertical

stress in the matrix soil increased, the lateral stress in the matrix soil also increased thus promoted the development of the interfacial shear stress. The improvement in the interfacial shears tress, however, was found to be insignificant in this study. As a result, the behavior of the unit cell and the isolated pier are quite similar in terms of the distribution with depth of the axial pier load.

13. The tangential stress was found to be the minor principal stress in the matrix soil adjacent to the pier. The tangential stress only became the intermediate principal in the soil element located at 0.75 m when the compressive load was less than 278 kN.

14. The vertical stress distribution underneath pier-supported footings can be well characterized by a bi-linear function obtained from FE results. Using the Westergaard's method can potentially result in an inaccurate stress distribution underneath pier-supported footings. The stiffness-based approach overestimated the total settlement of G_1 and underestimated the total settlement of G_2. Using the modulus-based method, the pier length can be accounted for in the analysis. Compared to the settlements calculated by the stiffness-based method, the modulus-based method provided better results which were very close to the measured values.

RECOMMENDATIONS FOR FURTHER STUDY

Some recommendations for further study are as follows:

1. The stress path control tests presented in Chapter 2 should be performed in a true triaxial compression system and/or hollow cylinder to distinguish the influences of the tangential stress and the radial stress.
2. Small strain LVTD should be attached along the samples to more accurately measure the modulus of the soil at small-strain condition.
3. The whole yield surface of the material including the extension part should be determined. This can be done by changing the orientation and direction of the stress path control tests.
4. Horizontal displacement during lateral consolidation should be measured.
5. A strain-softening constitutive model should be used to model the constitutive behaviors of the compacted aggregate.
6. The influences of the interface elements should be investigated. The stiffness of the interface elements can be estimated by calibrating the calculated load-settlement curve with the measured curve.
7. The cavity expansion modeling should be performed in the undrained condition. Time rate consolidation of the soil adjacent to rammed aggregate pier should be modeled. The increase in shear strength and stiffness of the adjacent soil after consolidation can be accounted for when using appropriate elasto-plastic models (e.g., Modified Cam-Clay model or hardening/softening cap models).
8. Behaviors of rammed aggregate piers in long-term condition (creep) should be modeled.

9. Vertical stress distribution along the pier shaft and the stress concentration ratio of rammed aggregate piers should be measured for different applications (e.g., embankment, storage tank, and floor slab support).
10. Variation in pore water pressure around rammed aggregate piers should be measured during pier installation and pier loading.
11. Long-term modulus load test should be performed to account for the consolidation settlement in the lower zone and also the creep of rammed aggregate piers.
12. Fully three-dimensional analysis should be performed to further investigate the group effect and stress concentration top of the piers. The three-dimensional model can also be used to investigate the support mechanism of rammed aggregate piers in embankment and slope stabilization.

GENERAL ACKNOWLEDGEMENT

I deeply appreciate the guidance throughout the course of my study at Iowa State University that I have received from my advisor, Dr. David J. White. This dissertation would have never been completed without his assistance and advice. His brilliance and passionate in research are far beyond my expectation.

The assistance that I have received from the members of the advisory committee, Dr. Vernon Schaefer, Dr. Radhey Sharma, Dr. Charles Jahren, and Dr. Igor Beresnev is gratefully appreciated.

The discussions with Dr. Kord Wissmann on the finite element modeling of rammed aggregate piers are extremely valuable. My special thanks go to Dr. Muhannad Suleiman, Mr. Donald Davidson Jr., Mr. Longjie Hong, and Mr. Hong Yang for their assistance and camaraderie.

My deepest appreciation is extended to my lovely wife, Hong Ha, and my two little boys, Truong Son and Truong Minh, for their constant love, understanding, and encouragement throughout this project. The help and the support that I have received from our Vietnamese friends in Ames are greatly appreciated.

Finally, the financial support from Geopier Foundation Company, Inc. in conducting this research is greatfully acknowledged.

APPENDIX A: DATA FROM STRESS PATH CONTROL TESTS

Table A.1. Test series CU (σ_3 = 25 kPa) - sample preparation:

Location					Loc No.		
Operator	HTP				Sample No.		B1
Test type	EX	CU	CD	UU	Date started	8/8/2003	17:30
Specimen type	Undisturbed	Remoulded	Recompacted		Nominal diameter		50
Specimen preparation	Compact in an 2.8x5.6 mold with 5 blows on each side						
Soil type and description	Western Iowa loess						

MEASUREMENTS (mm)			INITIAL CONDITIONS	
Initial length			Area Ao (cm^2)	19.63
			Volume Vo (cm^3)	196.25
Average L_o	mm	100	Density (g/cm^3)	1.94
Initial diameter			Moisture content (%)	21.02
Average D_o	mm	50	Dry density (g/cm^3)	1.605

WEIGHINGS	Trimmings	Specimen			LOCATION OF SPECIMEN
		initially	after test		
Container no.					
Specimen + cont.					
Container					
Mass of specimen	w_o	381.10	400.30	w_f	
Dry spec. + cont.					
Dry mass of spec.			314.90	w_d	
Moiture		66.20	85.40	M_f	
Moiture content		21.02	27.12		
Volume of solid		118.89			
Volume of the void		77.36			
Void ratio		0.65			

Table A.2. Test series CU (σ_3 = 25 kPa) - shearing:

Date					Location								Sample No.								0
Test	CD	CU	EX	UU	Membrane			With	side drains				Effective cell pressure							25	kPa
Rate of strain			0.615	mm/min	Operator		HTP	Without					Cell pressure							235	kPa
								Proving ring No.					Back pressure							210	kPa
Consolidated length			100	mm	Consolidated area					19.63	cm^2		Consolidated volume							9.10	cm^3
Corr.	Strain			Axial Load	Pore pressure			Deviator stress								Stress ratio					
Area	Displ.	Diff.	ε	Read	Load	U	Diff.	Stress	p'	p	q	p-cam	p'-cam	q-cam	σ1	σ3	σ'1	σ'3	σ'1/σ'3	p-p'
cm^2	mm		%	N	N	kPa	kPa	kPa	kPa	kPa	kPa	kPa	kPa	kPa	kPa	kPa	kPa	kPa	-	kPa
19.6	0.0	0.0	0.0	-63	0	211	0	0	25	235	0	235	25	0	235	235	25	25	1.0	25
19.7	0.3	0.3	0.3	-11	52	214	3	26	35	248	13	244	30	26	261	235	47	22	2.2	38
19.7	0.5	0.5	0.5	22	85	215	4	43	42	257	22	249	35	43	278	235	63	21	3.0	47
19.8	0.8	0.8	0.8	43	106	214	3	54	48	262	27	253	40	54	289	235	75	22	3.4	52
19.8	1.0	1.0	1.0	57	120	213	2	60	53	265	30	255	43	60	295	235	82	23	3.6	55
19.9	1.3	1.3	1.3	75	138	210	-1	69	60	270	35	258	49	69	304	235	94	26	3.6	60
19.9	1.5	1.5	1.5	87	150	209	-2	75	64	273	38	260	52	75	310	235	101	27	3.7	63
20.0	1.8	1.8	1.8	98	161	207	-4	81	69	275	40	262	56	81	316	235	109	29	3.7	65
20.0	2.0	2.0	2.0	107	170	204	-7	85	74	277	42	263	60	85	320	235	116	32	3.6	67
20.1	2.3	2.3	2.3	112	175	203	-8	87	76	279	44	264	62	87	322	235	119	33	3.6	69
20.1	2.5	2.5	2.5	120	183	202	-9	91	79	280	45	265	64	91	326	235	124	34	3.6	70
20.2	2.8	2.8	2.8	126	189	201	-10	94	81	282	47	266	66	94	329	235	128	35	3.6	72
20.2	3.0	3.0	3.0	131	194	200	-11	96	83	283	48	267	68	96	331	235	131	36	3.6	73
20.3	3.3	3.3	3.3	136	199	199	-12	98	86	284	49	268	69	98	333	235	134	37	3.6	74
20.3	3.5	3.5	3.5	139	202	198	-13	99	87	285	50	268	71	99	334	235	136	38	3.6	75
20.4	3.8	3.8	3.8	143	206	197	-14	101	89	285	50	269	72	101	336	235	139	39	3.6	75
20.4	4.0	4.0	4.0	148	211	196	-15	103	91	287	52	269	74	103	338	235	142	40	3.6	77
20.5	4.5	4.5	4.5	156	219	195	-16	107	94	288	53	271	76	107	342	235	147	41	3.6	78
20.7	5.0	5.0	5.0	164	227	194	-17	110	96	290	55	272	78	110	345	235	151	42	3.6	80
20.8	5.5	5.5	5.5	171	234	193	-18	113	99	291	56	273	80	113	348	235	155	43	3.6	81
20.9	6.0	6.0	6.0	176	239	192	-19	114	101	292	57	273	82	114	349	235	157	44	3.6	82
21.0	6.5	6.5	6.5	183	246	192	-20	117	103	294	59	274	83	117	352	235	161	45	3.6	84
21.1	7.0	7.0	7.0	189	252	191	-20	119	104	295	60	275	84	119	354	235	163	45	3.6	85
21.2	7.5	7.5	7.5	194	257	190	-21	121	106	296	61	275	86	121	356	235	166	46	3.6	86
21.3	8.0	8.0	8.0	200	263	189	-22	123	108	297	62	276	88	123	358	235	169	47	3.6	87
21.4	8.5	8.5	8.5	208	271	189	-23	126	110	298	63	277	89	126	361	235	173	48	3.6	88
21.6	9.0	9.0	9.0	211	274	188	-23	127	111	298	63	277	90	127	362	235	174	48	3.6	88
21.7	9.5	9.5	9.5	216	279	188	-24	129	112	299	64	278	91	129	364	235	176	49	3.6	89
21.8	10.0	10.0	10.0	220	283	187	-24	130	113	300	65	278	92	130	365	235	178	49	3.6	90
21.9	10.5	10.5	10.5	225	288	186	-25	131	115	301	66	279	93	131	366	235	180	50	3.6	91
22.1	11.0	11.0	11.0	230	293	186	-26	133	116	301	66	279	94	133	368	235	182	51	3.6	91
22.2	11.5	11.5	11.5	235	298	185	-26	134	118	302	67	280	95	134	369	235	184	51	3.6	92
22.3	12.0	12.0	12.0	238	301	185	-27	135	118	302	67	280	96	135	370	235	185	52	3.6	92
22.4	12.5	12.5	12.5	241	304	184	-27	135	119	303	68	280	97	135	370	235	186	52	3.6	93
22.6	13.0	13.0	13.0	246	309	184	-28	137	120	303	68	281	98	137	372	235	188	53	3.6	93
22.7	13.5	13.5	13.5	250	313	183	-28	138	121	304	69	281	99	138	373	235	190	53	3.6	94
22.8	14.0	14.0	14.0	254	317	183	-29	139	122	304	69	281	99	139	374	235	191	54	3.6	94
23.0	14.5	14.5	14.5	260	323	182	-29	141	124	305	70	282	101	141	376	235	194	54	3.6	95
23.1	15.0	15.0	15.0	262	325	182	-30	141	124	305	70	282	101	141	376	235	194	55	3.6	95
23.2	15.5	15.5	15.5	265	328	181	-30	141	125	306	71	282	102	141	376	235	195	55	3.5	96
23.4	16.0	16.0	16.0	271	334	181	-30	143	126	306	71	283	102	143	378	235	197	55	3.6	96
23.5	16.5	16.5	16.5	276	339	181	-31	144	127	307	72	283	103	144	379	235	199	56	3.6	97
23.6	17.0	17.0	17.0	278	341	180	-31	144	128	307	72	283	104	144	379	235	199	56	3.6	97
23.8	17.5	17.5	17.5	282	345	180	-32	145	128	307	72	283	104	145	380	235	200	57	3.5	97
23.9	18.0	18.0	18.0	287	350	179	-32	146	130	308	73	284	105	146	381	235	202	57	3.5	98
24.1	18.5	18.5	18.5	290	353	179	-32	147	130	308	73	284	106	147	382	235	203	57	3.6	98
24.2	19.0	19.0	19.0	294	357	178	-33	147	131	309	74	284	107	147	382	235	204	58	3.5	99
24.4	19.5	19.5	19.5	298	361	178	-34	148	132	309	74	284	108	148	383	235	206	59	3.5	99
24.5	20.0	20.0	20.0	301	364	178	-34	148	132	309	74	284	108	148	383	235	206	59	3.5	99

Note: Shaded area indicates the yielding zone

Table A.3. Test series CU (σ_3 = 50 kPa) - sample preparation:

Location					Loc No.		
Operator	HTP				Sample No.		B9
Test type	EX	CU	CD	UU	Date started	8/22/2003	10:00 AM
Specimen type	Undisturbed	Remoulded	Recompacted		Nominal diameter		50
Specimen preparation	Compact in an 2.8x5.6 mold with 5 blows on each side						
Soil type and description	Western Iowa loess						

MEASUREMENTS (mm)			INITIAL CONDITIONS	
Initial length			Area Ao (cm^2)	19.63
			Volume Vo (cm^3)	196.25
Average L_o	mm	100	Density (g/cm^3)	1.92
Initial diameter			Moisture content (%)	17.77
Average D_o	mm	50	Dry density (g/cm^3)	1.632

WEIGHINGS	Trimmings	Specimen			LOCATION OF SPECIMEN
		initially	after test		
Container no.					
Specimen + cont.					
Container					
Mass of specimen	w_o	377.10	398.40	w_f	
Dry spec. + cont.					
Dry mass of spec.			320.20	w_d	
Moiture		56.90	78.20	M_f	
Moiture content		17.77	24.42		
Volume of solid		120.89			
Volume of the void		75.36			
Void ratio		0.62			

Table A.4. Test series CU (σ_3 = 50 kPa) - shearing:

Date					Location								Sample No.							0
Test	CD	CU	EX	UU	Membrane			With	side drains				Effective cell pressure						50	kPa
Rate of strain			0.615	mm/min	Operator		HTP	Without					Cell pressure						260	kPa
								Proving ring No.					Back pressure						210	kPa
Consolidated length			100	mm	Consolidated area					19.63	cm^2		Consolidated volume						2.80	cm^3
Corr.	Strain			Axial Load	Pore pressure			Deviator stress								Stress ratio						
Area	Displ.	Diff.	ε	Read	Load	U	Diff.	Stress	p'	p	q	p-cam	p'-cam	q-cam	σ1	σ3	σ'1	σ'3	σ'1/σ'3	p-p'
cm^2	mm		%	N	N	kPa	kPa	kPa	kPa	kPa	kPa	kPa	kPa	kPa	kPa	kPa	kPa	kPa	-	kPa
19.6	0.0	0.0	0.0	19	0	213	0	0	50	260	0	260	50	0	260	260	50	50	1.0	50
19.7	0.3	0.3	0.3	96	77	215	2	39	66	280	20	273	60	39	299	260	84	48	1.8	70
19.7	0.5	0.5	0.5	153	134	216	5	68	77	294	34	283	67	68	328	260	110	45	2.4	84
19.8	0.8	0.8	0.8	189	170	218	5	86	86	303	43	289	73	86	346	260	128	45	2.8	93
19.8	1.0	1.0	1.0	215	196	217	4	99	94	309	49	293	78	99	359	260	142	46	3.1	99
19.9	1.3	1.3	1.3	235	216	215	2	109	101	314	54	296	83	109	369	260	154	48	3.2	104
19.9	1.5	1.5	1.5	246	227	214	1	114	104	317	57	298	86	114	374	260	160	49	3.3	107
20.0	1.8	1.8	1.8	257	238	212	-1	119	109	320	60	300	90	119	379	260	167	51	3.3	110
20.0	2.0	2.0	2.0	265	246	211	-2	123	112	321	61	301	92	123	383	260	172	52	3.3	111
20.1	2.3	2.3	2.3	271	252	210	-3	126	114	323	63	302	94	126	386	260	176	53	3.3	113
20.1	2.5	2.5	2.5	279	260	209	-4	129	117	325	65	303	96	129	389	260	180	54	3.3	115
20.2	2.8	2.8	2.8	284	265	209	-5	131	119	326	66	304	97	131	391	260	183	55	3.4	116
20.2	3.0	3.0	3.0	287	268	208	-5	132	120	326	66	304	98	132	392	260	184	55	3.4	116
20.3	3.3	3.3	3.3	293	274	207	-6	135	122	328	68	305	100	135	395	260	188	56	3.4	118
20.3	3.5	3.5	3.5	296	277	207	-6	136	123	328	68	305	100	136	396	260	189	56	3.4	118
20.4	3.8	3.8	3.8	301	282	207	-7	138	124	329	69	306	102	138	398	260	192	57	3.4	119
20.4	4.0	4.0	4.0	303	284	206	-7	139	125	329	69	306	102	139	399	260	193	57	3.4	119
20.5	4.5	4.5	4.5	310	291	205	-8	142	127	331	71	307	104	142	402	260	197	58	3.4	121
20.7	5.0	5.0	5.0	317	298	205	-9	144	129	332	72	308	106	144	404	260	200	59	3.4	122
20.8	5.5	5.5	5.5	324	305	204	-9	147	131	333	73	309	107	147	407	260	203	59	3.4	123
20.9	6.0	6.0	6.0	328	309	204	-9	148	132	334	74	309	107	148	408	260	204	59	3.5	124
21.0	6.5	6.5	6.5	335	316	204	-10	151	133	335	75	310	109	151	411	260	207	60	3.5	125
21.1	7.0	7.0	7.0	339	320	203	-10	152	134	336	76	311	110	152	412	260	209	60	3.5	126
21.2	7.5	7.5	7.5	346	327	203	-11	154	136	337	77	311	111	154	414	260	212	61	3.5	127
21.3	8.0	8.0	8.0	350	331	202	-11	155	137	338	78	312	112	155	415	260	213	61	3.5	128
21.4	8.5	8.5	8.5	355	336	202	-11	157	138	338	78	312	112	157	417	260	215	61	3.5	128
21.6	9.0	9.0	9.0	361	342	202	-11	159	139	339	79	313	113	159	419	260	217	61	3.6	129
21.7	9.5	9.5	9.5	366	347	201	-12	160	141	340	80	313	114	160	420	260	219	62	3.5	130
21.8	10.0	10.0	10.0	370	351	201	-13	161	141	340	80	314	115	161	421	260	220	63	3.5	130
21.9	10.5	10.5	10.5	375	356	200	-13	162	143	341	81	314	116	162	422	260	222	63	3.5	131
22.1	11.0	11.0	11.0	380	361	200	-13	164	143	342	82	315	117	164	424	260	224	63	3.6	132
22.2	11.5	11.5	11.5	384	365	200	-14	165	144	342	82	315	117	165	425	260	225	64	3.5	132
22.3	12.0	12.0	12.0	388	369	199	-14	165	145	343	83	315	118	165	425	260	226	64	3.5	133
22.4	12.5	12.5	12.5	394	375	199	-15	167	147	344	84	316	119	167	427	260	229	65	3.5	134
22.6	13.0	13.0	13.0	396	377	198	-15	167	147	344	84	316	120	167	427	260	229	65	3.5	134
22.7	13.5	13.5	13.5	396	377	198	-15	166	147	343	83	315	119	166	426	260	228	65	3.5	133
22.8	14.0	14.0	14.0	407	388	197	-16	170	150	345	85	317	122	170	430	260	233	66	3.5	135
23.0	14.5	14.5	14.5	410	391	197	-16	170	150	345	85	317	122	170	430	260	233	66	3.5	135
23.1	15.0	15.0	15.0	410	391	196	-17	169	150	345	85	316	122	169	429	260	233	67	3.5	135
23.3	15.8	15.8	15.8	418	399	196	-17	171	151	346	86	317	123	171	431	260	235	67	3.5	136
23.4	16.0	16.0	16.0	421	402	196	-18	172	152	346	86	317	124	172	432	260	237	68	3.5	136
23.5	16.5	16.5	16.5	424	405	195	-18	172	153	346	86	317	124	172	432	260	237	68	3.5	136
23.6	17.0	17.0	17.0	429	410	195	-18	173	153	347	87	318	125	173	433	260	238	68	3.5	137
23.8	17.5	17.5	17.5	427	408	194	-19	172	153	346	86	317	125	172	432	260	238	69	3.4	136
23.9	18.0	18.0	18.0	435	416	194	-19	174	154	347	87	318	126	174	434	260	240	69	3.5	137
24.1	18.5	18.5	18.5	440	421	194	-19	175	155	347	87	318	126	175	435	260	241	69	3.5	137
24.2	19.0	19.0	19.0	440	421	193	-20	174	155	347	87	318	127	174	434	260	241	70	3.4	137
24.4	19.5	19.5	19.5	448	429	193	-21	176	157	348	88	319	128	176	436	260	243	71	3.5	138
24.5	20.0	20.0	20.0	446	427	193	-21	174	156	347	87	318	128	174	434	260	242	71	3.4	137

Note: Shaded area indicates the yielding zone

Table A.5. Test series CU (σ_3 = 75 kPa) - sample preparation:

Location					Loc No.		
Operator	HTP				Sample No.		B3
Test type	EX	CU	CD	UU	Date started	8/11/2003	17:30
Specimen type	Undisturbed	Remoulded	Recompacted		Nominal diameter		50
Specimen preparation	Compact in an 2.8x5.6 mold with 5 blows on each side						
Soil type and description	Western Iowa loess						

MEASUREMENTS (mm)			INITIAL CONDITIONS	
Initial length			Area Ao (cm^2)	19.63
			Volume Vo (cm^3)	196.25
Average Lo	mm	100	Density (g/cm^3)	1.91
Initial diameter			Moisture content (%)	18.84
Average Do	mm	50	Dry density (g/cm^3)	1.604

WEIGHINGS	Trimmings	Specimen			LOCATION OF SPECIMEN
		initially	after test		
Container no.					
Specimen + cont.					
Container					
Mass of specimen	Wo	374	395.6	Wf	
Dry spec. + cont.					
Dry mass of spec.			314.7	Wd	
Moiture		59.30	80.90	Mf	
Moiture content		18.84	25.71		
Volume of solid		118.81			
Volume of the void		77.44			
Void ratio		0.65			

Table A.6. Test series CU (σ_3 = 75 kPa) - shearing:

Date					Location								Sample No.							0
Test	CD	CU	EX	UU	Membrane			With	side drains				Effective cell pressure						75	kPa
Rate of strain			0.615	mm / min	Operator		HTP	Without					Cell pressure						285	kPa
								Proving ring No.					Back pressure						210	kPa
Consolidated length			100	mm	Consolidated area					19.63	cm^2		Consolidated volume						11.50	cm^3
Corr.	Strain			Axial Load	Pore pressure			Deviator stress								Stress ratio				
Area	Displ.	Diff.	ε	Read	Load	U	Diff.	Stress	p'	p	q	p-cam	p'-cam	q-cam	σ1	σ3	σ'1	σ'3	σ'1/σ'3	p-p'
cm^2	mm		%	N	N	kPa	kPa	kPa	kPa	kPa	kPa	kPa	kPa	kPa	kPa	kPa	kPa	kPa	-	kPa
19.6	0.0	0.0	0.0	-81	0	211	0	0	75	285	0	285	75	0	285	285	75	75	1.0	75
19.7	0.3	0.3	0.3	89	170	215	4	86	114	328	43	314	100	86	371	285	156	71	2.2	118
19.7	0.5	0.5	0.5	138	219	215	4	111	126	341	56	322	108	111	396	285	181	71	2.5	131
19.8	0.8	0.8	0.8	153	234	215	3	118	130	344	59	324	111	118	403	285	189	72	2.6	134
19.8	1.0	1.0	1.0	155	236	214	2	119	131	344	59	325	112	119	404	285	190	73	2.6	134
19.9	1.3	1.3	1.3	202	283	213	2	142	143	356	71	332	120	142	427	285	214	73	2.9	146
19.9	1.5	1.5	1.5	213	294	213	2	148	147	359	74	334	122	148	433	285	220	73	3.0	149
20.0	1.8	1.8	1.8	198	279	213	2	140	143	355	70	332	120	140	425	285	212	73	2.9	145
20.0	2.0	2.0	2.0	194	275	213	1	137	142	354	69	331	119	137	422	285	210	74	2.8	144
20.1	2.3	2.3	2.3	201	282	212	1	140	143	355	70	332	120	140	425	285	213	74	2.9	145
20.1	2.5	2.5	2.5	209	290	213	1	144	145	357	72	333	121	144	429	285	217	74	2.9	147
20.2	2.8	2.8	2.8	242	323	213	2	160	153	365	80	338	126	160	445	285	232	73	3.2	155
20.2	3.0	3.0	3.0	247	328	213	2	162	154	366	81	339	127	162	447	285	234	73	3.2	156
20.3	3.3	3.3	3.3	250	331	213	2	163	154	367	82	339	127	163	448	285	235	73	3.2	157
20.3	3.5	3.5	3.5	253	334	213	2	164	155	367	82	340	128	164	449	285	236	73	3.2	157
20.4	3.8	3.8	3.8	258	339	213	2	166	156	368	83	340	128	166	451	285	238	73	3.2	158
20.5	4.0	4.0	4.0	261	342	213	2	167	156	369	84	341	129	167	452	285	239	73	3.3	159
20.5	4.3	4.3	4.3	242	323	213	2	158	152	364	79	338	125	158	443	285	230	73	3.1	154
20.5	4.5	4.5	4.5	264	345	213	2	168	157	369	84	341	129	168	453	285	240	73	3.3	159
20.6	4.8	4.8	4.8	269	350	213	2	170	157	370	85	342	129	170	455	285	242	73	3.3	160
20.7	5.0	5.0	5.0	245	326	213	2	158	151	364	79	338	125	158	443	285	229	73	3.1	154
20.8	5.5	5.5	5.5	278	359	213	2	173	159	371	86	343	130	173	458	285	244	73	3.3	161
20.9	6.0	6.0	6.0	261	342	213	2	164	154	367	82	340	127	164	449	285	235	73	3.2	157
21.0	6.5	6.5	6.5	287	368	214	2	175	160	373	88	343	131	175	460	285	246	73	3.4	163
21.1	7.0	7.0	7.0	291	372	213	2	176	160	373	88	344	131	176	461	285	248	73	3.4	163
21.2	7.5	7.5	7.5	297	378	213	2	178	161	374	89	344	132	178	463	285	250	73	3.4	164
21.3	8.0	8.0	8.0	280	361	213	2	169	157	370	85	341	129	169	454	285	241	73	3.3	160
21.5	8.5	8.5	8.5	305	386	213	2	180	162	375	90	345	132	180	465	285	251	73	3.4	165
21.6	9.0	9.0	9.0	310	391	213	2	181	163	376	91	345	133	181	466	285	253	73	3.5	166
21.7	9.6	9.6	9.6	316	397	213	2	183	164	376	91	346	134	183	468	285	255	73	3.5	166
21.8	10.0	10.0	10.0	319	400	213	2	183	164	377	92	346	134	183	468	285	255	73	3.5	167
21.9	10.6	10.6	10.6	324	405	213	2	185	165	377	92	347	134	185	470	285	257	73	3.5	167
22.1	11.0	11.0	11.0	329	410	213	1	186	166	378	93	347	135	186	471	285	258	74	3.5	168
22.2	11.5	11.5	11.5	310	391	212	1	176	161	373	88	344	132	176	461	285	249	74	3.4	163
22.3	12.1	12.1	12.1	338	419	212	1	188	167	379	94	348	136	188	473	285	260	74	3.5	169
22.4	12.5	12.5	12.5	340	421	212	1	188	168	379	94	348	137	188	473	285	261	75	3.5	169
22.6	13.0	13.0	13.0	324	405	212	1	180	164	375	90	345	134	180	465	285	253	75	3.4	165
22.7	13.5	13.5	13.5	351	432	211	0	190	170	380	95	348	138	190	475	285	264	75	3.5	170
22.8	14.0	14.0	14.0	354	435	211	0	191	170	380	95	349	138	191	476	285	264	75	3.5	170
23.0	14.5	14.5	14.5	360	441	211	-1	192	171	381	96	349	139	192	477	285	266	76	3.5	171
23.1	15.0	15.0	15.0	362	443	211	-1	192	171	381	96	349	139	192	477	285	267	76	3.5	171
23.2	15.5	15.5	15.5	368	449	210	-1	193	172	382	97	349	140	193	478	285	268	76	3.5	172
23.4	16.0	16.0	16.0	371	452	210	-2	193	173	382	97	349	141	193	478	285	269	77	3.5	172
23.5	16.5	16.5	16.5	375	456	209	-2	194	173	382	97	350	141	194	479	285	269	77	3.5	172
23.6	17.0	17.0	17.0	354	435	209	-2	184	168	377	92	346	138	184	469	285	260	77	3.4	167
23.8	17.5	17.5	17.5	381	462	209	-3	194	174	382	97	350	142	194	479	285	271	78	3.5	172
23.9	18.0	18.0	18.0	351	432	208	-3	181	168	375	90	345	138	181	466	285	258	78	3.3	165
24.1	18.5	18.5	18.5	387	468	208	-3	194	175	382	97	350	143	194	479	285	271	78	3.5	172
24.2	19.0	19.0	19.0	353	434	208	-4	179	168	375	90	345	138	179	464	285	256	79	3.3	165
24.4	19.5	19.5	19.5	395	476	207	-4	195	176	383	98	350	144	195	480	285	273	79	3.5	173
24.5	20	20.0	20.0	353	434	207	-4	177	167	373	88	344	138	177	462	285	255	79	3.2	163

Note: Shaded area indicates the yielding zone

Table A.7. Test series CU (σ_3 = 100 kPa) - sample preparation:

Location					Loc No.		
Operator	HTP				Sample No.		B4
Test type	EX	CU	CD	UU	Date started	8/12/2003	3:30 PM
Specimen type	Undisturbed	Remoulded	Recompacted		Nominal diameter		50
Specimen preparation	Compact in an 2.8x5.6 mold with 5 blows on each side						
Soil type and description	Western Iowa loess						

MEASUREMENTS (mm)			INITIAL CONDITIONS	
Initial length			Area Ao (cm^2)	19.63
			Volume Vo (cm^3)	196.25
Average L_o	mm	100	Density (g/cm^3)	1.91
Initial diameter			Moisture content (%)	19.16
Average D_o	mm	50	Dry density (g/cm^3)	1.606

WEIGHINGS	Trimmings	Specimen			LOCATION OF SPECIMEN
		initially	after test		
Container no.					
Specimen + cont.					
Container					
Mass of specimen	W_o	375.6	397.7	W_f	
Dry spec. + cont.					
Dry mass of spec.			315.2	W_d	
Moiture		60.40	82.50	M_f	
Moiture content		19.16	26.17		
Volume of solid		119.00			
Volume of the void		77.25			
Void ratio		0.65			

Table A.8. Test series CU (σ_3 = 100 kPa) - shearing:

Date					Location										Sample No.						0
Test	CD	CU	EX	UU	Membrane			With	side drains						Effective cell pressure					100	kPa
Rate of strain			0.615	mm/min	Operator	HTP		Without							Cell pressure					310	kPa
								Proving ring No.							Back pressure					210	kPa
Consolidated length			100	mm	Consolidated area					19.63	cm^2				Consolidated volume					4.02	cm^3
Corr.	Strain			Axial Load	Pore pressure			Deviator stress							Stress ratio						
Area	Displ.	Diff.	ε	Read	Load	U	Diff.	Stress	p'	p	q	p-cam	p'-cam	q-cam	σ1	σ3	σ'1	σ'3	σ'1/σ'3	p-p'	
cm^2	mm		%	N	N	kPa	kPa	kPa	kPa	kPa	kPa	kPa	kPa	kPa	kPa	kPa	kPa	kPa	-	kPa	
19.6	0.0	0.0	0.0	-150	0	213	0	0	100	310	0	310	100	0	310	310	100	100	1.0	100	
19.7	0.3	0.3	0.3	-76	74	213	0	38	117	329	19	323	112	38	348	310	135	100	1.3	119	
19.7	0.5	0.5	0.5	-20	130	213	0	66	131	343	33	332	121	66	376	310	163	100	1.6	133	
19.8	0.8	0.8	0.8	30	180	216	3	91	141	356	46	340	126	91	401	310	185	97	1.9	146	
19.8	1.0	1.0	1.0	87	237	220	7	120	151	370	60	350	132	120	430	310	210	93	2.3	160	
19.9	1.3	1.3	1.3	139	289	223	10	145	161	383	73	358	137	145	455	310	232	90	2.6	173	
19.9	1.5	1.5	1.5	174	324	225	12	163	168	391	81	364	141	163	473	310	248	88	2.8	181	
20.0	1.8	1.8	1.8	198	348	226	13	174	173	397	87	368	144	174	484	310	258	87	3.0	187	
20.0	2.0	2.0	2.0	213	363	227	14	181	175	401	91	370	145	181	491	310	264	86	3.1	191	
20.1	2.3	2.3	2.3	224	374	227	14	186	178	403	93	372	147	186	496	310	269	86	3.1	193	
20.1	2.5	2.5	2.5	235	385	228	15	191	179	406	96	374	148	191	501	310	273	85	3.2	196	
20.2	2.8	2.8	2.8	244	394	228	15	195	181	408	98	375	149	195	505	310	277	85	3.3	198	
20.2	3.0	3.0	3.0	252	402	228	15	199	183	409	99	376	150	199	509	310	281	85	3.3	199	
20.3	3.3	3.3	3.3	262	412	229	16	203	184	412	102	378	151	203	513	310	284	84	3.4	202	
20.3	3.5	3.5	3.5	263	413	229	16	203	184	412	102	378	151	203	513	310	284	84	3.4	202	
20.4	3.8	3.8	3.8	271	421	229	16	206	186	413	103	379	152	206	516	310	287	84	3.4	203	
20.4	4.0	4.0	4.0	273	423	230	17	207	185	413	103	379	151	207	517	310	287	83	3.5	203	
20.5	4.3	4.3	4.3	282	432	230	17	211	187	415	105	380	152	211	521	310	291	83	3.5	205	
20.7	5.0	5.0	5.0	293	443	230	17	214	189	417	107	381	153	214	524	310	294	83	3.5	207	
20.8	5.5	5.5	5.5	300	450	231	18	217	189	418	108	382	154	217	527	310	296	83	3.6	208	
20.9	6.0	6.0	6.0	309	459	231	18	220	191	420	110	383	155	220	530	310	299	83	3.6	210	
21.0	6.5	6.5	6.5	312	462	231	18	220	191	420	110	383	155	220	530	310	300	83	3.6	210	
21.1	7.0	7.0	7.0	323	473	231	18	224	193	422	112	385	156	224	534	310	304	83	3.7	212	
21.2	7.5	7.5	7.5	326	476	231	18	224	193	422	112	385	156	224	534	310	304	83	3.7	212	
21.3	8.0	8.0	8.0	331	481	230	17	225	194	423	113	385	157	225	535	310	305	83	3.7	213	
21.4	8.5	8.5	8.5	336	486	230	17	227	195	423	113	386	158	227	537	310	307	83	3.7	213	
21.6	9.0	9.0	9.0	347	497	230	17	230	197	425	115	387	159	230	540	310	310	83	3.7	215	
21.7	9.5	9.5	9.5	350	500	230	17	231	197	425	115	387	159	231	541	310	311	84	3.7	215	
21.8	10.0	10.0	10.0	358	508	229	16	233	199	426	116	388	161	233	543	310	314	84	3.7	216	
21.9	10.5	10.5	10.5	364	514	229	16	234	200	427	117	388	162	234	544	310	316	85	3.7	217	
22.1	11.0	11.0	11.0	366	516	228	15	234	201	427	117	388	162	234	544	310	316	85	3.7	217	
22.2	11.5	11.5	11.5	372	522	228	15	235	201	428	118	388	162	235	545	310	317	85	3.7	218	
22.3	12.0	12.0	12.0	380	530	228	15	238	203	429	119	389	164	238	548	310	320	86	3.7	219	
22.4	12.5	12.5	12.5	383	533	227	14	238	203	429	119	389	164	238	548	310	321	86	3.7	219	
22.6	13.0	13.0	13.0	391	541	227	14	240	204	430	120	390	165	240	550	310	323	86	3.8	220	
22.7	13.5	13.5	13.5	391	541	227	14	238	204	429	119	389	165	238	548	310	322	87	3.7	219	
22.8	14.0	14.0	14.0	399	549	226	13	241	206	430	120	390	166	241	551	310	325	87	3.7	220	
23.0	14.5	14.5	14.5	407	557	225	12	243	208	431	121	391	168	243	553	310	328	88	3.7	221	
23.1	15.0	15.0	15.0	407	557	225	12	241	207	431	121	390	167	241	551	310	326	88	3.7	221	
23.2	15.5	15.5	15.5	411	561	225	12	242	208	431	121	391	168	242	552	310	327	89	3.7	221	
23.4	16.0	16.0	16.0	418	568	224	11	243	209	432	122	391	169	243	553	310	329	89	3.7	222	
23.5	16.5	16.5	16.5	418	568	224	11	242	208	431	121	391	169	242	552	310	328	89	3.7	221	
23.6	17.0	17.0	17.0	427	577	224	11	244	210	432	122	391	170	244	554	310	331	90	3.7	222	
23.8	17.5	17.5	17.5	432	582	223	10	245	211	432	122	392	171	245	555	310	332	90	3.7	222	
23.9	18.0	18.0	18.0	432	582	223	10	243	211	432	122	391	171	243	553	310	331	91	3.7	222	
24.1	18.5	18.5	18.5	440	590	222	9	245	212	433	123	392	172	245	555	310	333	91	3.7	223	
24.2	19.0	19.0	19.0	446	596	222	9	246	212	433	123	392	172	246	556	310	334	91	3.7	223	
24.4	19.5	19.5	19.5	446	596	222	9	244	212	432	122	391	172	244	554	310	333	92	3.6	222	
24.5	20.0	20.0	20.0	454	604	221	8	246	214	433	123	392	173	246	556	310	335	92	3.6	223	

Note: Shaded area indicates the yielding zone

Table A.9. Test series CU (σ_3 = 125 kPa) - sample preparation:

Location					Loc No.		
Operator	HTP				Sample No.		B6
Test type	EX	CU	CD	UU	Date started	8/16/2003	4:00 PM
Specimen type	Undisturbed	Remoulded	Recompacted		Nominal diameter		50
Specimen preparation	Compact in an 2.8x5.6 mold with 5 blows on each side						
Soil type and description	Western Iowa loess						

MEASUREMENTS (mm)			INITIAL CONDITIONS	
Initial length			Area Ao (cm^2)	19.63
			Volume Vo (cm^3)	196.25
Average L_o	mm	100	Density (g/cm^3)	1.94
Initial diameter			Moisture content (%)	20.79
Average D_o	mm	50	Dry density (g/cm^3)	1.606

WEIGHINGS	Trimmings	Specimen			LOCATION OF SPECIMEN
		initially	after test		
Container no.					
Specimen + cont.					
Container					
Mass of specimen	Wo	380.6	397.5	Wf	
Dry spec. + cont.					
Dry mass of spec.			315.1	Wd	
Moiture		65.50	82.40	Mf	
Moiture content		20.79	26.15		
Volume of solid		118.96			
Volume of the void		77.29			
Void ratio		0.65			

Table A.10. Test series CU (σ_3 = 125 kPa) - shearing:

Date					Location								Sample No.								0
Test	CD	CU	EX	UU	Membrane			With	side drains				Effective cell pressure							125	kPa
Rate of strain			0.615	mm/min	Operator	HTP		Without					Cell pressure							335	kPa
								Proving ring No.					Back pressure							210	kPa
Consolidated length			100	mm	Consolidated area					19.63	cm^2		Consolidated volume							3.55	cm^3
Corr.	Strain			Axial Load	Pore pressure			Deviator stress								Stress ratio					
Area	Displ.	Diff.	ε	Read	Load	U	Diff.	Stress	p'	p	q	p-cam	p'-cam	q-cam	σ1	σ3	σ'1	σ'3	σ'1/σ'3	p-p'
cm^2	mm		%	N	N	kPa	kPa	kPa	kPa	kPa	kPa	kPa	kPa	kPa	kPa	kPa	kPa	kPa	-	kPa
19.6	0.0	0.0	0.0	17	0	215	0	0	125	335	0	335	125	0	335	335	125	125	1.0	125
19.7	0.3	0.3	0.3	44	27	216	1	14	129	342	7	340	127	14	349	335	133	125	1.1	132
19.7	0.5	0.5	0.5	91	74	216	1	38	140	354	19	348	135	38	373	335	157	124	1.3	144
19.8	0.8	0.8	0.8	221	204	223	8	103	167	387	52	369	150	103	438	335	216	118	1.8	177
19.8	1.0	1.0	1.0	307	290	228	13	146	183	408	73	384	159	146	481	335	253	112	2.3	198
19.9	1.3	1.3	1.3	345	328	231	16	165	189	418	83	390	162	165	500	335	269	109	2.5	208
19.9	1.5	1.5	1.5	373	356	233	18	179	194	424	89	395	165	179	514	335	281	107	2.6	214
20.0	1.8	1.8	1.8	392	375	235	20	188	196	429	94	398	166	188	523	335	288	105	2.7	219
20.0	2.0	2.0	2.0	405	388	236	21	194	198	432	97	400	167	194	529	335	293	104	2.8	222
20.1	2.3	2.3	2.3	414	397	237	22	198	199	434	99	401	167	198	533	335	296	103	2.9	224
20.1	2.5	2.5	2.5	424	407	238	23	202	201	436	101	402	168	202	537	335	299	102	2.9	226
20.2	2.8	2.8	2.8	430	413	239	24	205	201	437	102	403	168	205	540	335	301	101	3.0	227
20.2	3.0	3.0	3.0	436	419	240	25	207	202	439	104	404	168	207	542	335	303	101	3.0	229
20.3	3.3	3.3	3.3	442	425	241	26	210	202	440	105	405	168	210	545	335	304	100	3.1	230
20.3	3.5	3.5	3.5	449	432	241	26	212	203	441	106	406	168	212	547	335	306	99	3.1	231
20.4	3.8	3.8	3.8	455	438	242	27	215	203	442	107	407	168	215	550	335	308	98	3.1	232
20.4	4.0	4.0	4.0	460	443	242	27	217	204	443	108	407	169	217	552	335	310	98	3.2	233
20.5	4.3	4.3	4.3	468	451	243	28	220	205	445	110	408	169	220	555	335	312	97	3.2	235
20.7	5.0	5.0	5.0	477	460	243	28	223	206	446	111	409	170	223	558	335	315	97	3.2	236
20.8	5.5	5.5	5.5	485	468	243	28	225	207	448	113	410	170	225	560	335	317	97	3.3	238
20.9	6.0	6.0	6.0	493	476	243	28	228	208	449	114	411	171	228	563	335	320	97	3.3	239
21.0	6.5	6.5	6.5	501	484	243	28	231	210	450	115	412	172	231	566	335	323	97	3.3	240
21.1	7.0	7.0	7.0	507	490	243	28	232	211	451	116	412	173	232	567	335	324	97	3.3	241
21.2	7.5	7.5	7.5	518	501	243	28	236	213	453	118	414	174	236	571	335	328	97	3.4	243
21.3	8.0	8.0	8.0	523	506	243	28	237	213	454	119	414	174	237	572	335	329	97	3.4	244
21.4	8.5	8.5	8.5	534	517	243	28	241	216	456	121	415	176	241	576	335	334	98	3.4	246
21.6	9.0	9.0	9.0	539	522	242	27	242	217	456	121	416	177	242	577	335	335	98	3.4	246
21.7	9.5	9.5	9.5	545	528	242	27	243	217	457	122	416	177	243	578	335	336	98	3.4	247
21.8	10.0	10.0	10.0	553	536	241	26	246	219	458	123	417	179	246	581	335	340	99	3.4	248
21.9	10.5	10.5	10.5	561	544	241	26	248	221	459	124	418	180	248	583	335	342	99	3.5	249
22.1	11.0	11.0	11.0	569	552	240	25	250	223	460	125	418	182	250	585	335	345	100	3.5	250
22.2	11.5	11.5	11.5	575	558	240	25	252	223	461	126	419	182	252	587	335	347	100	3.5	251
22.3	12.0	12.0	12.0	581	564	239	24	253	225	461	126	419	184	253	588	335	349	101	3.5	251
22.4	12.5	12.5	12.5	588	571	239	24	255	226	462	127	420	185	255	590	335	351	102	3.5	252
22.6	13.0	13.0	13.0	595	578	238	23	256	228	463	128	420	186	256	591	335	353	102	3.5	253
22.7	13.5	13.5	13.5	602	585	238	23	258	229	464	129	421	187	258	593	335	355	103	3.5	254
22.8	14.0	14.0	14.0	611	594	237	22	260	231	465	130	422	188	260	595	335	358	103	3.5	255
23.0	14.5	14.5	14.5	613	596	236	21	260	231	465	130	422	189	260	595	335	359	104	3.4	255
23.1	15.0	15.0	15.0	623	606	236	21	262	233	466	131	422	190	262	597	335	361	104	3.5	256
23.2	15.5	15.5	15.5	630	613	235	20	264	234	467	132	423	191	264	599	335	364	105	3.5	257
23.4	16.0	16.0	16.0	635	618	234	19	265	236	467	132	423	193	265	600	335	366	106	3.4	257
23.5	16.5	16.5	16.5	641	624	234	19	265	236	468	133	423	193	265	600	335	366	106	3.5	258
23.6	17.0	17.0	17.0	646	629	233	18	266	238	468	133	424	194	266	601	335	368	107	3.4	258
23.8	17.5	17.5	17.5	652	635	232	17	267	239	468	133	424	195	267	602	335	370	108	3.4	258
23.9	18.0	18.0	18.0	660	643	232	17	269	240	469	134	425	196	269	604	335	372	109	3.4	259
24.1	18.5	18.5	18.5	665	648	231	16	269	241	470	135	425	197	269	604	335	373	109	3.4	260
24.2	19.0	19.0	19.0	671	654	231	16	270	242	470	135	425	198	270	605	335	374	110	3.4	260
24.4	19.5	19.5	19.5	676	659	230	15	270	243	470	135	425	198	270	605	335	375	110	3.4	260
24.5	20.0	20.0	20.0	684	667	230	15	272	244	471	136	426	199	272	607	335	377	111	3.4	261

Note: Shaded area indicates the yielding zone

Table A.11. Test series CU (σ_3 = 150 kPa) - sample preparation:

Location					Loc No.		
Operator	HTP				Sample No.		B7
Test type	EX	CU	CD	UU	Date started	8/18/2003	6:15 PM
Specimen type	Undisturbed	Remoulded	Recompacted		Nominal diameter		50
Specimen preparation	Compact in an 2.8x5.6 mold with 5 blows on each side						
Soil type and description	Western Iowa loess						

MEASUREMENTS (mm)			INITIAL CONDITIONS	
Initial length			Area Ao (cm^2)	19.63
			Volume Vo (cm^3)	196.25
Average L_o	mm	100	Density (g/cm^3)	1.93
Initial diameter			Moisture content (%)	20.51
Average D_o	mm	50	Dry density (g/cm^3)	1.605

WEIGHINGS	Trimmings	Specimen			LOCATION OF SPECIMEN
		initially	after test		
Container no.					
Specimen + cont.					
Container					
Mass of specimen	w_o	379.6	396.3	w_f	
Dry spec. + cont.					
Dry mass of spec.			315	w_d	
Moiture		64.60	81.30	Mf	
Moiture content		20.51	25.81		
Volume of solid		118.93			
Volume of the void		77.32			
Void ratio		0.65			

Table A.12. Test series CU (σ_3 = 150 kPa) - shearing:

Date					Location							Sample No.								0
Test	CD	CU	EX	UU	Membrane			With	side drains			Effective cell pressure							150	kPa
Rate of strain			0.615	mm/min	Operator		HTP	Without				Cell pressure							360	kPa
								Proving ring No.				Back pressure							210	kPa
Consolidated length			100	mm	Consolidated area					19.63	cm^2	Consolidated volume							5.15	cm^3
Corr.	Strain			Axial Load		Pore pressure		Deviator stress							Stress ratio					
Area	Displ.	Diff.	ε	Read	Load	U	Diff.	Stress	p'	p	q	p-cam	p'-cam	q-cam	σ1	σ3	σ'1	σ'3	σ'1/σ'3	p-p'
cm^2	mm		%	N	N	kPa	kPa	kPa	kPa	kPa	kPa	kPa	kPa	kPa	kPa	kPa	kPa	kPa	-	kPa
19.6	0.0	0.0	0.0	-20	0	219	0	0	150	360	0	360	150	0	360	360	150	150	1.0	150
19.7	0.3	0.3	0.3	80	100	220	1	51	170	385	25	377	163	51	411	360	191	149	1.3	175
19.7	0.5	0.5	0.5	207	227	224	5	115	198	418	58	398	180	115	475	360	251	145	1.7	208
19.8	0.8	0.8	0.8	282	302	231	12	153	210	436	76	411	186	153	513	360	282	138	2.0	226
19.8	1.0	1.0	1.0	328	348	237	18	176	215	448	88	419	188	176	536	360	299	132	2.3	238
19.9	1.3	1.3	1.3	362	382	242	23	192	219	456	96	424	188	192	552	360	310	127	2.4	246
19.9	1.5	1.5	1.5	388	408	246	27	205	221	462	102	428	188	205	565	360	319	123	2.6	252
20.0	1.8	1.8	1.8	399	419	249	30	210	220	465	105	430	187	210	570	360	321	120	2.7	255
20.0	2.0	2.0	2.0	414	434	252	33	217	221	468	108	432	187	217	577	360	325	118	2.8	258
20.1	2.3	2.3	2.3	425	445	254	35	222	221	471	111	434	186	222	582	360	328	115	2.8	261
20.1	2.5	2.5	2.5	434	454	256	37	226	221	473	113	435	185	226	586	360	330	113	2.9	263
20.2	2.8	2.8	2.8	441	461	258	39	228	221	474	114	436	184	228	588	360	330	111	3.0	264
20.2	3.0	3.0	3.0	448	468	259	40	231	221	476	116	437	184	231	591	360	332	110	3.0	266
20.3	3.3	3.3	3.3	454	474	261	42	234	220	477	117	438	183	234	594	360	333	108	3.1	267
20.3	3.5	3.5	3.5	462	482	262	43	237	222	479	119	439	184	237	597	360	336	108	3.1	269
20.4	3.8	3.8	3.8	463	483	263	44	237	220	478	118	439	182	237	597	360	334	106	3.1	268
20.4	4.0	4.0	4.0	470	490	264	45	240	220	480	120	440	182	240	600	360	336	105	3.2	270
20.5	4.5	4.5	4.5	478	498	265	46	242	221	481	121	441	182	242	602	360	337	104	3.2	271
20.7	5.0	5.0	5.0	487	507	267	48	245	221	483	123	442	181	245	605	360	339	103	3.3	273
20.8	5.5	5.5	5.5	492	512	267	48	247	221	483	123	442	181	247	607	360	340	102	3.3	273
20.9	6.0	6.0	6.0	503	523	268	49	251	222	485	125	444	182	251	611	360	343	102	3.4	275
21.0	6.5	6.5	6.5	509	529	268	49	252	223	486	126	444	182	252	612	360	344	101	3.4	276
21.1	7.0	7.0	7.0	517	537	268	49	254	224	487	127	445	183	254	614	360	346	101	3.4	277
21.2	7.5	7.5	7.5	528	548	268	49	258	226	489	129	446	184	258	618	360	350	101	3.5	279
21.3	8.0	8.0	8.0	536	556	268	49	261	227	490	130	447	185	261	621	360	353	101	3.5	280
21.4	8.5	8.5	8.5	541	561	268	49	262	227	491	131	447	185	262	622	360	354	101	3.5	281
21.6	9.0	9.0	9.0	549	569	268	49	264	229	492	132	448	186	264	624	360	356	102	3.5	282
21.7	9.5	9.5	9.5	555	575	268	49	265	230	493	133	448	187	265	625	360	358	102	3.5	283
21.8	10.0	10.0	10.0	563	583	267	48	267	231	494	134	449	188	267	627	360	360	102	3.5	284
21.9	10.5	10.5	10.5	577	597	266	47	272	235	496	136	451	191	272	632	360	366	103	3.6	286
22.1	11.0	11.0	11.0	579	599	266	47	272	234	496	136	451	191	272	632	360	366	103	3.5	286
22.2	11.5	11.5	11.5	586	606	265	46	273	236	497	137	451	192	273	633	360	368	104	3.5	287
22.3	12.0	12.0	12.0	597	617	265	46	277	238	498	138	452	193	277	637	360	372	104	3.6	288
22.4	12.5	12.5	12.5	601	621	264	45	277	239	498	138	452	194	277	637	360	373	105	3.6	288
22.6	13.0	13.0	13.0	607	627	264	45	278	239	499	139	453	195	278	638	360	374	105	3.6	289
22.7	13.5	13.5	13.5	609	629	263	44	277	240	499	139	452	195	277	637	360	374	106	3.5	289
22.8	14.0	14.0	14.0	625	645	262	43	283	244	501	141	454	198	283	643	360	381	107	3.6	291
23.0	14.5	14.5	14.5	629	649	262	43	283	244	501	141	454	199	283	643	360	381	108	3.5	291
23.1	15.0	15.0	15.0	634	654	261	42	283	246	502	142	454	200	283	643	360	383	109	3.5	292
23.3	15.8	15.8	15.8	645	665	260	41	285	248	503	143	455	202	285	645	360	386	110	3.5	293
23.4	16.0	16.0	16.0	653	673	259	40	288	250	504	144	456	203	288	648	360	389	110	3.5	294
23.5	16.5	16.5	16.5	659	679	259	40	289	250	504	144	456	204	289	649	360	390	111	3.5	294
23.6	17.0	17.0	17.0	667	687	258	39	291	252	505	145	457	205	291	651	360	393	111	3.5	295
23.8	17.5	17.5	17.5	673	693	257	38	291	253	506	146	457	206	291	651	360	394	112	3.5	296
23.9	18.0	18.0	18.0	675	695	257	38	290	253	505	145	457	206	290	650	360	393	112	3.5	295
24.1	18.5	18.5	18.5	680	700	256	37	291	254	505	145	457	207	291	651	360	395	113	3.5	295
24.2	19.0	19.0	19.0	684	704	255	36	291	255	505	145	457	208	291	651	360	396	114	3.5	295
24.4	19.5	19.5	19.5	697	717	255	36	294	257	507	147	458	210	294	654	360	400	115	3.5	297
24.5	20.0	20.0	20.0	697	717	254	35	292	257	506	146	457	209	292	652	360	398	115	3.5	296

Note: Shaded area indicates the yielding zone

Table A.13. Test series CU (σ_3 = 175 kPa) - sample preparation:

Location					Loc No.		
Operator	HTP				Sample No.		B8
Test type	EX	CU	CD	UU	Date started	8/20/2003	4:30 PM
Specimen type	Undisturbed	Remoulded	Recompacted		Nominal diameter		50
Specimen preparation	Compact in an 2.8x5.6 mold with 5 blows on each side						
Soil type and description	Western Iowa loess						

MEASUREMENTS (mm)			INITIAL CONDITIONS	
Initial length			Area Ao (cm^2)	19.63
			Volume Vo (cm^3)	196.25
Average L_o	mm	100	Density (g/cm^3)	1.96
Initial diameter			Moisture content (%)	21.00
Average D_o	mm	50	Dry density (g/cm^3)	1.616

WEIGHINGS	Trimmings	Specimen			LOCATION OF SPECIMEN
		initially	after test		
Container no.					
Specimen + cont.					
Container					
Mass of specimen	Wo	383.7	398.9	Wf	
Dry spec. + cont.					
Dry mass of spec.			317.1	Wd	
Moiture		66.60	81.80	Mf	
Moiture content		21.00	25.80		
Volume of solid		119.72			
Volume of the void		76.53			
Void ratio		0.64			

Table A.14. Test series CU (σ_3 = 175 kPa) - shearing:

Date					Location								Sample No.							0
Test	CD	CU	EX	UU	Membrane			With	side drains				Effective cell pressure						175	kPa
Rate of strain			0.615	mm/min	Operator		HTP	Without					Cell pressure						385	kPa
								Proving ring No.					Back pressure						210	kPa
Consolidated length			100	mm	Consolidated area					19.63	cm^2		Consolidated volume						4.59	cm^3
Corr.	Strain			Axial Load	Pore pressure			Deviator stress								Stress ratio					
Area	Displ.	Diff.	ε	Read	Load	U	Diff.	Stress	p'	p	q	p-cam	p'-cam	q-cam	σ1	σ3	σ'1	σ'3	σ'1/σ'3	p-p'
cm^2	mm		%	N	N	kPa	kPa	kPa	kPa	kPa	kPa	kPa	kPa	kPa	kPa	kPa	kPa	kPa	-	kPa
19.6	0.0	0.0	0.0	52	0	217	0	0	175	385	0	385	175	0	385	385	175	175	1.0	175
19.7	0.3	0.3	0.3	118	66	218	1	34	187	402	17	396	183	34	419	385	201	174	1.2	192
19.7	0.5	0.5	0.5	252	200	222	5	101	217	436	51	419	201	101	486	385	264	170	1.6	226
19.8	0.8	0.8	0.8	339	287	229	12	145	232	458	73	433	209	145	530	385	301	163	1.8	248
19.8	1.0	1.0	1.0	396	344	235	18	174	241	472	87	443	213	174	559	385	324	158	2.1	262
19.9	1.3	1.3	1.3	440	388	239	22	195	247	483	98	450	216	195	580	385	341	153	2.2	273
19.9	1.5	1.5	1.5	468	416	244	27	209	249	489	104	455	216	209	594	385	350	149	2.4	279
20.0	1.8	1.8	1.8	489	437	247	30	219	251	494	109	458	216	219	604	385	357	145	2.5	284
20.0	2.0	2.0	2.0	508	456	251	34	228	252	499	114	461	215	228	613	385	362	142	2.6	289
20.1	2.3	2.3	2.3	522	470	253	36	234	253	502	117	463	215	234	619	385	366	139	2.6	292
20.1	2.5	2.5	2.5	532	480	256	39	238	252	504	119	464	214	238	623	385	368	137	2.7	294
20.2	2.8	2.8	2.8	541	489	257	40	242	253	506	121	466	213	242	627	385	370	135	2.7	296
20.2	3.0	3.0	3.0	550	498	259	42	246	253	508	123	467	213	246	631	385	372	133	2.8	298
20.3	3.3	3.3	3.3	555	503	261	44	248	252	509	124	468	212	248	633	385	372	132	2.8	299
20.3	3.5	3.5	3.5	563	511	262	45	251	252	511	126	469	211	251	636	385	374	130	2.9	301
20.4	3.8	3.8	3.8	567	515	263	46	253	252	511	126	469	211	253	638	385	375	129	2.9	301
20.4	4.0	4.0	4.0	571	519	264	47	254	251	512	127	470	210	254	639	385	375	128	2.9	302
20.5	4.5	4.5	4.5	582	530	267	50	258	251	514	129	471	209	258	643	385	376	126	3.0	304
20.7	5.0	5.0	5.0	591	539	268	51	261	251	515	130	472	209	261	646	385	378	125	3.0	305
20.8	5.5	5.5	5.5	601	549	269	52	264	252	517	132	473	209	264	649	385	381	124	3.1	307
20.9	6.0	6.0	6.0	610	558	270	53	267	252	519	134	474	209	267	652	385	382	122	3.1	309
21.0	6.5	6.5	6.5	618	566	271	54	270	253	520	135	475	209	270	655	385	384	122	3.2	310
21.1	7.0	7.0	7.0	626	574	271	54	272	254	521	136	476	210	272	657	385	387	122	3.2	311
21.2	7.5	7.5	7.5	637	585	271	54	276	255	523	138	477	211	276	661	385	390	121	3.2	313
21.3	8.0	8.0	8.0	644	592	271	54	278	256	524	139	478	211	278	663	385	392	121	3.2	314
21.4	8.5	8.5	8.5	656	604	271	54	282	258	526	141	479	213	282	667	385	396	121	3.3	316
21.6	9.0	9.0	9.0	664	612	271	54	284	260	527	142	480	214	284	669	385	398	122	3.3	317
21.7	9.5	9.5	9.5	671	619	270	53	285	261	528	143	480	215	285	670	385	400	122	3.3	318
21.8	10.0	10.0	10.0	681	629	270	53	288	263	529	144	481	216	288	673	385	403	122	3.3	319
21.9	10.5	10.5	10.5	692	640	270	53	292	264	531	146	482	217	292	677	385	407	122	3.3	321
22.1	11.0	11.0	11.0	700	648	269	52	294	266	532	147	483	219	294	679	385	410	123	3.3	322
22.2	11.5	11.5	11.5	708	656	268	51	296	268	533	148	484	220	296	681	385	413	124	3.3	323
22.3	12.0	12.0	12.0	717	665	268	51	298	270	534	149	484	222	298	683	385	416	125	3.3	324
22.4	12.5	12.5	12.5	725	673	267	50	300	272	535	150	485	223	300	685	385	418	125	3.3	325
22.6	13.0	13.0	13.0	733	681	267	50	302	273	536	151	486	224	302	687	385	420	126	3.3	326
22.7	13.5	13.5	13.5	741	689	266	49	304	274	537	152	486	225	304	689	385	423	126	3.4	327
22.8	14.0	14.0	14.0	749	697	265	48	305	276	538	153	487	226	305	690	385	425	127	3.3	328
23.0	14.5	14.5	14.5	757	705	264	47	307	278	539	154	487	228	307	692	385	428	128	3.3	329
23.1	15.0	15.0	15.0	766	714	264	47	309	279	540	155	488	229	309	694	385	430	128	3.4	330
23.3	15.8	15.8	15.8	774	722	263	46	310	280	540	155	488	230	310	695	385	432	129	3.3	330
23.4	16.0	16.0	16.0	779	727	262	45	311	282	541	156	489	231	311	696	385	434	130	3.3	331
23.5	16.5	16.5	16.5	790	738	262	45	314	284	542	157	490	232	314	699	385	437	130	3.4	332
23.6	17.0	17.0	17.0	796	744	261	44	315	285	542	157	490	234	315	700	385	439	131	3.3	332
23.8	17.5	17.5	17.5	804	752	260	43	316	287	543	158	490	235	316	701	385	441	132	3.3	333
23.9	18.0	18.0	18.0	812	760	260	43	318	288	544	159	491	236	318	703	385	443	133	3.3	334
24.1	18.5	18.5	18.5	815	763	259	42	317	288	543	158	491	236	317	702	385	443	133	3.3	333
24.2	19.0	19.0	19.0	826	774	258	41	319	290	545	160	491	238	319	704	385	446	134	3.3	335
24.4	19.5	19.5	19.5	834	782	257	40	321	292	545	160	492	240	321	706	385	449	135	3.3	335
24.5	20.0	20.0	20.0	836	784	256	39	320	292	545	160	492	240	320	705	385	449	136	3.3	335

Note: Shaded area indicates the yielding zone

Table A.15. Test series CU (σ_3 = 200 kPa) - sample preparation:

Location					Loc No.		
Operator	HTP				Sample No.		B4
Test type	EX	CU	CD	UU	Date started	8/14/2003	5:30 PM
Specimen type	Undisturbed	Remoulded	Recompacted		Nominal diameter		50
Specimen preparation	Compact in an 2.8x5.6 mold with 5 blows on each side						
Soil type and description	Western Iowa loess						

MEASUREMENTS (mm)			INITIAL CONDITIONS	
Initial length			Area Ao (cm^2)	19.63
			Volume Vo (cm^3)	196.25
Average L_o	mm	100	Density (g/cm^3)	1.97
Initial diameter			Moisture content (%)	21.08
Average D_o	mm	50	Dry density (g/cm^3)	1.624

WEIGHINGS	Trimmings	Specimen			LOCATION OF SPECIMEN
		initially	after test		
Container no.					
Specimen + cont.					
Container					
Mass of specimen	w_o	386	399.6	w_f	
Dry spec. + cont.					
Dry mass of spec.			318.8	w_d	
Moiture		67.20	80.80	M_f	
Moiture content		21.08	25.35		
Volume of solid		120.36			
Volume of the void		75.89			
Void ratio		0.63			

Table A. 16. Test series CU (σ_3 = 200 kPa) - shearing:

Date					Location								Sample No.								0
Test	CD	CU	EX	UU	Membrane			With	side drains				Effective cell pressure							200	kPa
Rate of strain			0.615	mm/min	Operator		HTP	Without					Cell pressure							410	kPa
								Proving ring No.					Back pressure							210	kPa
Consolidated length			100	mm	Consolidated area					19.63	cm^2		Consolidated volume							3.89	cm^3
Corr.	Strain			Axial Load	Pore pressure			Deviator stress								Stress ratio					
Area	Displ.	Diff.	ε	Read	Load	U	Diff.	Stress	p'	p	q	p-cam	p'-cam	q-cam	σ1	σ3	σ'1	σ'3	σ'1/σ'3	p-p'
cm^2	mm		%	N	N	kPa	kPa	kPa	kPa	kPa	kPa	kPa	kPa	kPa	kPa	kPa	kPa	kPa	-	kPa
19.6	0.0	0.0	0.0	0	0	232	0	0	200	410	0	410	200	0	410	410	200	200	1.0	200
19.7	0.3	0.3	0.3	303	303	244	13	154	254	487	77	461	232	154	564	410	320	188	1.7	277
19.7	0.5	0.5	0.5	367	367	251	20	186	263	503	93	472	235	186	596	410	345	181	1.9	293
19.8	0.8	0.8	0.8	410	410	259	28	207	265	514	104	479	234	207	617	410	358	173	2.1	304
19.8	1.0	1.0	1.0	421	421	264	33	212	263	516	106	481	231	212	622	410	358	168	2.1	306
19.9	1.3	1.3	1.3	448	448	269	38	225	264	523	113	485	230	225	635	410	366	163	2.3	313
19.9	1.5	1.5	1.5	457	457	272	40	229	264	525	115	486	229	229	639	410	368	160	2.3	315
20.0	1.8	1.8	1.8	476	476	275	44	238	265	529	119	489	229	238	648	410	373	157	2.4	319
20.0	2.0	2.0	2.0	487	487	279	48	243	263	532	122	491	226	243	653	410	374	153	2.5	322
20.1	2.3	2.3	2.3	489	489	281	50	244	262	532	122	491	225	244	654	410	373	151	2.5	322
20.1	2.5	2.5	2.5	497	497	283	52	247	261	533	123	492	224	247	657	410	374	149	2.5	323
20.2	2.8	2.8	2.8	498	498	285	54	247	259	533	123	492	222	247	657	410	372	147	2.5	323
20.2	3.0	3.0	3.0	506	506	287	55	250	259	535	125	493	221	250	660	410	374	145	2.6	325
20.3	3.3	3.3	3.3	513	513	288	56	253	260	536	126	494	221	253	663	410	375	144	2.6	326
20.3	3.5	3.5	3.5	514	514	289	57	253	259	536	126	494	220	253	663	410	374	143	2.6	326
20.4	3.8	3.8	3.8	522	522	290	59	256	259	538	128	495	220	256	666	410	376	142	2.7	328
20.4	4.0	4.0	4.0	528	528	291	60	258	259	539	129	496	219	258	668	410	377	141	2.7	329
20.5	4.5	4.5	4.5	536	536	292	61	261	259	540	130	497	219	261	671	410	379	140	2.7	330
20.7	5.0	5.0	5.0	541	541	293	61	262	259	541	131	497	219	262	672	410	379	139	2.7	331
20.8	5.5	5.5	5.5	558	558	294	62	269	262	544	134	500	220	269	679	410	385	138	2.8	334
20.9	6.0	6.0	6.0	566	566	294	62	271	263	546	136	500	221	271	681	410	388	138	2.8	336
21.0	6.5	6.5	6.5	574	574	294	62	273	264	547	137	501	222	273	683	410	390	138	2.8	337
21.1	7.0	7.0	7.0	585	585	294	62	277	266	549	139	502	223	277	687	410	394	138	2.9	339
21.2	7.5	7.5	7.5	596	596	294	62	281	268	550	140	504	224	281	691	410	397	138	2.9	340
21.3	8.0	8.0	8.0	603	603	293	62	283	269	551	141	504	226	283	693	410	400	139	2.9	341
21.4	8.5	8.5	8.5	615	615	293	61	287	272	553	143	506	227	287	697	410	404	139	2.9	343
21.6	9.0	9.0	9.0	629	629	292	61	292	275	556	146	507	230	292	702	410	410	140	2.9	346
21.7	9.5	9.5	9.5	637	637	291	60	294	277	557	147	508	231	294	704	410	413	141	2.9	347
21.8	10.0	10.0	10.0	645	645	291	60	296	278	558	148	509	232	296	706	410	415	141	3.0	348
21.9	10.5	10.5	10.5	653	653	290	59	298	280	559	149	509	234	298	708	410	418	142	3.0	349
22.1	11.0	11.0	11.0	670	670	289	58	304	284	562	152	511	237	304	714	410	425	143	3.0	352
22.2	11.5	11.5	11.5	681	681	288	57	307	286	564	154	512	239	307	717	410	429	144	3.0	354
22.3	12.0	12.0	12.0	686	686	287	56	308	288	564	154	513	240	308	718	410	431	145	3.0	354
22.4	12.5	12.5	12.5	694	694	286	55	309	289	565	155	513	241	309	719	410	433	146	3.0	355
22.6	13.0	13.0	13.0	700	700	285	54	310	291	565	155	513	243	310	720	410	435	147	3.0	355
22.7	13.5	13.5	13.5	719	719	284	53	317	295	568	158	516	246	317	727	410	443	148	3.0	358
22.8	14.0	14.0	14.0	723	723	283	52	317	296	568	158	516	247	317	727	410	444	149	3.0	358
23.0	14.5	14.5	14.5	733	733	282	51	319	298	570	160	516	249	319	729	410	447	150	3.0	360
23.1	15.0	15.0	15.0	749	749	281	50	324	302	572	162	518	251	324	734	410	453	151	3.0	362
23.2	15.5	15.5	15.5	755	755	281	50	325	302	573	163	518	252	325	735	410	454	151	3.0	363
23.4	16.0	16.0	16.0	762	762	279	48	326	305	573	163	519	254	326	736	410	457	153	3.0	363
23.5	16.5	16.5	16.5	770	770	278	47	328	307	574	164	519	256	328	738	410	460	154	3.0	364
23.6	17.0	17.0	17.0	784	784	277	46	332	310	576	166	521	258	332	742	410	465	155	3.0	366
23.8	17.5	17.5	17.5	793	793	276	45	333	311	577	167	521	259	333	743	410	467	156	3.0	367
23.9	18.0	18.0	18.0	799	799	275	44	334	313	577	167	521	261	334	744	410	469	157	3.0	367
24.1	18.5	18.5	18.5	802	802	274	43	333	313	577	167	521	261	333	743	410	469	158	3.0	367
24.2	19.0	19.0	19.0	820	820	273	42	338	317	579	169	523	264	338	748	410	475	159	3.0	369
24.4	19.5	19.5	19.5	823	823	272	41	338	318	579	169	523	265	338	748	410	476	160	3.0	369
24.5	20.0	20.0	20.0	837	837	271	40	341	320	581	171	524	267	341	751	410	480	161	3.0	371

Note: Shaded area indicates the yielding zone

Table A.17. Test series LCU-K_{iso} (K = 1.0) - sample preparation:

Location					Loc No.		
Operator	HTP				Sample No.		B48
Test type	EX	CU	CD	UU	Date started	11/27/2003	
Specimen type	Undisturbed	Remoulded	Recompacted		Nominal diameter		50
Specimen preparation	Compact in an 2.8x5.6 mold with 5 blows on each side						
Soil type and description	Western Iowa loess						

MEASUREMENTS (mm)			INITIAL CONDITIONS	
Initial length			Area Ao (cm^2)	19.63
			Volume Vo (cm^3)	196.25
Average L_o	mm	100	Density (g/cm^3)	1.93
Initial diameter			Moisture content (%)	18.74
Average D_o	mm	50	Dry density (g/cm^3)	1.626

WEIGHINGS	Trimmings	Specimen			LOCATION OF SPECIMEN
		initially	after test		
Container no.					
Specimen + cont.					
Container					
Mass of specimen	w_o	378.9	402.5	w_f	
Dry spec. + cont.					
Dry mass of spec.			319.1	w_d	
Moiture		59.80	83.40	M_f	
Moiture content		18.74	26.14		
Volume of solid		120.47			
Volume of the void		75.78			
Void ratio		0.63			

Table A.18. Test series LCU-K_{iso} (K = 1.0) - shearing:

Date					Location									Sample No.					B48
Test CD CU EX UU					Membrane			With / Without side drains						Ram pressure			0	kPa	
Rate of strain			0.635	mm / min	Operator		HTP	Proving ring No.						Tensile pressure			0	kPa	
Consolidated length			100	mm	Consolidated area			19.63					cm^2	Cell pressure			260	kPa	
														Pore pressure			211.3	kPa	
Corr.	Strain		Axial Load		Pore pressure		Deviator stress							Principal stresses					
Area	Displ.	ε	Read	Load	U	ΔU	σa	p'	p	q	p-cam	p'-cam	q-cam	σ1	σ3	σ'1	σ'3	σ'1/σ'3	A
cm^2	mm	%	N	N	kPa	kPa	kPa	kPa	kPa	kPa	kPa	kPa	kPa	kPa	kPa	kPa	kPa	-	
19.63	0.0	0.0	-85	0	211	0	0	49	260	0	260	49	0	260	260	49	49	1.0	
19.68	0.3	0.3	3	88	218	6	45	65	282	22	275	57	45	305	260	87	42	2.1	0.14
19.73	0.5	0.5	34	119	220	9	60	70	290	30	280	60	60	320	260	100	40	2.5	0.15
19.78	0.8	0.8	60	145	221	10	73	75	297	37	284	63	73	333	260	112	39	2.9	0.14
19.83	1.0	1.0	79	164	221	10	83	81	301	41	288	67	83	343	260	122	39	3.1	0.12
19.88	1.3	1.3	79	164	221	10	83	80	301	41	288	67	83	343	260	122	39	3.1	0.12
19.93	1.5	1.5	101	186	220	9	93	86	307	47	291	71	93	353	260	133	40	3.4	0.10
19.98	1.8	1.8	116	201	219	8	101	91	310	50	294	74	101	361	260	141	41	3.5	0.08
20.04	2.0	2.0	129	214	219	7	107	95	313	53	296	77	107	367	260	148	42	3.6	0.07
20.08	2.3	2.3	127	212	218	6	105	95	313	53	295	77	105	365	260	148	42	3.5	0.06
20.14	2.5	2.5	139	224	217	6	111	99	316	56	297	80	111	371	260	154	43	3.6	0.05
20.19	2.8	2.8	145	230	216	5	114	101	317	57	298	82	114	374	260	158	44	3.6	0.04
20.24	3.0	3.0	145	230	216	4	114	101	317	57	298	82	114	374	260	158	44	3.6	0.04
20.30	3.3	3.3	150	235	215	4	116	103	318	58	299	84	116	376	260	161	45	3.6	0.03
20.35	3.5	3.5	164	249	215	3	122	107	321	61	301	86	122	382	260	168	46	3.7	0.03
20.40	3.8	3.8	164	249	214	3	122	107	321	61	301	87	122	382	260	168	46	3.7	0.02
20.45	4.0	4.0	164	249	213	2	122	107	321	61	301	87	122	382	260	168	47	3.6	0.02
20.50	4.3	4.3	174	259	213	2	126	110	323	63	302	89	126	386	260	173	47	3.7	0.01
20.55	4.5	4.5	171	256	212	1	124	110	322	62	301	89	124	384	260	172	48	3.6	0.01
20.61	4.8	4.8	175	260	212	1	126	111	323	63	302	90	126	386	260	174	48	3.6	0.00
20.67	5.0	5.0	186	271	212	0	131	114	326	66	304	92	131	391	260	179	48	3.7	0.00
20.78	5.5	5.5	184	269	211	-1	129	114	325	65	303	92	129	389	260	179	49	3.6	0.00
20.89	6.0	6.0	198	283	210	-1	136	118	328	68	305	95	136	396	260	185	50	3.7	-0.01
21.00	6.5	6.5	194	279	210	-2	133	117	326	66	304	95	133	393	260	183	50	3.6	-0.01
21.11	7.0	7.0	208	293	209	-3	139	121	329	69	306	98	139	399	260	190	51	3.7	-0.02
21.23	7.5	7.5	206	291	208	-3	137	120	329	69	306	98	137	397	260	189	52	3.6	-0.02
21.34	8.0	8.0	222	307	208	-4	144	124	332	72	308	100	144	404	260	196	52	3.7	-0.03
21.46	8.5	8.5	224	309	207	-4	144	125	332	72	308	101	144	404	260	197	53	3.7	-0.03
21.57	9.0	9.0	222	307	207	-5	142	125	331	71	307	101	142	402	260	196	54	3.7	-0.03
21.69	9.5	9.5	235	320	206	-5	148	128	334	74	309	103	148	408	260	201	54	3.7	-0.04
21.81	10.0	10.0	230	315	205	-6	144	127	332	72	308	103	144	404	260	199	55	3.6	-0.04
21.94	10.5	10.5	243	328	205	-6	150	129	335	75	310	104	150	410	260	204	55	3.7	-0.04
22.06	11.0	11.0	238	323	205	-7	146	129	333	73	309	104	146	406	260	202	56	3.6	-0.05
22.19	11.5	11.5	252	337	204	-7	152	132	336	76	311	106	152	412	260	208	56	3.7	-0.05
22.31	12.0	12.0	249	334	204	-8	150	131	335	75	310	106	150	410	260	206	56	3.7	-0.05
22.44	12.5	12.5	257	342	203	-8	152	133	336	76	311	108	152	412	260	209	57	3.7	-0.05
22.57	13.0	13.0	263	348	203	-8	154	134	337	77	311	108	154	414	260	211	57	3.7	-0.05
22.70	13.5	13.5	257	342	202	-9	151	133	335	75	310	108	151	411	260	208	58	3.6	-0.06
22.83	14.0	14.0	271	356	202	-9	156	136	338	78	312	110	156	416	260	214	58	3.7	-0.06
22.94	14.4	14.4	266	351	202	-10	153	135	337	77	311	109	153	413	260	211	58	3.6	-0.06
23.09	15.0	15.0	248	333	201	-10	144	131	332	72	308	107	144	404	260	203	59	3.5	-0.07
23.24	15.5	15.5	272	357	201	-11	153	136	337	77	311	111	153	413	260	213	59	3.6	-0.07
23.37	16.0	16.0	265	350	200	-11	150	135	335	75	310	110	150	410	260	210	60	3.5	-0.07
23.52	16.5	16.5	279	364	200	-11	155	137	337	77	312	111	155	415	260	215	60	3.6	-0.07
23.66	17.0	17.0	292	377	200	-12	159	140	340	80	313	114	159	419	260	220	60	3.6	-0.07
23.80	17.5	17.5	287	372	199	-12	156	139	338	78	312	113	156	416	260	217	61	3.6	-0.08
23.94	18.0	18.0	265	350	199	-12	146	134	333	73	309	110	146	406	260	207	61	3.4	-0.08
24.09	18.5	18.5	290	375	199	-13	156	139	338	78	312	113	156	416	260	217	62	3.5	-0.08
24.24	19.0	19.0	306	391	198	-13	161	143	341	81	314	116	161	421	260	223	62	3.6	-0.08
24.39	19.5	19.5	298	383	198	-13	157	141	339	79	312	114	157	417	260	219	62	3.5	-0.08
24.54	20.0	20.0	308	393	197	-14	160	143	340	80	313	116	160	420	260	223	63	3.6	-0.09
24.69	20.5	20.5	304	389	197	-14	157	141	339	79	312	115	157	417	260	220	63	3.5	-0.09
24.85	21.0	21.0	282	367	197	-14	148	137	334	74	309	112	148	408	260	211	63	3.3	-0.10
25.01	21.5	21.5	309	394	196	-15	158	142	339	79	313	116	158	418	260	221	64	3.5	-0.09
25.17	22.0	22.0	306	391	196	-15	155	141	338	78	312	115	155	415	260	219	64	3.4	-0.10
25.33	22.5	22.5	325	410	196	-15	162	145	341	81	314	118	162	422	260	226	64	3.5	-0.09
25.49	23.0	23.0	317	402	196	-15	158	143	339	79	313	117	158	418	260	222	64	3.5	-0.10
25.66	23.5	23.5	328	413	196	-16	161	145	340	80	314	118	161	421	260	225	64	3.5	-0.10
25.83	24.0	24.0	321	406	195	-16	157	143	339	79	312	117	157	417	260	222	65	3.4	-0.10

Note: Shaded area indicates the yielding zone

Table A.19. Test series LCU-K_{iso} (K = 1.5) - sample preparation:

Location					Loc No.		
Operator	HTP				Sample No.		B44
Test type	EX	CU	CD	UU	Date started	11/28/2003	
Specimen type	Undisturbed	Remoulded	Recompacted		Nominal diameter		50
Specimen preparation	Compact in an 2.8x5.6 mold with 5 blows on each side						
Soil type and description	Western Iowa loess						

MEASUREMENTS (mm)			INITIAL CONDITIONS	
Initial length			Area Ao (cm^2)	19.63
			Volume Vo (cm^3)	196.25
Average Lc	mm	100	Density (g/cm^3)	1.92
Initial diameter			Moisture content (%)	18.50
Average Do	mm	50	Dry density (g/cm^3)	1.622

WEIGHINGS	Trimmings	Specimen			LOCATION OF SPECIMEN
		initially	after test		
Container no.					
Specimen + cont.					
Container					
Mass of specimen	Wo	377.2	400.6	Wf	
Dry spec. + cont.					
Dry mass of spec.			318.3	Wd	
Moiture		58.90	82.30	Mf	
Moiture content		18.50	25.86		
Volume of solid		120.17			
Volume of the void		76.08			
Void ratio		0.63			

Table A.20. Test series LCU-K_{iso} (K = 1.5) - shearing:

Date					Location									Sample No.					B44
Test	CD	CU	EX	UU	Membrane		With		side drains					Ram pressure			0	kPa	
Rate of strain			0.635	mm/min	Operator	HTP	Without							Tensile pressure			0	kPa	
							Proving ring No.							Cell pressure			285	kPa	
Consolidated length			100	mm	Consolidated area			19.63					cm^2	Pore pressure			210.9	kPa	
Corr.	Strain		Axial Load		Pore pressure		Deviator stress							Principal stresses					
Area cm^2	Displ. mm	ε %	Read N	Load N	U kPa	ΔU kPa	σa kPa	p' kPa	p kPa	q kPa	p-cam kPa	p'-cam kPa	q-cam kPa	σ1 kPa	σ3 kPa	σ'1 kPa	σ'3 kPa	σ'1/σ'3 -	A
19.63	0.0	0.0	-134	0	211	0	0	74	285	0	285	74	0	285	285	74	74	1.0	
19.69	0.3	0.3	43	177	226	15	90	104	330	45	315	89	90	375	285	149	59	2.5	0.16
19.74	0.5	0.5	52	186	228	17	94	104	332	47	316	89	94	379	285	152	57	2.6	0.18
19.79	0.8	0.8	112	246	229	18	124	118	347	62	326	98	124	409	285	180	56	3.2	0.14
19.83	1.0	1.0	129	262	229	19	132	122	351	66	329	100	132	417	285	188	56	3.4	0.14
19.88	1.3	1.3	148	282	229	18	142	127	356	71	332	103	142	427	285	198	56	3.5	0.13
19.94	1.5	1.5	159	293	228	18	147	130	358	73	334	106	147	432	285	203	57	3.6	0.12
19.99	1.8	1.8	148	282	228	17	141	128	355	70	332	104	141	426	285	198	57	3.5	0.12
20.03	2.0	2.0	156	290	227	16	145	130	357	72	333	106	145	430	285	203	58	3.5	0.11
20.08	2.3	2.3	189	323	227	16	161	139	365	80	339	112	161	446	285	219	58	3.8	0.10
20.14	2.5	2.5	197	331	226	15	164	141	367	82	340	114	164	449	285	223	59	3.8	0.09
20.19	2.8	2.8	203	337	226	15	167	143	368	83	341	115	167	452	285	226	59	3.8	0.09
20.24	3.0	3.0	191	325	225	14	161	140	365	80	339	113	161	446	285	221	60	3.7	0.09
20.29	3.3	3.3	216	350	225	14	172	146	371	86	342	117	172	457	285	232	60	3.9	0.08
20.35	3.5	3.5	189	323	225	14	159	140	364	79	338	113	159	444	285	219	61	3.6	0.09
20.39	3.8	3.8	207	341	224	13	167	145	369	84	341	117	167	452	285	228	61	3.7	0.08
20.45	4.0	4.0	230	364	224	13	178	150	374	89	344	120	178	463	285	239	61	3.9	0.07
20.51	4.3	4.3	207	341	224	13	166	145	368	83	340	117	166	451	285	228	62	3.7	0.08
20.55	4.5	4.5	213	347	223	12	169	146	369	84	341	118	169	454	285	231	62	3.7	0.07
20.61	4.8	4.8	241	375	223	12	182	153	376	91	346	123	182	467	285	244	62	3.9	0.07
20.67	5.1	5.1	246	380	223	12	184	154	377	92	346	124	184	469	285	246	63	3.9	0.06
20.77	5.5	5.5	222	356	222	11	171	149	371	86	342	120	171	456	285	234	63	3.7	0.06
20.89	6.0	6.0	257	391	222	11	187	157	379	94	347	126	187	472	285	251	63	4.0	0.06
20.99	6.5	6.5	246	380	221	11	181	154	376	91	345	124	181	466	285	245	64	3.8	0.06
21.11	7.0	7.0	271	405	221	10	192	160	381	96	349	128	192	477	285	256	64	4.0	0.05
21.22	7.5	7.5	276	410	220	10	193	161	382	97	349	129	193	478	285	258	65	4.0	0.05
21.35	8.0	8.0	284	418	220	9	196	163	383	98	350	131	196	481	285	261	65	4.0	0.05
21.45	8.5	8.5	290	424	219	8	198	164	384	99	351	132	198	483	285	263	66	4.0	0.04
21.58	9.1	9.1	263	396	219	8	184	158	377	92	346	127	184	469	285	250	66	3.8	0.04
21.69	9.5	9.5	298	432	218	7	199	166	385	100	351	133	199	484	285	266	67	4.0	0.04
21.81	10.0	10.0	265	399	218	7	183	159	377	92	346	128	183	468	285	250	67	3.7	0.04
21.94	10.5	10.5	306	440	217	6	201	168	385	100	352	135	201	486	285	268	68	4.0	0.03
22.06	11.0	11.0	312	446	217	6	202	169	386	101	352	135	202	487	285	270	68	4.0	0.03
22.19	11.6	11.6	312	446	217	6	201	169	385	100	352	135	201	486	285	269	68	3.9	0.03
22.31	12.0	12.0	323	457	216	5	205	171	387	102	353	137	205	490	285	274	69	4.0	0.03
22.43	12.5	12.5	298	432	216	5	193	166	381	96	349	134	193	478	285	262	69	3.8	0.02
22.57	13.0	13.0	331	465	215	4	206	173	388	103	354	139	206	491	285	276	70	3.9	0.02
22.70	13.5	13.5	312	446	215	4	196	169	383	98	350	136	196	481	285	267	71	3.8	0.02
22.84	14.0	14.0	336	470	214	4	206	174	388	103	354	139	206	491	285	277	71	3.9	0.02
22.96	14.5	14.5	342	476	214	3	207	175	389	104	354	140	207	492	285	278	71	3.9	0.01
23.10	15.0	15.0	347	481	214	3	208	176	389	104	354	141	208	493	285	280	71	3.9	0.01
23.23	15.5	15.5	328	462	213	3	199	171	384	99	351	138	199	484	285	271	72	3.8	0.01
23.37	16.0	16.0	355	489	213	2	209	177	390	105	355	142	209	494	285	281	72	3.9	0.01
23.51	16.5	16.5	333	467	212	2	199	172	384	99	351	139	199	484	285	271	73	3.7	0.01
23.66	17.0	17.0	361	495	212	2	209	177	390	105	355	142	209	494	285	282	73	3.9	0.01
23.79	17.5	17.5	342	476	212	1	200	173	385	100	352	140	200	485	285	273	73	3.7	0.00
23.94	18.0	18.0	366	500	211	0	209	178	389	104	355	143	209	494	285	283	74	3.8	0.00
24.10	18.6	18.6	370	504	211	0	209	178	390	105	355	143	209	494	285	283	74	3.8	0.00
24.24	19.0	19.0	375	509	211	0	210	179	390	105	355	144	210	495	285	284	74	3.8	0.00
24.40	19.5	19.5	380	513	210	-1	210	180	390	105	355	145	210	495	285	285	75	3.8	0.00
24.54	20.0	20.0	374	508	210	-1	207	178	389	104	354	144	207	492	285	282	75	3.8	0.00
24.69	20.5	20.5	351	485	210	-1	196	173	383	98	350	141	196	481	285	272	75	3.6	-0.01
24.85	21.0	21.0	388	522	210	-1	210	180	390	105	355	145	210	495	285	285	75	3.8	-0.01
25.01	21.5	21.5	355	489	209	-2	196	173	383	98	350	141	196	481	285	271	76	3.6	-0.01
25.17	22.0	22.0	388	522	209	-2	207	180	389	104	354	145	207	492	285	283	76	3.7	-0.01
25.33	22.5	22.5	399	533	209	-2	210	181	390	105	355	146	210	495	285	286	76	3.8	-0.01
25.49	23.0	23.0	394	528	209	-2	207	180	388	103	354	145	207	492	285	283	76	3.7	-0.01
25.66	23.5	23.5	405	539	209	-2	210	181	390	105	355	146	210	495	285	286	76	3.7	-0.01
25.83	24.0	24.0	375	509	208	-3	197	175	384	99	351	142	197	482	285	274	77	3.6	-0.01

Note: Shaded area indicates yielding zone

Table A.21. Test series LCU-K_{iso} (K = 2.0) - sample preparation:

Location					Loc No.		
Operator	HTP				Sample No.		B45
Test type	EX	CU	CD	UU	Date started	11/29/2003	
Specimen type	Undisturbed	Remoulded	Recompacted		Nominal diameter		50
Specimen preparation	Compact in an 2.8x5.6 mold with 5 blows on each side						
Soil type and description	Western Iowa loess						

MEASUREMENTS (mm)			INITIAL CONDITIONS	
Initial length			Area Ao (cm^2)	19.63
			Volume Vo (cm^3)	196.25
Average L_o	mm	100	Density (g/cm^3)	1.92
Initial diameter			Moisture content (%)	18.35
Average D_o	mm	50	Dry density (g/cm^3)	1.622

WEIGHINGS	Trimmings	Specimen			LOCATION OF SPECIMEN
		initially	after test		
Container no.					
Specimen + cont.					
Container					
Mass of specimen	Wo	376.7	400.3	Wf	
Dry spec. + cont.					
Dry mass of spec.			318.3	Wd	
Moiture		58.40	82.00	Mf	
Moiture content		18.35	25.76		
Volume of solid		120.17			
Volume of the void		76.08			
Void ratio		0.63			

Table A.22. Test series LCU-K_{iso} (K = 2.0) - shearing:

Date					Location										Sample No.					B45
Test	CD	CU	EX	UU	Membrane			With		side drains					Ram pressure			0	kPa	
Rate of strain			0.635	mm/min	Operator		HTP	Without							Tensile pressure			0	kPa	
								Proving ring No.							Cell pressure			285	kPa	
Consolidated length			100	mm	Consolidated area				19.63					cm^2	Pore pressure			211.8	kPa	
Corr.	Strain		Axial Load		Pore pressure		Deviator stress								Principal stresses					
Area	Displ.	ε	Read	Load	U	ΔU	σa	p'	p	q	p-cam	p'-cam	q-cam		σ1	σ3	σ'1	σ'3	σ'1/σ'3	A
cm^2	mm	%	N	N	kPa	kPa	kPa	kPa	kPa	kPa	kPa	kPa	kPa		kPa	kPa	kPa	kPa	-	
19.63	0.0	0.0	-159	0	212	0	0	73	285	0	285	73	0		285	285	73	73	1.0	
19.69	0.3	0.3	30	189	222	10	96	111	333	48	317	95	96		381	285	159	63	2.5	0.11
19.74	0.5	0.5	85	244	227	15	124	120	347	62	326	99	124		409	285	182	58	3.1	0.12
19.79	0.8	0.8	117	276	231	19	139	124	355	70	331	101	139		424	285	194	54	3.6	0.14
19.83	1.0	1.0	157	316	233	21	159	131	365	80	338	105	159		444	285	211	52	4.1	0.13
19.88	1.3	1.3	180	339	234	23	171	136	370	85	342	108	171		456	285	221	51	4.4	0.13
19.94	1.5	1.5	184	343	236	24	172	136	371	86	342	107	172		457	285	222	50	4.5	0.14
19.99	1.8	1.8	214	373	236	24	187	142	378	93	347	111	187		472	285	236	49	4.8	0.13
20.03	2.0	2.0	196	355	236	25	177	137	374	89	344	108	177		462	285	226	49	4.6	0.14
20.08	2.3	2.3	216	375	236	25	187	142	378	93	347	111	187		472	285	235	49	4.8	0.13
20.14	2.5	2.5	239	398	236	25	198	147	384	99	351	115	198		483	285	246	49	5.1	0.12
20.19	2.8	2.8	249	408	236	25	202	150	386	101	352	116	202		487	285	251	49	5.2	0.12
20.24	3.0	3.0	230	389	236	25	192	145	381	96	349	113	192		477	285	241	49	5.0	0.13
20.29	3.3	3.3	260	419	236	25	206	152	388	103	354	117	206		491	285	255	49	5.2	0.12
20.35	3.5	3.5	265	424	236	24	208	153	389	104	354	119	208		493	285	258	49	5.2	0.12
20.39	3.8	3.8	232	391	236	24	192	145	381	96	349	113	192		477	285	241	49	4.9	0.13
20.45	4.0	4.0	276	435	236	24	213	155	391	106	356	120	213		498	285	262	49	5.3	0.11
20.51	4.3	4.3	279	438	236	24	214	156	392	107	356	120	214		499	285	263	49	5.3	0.11
20.55	4.5	4.5	250	409	235	24	199	149	385	100	351	116	199		484	285	249	50	5.0	0.12
20.61	4.8	4.8	289	448	235	24	218	158	394	109	358	122	218		503	285	267	50	5.4	0.11
20.67	5.1	5.1	253	412	235	24	199	149	385	100	351	116	199		484	285	249	50	5.0	0.12
20.77	5.5	5.5	300	459	235	23	221	161	396	111	359	124	221		506	285	271	50	5.4	0.10
20.89	6.0	6.0	306	465	235	23	223	162	396	111	359	124	223		508	285	273	50	5.4	0.10
20.99	6.5	6.5	276	435	234	23	207	154	389	104	354	120	207		492	285	258	51	5.1	0.11
21.11	7.0	7.0	320	479	234	23	227	164	398	113	361	126	227		512	285	278	51	5.5	0.10
21.22	7.5	7.5	327	486	234	22	229	166	399	114	361	128	229		514	285	280	51	5.5	0.10
21.35	8.0	8.0	292	451	233	21	211	157	391	106	355	122	211		496	285	263	52	5.1	0.10
21.45	8.5	8.5	318	477	233	21	222	163	396	111	359	126	222		507	285	274	52	5.3	0.10
21.58	9.1	9.1	302	461	233	21	214	159	392	107	356	124	214		499	285	266	52	5.1	0.10
21.69	9.5	9.5	328	487	232	20	225	165	397	112	360	128	225		510	285	277	53	5.2	0.09
21.81	10.0	10.0	356	515	232	20	236	171	403	118	364	132	236		521	285	289	53	5.5	0.09
21.94	10.5	10.5	339	498	232	20	227	167	398	113	361	129	227		512	285	280	53	5.3	0.09
22.06	11.0	11.0	366	525	231	19	238	173	404	119	364	133	238		523	285	292	54	5.4	0.08
22.19	11.6	11.6	372	531	231	19	239	174	405	120	365	134	239		524	285	293	54	5.4	0.08
22.31	12.0	12.0	345	504	230	18	226	168	398	113	360	130	226		511	285	281	55	5.1	0.08
22.43	12.5	12.5	380	539	230	18	240	175	405	120	365	135	240		525	285	295	55	5.4	0.08
22.57	13.0	13.0	364	523	229	18	232	171	401	116	362	133	232		517	285	287	56	5.2	0.08
22.70	13.5	13.5	391	550	229	17	242	177	406	121	366	137	242		527	285	298	56	5.3	0.07
22.84	14.0	14.0	394	553	228	17	242	178	406	121	366	137	242		527	285	299	57	5.3	0.07
22.96	14.5	14.5	355	514	228	16	224	169	397	112	360	132	224		509	285	281	57	4.9	0.07
23.10	15.0	15.0	405	564	228	16	244	179	407	122	366	139	244		529	285	301	57	5.3	0.07
23.23	15.5	15.5	407	566	227	16	244	180	407	122	366	139	244		529	285	302	58	5.2	0.06
23.37	16.0	16.0	388	547	227	15	234	175	402	117	363	136	234		519	285	292	58	5.0	0.06
23.51	16.5	16.5	416	575	226	14	244	181	407	122	366	140	244		529	285	303	59	5.2	0.06
23.66	17.0	17.0	394	553	226	14	234	176	402	117	363	137	234		519	285	293	59	4.9	0.06
23.79	17.5	17.5	424	583	226	14	245	182	407	122	367	141	245		530	285	304	59	5.1	0.06
23.94	18.0	18.0	402	561	225	13	234	177	402	117	363	138	234		519	285	294	60	4.9	0.06
24.10	18.6	18.6	430	589	225	13	244	182	407	122	366	142	244		529	285	305	60	5.1	0.05
24.24	19.0	19.0	399	558	225	13	230	176	400	115	362	137	230		515	285	291	60	4.8	0.06
24.40	19.5	19.5	437	596	224	12	244	183	407	122	366	142	244		529	285	305	61	5.0	0.05
24.54	20.0	20.0	406	565	224	12	230	177	400	115	362	138	230		515	285	292	61	4.8	0.05
24.69	20.5	20.5	446	605	224	12	245	184	407	122	367	143	245		530	285	306	61	5.0	0.05
24.85	21.0	21.0	448	607	224	12	244	184	407	122	366	143	244		529	285	306	61	5.0	0.05
25.01	21.5	21.5	402	561	223	11	224	174	397	112	360	137	224		509	285	286	62	4.6	0.05
25.17	22.0	22.0	456	615	223	11	244	185	407	122	366	144	244		529	285	307	63	4.9	0.04
25.33	22.5	22.5	459	618	223	11	244	185	407	122	366	144	244		529	285	307	63	4.9	0.04
25.49	23.0	23.0	462	621	222	10	244	185	407	122	366	144	244		529	285	306	63	4.9	0.04
25.66	23.5	23.5	419	578	222	10	225	176	398	113	360	138	225		510	285	288	63	4.6	0.05
25.83	24.0	24.0	470	629	222	10	244	185	407	122	366	144	244		529	285	307	63	4.9	0.04

Note: Shaded area indicates yielding zone

Table A. 23. Test series LCU-K_{iso} (K = 2.5) - sample preparation:

Location					Loc No.		
Operator	HTP				Sample No.		B46
Test type	EX	CU	CD	UU	Date started	11/30/2003	
Specimen type	Undisturbed	Remoulded	Recompacted		Nominal diameter		50
Specimen preparation	Compact in an 2.8x5.6 mold with 5 blows on each side						
Soil type and description	Western Iowa loess						

MEASUREMENTS (mm)			INITIAL CONDITIONS	
Initial length			Area Ao (cm^2)	19.63
			Volume Vo (cm^3)	196.25
Average L_o	mm	100	Density (g/cm^3)	1.92
Initial diameter			Moisture content (%)	18.08
Average D_o	mm	50	Dry density (g/cm^3)	1.626

WEIGHINGS	Trimmings	Specimen			LOCATION OF SPECIMEN
		initially	after test		
Container no.					
Specimen + cont.					
Container					
Mass of specimen	w_o	376.9	398.8	w_f	
Dry spec. + cont.					
Dry mass of spec.			319.2	w_d	
Moiture		57.70	79.60	M_f	
Moiture content		18.08	24.94		
Volume of solid		120.51			
Volume of the void		75.74			
Void ratio		0.63			

Table A.24. Test series LCU-K_{iso} (K = 2.5) - shearing:

Date					Location										Sample No.					B46
Test	CD	CU	EX	UU	Membrane			With		side drains					Ram pressure			0	kPa	
Rate of strain			0.635	mm/min	Operator		HTP	Without							Tensile pressure			0	kPa	
								Proving ring No.							Cell pressure			310	kPa	
Consolidated length			100	mm	Consolidated area					19.63				cm^2	Pore pressure			211.3	kPa	
Corr.	Strain		Axial Load		Pore pressure		Deviator stress								Principal stresses					
Area	Displ.	ε	Read	Load	U	ΔU	σa	p'	p	q	p-cam	p'-cam	q-cam		σ1	σ3	σ'1	σ'3	σ'1/σ'3	A
cm^2	mm	%	N	N	kPa	kPa	kPa	kPa	kPa	kPa	kPa	kPa	kPa		kPa	kPa	kPa	kPa	-	
19.63	0.0	0.0	-189	0	211	0	0	99	310	0	310	99	0		310	310	99	99	1.0	
19.68	0.3	0.3	16	205	225	14	104	137	362	52	345	120	104		414	310	189	85	2.2	0.13
19.74	0.5	0.5	96	285	233	22	144	149	382	72	358	125	144		454	310	221	77	2.9	0.15
19.78	0.8	0.8	142	331	237	26	167	156	394	84	366	129	167		477	310	240	73	3.3	0.15
19.84	1.0	1.0	164	353	241	29	178	158	399	89	369	129	178		488	310	247	69	3.6	0.17
19.88	1.3	1.3	197	386	243	32	194	164	407	97	375	132	194		504	310	261	67	3.9	0.16
19.93	1.5	1.5	213	402	244	33	202	167	411	101	377	133	202		512	310	267	66	4.1	0.16
19.98	1.8	1.8	208	397	245	34	199	164	409	99	376	131	199		509	310	264	65	4.1	0.17
20.03	2.0	2.0	238	427	246	35	213	171	417	107	381	135	213		523	310	277	64	4.3	0.16
20.09	2.3	2.3	249	438	247	36	218	172	419	109	383	136	218		528	310	281	63	4.5	0.16
20.14	2.5	2.5	258	447	248	36	222	173	421	111	384	136	222		532	310	284	62	4.6	0.16
20.19	2.8	2.8	265	454	248	37	225	174	422	112	385	137	225		535	310	287	62	4.6	0.16
20.24	3.0	3.0	268	457	248	37	226	175	423	113	385	137	226		536	310	288	62	4.6	0.16
20.30	3.3	3.3	273	462	249	37	228	175	424	114	386	137	228		538	310	289	61	4.7	0.16
20.35	3.5	3.5	281	470	249	37	231	177	426	116	387	138	231		541	310	292	61	4.8	0.16
20.40	3.8	3.8	282	471	249	38	231	176	426	116	387	138	231		541	310	292	61	4.8	0.16
20.45	4.0	4.0	288	477	249	38	233	177	427	117	388	139	233		543	310	294	61	4.8	0.16
20.50	4.3	4.3	293	482	249	38	235	178	428	118	388	139	235		545	310	296	61	4.9	0.16
20.55	4.5	4.5	296	485	250	38	236	178	428	118	389	139	236		546	310	296	60	4.9	0.16
20.61	4.8	4.8	301	490	250	38	238	179	429	119	389	139	238		548	310	298	60	4.9	0.16
20.66	5.0	5.0	306	495	250	38	240	180	430	120	390	140	240		550	310	300	60	5.0	0.16
20.77	5.5	5.5	312	501	250	38	241	181	431	121	390	141	241		551	310	301	60	5.0	0.16
20.89	6.0	6.0	320	509	250	38	244	182	432	122	391	141	244		554	310	304	60	5.0	0.16
20.99	6.5	6.5	333	522	250	38	249	185	434	124	393	143	249		559	310	309	60	5.1	0.15
21.11	7.0	7.0	337	526	250	38	249	185	435	125	393	143	249		559	310	310	60	5.1	0.15
21.22	7.5	7.5	345	534	249	38	251	186	436	126	394	144	251		561	310	312	61	5.1	0.15
21.34	8.0	8.0	347	536	249	38	251	186	436	126	394	145	251		561	310	312	61	5.1	0.15
21.46	8.5	8.5	350	539	249	38	251	187	436	126	394	145	251		561	310	312	61	5.1	0.15
21.57	9.0	9.0	356	545	249	37	253	188	436	126	394	146	253		563	310	314	61	5.1	0.15
21.69	9.5	9.5	362	551	248	37	254	189	437	127	395	146	254		564	310	316	62	5.1	0.15
21.82	10.0	10.0	377	566	248	37	260	192	440	130	397	148	260		570	310	321	62	5.2	0.14
21.94	10.5	10.5	375	564	248	36	257	191	438	128	396	148	257		567	310	319	62	5.1	0.14
22.06	11.0	11.0	361	550	247	36	249	188	435	125	393	146	249		559	310	312	63	5.0	0.14
22.19	11.5	11.5	386	575	247	36	259	192	439	129	396	149	259		569	310	322	63	5.1	0.14
22.31	12.0	12.0	391	580	247	35	260	193	440	130	397	150	260		570	310	323	64	5.1	0.14
22.44	12.5	12.5	402	591	246	35	263	195	442	132	398	151	263		573	310	327	64	5.1	0.13
22.57	13.0	13.0	402	591	246	35	262	195	441	131	397	151	262		572	310	326	64	5.1	0.13
22.70	13.5	13.5	411	600	246	34	264	197	442	132	398	153	264		574	310	329	65	5.1	0.13
22.83	14.0	14.0	410	599	245	34	262	196	441	131	397	153	262		572	310	327	65	5.0	0.13
22.96	14.5	14.5	403	592	244	33	258	195	439	129	396	152	258		568	310	324	66	4.9	0.13
23.10	15.0	15.0	421	610	244	33	264	198	442	132	398	154	264		574	310	330	66	5.0	0.12
23.23	15.5	15.5	411	600	243	32	258	196	439	129	396	153	258		568	310	325	67	4.9	0.12
23.37	16.0	16.0	429	618	243	32	264	199	442	132	398	155	264		574	310	332	67	4.9	0.12
23.51	16.5	16.5	402	591	242	31	251	193	436	126	394	151	251		561	310	319	68	4.7	0.12
23.66	17.0	17.0	438	627	242	30	265	201	443	133	398	157	265		575	310	333	68	4.9	0.11
23.79	17.5	17.5	416	605	241	30	254	196	437	127	395	153	254		564	310	323	69	4.7	0.12
23.94	18.0	18.0	446	635	241	29	265	202	443	133	398	158	265		575	310	334	69	4.8	0.11
24.09	18.5	18.5	448	637	240	29	265	202	442	132	398	158	265		575	310	335	70	4.8	0.11
24.24	19.0	19.0	451	640	240	28	264	202	442	132	398	158	264		574	310	334	70	4.8	0.11
24.39	19.5	19.5	462	651	240	28	267	204	443	133	399	159	267		577	310	337	71	4.8	0.11
24.54	20.0	20.0	459	648	239	28	264	203	442	132	398	159	264		574	310	335	71	4.7	0.11
24.69	20.5	20.5	470	659	239	27	267	205	443	133	399	160	267		577	310	338	72	4.7	0.10
24.85	21.0	21.0	465	654	239	27	263	203	442	132	398	159	263		573	310	335	72	4.7	0.10
25.01	21.5	21.5	443	632	238	27	253	198	436	126	394	156	253		563	310	325	72	4.5	0.11
25.17	22.0	22.0	473	662	238	26	263	204	442	132	398	160	263		573	310	336	73	4.6	0.10
25.33	22.5	22.5	461	650	237	26	257	201	438	128	396	159	257		567	310	330	73	4.5	0.10
25.49	23.0	23.0	478	667	237	26	262	204	441	131	397	160	262		572	310	335	73	4.6	0.10
25.66	23.5	23.5	481	670	237	25	261	204	441	131	397	161	261		571	310	335	74	4.6	0.10
25.83	24.0	24.0	430	619	236	25	240	193	430	120	390	153	240		550	310	313	74	4.3	0.10

Note: Shaded area indicates yielding zone

Table A.25. Test series LCU-K_{iso} (K = 3.0) - sample preparation:

Location					Loc No.		
Operator	HTP				Sample No.		B47
Test type	EX	CU	CD	UU	Date started	12/1/2003	
Specimen type	Undisturbed	Remoulded	Recompacted		Nominal diameter		50
Specimen preparation	Compact in an 2.8x5.6 mold with 5 blows on each side						
Soil type and description	Western Iowa loess						

MEASUREMENTS (mm)			INITIAL CONDITIONS	
Initial length			Area Ao (cm^2)	19.63
			Volume Vo (cm^3)	196.25
Average L_o	mm	100	Density (g/cm^3)	1.93
Initial diameter			Moisture content (%)	18.61
Average D_o	mm	50	Dry density (g/cm^3)	1.624

WEIGHINGS	Trimmings	Specimen			LOCATION OF SPECIMEN
		initially	after test		
Container no.					
Specimen + cont.					
Container					
Mass of specimen	W_o	378	400.6	W_f	
Dry spec. + cont.					
Dry mass of spec.			318.7	W_d	
Moiture		59.30	81.90	M_f	
Moiture content		18.61	25.70		
Volume of solid		120.32			
Volume of the void		75.93			
Void ratio		0.63			

Table A.26. Test series LCU-K_{iso} (K = 3.0) - shearing:

Date					Location										Sample No.					B47
Test	CD	CU	EX	UU	Membrane		With	side drains							Ram pressure		0	kPa		
Rate of strain			0.635	mm/min	Operator	HTP	Without								Tensile pressure		0	kPa		
							Proving ring No.								Cell pressure		310	kPa		
Consolidated length			100	mm	Consolidated area		19.63							cm^2	Pore pressure		215	kPa		
Corr.	Strain		Axial Load		Pore pressure		Deviator stress								Principal stresses					
Area	Displ.	ε	Read	Load	U	ΔU	σa	p'	p	q	p-cam	p'-cam	q-cam		σ1	σ3	σ'1	σ'3	σ'1/σ'3	A
cm^2	mm	%	N	N	kPa	kPa	kPa	kPa	kPa	kPa	kPa	kPa	kPa		kPa	kPa	kPa	kPa	-	
19.63	0.0	0.0	-219	0	215	0	0	95	310	0	310	95	0		310	310	95	95	1.0	
19.69	0.3	0.3	11	230	227	12	117	141	368	58	349	122	117		427	310	200	83	2.4	0.11
19.73	0.5	0.5	66	285	235	20	144	147	382	72	358	123	144		454	310	219	75	2.9	0.14
19.78	0.8	0.8	159	378	242	27	191	164	405	95	374	132	191		501	310	259	69	3.8	0.14
19.83	1.0	1.0	194	413	246	31	208	168	414	104	379	133	208		518	310	272	64	4.3	0.15
19.88	1.3	1.3	226	445	250	35	224	172	422	112	385	134	224		534	310	284	60	4.8	0.16
19.94	1.5	1.5	247	466	253	38	234	174	427	117	388	135	234		544	310	291	57	5.1	0.16
19.98	1.8	1.8	252	471	255	40	235	173	428	118	388	133	235		545	310	290	55	5.3	0.17
20.03	2.0	2.0	265	484	257	42	242	174	431	121	391	133	242		552	310	295	53	5.6	0.17
20.09	2.3	2.3	279	498	259	44	248	175	434	124	393	134	248		558	310	299	51	5.8	0.18
20.14	2.5	2.5	298	517	260	45	257	178	438	128	396	136	257		567	310	307	50	6.1	0.18
20.19	2.8	2.8	306	525	261	46	260	179	440	130	397	135	260		570	310	309	49	6.4	0.18
20.24	3.0	3.0	301	520	262	47	257	176	438	128	396	134	257		567	310	305	48	6.4	0.18
20.30	3.3	3.3	309	528	263	48	260	177	440	130	397	134	260		570	310	307	47	6.5	0.18
20.35	3.5	3.5	325	544	264	49	268	180	444	134	399	136	268		578	310	314	46	6.8	0.18
20.39	3.8	3.8	320	539	264	49	264	178	442	132	398	134	264		574	310	310	46	6.8	0.19
20.45	4.0	4.0	338	557	265	50	272	181	446	136	401	136	272		582	310	317	45	7.0	0.18
20.51	4.3	4.3	339	558	265	50	272	181	446	136	401	136	272		582	310	317	45	7.1	0.18
20.55	4.5	4.5	347	566	266	51	275	182	448	138	402	136	275		585	310	320	44	7.2	0.18
20.61	4.8	4.8	336	555	266	51	269	178	445	135	400	133	269		579	310	313	44	7.2	0.19
20.67	5.0	5.0	350	569	267	52	275	181	448	138	402	135	275		585	310	319	44	7.3	0.19
20.77	5.5	5.5	345	564	267	52	271	179	446	136	400	133	271		581	310	314	43	7.3	0.19
20.88	6.0	6.0	365	584	267	52	280	183	450	140	403	136	280		590	310	322	43	7.5	0.19
20.99	6.5	6.5	358	577	268	53	275	180	447	137	402	134	275		585	310	317	42	7.5	0.19
21.11	7.0	7.0	380	599	268	53	284	184	452	142	405	137	284		594	310	326	42	7.7	0.19
21.23	7.5	7.5	373	592	268	53	279	181	449	139	403	135	279		589	310	321	42	7.6	0.19
21.34	8.0	8.0	395	614	268	53	287	185	454	144	406	137	287		597	310	329	42	7.9	0.19
21.46	8.5	8.5	383	602	268	53	280	182	450	140	403	135	280		590	310	322	42	7.7	0.19
21.58	9.0	9.0	407	626	268	53	290	187	455	145	407	139	290		600	310	332	42	7.9	0.18
21.69	9.5	9.5	394	613	268	53	282	183	451	141	404	136	282		592	310	325	42	7.7	0.19
21.82	10.0	10.0	421	640	268	53	293	189	457	147	408	140	293		603	310	335	42	8.0	0.18
21.93	10.5	10.5	427	646	268	53	294	189	457	147	408	140	294		604	310	336	42	8.0	0.18
22.06	11.0	11.0	402	621	267	52	281	183	451	141	404	137	281		591	310	324	43	7.6	0.19
22.19	11.5	11.5	435	654	267	52	295	190	457	147	408	141	295		605	310	337	43	7.9	0.18
22.31	12.0	12.0	421	640	267	52	287	187	453	143	406	139	287		597	310	330	43	7.6	0.18
22.44	12.5	12.5	446	665	267	52	296	191	458	148	409	142	296		606	310	339	43	7.9	0.17
22.57	13.0	13.0	432	651	266	51	288	188	454	144	406	140	288		598	310	332	44	7.6	0.18
22.70	13.5	13.5	457	676	266	51	298	193	459	149	409	144	298		608	310	342	44	7.7	0.17
22.83	14.0	14.0	462	681	266	51	298	194	459	149	409	144	298		608	310	343	44	7.7	0.17
22.96	14.5	14.5	443	662	265	50	288	189	454	144	406	141	288		598	310	333	45	7.4	0.17
23.10	15.0	15.0	468	687	265	50	297	194	459	149	409	144	297		607	310	343	45	7.6	0.17
23.23	15.5	15.5	433	652	264	49	281	186	450	140	404	139	281		591	310	326	46	7.2	0.18
23.37	16.0	16.0	476	695	264	49	297	195	459	149	409	145	297		607	310	343	46	7.5	0.17
23.51	16.5	16.5	432	651	264	49	277	185	448	138	402	139	277		587	310	323	46	7.0	0.18
23.65	17.0	17.0	484	703	264	49	297	195	459	149	409	145	297		607	310	344	46	7.4	0.16
23.79	17.5	17.5	446	665	263	48	279	187	450	140	403	140	279		589	310	326	47	7.0	0.17
23.94	18.0	18.0	468	687	263	48	287	190	453	143	406	142	287		597	310	334	47	7.1	0.17
24.09	18.5	18.5	492	711	263	48	295	195	458	148	408	146	295		605	310	343	48	7.2	0.16
24.24	19.0	19.0	473	692	263	48	286	190	453	143	405	143	286		596	310	333	48	7.0	0.17
24.39	19.5	19.5	503	722	263	48	296	196	458	148	409	146	296		606	310	344	48	7.2	0.16
24.54	20.0	20.0	482	701	262	47	286	191	453	143	405	143	286		596	310	334	48	7.0	0.16
24.69	20.5	20.5	506	725	262	47	294	195	457	147	408	146	294		604	310	342	48	7.1	0.16
24.85	21.0	21.0	484	703	262	47	283	190	451	141	404	143	283		593	310	331	49	6.8	0.16
25.01	21.5	21.5	470	689	261	46	276	187	448	138	402	141	276		586	310	324	49	6.6	0.17
25.17	22.0	22.0	513	732	261	46	291	194	455	145	407	146	291		601	310	340	49	6.9	0.16
25.33	22.5	22.5	492	711	261	46	281	189	450	140	404	143	281		591	310	330	49	6.7	0.16
25.49	23.0	23.0	520	739	261	46	290	194	455	145	407	146	290		600	310	339	49	6.9	0.16
25.66	23.5	23.5	495	714	260	45	278	189	449	139	403	142	278		588	310	328	50	6.6	0.16
25.83	24.0	24.0	522	741	260	45	287	193	453	143	406	145	287		597	310	337	50	6.8	0.16

Note: Shaded area indicates yielding zone

Table A.27. Test series LCU-K_o (K = 1.0) – sampe preparation:

Location					Loc No.		
Operator	HTP				Sample No.		B35
Test type	EX	CU	CD	UU	Date started	11/14/2003	
Specimen type	Undisturbed	Remoulded	Recompacted		Nominal diameter		50
Specimen preparation	Compact in an 2.8x5.6 mold with 5 blows on each side						
Soil type and description	Western Iowa loess						

MEASUREMENTS (mm)			INITIAL CONDITIONS	
Initial length			Area Ao (cm^2)	19.63
			Volume Vo (cm^3)	196.25
Average L_o	mm	100	Density (g/cm^3)	1.93
Initial diameter			Moisture content (%)	18.88
Average D_o	mm	50	Dry density (g/cm^3)	1.619

WEIGHINGS	Trimmings	Specimen			LOCATION OF SPECIMEN
		initially	after test		
Container no.					
Specimen + cont.					
Container					
Mass of specimen	Wo	377.8	398.4	Wf	
Dry spec. + cont.					
Dry mass of spec.			317.8	Wd	
Moiture		60.00	80.60	Mf	
Moiture content		18.88	25.36		
Volume of solid		119.98			
Volume of the void		76.27			
Void ratio		0.64			

Table A.28. Test series LCU-K_o (K = 1.0) – shearing:

Date					Location									Sample No.					B35
Test	CD	CU	EX	UU	Membrane		With		side drains					Ram pressure			50	kPa	
Rate of strain			0.635	mm / min	Operator	HTP	Without							Tensile pressure			0	kPa	
							Proving ring No.							Cell pressure			310	kPa	
Consolidated length			100	mm	Consolidated area				19.63				cm^2	Pore pressure			210.2	kPa	
Corr.	Strain		Axial Load		Pore pressure		Deviator stress							Principal stresses					
Area	Displ.	ε	Read	Load	U	ΔU	σa	p'	p	q	p-cam	p'-cam	q-cam	σ1	σ3	σ'1	σ'3	σ'1/σ'3	A
cm^2	mm	%	N	N	kPa	kPa	kPa	kPa	kPa	kPa	kPa	kPa	kPa	kPa	kPa	kPa	kPa	-	
19.63	0.0	0.0	-93	0	210	0	0	125	335	25	327	116	50	360	310	150	100	1.5	
19.69	0.3	0.3	52	145	220	10	74	152	372	62	351	131	124	434	310	214	90	2.4	0.13
19.73	0.5	0.5	87	180	220	10	91	161	381	71	357	137	141	451	310	231	90	2.6	0.11
19.79	0.8	0.8	112	205	218	8	104	168	387	77	361	143	154	464	310	245	92	2.7	0.08
19.83	1.0	1.0	129	222	217	6	112	174	391	81	364	147	162	472	310	255	93	2.7	0.06
19.88	1.3	1.3	145	238	216	5	120	179	395	85	367	151	170	480	310	264	94	2.8	0.05
19.93	1.5	1.5	157	250	214	4	126	184	398	88	369	155	176	486	310	272	96	2.8	0.03
19.99	1.8	1.8	168	261	212	2	130	188	400	90	370	158	180	490	310	278	98	2.8	0.02
20.03	2.0	2.0	178	271	211	1	135	191	403	93	372	160	185	495	310	284	99	2.9	0.01
20.08	2.3	2.3	183	276	210	0	138	194	404	94	373	162	188	498	310	287	100	2.9	0.00
20.14	2.5	2.5	189	282	209	-1	140	196	405	95	373	164	190	500	310	291	101	2.9	-0.01
20.19	2.8	2.8	196	289	209	-2	143	198	406	96	374	166	193	503	310	294	101	2.9	-0.01
20.24	3.0	3.0	197	290	208	-3	143	199	407	97	374	167	193	503	310	296	102	2.9	-0.02
20.29	3.3	3.3	205	298	207	-3	147	201	408	98	376	169	197	507	310	300	103	2.9	-0.02
20.35	3.5	3.5	209	302	206	-4	148	203	409	99	376	170	198	508	310	302	104	2.9	-0.03
20.40	3.8	3.8	202	295	206	-5	145	202	407	97	375	169	195	505	310	299	104	2.9	-0.03
20.45	4.0	4.0	216	309	205	-5	151	205	411	101	377	172	201	511	310	306	105	2.9	-0.03
20.51	4.3	4.3	221	314	205	-6	153	207	412	102	378	173	203	513	310	309	106	2.9	-0.04
20.55	4.5	4.5	208	301	204	-6	146	204	408	98	375	172	196	506	310	303	106	2.8	-0.04
20.61	4.8	4.8	227	320	204	-6	155	209	413	103	378	175	205	515	310	311	106	2.9	-0.04
20.67	5.0	5.0	232	325	203	-7	157	210	414	104	379	176	207	517	310	314	107	2.9	-0.04
20.77	5.5	5.5	229	322	202	-8	155	210	413	103	378	176	205	515	310	313	108	2.9	-0.05
20.89	6.0	6.0	246	339	202	-9	162	214	416	106	381	179	212	522	310	321	108	3.0	-0.05
20.99	6.5	6.5	235	328	201	-9	156	212	413	103	379	178	206	516	310	315	109	2.9	-0.06
21.12	7.0	7.0	257	350	201	-10	166	217	418	108	382	181	216	526	310	325	109	3.0	-0.06
21.22	7.5	7.5	262	355	200	-10	167	219	419	109	382	182	217	527	310	327	110	3.0	-0.06
21.34	8.0	8.0	268	361	200	-11	169	220	420	110	383	183	219	529	310	330	110	3.0	-0.06
21.46	8.5	8.5	271	364	199	-11	169	221	420	110	383	184	219	529	310	330	111	3.0	-0.07
21.57	9.0	9.0	279	372	199	-12	172	223	421	111	384	186	222	532	310	334	112	3.0	-0.07
21.70	9.5	9.5	282	375	198	-12	173	223	421	111	384	186	223	533	310	335	112	3.0	-0.07
21.81	10.0	10.0	274	367	197	-13	168	222	419	109	383	185	218	528	310	331	113	2.9	-0.08
21.94	10.5	10.5	291	384	197	-13	175	226	422	112	385	188	225	535	310	338	113	3.0	-0.08
22.06	11.0	11.0	295	388	196	-14	176	227	423	113	385	189	226	536	310	340	114	3.0	-0.08
22.19	11.5	11.5	304	397	196	-14	179	228	424	114	386	190	229	539	310	342	114	3.0	-0.08
22.31	12.0	12.0	304	397	196	-14	178	228	424	114	386	190	228	538	310	342	114	3.0	-0.08
22.43	12.5	12.5	298	391	195	-15	174	227	422	112	385	189	224	534	310	339	115	3.0	-0.09
22.57	13.0	13.0	317	410	195	-15	182	231	426	116	387	192	232	542	310	347	115	3.0	-0.08
22.70	13.5	13.5	317	410	194	-16	181	231	425	115	387	192	231	541	310	346	116	3.0	-0.09
22.83	14.0	14.0	328	421	194	-16	184	233	427	117	388	194	234	544	310	350	116	3.0	-0.09
22.96	14.5	14.5	326	419	193	-17	183	233	426	116	388	194	233	543	310	349	117	3.0	-0.09
23.10	15.0	15.0	336	429	193	-18	186	235	428	118	389	196	236	546	310	353	117	3.0	-0.09
23.23	15.5	15.5	334	427	193	-18	184	234	427	117	388	195	234	544	310	351	117	3.0	-0.10
23.37	16.0	16.0	342	435	192	-18	186	236	428	118	389	197	236	546	310	354	118	3.0	-0.10
23.51	16.5	16.5	339	432	192	-19	184	235	427	117	388	196	234	544	310	352	118	3.0	-0.10
23.65	17.0	17.0	352	445	192	-19	188	237	429	119	389	198	238	548	310	357	118	3.0	-0.10
23.80	17.5	17.5	350	443	191	-20	186	237	428	118	389	198	236	546	310	355	119	3.0	-0.10
23.95	18.0	18.0	355	448	191	-20	187	238	429	119	389	199	237	547	310	357	120	3.0	-0.11
24.09	18.5	18.5	339	432	190	-20	179	235	425	115	386	196	229	539	310	349	120	2.9	-0.11
24.24	19.0	19.0	361	454	190	-20	187	239	429	119	389	199	237	547	310	357	120	3.0	-0.11
24.39	19.5	19.5	339	432	189	-21	177	234	424	114	386	196	227	537	310	348	121	2.9	-0.12
24.54	20.0	20.0	372	465	189	-21	189	241	430	120	390	201	239	549	310	361	121	3.0	-0.11
24.69	20.5	20.5	361	454	189	-22	184	238	427	117	388	199	234	544	310	355	121	2.9	-0.12
24.85	21.0	21.0	350	443	188	-22	178	236	424	114	386	198	228	538	310	350	122	2.9	-0.12
25.01	21.5	21.5	380	473	188	-22	189	242	430	120	390	202	239	549	310	361	122	3.0	-0.12
25.17	22.0	22.0	392	485	188	-23	193	244	431	121	391	203	243	553	310	365	122	3.0	-0.12
25.33	22.5	22.5	388	481	187	-23	190	243	430	120	390	203	240	550	310	363	123	3.0	-0.12
25.49	23.0	23.0	402	495	187	-23	194	245	432	122	391	205	244	554	310	367	123	3.0	-0.12
25.66	23.5	23.5	394	487	187	-24	190	243	430	120	390	203	240	550	310	363	124	2.9	-0.12
25.83	24.0	24.0	386	479	186	-24	185	241	428	118	388	202	235	545	310	359	124	2.9	-0.13

Note: Shaded area indicates yielding zone

Table A.29. Test series LCU-K_o (K = 1.5) – sample preparation:

Location					Loc No.		
Operator	HTP				Sample No.		B31
Test type	EX	CU	CD	UU	Date started	11/8/2003	
Specimen type	Undisturbed	Remoulded	Recompacted		Nominal diameter		50
Specimen preparation	Compact in an 2.8x5.6 mold with 5 blows on each side						
Soil type and description	Western Iowa loess						

MEASUREMENTS (mm)			INITIAL CONDITIONS	
Initial length			Area Ao (cm^2)	19.63
			Volume Vo (cm^3)	196.25
Average L_o	mm	100	Density (g/cm^3)	1.95
Initial diameter			Moisture content (%)	19.81
Average D_o	mm	50	Dry density (g/cm^3)	1.629

WEIGHINGS	Trimmings	Specimen			LOCATION OF SPECIMEN
		initially	after test		
Container no.					
Specimen + cont.					
Container					
Mass of specimen	Wo	382.9	401.4	Wf	
Dry spec. + cont.					
Dry mass of spec.			319.6	Wd	
Moiture		63.30	81.80	Mf	
Moiture content		19.81	25.59		
Volume of solid		120.66			
Volume of the void		75.59			
Void ratio		0.63			

Table A.30. Test series LCU-K_o (K = 1.5) – shearing:

Date					Location									Sample No.					B31
Test	CD	CU	EX	UU	Membrane		With		side drains					Ram pressure		75	kPa		
Rate of strain			0.635	mm min	Operator	HTP	Without							Tensile pressure		0	kPa		
							Proving ring No.							Cell pressure		310	kPa		
Consolidated length			100	mm	Consolidated area		19.63						cm²	Pore pressure		211.3	kPa		
Corr.	Strain		Axial Load		Pore pressure		Deviator stress							Principal stresses					
Area	Displ.	ε	Read	Load	U	ΔU	σa	p'	p	q	p-cam	p'-cam	q-cam	σ1	σ3	σ'1	σ'3	σ'1/σ'3	A
cm²	mm	%	N	N	kPa	kPa	kPa	kPa	kPa	kPa	kPa	kPa	kPa	kPa	kPa	kPa	kPa	-	
19.65	0.1	0.1	-104	0	211	0	0	136	348	38	335	124	75	385	310	174	99	1.8	
19.68	0.3	0.3	71	175	222	11	89	170	392	82	365	143	164	474	310	252	88	2.9	0.12
19.73	0.5	0.5	112	216	224	13	109	178	402	92	371	148	184	494	310	270	86	3.1	0.11
19.78	0.8	0.8	139	243	225	13	123	184	409	99	376	151	198	508	310	283	85	3.3	0.11
19.83	1.0	1.0	161	265	224	13	134	190	414	104	380	155	209	519	310	294	86	3.4	0.10
19.88	1.3	1.3	166	270	224	12	136	192	415	105	380	157	211	521	310	297	86	3.4	0.09
19.94	1.5	1.5	180	284	223	12	142	196	419	109	382	159	217	527	310	304	87	3.5	0.08
19.99	1.8	1.8	200	304	223	11	152	201	423	113	386	163	227	537	310	314	87	3.6	0.08
20.03	2.0	2.0	196	300	222	11	150	200	422	112	385	163	225	535	310	313	88	3.6	0.07
20.09	2.3	2.3	213	317	222	11	158	204	426	116	388	166	233	543	310	321	88	3.6	0.07
20.14	2.5	2.5	221	325	221	10	161	207	428	118	389	167	236	546	310	325	89	3.7	0.06
20.19	2.8	2.8	218	322	221	10	160	206	427	117	388	167	235	545	310	324	89	3.6	0.06
20.24	3.0	3.0	232	336	220	9	166	210	430	120	390	170	241	551	310	331	90	3.7	0.05
20.30	3.3	3.3	238	342	220	9	168	212	432	122	391	171	243	553	310	333	90	3.7	0.05
20.34	3.5	3.5	240	344	220	9	169	212	432	122	391	172	244	554	310	334	90	3.7	0.05
20.40	3.8	3.8	247	351	219	8	172	214	434	124	392	173	247	557	310	338	91	3.7	0.05
20.45	4.0	4.0	251	355	219	8	174	215	434	124	393	174	249	559	310	339	91	3.7	0.05
20.50	4.3	4.3	254	358	219	8	174	216	435	125	393	174	249	559	310	341	91	3.7	0.04
20.55	4.5	4.5	256	360	218	7	175	217	435	125	393	175	250	560	310	342	92	3.7	0.04
20.61	4.8	4.8	261	365	218	7	177	218	436	126	394	176	252	562	310	344	92	3.7	0.04
20.67	5.0	5.0	265	369	218	6	179	219	437	127	395	177	254	564	310	346	92	3.7	0.04
20.77	5.5	5.5	273	377	217	6	181	221	438	128	395	178	256	566	310	349	93	3.8	0.03
20.89	6.0	6.0	278	382	217	6	183	222	439	129	396	179	258	568	310	351	93	3.8	0.03
20.99	6.5	6.5	284	388	217	5	185	223	440	130	397	180	260	570	310	353	94	3.8	0.03
21.12	7.0	7.0	292	396	216	5	188	225	441	131	398	181	263	573	310	356	94	3.8	0.03
21.23	7.5	7.5	295	399	216	4	188	226	441	131	398	182	263	573	310	357	94	3.8	0.02
21.34	8.0	8.0	303	407	215	4	191	228	443	133	399	184	266	576	310	361	95	3.8	0.02
21.46	8.5	8.5	308	412	215	3	192	229	444	134	399	185	267	577	310	363	96	3.8	0.02
21.57	9.0	9.0	306	410	214	3	190	228	442	132	398	184	265	575	310	361	96	3.8	0.01
21.69	9.5	9.5	322	426	214	2	196	232	446	136	400	187	271	581	310	368	96	3.8	0.01
21.81	10.0	10.0	317	421	213	2	193	231	444	134	399	186	268	578	310	365	97	3.8	0.01
21.94	10.5	10.5	330	434	213	1	198	234	446	136	401	188	273	583	310	370	98	3.8	0.01
22.06	11.0	11.0	336	440	212	1	199	235	447	137	401	189	274	584	310	372	98	3.8	0.01
22.18	11.5	11.5	339	443	212	1	200	236	447	137	402	190	275	585	310	373	98	3.8	0.00
22.31	12.0	12.0	344	448	211	0	201	237	448	138	402	191	276	586	310	374	99	3.8	0.00
22.43	12.5	12.5	341	445	211	-1	198	236	447	137	401	190	273	583	310	373	99	3.8	0.00
22.57	13.0	13.0	352	456	210	-1	202	238	449	139	402	192	277	587	310	377	100	3.8	-0.01
22.69	13.5	13.5	344	448	210	-2	197	236	446	136	401	191	272	582	310	373	100	3.7	-0.01
22.84	14.0	14.0	363	467	210	-2	205	240	450	140	403	193	280	590	310	380	100	3.8	-0.01
22.96	14.5	14.5	367	471	209	-2	205	241	450	140	403	194	280	590	310	381	101	3.8	-0.01
23.10	15.0	15.0	371	475	209	-3	206	242	450	140	404	195	281	591	310	382	101	3.8	-0.01
23.23	15.5	15.5	371	475	208	-3	205	241	450	140	403	195	280	590	310	381	102	3.7	-0.01
23.38	16.0	16.0	377	481	208	-3	206	242	450	140	404	195	281	591	310	383	102	3.8	-0.02
23.51	16.5	16.5	369	473	208	-4	201	240	448	138	402	194	276	586	310	378	102	3.7	-0.02
23.66	17.0	17.0	389	493	207	-4	208	245	452	142	404	197	283	593	310	386	103	3.8	-0.02
23.79	17.5	17.5	377	481	207	-5	202	242	449	139	402	196	277	587	310	381	104	3.7	-0.02
23.95	18.0	18.0	398	502	207	-5	210	246	452	142	405	198	285	595	310	388	104	3.7	-0.02
24.09	18.5	18.5	400	504	206	-5	209	246	452	142	405	199	284	594	310	388	104	3.7	-0.03
24.24	19.0	19.0	401	505	205	-6	208	246	452	142	404	199	283	593	310	388	105	3.7	-0.03
24.39	19.5	19.5	409	513	205	-6	210	248	453	143	405	200	285	595	310	390	105	3.7	-0.03
24.54	20.0	20.0	412	516	205	-7	210	248	453	143	405	201	285	595	310	391	106	3.7	-0.03
24.69	20.5	20.5	399	503	204	-7	204	245	449	139	403	198	279	589	310	384	106	3.6	-0.03
24.85	21.0	21.0	415	519	204	-8	209	248	452	142	405	201	284	594	310	390	106	3.7	-0.04
25.01	21.5	21.5	419	523	204	-8	209	248	452	142	405	201	284	594	310	390	106	3.7	-0.04
25.17	22.0	22.0	426	530	203	-8	211	249	453	143	405	202	286	596	310	392	107	3.7	-0.04
25.33	22.5	22.5	426	530	203	-8	209	249	452	142	405	201	284	594	310	391	107	3.7	-0.04
25.49	23.0	23.0	434	538	203	-9	211	250	453	143	405	203	286	596	310	393	107	3.7	-0.04
25.66	23.5	23.5	433	537	203	-9	209	249	452	142	405	202	284	594	310	392	107	3.7	-0.04
25.83	24.0	24.0	412	516	202	-9	200	245	447	137	402	199	275	585	310	383	108	3.6	-0.05

Note: Shaded area indicates yielding zone

Table A.31. Test series LCU-K_o (K = 2.0) – sample preparation:

Location					Loc No.		
Operator	HTP				Sample No.		B29
Test type	EX	CU	CD	UU	Date started	11/6/2003	
Specimen type	Undisturbed	Remoulded	Recompacted		Nominal diameter		50
Specimen preparation	Compact in an 2.8x5.6 mold with 5 blows on each side						
Soil type and description	Western Iowa loess						

MEASUREMENTS (mm)			INITIAL CONDITIONS	
Initial length			Area Ao (cm^2)	19.63
			Volume Vo (cm^3)	196.25
Average Lo	mm	100	Density (g/cm^3)	1.96
Initial diameter			Moisture content (%)	20.50
			Dry density (g/cm^3)	1.628
Average Do	mm	50		

WEIGHINGS	Trimmings	Specimen			LOCATION OF SPECIMEN
		initially	after test		
Container no.					
Specimen + cont.					
Container					
Mass of specimen	Wo	385	401.1	Wf	
Dry spec. + cont.					
Dry mass of spec.			319.5	Wd	
Moiture		65.50	81.60	Mf	
Moiture content		20.50	25.54		
Volume of solid		120.63			
Volume of the void		75.62			
Void ratio		0.63			

Table A.32. Test series LCU-K_o (K = 2.0) – shearing:

Date					Location										Sample No.					B29
Test	CD	CU	EX	UU	Membrane			With	side drains						Ram pressure			100	kPa	
Rate of strain			0.635	mm/min	Operator		HTP	Without							Tensile pressure			0	kPa	
								Proving ring No.							Cell pressure			310	kPa	
Consolidated length			100	mm	Consolidated area			19.63						cm^2	Pore pressure			210.4	kPa	
Corr.	Strain		Axial Load		Pore pressure		Deviator stress								Principal stresses					
Area	Displ.	ε	Read	Load	U	ΔU	σa	p'	p	q	p-cam	p'-cam	q-cam		σ1	σ3	σ'1	σ'3	σ'1/σ'3	A
cm^2	mm	%	N	N	kPa	kPa	kPa	kPa	kPa	kPa	kPa	kPa	kPa		kPa	kPa	kPa	kPa	-	
19.65	0.1	0.1	-128	0	210	0	0	150	360	50	343	133	100		410	310	200	100	2.0	
19.69	0.3	0.3	36	164	223	13	83	179	402	92	371	148	183		493	310	270	87	3.1	0.15
19.73	0.5	0.5	122	250	228	18	127	195	423	113	386	158	227		537	310	309	82	3.8	0.14
19.78	0.8	0.8	161	289	230	20	146	203	433	123	392	162	246		556	310	326	80	4.1	0.13
19.83	1.0	1.0	184	312	231	20	157	208	439	129	396	165	257		567	310	337	79	4.2	0.13
19.89	1.3	1.3	211	339	232	21	171	214	445	135	400	168	271		581	310	349	78	4.5	0.12
19.93	1.5	1.5	211	339	232	21	170	213	445	135	400	168	270		580	310	348	78	4.5	0.13
19.99	1.8	1.8	223	351	232	22	176	215	448	138	402	170	276		586	310	353	78	4.5	0.12
20.03	2.0	2.0	241	369	232	22	184	220	452	142	405	172	284		594	310	362	78	4.7	0.12
20.08	2.3	2.3	220	347	232	22	173	215	447	137	401	169	273		583	310	351	78	4.5	0.12
20.14	2.5	2.5	247	375	232	22	186	221	453	143	405	173	286		596	310	364	78	4.7	0.12
20.19	2.8	2.8	263	391	232	22	194	225	457	147	408	176	294		604	310	372	78	4.8	0.11
20.24	3.0	3.0	266	394	232	22	195	225	457	147	408	176	295		605	310	372	78	4.8	0.11
20.29	3.3	3.3	261	389	232	22	192	223	456	146	407	175	292		602	310	369	78	4.8	0.11
20.35	3.5	3.5	269	397	232	22	195	225	457	147	408	176	295		605	310	373	78	4.8	0.11
20.40	3.8	3.8	282	410	232	22	201	228	461	151	410	178	301		611	310	379	78	4.9	0.11
20.45	4.0	4.0	274	402	232	22	197	226	458	148	409	177	297		607	310	374	78	4.8	0.11
20.51	4.3	4.3	282	410	232	21	200	228	460	150	410	178	300		610	310	378	78	4.8	0.11
20.56	4.5	4.5	299	427	232	22	208	232	464	154	413	181	308		618	310	386	78	4.9	0.10
20.61	4.8	4.8	278	405	232	21	197	227	458	148	409	177	297		607	310	375	78	4.8	0.11
20.67	5.0	5.0	291	419	232	21	203	230	461	151	411	179	303		613	310	381	78	4.9	0.11
20.77	5.5	5.5	310	438	232	21	211	234	465	155	414	182	311		621	310	389	78	5.0	0.10
20.89	6.0	6.0	315	443	232	21	212	234	466	156	414	182	312		622	310	391	78	5.0	0.10
21.00	6.5	6.5	329	457	231	21	218	238	469	159	416	185	318		628	310	396	79	5.0	0.10
21.11	7.0	7.0	321	449	231	20	213	235	466	156	414	183	313		623	310	392	79	4.9	0.10
21.22	7.5	7.5	302	430	231	20	202	231	461	151	411	180	302		612	310	382	80	4.8	0.10
21.34	8.0	8.0	343	471	231	20	221	240	470	160	417	186	321		631	310	400	80	5.0	0.09
21.46	8.5	8.5	351	479	230	20	223	241	472	162	418	188	323		633	310	403	80	5.0	0.09
21.58	9.0	9.0	345	473	230	19	219	240	470	160	416	187	319		629	310	400	80	5.0	0.09
21.70	9.5	9.5	367	495	229	19	228	245	474	164	419	190	328		638	310	409	81	5.1	0.08
21.81	10.0	10.0	373	501	229	19	229	246	475	165	420	191	329		639	310	410	81	5.1	0.08
21.94	10.5	10.5	354	481	228	18	219	242	470	160	416	188	319		629	310	401	82	4.9	0.08
22.06	11.0	11.0	381	509	228	18	231	247	475	165	420	192	331		641	310	413	82	5.0	0.08
22.18	11.5	11.5	375	503	228	17	227	246	473	163	419	191	327		637	310	409	83	5.0	0.08
22.31	12.0	12.0	399	527	227	17	236	251	478	168	422	195	336		646	310	419	83	5.0	0.07
22.44	12.5	12.5	389	517	226	16	230	249	475	165	420	194	330		640	310	414	84	5.0	0.07
22.56	13.0	13.0	373	501	226	16	222	245	471	161	417	191	322		632	310	406	84	4.8	0.07
22.69	13.5	13.5	412	540	225	15	238	254	479	169	423	197	338		648	310	423	85	5.0	0.06
22.83	14.0	14.0	406	533	225	14	234	252	477	167	421	196	334		644	310	419	85	4.9	0.06
22.96	14.5	14.5	425	553	224	14	241	256	480	170	424	199	341		651	310	426	86	5.0	0.06
23.10	15.0	15.0	411	539	224	13	233	253	477	167	421	197	333		643	310	420	86	4.9	0.06
23.24	15.5	15.5	436	563	223	13	242	258	481	171	424	201	342		652	310	429	87	4.9	0.05
23.37	16.0	16.0	411	539	222	12	231	253	475	165	420	198	331		641	310	418	88	4.8	0.05
23.52	16.5	16.5	430	558	222	12	237	257	479	169	422	200	337		647	310	425	88	4.8	0.05
23.65	17.0	17.0	422	550	221	11	232	255	476	166	421	200	332		642	310	421	89	4.7	0.05
23.79	17.5	17.5	455	583	221	11	245	261	482	172	425	204	345		655	310	434	89	4.9	0.04
23.95	18.0	18.0	460	588	221	10	246	262	483	173	425	205	346		656	310	435	90	4.9	0.04
24.09	18.5	18.5	447	574	220	10	238	259	479	169	423	203	338		648	310	428	90	4.8	0.04
24.24	19.0	19.0	422	550	219	9	227	254	473	163	419	200	327		637	310	418	91	4.6	0.04
24.39	19.5	19.5	455	583	219	9	239	261	479	169	423	204	339		649	310	430	91	4.7	0.04
24.54	20.0	20.0	478	606	218	8	247	265	484	174	426	207	347		657	310	439	92	4.8	0.03
24.69	20.5	20.5	462	589	218	8	239	261	479	169	423	205	339		649	310	431	92	4.7	0.03
24.85	21.0	21.0	490	618	217	7	249	267	484	174	426	209	349		659	310	441	93	4.8	0.03
25.01	21.5	21.5	493	621	217	6	248	267	484	174	426	209	348		658	310	441	93	4.7	0.03
25.17	22.0	22.0	463	591	216	6	235	261	477	167	422	205	335		645	310	428	94	4.6	0.03
25.33	22.5	22.5	499	627	216	6	248	267	484	174	426	210	348		658	310	441	94	4.7	0.02
25.49	23.0	23.0	483	611	216	5	239	264	480	170	423	207	339		649	310	434	94	4.6	0.02
25.66	23.5	23.5	507	635	215	5	247	268	484	174	426	211	347		657	310	442	95	4.7	0.02
25.83	24.0	24.0	447	574	217	7	222	254	471	161	417	201	322		632	310	416	93	4.5	0.03

Note: Shaded area indicates yielding zone

Table A.33. Test series LCU-K_o (K = 2.5) – sample preparation:

Location					Loc No.		
Operator	HTP				Sample No.		B33
Test type	EX	CU	CD	UU	Date started	11/11/2003	
Specimen type	Undisturbed	Remoulded	Recompacted		Nominal diameter		50
Specimen preparation	Compact in an 2.8x5.6 mold with 5 blows on each side						
Soil type and description	Western Iowa loess						

MEASUREMENTS (mm)			INITIAL CONDITIONS	
Initial length			Area Ao (cm^2)	19.63
			Volume Vo (cm^3)	196.25
Average L_o	mm	100	Density (g/cm^3)	1.93
Initial diameter			Moisture content (%)	18.81
			Dry density (g/cm^3)	1.625
Average D_o	mm	50		

WEIGHINGS	Trimmings	Specimen			LOCATION OF SPECIMEN
		initially	after test		
Container no.					
Specimen + cont.					
Container					
Mass of specimen	W_o	379	397.9	W_f	
Dry spec. + cont.					
Dry mass of spec.			319	W_d	
Moiture		60.00	78.90	M_f	
Moiture content		18.81	24.73		
Volume of solid		120.44			
Volume of the void		75.81			
Void ratio		0.63			

Table A.34. Test series LCU-K_o (K = 2.5) – shearing:

Date					Location									Sample No.					B34
Test	CD	CU	EX	UU	Membrane			With		side drains				Ram pressure			125	kPa	
Rate of strain			0.635	mm / min	Operator		HTP	Without						Tensile pressure			0	kPa	
								Proving ring No.						Cell pressure			360	kPa	
Consolidated length			100	mm	Consolidated area			19.63					cm^2	Pore pressure			210.8	kPa	
Corr.	Strain		Axial Load		Pore pressure		Deviator stress							Principal stresses					
Area	Displ.	ε	Read	Load	U	ΔU	σa	p'	p	q	p-cam	p'-cam	q-cam	σ1	σ3	σ'1	σ'3	σ'1/σ'3	A
cm^2	mm	%	N	N	kPa	kPa	kPa	kPa	kPa	kPa	kPa	kPa	kPa	kPa	kPa	kPa	kPa	-	
19.63	0.0	0.0	-157	0	211	0	0	212	423	63	402	191	125	485	360	274	149	1.8	
19.68	0.3	0.3	46	203	226	15	103	248	474	114	436	210	228	588	360	362	134	2.7	0.14
19.73	0.5	0.5	131	288	233	22	146	263	495	135	450	218	271	631	360	398	127	3.1	0.15
19.78	0.8	0.8	180	337	236	26	170	271	508	148	458	222	295	655	360	419	124	3.4	0.15
19.83	1.0	1.0	185	342	239	28	173	270	509	149	459	221	298	658	360	419	122	3.5	0.16
19.88	1.3	1.3	243	400	241	30	201	282	523	163	469	228	326	686	360	445	119	3.7	0.15
19.93	1.5	1.5	259	416	242	31	209	285	527	167	471	230	334	694	360	452	118	3.8	0.15
19.98	1.8	1.8	265	422	242	32	211	286	528	168	472	230	336	696	360	454	118	3.9	0.15
20.03	2.0	2.0	278	435	243	32	217	288	531	171	474	231	342	702	360	459	117	3.9	0.15
20.08	2.3	2.3	295	452	243	32	225	292	535	175	477	234	350	710	360	467	117	4.0	0.14
20.13	2.5	2.5	287	444	243	32	220	290	533	173	475	232	345	705	360	462	117	3.9	0.15
20.19	2.8	2.8	303	460	243	33	228	293	536	176	478	234	353	713	360	470	117	4.0	0.14
20.24	3.0	3.0	319	476	244	33	235	297	540	180	480	237	360	720	360	477	117	4.1	0.14
20.29	3.3	3.3	328	485	244	33	239	298	542	182	481	237	364	724	360	480	116	4.1	0.14
20.34	3.5	3.5	311	468	243	33	230	294	538	178	478	235	355	715	360	472	117	4.0	0.14
20.40	3.8	3.8	328	485	244	33	238	298	541	181	481	237	363	723	360	479	116	4.1	0.14
20.45	4.0	4.0	344	501	244	33	245	301	545	185	483	239	370	730	360	486	116	4.2	0.14
20.51	4.3	4.3	349	506	244	33	247	302	546	186	484	240	372	732	360	488	116	4.2	0.13
20.56	4.5	4.5	341	498	244	33	242	300	544	184	482	239	367	727	360	484	116	4.2	0.14
20.62	4.8	4.8	355	512	244	33	248	303	547	187	484	241	373	733	360	489	116	4.2	0.13
20.67	5.0	5.0	325	482	243	33	233	296	539	179	479	236	358	718	360	475	117	4.1	0.14
20.78	5.5	5.5	363	520	243	33	250	304	548	188	485	242	375	735	360	492	117	4.2	0.13
20.89	6.0	6.0	341	498	243	32	239	299	542	182	481	238	364	724	360	481	117	4.1	0.13
21.00	6.5	6.5	384	541	243	32	257	308	551	191	487	244	382	742	360	499	117	4.3	0.13
21.11	7.0	7.0	395	552	243	32	261	310	553	193	489	246	386	746	360	503	117	4.3	0.12
21.23	7.5	7.5	390	547	242	32	258	309	551	191	488	245	383	743	360	501	118	4.3	0.12
21.34	8.0	8.0	380	537	242	31	251	307	548	188	485	244	376	736	360	495	118	4.2	0.12
21.46	8.5	8.5	407	564	242	31	263	312	554	194	489	248	388	748	360	506	118	4.3	0.12
21.57	9.0	9.0	393	550	241	30	255	309	550	190	487	246	380	740	360	499	119	4.2	0.12
21.70	9.5	9.5	421	578	241	30	266	315	556	196	490	250	391	751	360	510	119	4.3	0.11
21.81	10.0	10.0	404	561	240	29	257	311	551	191	487	247	382	742	360	502	120	4.2	0.11
21.94	10.5	10.5	434	591	240	29	269	317	557	197	491	251	394	754	360	514	120	4.3	0.11
22.06	11.0	11.0	410	567	239	28	257	312	551	191	487	248	382	742	360	503	121	4.2	0.11
22.19	11.5	11.5	445	602	239	28	271	319	558	198	492	253	396	756	360	518	121	4.3	0.10
22.31	12.0	12.0	453	610	239	28	274	321	559	199	493	254	399	759	360	520	122	4.3	0.10
22.44	12.5	12.5	464	621	238	27	277	323	561	201	494	256	402	762	360	524	123	4.3	0.10
22.57	13.0	13.0	462	619	237	26	274	323	560	200	493	256	399	759	360	522	123	4.2	0.10
22.70	13.5	13.5	437	594	236	26	262	317	553	193	489	252	387	747	360	510	124	4.1	0.10
22.83	14.0	14.0	475	632	236	26	277	325	561	201	494	258	402	762	360	526	124	4.3	0.09
22.96	14.5	14.5	454	611	235	25	266	320	556	196	490	255	391	751	360	516	125	4.1	0.09
23.09	15.0	15.0	503	660	235	25	286	330	565	205	497	262	411	771	360	535	125	4.3	0.09
23.23	15.5	15.5	464	621	234	24	267	322	556	196	491	257	392	752	360	518	126	4.1	0.09
23.38	16.0	16.0	497	654	234	23	280	328	562	202	495	261	405	765	360	531	126	4.2	0.08
23.51	16.5	16.5	510	667	233	23	284	331	564	204	496	263	409	769	360	535	127	4.2	0.08
23.65	17.0	17.0	508	665	233	22	281	330	563	203	495	262	406	766	360	533	127	4.2	0.08
23.80	17.5	17.5	530	687	233	22	289	334	567	207	498	265	414	774	360	541	127	4.2	0.08
23.94	18.0	18.0	494	651	232	21	272	327	559	199	492	261	397	757	360	525	128	4.1	0.08
24.09	18.5	18.5	541	698	232	21	290	336	567	207	498	267	415	775	360	543	128	4.2	0.07
24.23	19.0	19.0	511	668	231	20	276	329	560	200	494	263	401	761	360	530	129	4.1	0.07
24.39	19.5	19.5	535	692	231	20	284	334	564	204	496	266	409	769	360	538	130	4.2	0.07
24.54	20.0	20.0	503	660	230	19	269	327	557	197	491	261	394	754	360	524	130	4.0	0.07
24.69	20.5	20.5	551	708	230	19	287	336	566	206	497	267	412	772	360	542	130	4.2	0.07
24.85	21.0	21.0	560	717	229	19	289	337	567	207	498	268	414	774	360	544	131	4.2	0.06
25.01	21.5	21.5	566	723	229	18	289	338	567	207	498	269	414	774	360	545	131	4.2	0.06
25.17	22.0	22.0	552	709	228	18	282	335	563	203	496	267	407	767	360	538	132	4.1	0.06
25.33	22.5	22.5	576	733	228	18	290	339	567	207	498	270	415	775	360	546	132	4.1	0.06
25.49	23.0	23.0	558	715	227	17	280	335	563	203	495	268	405	765	360	538	133	4.1	0.06
25.66	23.5	23.5	585	742	227	17	289	340	567	207	498	271	414	774	360	547	133	4.1	0.06
25.83	24.0	24.0	565	722	227	16	280	336	562	202	495	268	405	765	360	538	134	4.0	0.06

Note: Shaded area indicates yielding zone

Table A.35. Test series LCU-K_o (K = 3.0) – sample preparation:

Location					Loc No.		
Operator	HTP				Sample No.		B34
Test type	EX	CU	CD	UU	Date started	11/12/2003	
Specimen type	Undisturbed	Remoulded	Recompacted		Nominal diameter		50
Specimen preparation	Compact in an 2.8x5.6 mold with 5 blows on each side						
Soil type and description	Western Iowa loess						

MEASUREMENTS (mm)			INITIAL CONDITIONS	
Initial length			Area Ao (cm^2)	19.63
			Volume Vo (cm^3)	196.25
Average L_o	mm	100	Density (g/cm^3)	1.93
Initial diameter			Moisture content (%)	18.76
Average D_o	mm	50	Dry density (g/cm^3)	1.622

WEIGHINGS	Trimmings	Specimen			LOCATION OF SPECIMEN
		initially	after test		
Container no.					
Specimen + cont.					
Container					
Mass of specimen	W_o	378	379.2	W_f	
Dry spec. + cont.					
Dry mass of spec.			318.3	W_d	
Moiture		59.70	60.90	M_f	
Moiture content		18.76	19.13		
Volume of solid		120.17			
Volume of the void		76.08			
Void ratio		0.63			

Table A.36. Test series LCU-K_o (K = 3.0) – shearing:

Date					Location									Sample No.					B34
Test	CD	CU	EX	UU	Membrane			With		side drains				Ram pressure			150	kPa	
Rate of strain			0.635	mm / min	Operator		HTP	Without						Tensile pressure			0	kPa	
								Proving ring No.						Cell pressure			360	kPa	
Consolidated length			100	mm	Consolidated area			19.63					cm^2	Pore pressure			210.9	kPa	
Corr.	Strain		Axial Load		Pore pressure		Deviator stress							Principal stresses					
Area	Displ.	ε	Read	Load	U	ΔU	σa	p'	p	q	p-cam	p'-cam	q-cam	σ1	σ3	σ'1	σ'3	σ'1/σ'3	A
cm^2	mm	%	N	N	kPa	kPa	kPa	kPa	kPa	kPa	kPa	kPa	kPa	kPa	kPa	kPa	kPa	-	
19.65	0.1	0.1	-178	0	211	0	0	224	435	75	410	199	150	510	360	299	149	2.0	
19.68	0.3	0.3	77	255	229	18	129	271	500	140	453	225	279	639	360	411	132	3.1	0.14
19.74	0.5	0.5	131	309	236	25	157	277	513	153	462	226	307	667	360	431	124	3.5	0.16
19.79	0.8	0.8	180	358	241	30	181	285	526	166	470	230	331	691	360	450	119	3.8	0.17
19.84	1.0	1.0	224	402	244	33	203	292	536	176	478	234	353	713	360	469	116	4.0	0.16
19.89	1.3	1.3	232	410	246	35	206	292	538	178	479	233	356	716	360	470	114	4.1	0.17
19.94	1.6	1.6	271	449	248	37	225	299	548	188	485	237	375	735	360	487	112	4.4	0.17
19.98	1.8	1.8	277	455	249	38	228	300	549	189	486	237	378	738	360	489	111	4.4	0.17
20.03	2.0	2.0	290	468	250	39	234	302	552	192	488	238	384	744	360	494	110	4.5	0.17
20.09	2.3	2.3	301	479	251	40	238	303	554	194	489	239	388	748	360	498	109	4.6	0.17
20.13	2.5	2.5	298	476	251	40	236	302	553	193	489	238	386	746	360	495	109	4.6	0.17
20.19	2.8	2.8	317	495	252	41	245	306	558	198	492	240	395	755	360	503	108	4.7	0.17
20.24	3.0	3.0	328	506	252	41	250	308	560	200	493	241	400	760	360	508	108	4.7	0.16
20.30	3.3	3.3	335	513	252	42	253	309	561	201	494	242	403	763	360	510	108	4.7	0.16
20.34	3.5	3.5	325	503	252	42	247	306	559	199	492	240	397	757	360	505	108	4.7	0.17
20.40	3.8	3.8	345	523	253	42	257	311	563	203	496	243	407	767	360	514	107	4.8	0.16
20.46	4.1	4.1	350	528	253	42	258	311	564	204	496	243	408	768	360	515	107	4.8	0.16
20.50	4.3	4.3	353	531	253	42	259	312	564	204	496	243	409	769	360	516	107	4.8	0.16
20.56	4.5	4.5	358	536	253	42	261	313	565	205	497	244	411	771	360	518	107	4.8	0.16
20.62	4.8	4.8	361	539	253	42	261	313	566	206	497	244	411	771	360	518	107	4.8	0.16
20.66	5.0	5.0	354	532	253	42	257	311	564	204	496	243	407	767	360	514	107	4.8	0.16
20.77	5.5	5.5	361	539	253	42	259	312	565	205	496	244	409	769	360	517	107	4.8	0.16
20.89	6.1	6.1	388	566	253	42	271	318	570	210	500	247	421	781	360	528	107	4.9	0.15
21.00	6.5	6.5	397	575	253	42	274	319	572	212	501	248	424	784	360	531	107	5.0	0.15
21.11	7.0	7.0	372	550	252	41	260	313	565	205	497	245	410	770	360	518	108	4.8	0.16
21.23	7.5	7.5	407	585	252	41	276	321	573	213	502	250	426	786	360	533	108	5.0	0.15
21.34	8.0	8.0	388	566	252	41	265	315	568	208	498	246	415	775	360	523	108	4.9	0.16
21.46	8.5	8.5	427	605	252	41	282	324	576	216	504	252	432	792	360	539	108	5.0	0.15
21.57	9.0	9.0	418	596	251	40	276	322	573	213	502	251	426	786	360	536	109	4.9	0.14
21.70	9.5	9.5	424	602	251	40	277	323	574	214	502	252	427	787	360	537	109	4.9	0.14
21.81	10.0	10.0	429	607	250	39	278	324	574	214	503	253	428	788	360	539	110	4.9	0.14
21.94	10.5	10.5	454	632	250	39	288	329	579	219	506	256	438	798	360	548	110	5.0	0.13
22.06	11.0	11.0	464	642	249	38	291	331	581	221	507	258	441	801	360	552	111	5.0	0.13
22.19	11.5	11.5	465	643	249	38	290	331	580	220	507	258	440	800	360	551	111	5.0	0.13
22.31	12.0	12.0	475	653	248	37	293	333	581	221	508	259	443	803	360	555	112	5.0	0.13
22.43	12.5	12.5	465	643	248	37	287	331	578	218	506	258	437	797	360	549	112	4.9	0.13
22.57	13.0	13.0	488	666	247	36	295	335	582	222	508	261	445	805	360	558	113	4.9	0.12
22.69	13.5	13.5	473	651	246	35	287	332	578	218	506	260	437	797	360	551	114	4.8	0.12
22.83	14.0	14.0	481	659	246	35	289	333	579	219	506	260	439	799	360	553	114	4.8	0.12
22.96	14.5	14.5	487	665	245	34	290	335	580	220	507	261	440	800	360	554	115	4.8	0.12
23.10	15.0	15.0	511	689	245	34	298	339	584	224	509	265	448	808	360	563	115	4.9	0.11
23.23	15.5	15.5	482	660	244	33	284	333	577	217	505	260	434	794	360	550	116	4.8	0.12
23.37	16.0	16.0	522	700	244	33	300	341	585	225	510	266	450	810	360	566	116	4.9	0.11
23.51	16.5	16.5	492	670	243	32	285	335	578	218	505	262	435	795	360	552	117	4.7	0.11
23.66	17.0	17.0	513	691	243	32	292	338	581	221	507	265	442	802	360	559	117	4.8	0.11
23.80	17.5	17.5	517	695	242	31	292	339	581	221	507	265	442	802	360	560	118	4.8	0.11
23.94	18.0	18.0	541	719	242	31	300	344	585	225	510	268	450	810	360	569	118	4.8	0.10
24.10	18.5	18.5	547	725	241	30	301	344	585	225	510	269	451	811	360	570	119	4.8	0.10
24.23	19.0	19.0	552	730	241	30	301	345	586	226	510	270	451	811	360	571	119	4.8	0.10
24.39	19.5	19.5	558	736	240	29	302	346	586	226	511	270	452	812	360	571	120	4.8	0.10
24.54	20.0	20.0	558	736	240	29	300	345	585	225	510	270	450	810	360	570	120	4.7	0.10
24.69	20.5	20.5	567	745	239	28	302	347	586	226	511	272	452	812	360	573	121	4.7	0.09
24.85	21.0	21.0	571	749	239	28	302	347	586	226	511	272	452	812	360	573	122	4.7	0.09
25.01	21.5	21.5	577	755	238	27	302	348	586	226	511	273	452	812	360	574	122	4.7	0.09
25.17	22.0	22.0	578	756	238	27	300	348	585	225	510	272	450	810	360	573	122	4.7	0.09
25.33	22.5	22.5	547	725	237	26	286	341	578	218	505	268	436	796	360	559	123	4.5	0.09
25.49	23.0	23.0	588	766	237	26	300	348	585	225	510	273	450	810	360	573	123	4.7	0.09
25.66	23.5	23.5	561	739	236	25	288	343	579	219	506	270	438	798	360	562	124	4.5	0.09
25.83	24.0	24.0	596	774	236	25	300	349	585	225	510	274	450	810	360	574	124	4.6	0.08

Note: Shaded area indicates yielding zone

APPENDIX B: COMPUTATIONAL PROCEDURE FOR CALCULATING BEARING CAPACITY AND SETTLEMENT OF RIGID FOOTINGS SUPPORTED BY RAMMED AGGREGATE PIERS

CALCULATION OF SETTLEMENT OF PIER-SUPPORTED FOOTINGS

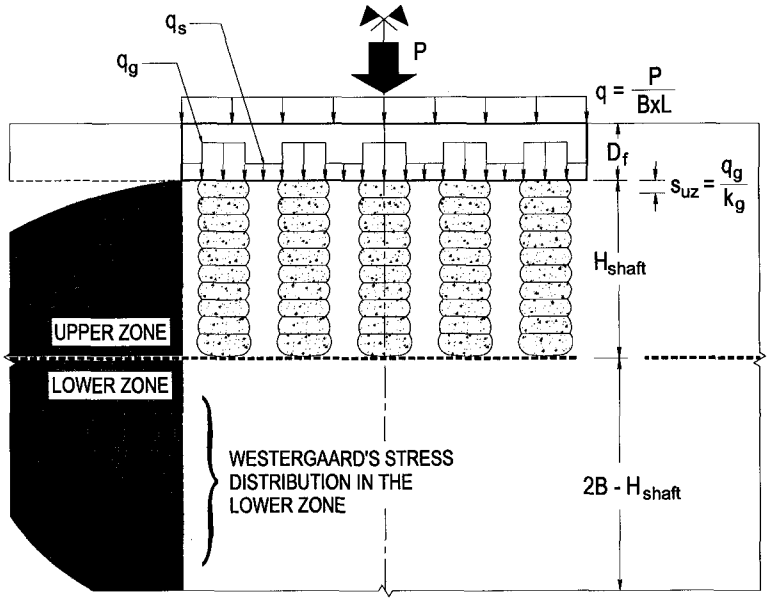

Figure B.1. Computational scheme for settlement of rammed aggregate pier-supported footings

Figure B.1 shows the computational scheme for the settlement of a rigid footing supported by rammed aggregate piers. The soil underneath the footing can be divided into two zones named as the upper zone and the lower zone (Fig. B.1). The thickness of the upper zone (H_{shaft}) is defined as summation of drilling depth, H_o, and the pier nominal diameter (d_{shaft}). According to Lawton and Warner (2004), the total settlement, S_T, of a pier-supported rigid footing is:

$$S_T = S_{UZ} + S_{LZ} = S_{UZ} + S_{i,LZ} + S_{c,LZ} + S_{s,LZ} + S_{m,LZ} \qquad [B.1]$$

where S_{UZ} is the immediate settlement of the upper zone, S_{LZ} is the total settlement of the lower zone, $S_{i,LZ}$ is the immediate settlement of the lower zone, $S_{c,LZ}$ is the primary consolidation settlement in the lower zone, $S_{s,LZ}$ is the secondary consolidation settlement of

the lower zone, and $S_{m,LZ}$ is the settlement due to changes in moisture within the lower zone. If the secondary consolidation settlement and the settlement due to changes in moisture are assumed to be negligible then the total settlement of the footing can be simplified as:

$$S_T = S_{UZ} + S_{i,LZ} + S_{c,LZ} \qquad [B.2]$$

Upper Zone Settlement

If the footing is assumed to be perfectly rigid then the immediate settlement of the upper zone is equal to the settlement of the pier and can be estimated as:

$$S_{UZ} = \frac{q_g}{k_g} \qquad [B.3]$$

where q_g is the stress distributed to the top of the pier element and k_g is the modulus of subgrade reaction (i.e., stiffness) of the pier element. In practice, the modulus of subgrade reaction, k_g, is routinely estimated from *on-site* modulus load test performed on a representative isolated pier built in the construction site. The stress distributed to the top of the pier (q_g) and the matrix soil (q_m) can be estimated based on the spring analogy as follows:

$$q_g = \frac{qR_s}{R_a(R_s - 1) + 1} \qquad [B.4]$$

$$q_m = \frac{q}{R_a(R_s - 1) + 1} \qquad [B.5]$$

$$R_s = n_s = \frac{k_g}{k_m} \qquad \textit{(for perfectly rigid footings)} \qquad [B.6]$$

where q is the average footing-bottom stress, R_s is the pier-soil stiffness ratio, R_a is the area replacement ratio which is defined as the ratio of the gross area of the piers in the footing over the footing area, and k_m is the modulus of subgrade reaction of the matrix soil. For

perfectly rigid footings, the pier-soil stiffness ratio, R_s, is equal to the stress concentration ratio, n_s. According to Bowles (1996, p. 503), k_m can be estimated from the elastic modulus of the soil (E_s), Poisson's ratio (v), footing width (B), and influence factors (I_s, I_F) as follows:

$$k_m = \frac{1}{BE_s' I_s I_F} \qquad [B.7]$$

$$E_s' = \frac{(1-v^2)}{E_s} \qquad [B.8]$$

Lower Zone Settlement

The immediate settlement of the lower zone is calculated using elastic solution as follows:

$$S_{i,LZ} = \frac{qI_q H_{LZ}}{E_{LZ}} \qquad [B.9]$$

For square or circular footings:

$$H_{LZ} = 2B - H_{shaft} = 2B - H_0 - d_{shaft} \qquad [B.10]$$

where I_q is the Westergaard's influence factor (Bowles 1996), H_{LZ} is the thickness of the lower zone, E_{LZ} is the average elastic modulus of the lower zone, and B is the footing width. The primary consolidation settlement of the lower zone is calculated using the data from the oedometer test:

$$S_{c,LZ} = \frac{C_\varepsilon H_{LZ}}{1+e_o} log\left(\frac{p_o' + \delta p}{p_o'}\right) \qquad [B.11]$$

where C_ε is the compression or recompression index, p'_o is *in-situ* vertical effective stress, δp is the vertical stress increase, and e_o is the initial void ratio.

CALCULATION OF BEARING CAPACITY OF PIER-SUPPORTED FOOTINGS

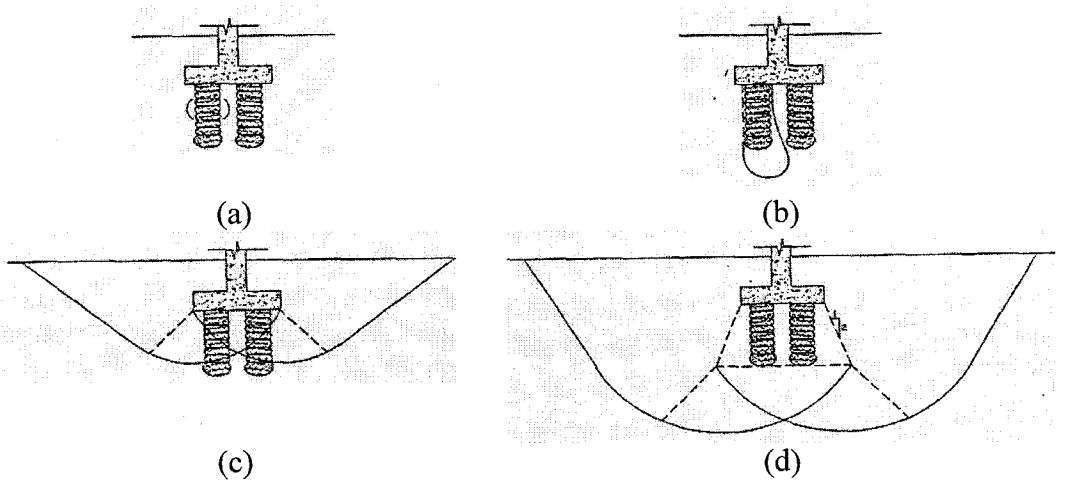

Figure B.2. Bearing capacity failure mechanisms of rammed aggregate pier-supported footings: (a) bulging of individual pier; (b) shearing below individual pier; (c) shearing within the pier-reinforced zone; and (d) shearing below the pier-reinforced zone (from Fox and Cowell 1998)

The allowable bearing pressure for rammed aggregate pier-supported footings is defined as the minimum pressure among those computed using limit equilibrium equations derived from four possible modes of failure (Fig. B.2):

Bulging of Individual Pier Element

If the shaft of the pier element is sufficiently long, the stress applied to the top of the pier may cause a full mobilization of shear strength in the aggregate within the pier element before it can be transferred to the tip. The development of shearing surface within the pier element causes the pier element to bulge outward (Fig. B.2a). The bearing capacity of an individual pier subjected to bulging deflection, $q_{ult,g}$, is proposed by Hughes and Withers (1974) as follows:

$$q_{ult,g} = \sigma_{r,lim} \tan^2(45 + \frac{\phi_g}{2}) \quad [B.12]$$

$$\sigma_{r,lim} = \sigma_{ro} + s_u[1 + ln\frac{E_u}{2s_u(1+\nu_u)}] \quad [B.13]$$

where $\sigma_{r,lim}$ is the Rankine's passive stress, ϕ_g is the friction angle of the pier material, σ_{ro} is the total radial stress after pier installation, s_u, E_u, and ν_u are undrained shear strength, modulus, and Poisson's ratio of the matrix soil, respectively. The total radial stress, σ_{ro}, can be calculated from the effective vertical stress and pore-water pressure as follows:

$$\sigma_{ro} = \sigma'_{vo} K_p + u_o \quad [B.14]$$

where K_p is Rankine's passive earth pressure coefficient, σ'_{vo} and u_o are vertical effective stress and pore-water pressure after pier installation, respectively. If the matrix soil underneath the footing is homogeneous then the bulging depth, z_b, can be estimated from the friction angle of the pier material (ϕ_g) and the footing depth (D_f) as follows:

$$z_b = D_f + \frac{1}{2} d_{shaft} \tan(45 + \frac{\phi_g}{2}) \quad [B.15]$$

Shearing Below the Tip of Individual Pier Element

When the shaft of the pier element is short, a significant portion of the stress applied to the top of the pier may be transferred to the pier tip and causes shearing in the soil below the tip of the pier element (Fig. B.2b). In this case, the ultimate bearing capacity can be calculated as:

$$q_{ult,g} = \frac{1}{A_g}(f_s A_{shaft} + q_{tip,g} A_g) = \frac{4}{d^2} f_s d_{shaft} H_{shaft} + q_{tip,g} \quad [B.16]$$

For undrained condition:

$$f_s = s_u \quad [B.17]$$

$$q_{tip,g} = s_u N_c \quad [B.18]$$

For drained condition:

$$f_s = \sigma'_{v,ave} \tan(\phi_s) K_p = (D_f + \frac{H_{shaft}}{2}) \gamma \tan(\phi_s) \tan^2(45 + \frac{\phi_s}{2}) \quad [B.19]$$

$$q_{tip,g} = c' N_c + 0.5 d_{shaft} \gamma N_\gamma + \sigma'_v N_q \quad [B.20]$$

where A_g is the cross-sectional area of the pier element, A_{shaft} is the area of the pier shaft, $q_{tip,g}$ is the stress resisted at tip of the pier element, f_s is the unit friction along the pier shaft, d is the effective diameter of the pier element and is approximately 110% of d_{shaft}, N_c, N_q, N_γ are dimensionless bearing capacity factors, $\sigma'_{v,ave}$ is the average vertical effective stress along the shaft of the pier, ϕ_s is the friction angle of the matrix soil, γ is the buoyant unit weight of the matrix soil, and σ'_v is the vertical effective stress at the footing-bottom elevation.

Shearing Within the Pier-Soil Matrix Zone

For this possible mode of failure, the shear plane is assumed to pass through pier-reinforced zone (Fig. B.2c). The shear strength of the materials along the assumed failure plane depends on the frictional resistance to shearing within the matrix soil (τ_s) and the frictional resistance to shearing offered by the pier elements (τ_g). The composite friction angle, ϕ_{comp}, and cohesion intercept, c_{comp}, of the pier-reinforced zone is calculated using the equation proposed by Priebe (1978) as follows:

$$\phi_{comp} = \tan^{-1}[R_a n_s \tan(\phi_g) + (1 - R_a n_s) \tan(\phi_s)] \quad [B.21]$$

$$c_{comp} = (1 - R_a n_s) c \quad [B.22]$$

where n_s is the stress concentration ratio and ϕ_g is the friction angle of the pier element. To account for the change in stress and the orientation of the failure plane, n_s value of 2.8 is recommended (Wissmann 1999). Once the composite shear strength parameters (c_{comp} and ϕ_{comp}) are determined, the bearing capacity of the pier-supported footing can be estimated using Eq. B.20.

Shearing Below the Bottom of the Pier-Soil Matrix Zone

General bearing capacity failure may occur below the pier-reinforced zone (Fig. B.2d). The conventional solution for this problem can be achieved by comparing the stresses induced at the bottom of the pier-reinforced zone with the allowable bearing pressure computed using Eq. B.20. Assuming that load spreading increases at a rate of 2:1 (vertical to horizontal) below the bottom of the footing, the stress induced at the bottom of the pier-reinforced zone, q_{bottom}, may be estimated from footing dimensions (B and L) as follows:

$$q_{bottom} = \frac{qBL}{(B + H_{UZ})(L + H_{UZ})} \qquad [B.23]$$

References

1. Bowles, J.E. (1996). *Foundation analysis and design.* 5th Edition, McGraw-Hill Companies, Inc.
2. Hughes, J.M.O., and Withers, N.J. (1974). "Reinforcing of soft cohesive soils with stone columns." *Ground Engineering*, 7(3), 42-49.
3. Priebe, H. (1978). "Abschaetzung des Scherwiderstanes eines durch Stopfverdichtung verbesserten Baugrundes." Die Bautechnik, 55(8), 281-284.

4. Wissmann, K.J. (1999). "Bearing capacity of Geopier-supported foundation systems." *Technical Bulletin No. 2*, Geopier Foundation Company, Inc., Blacksburg, VA, USA.

APPENDIX C: NUMERICAL CALCULATIONS OF BEARING CAPACITY AND SETTLEMENT

BEARING CAPACITY COMPUTATIONS

Input:

Dimensions:

$B = L = 2.29(m)$

$D_f = 0.46(m)$

$H_O^{(1)} = 2.79(m);\ H_O^{(2)} = 5.10(m)$

$H_{Shaft}^{(1)} = 2.33(m);\ H_{Shaft}^{(2)} = 4.64(m)$

$d_{Shaft} = 0.76(m)\ ; d' = 0.76 + 0.076 = 0.84(m)$

GWT = 2.0 (m)

Soil properties:

a) Desiccated fill: $\gamma_1 = 18.87\ (kN/m^3);\ E_s^1 = 8.0(MPa)$

$c_1' = 2\ (kPa);\ \phi_1 = 35^0;\ s_u^{(1)} = 150(kPa)$

b) Alluvial clay: $\gamma_2 = 18.87\ (kN/m^3);\ E_s^2 = 3.5(MPa)\ ;\ E_u = 2.5\ (MPa)$

$c_2' = 2\ (kPa);\ \phi_2 = 24^0;\ s_u^{(2)} = 30(kPa)$

c) Compacted clay: $\gamma_G = 20.6\ (kN/m^3);\ E_s^G = 85(MPa)$

$c_G' = 4\ (kPa);\ \phi_G = 47^0;\ s_u = 0$

Bulging of individual pier element:

$q_{ult,g} = \sigma_{r1\,lim}\, tan^2(\phi_G / 2 + 45^0)$

$$= [\sigma_{r1o} + s_u(1 + ln\frac{E_u}{2s_u(1+v_u)})]tan^2(\frac{\phi_G}{2} + 45)$$

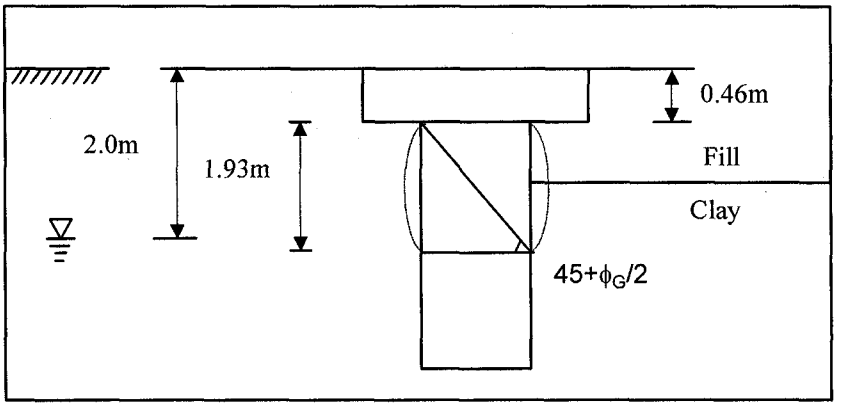

* Determination of bulging depth:

$$z_b = (0.46) + [\frac{0.76}{2}tan^2(68.5)] = 1.68(m)$$

* $\sigma_{r_0}' = \sigma_v' K_p^s$ where: $K_p^s = tan^2(45 + 24/2) = 2.37$

$$\sigma_v' = (18.87)(1.68) = 31.7(kPa)$$

$\sigma_{r1o}' = (31.7)(2.37) = 75(kPa)$; u = 0 (kPa)

$\sigma_{r1o} = 75 + u = 75 + 0 = 75(kPa)$

$\sigma_{r1\,lim} = [75 + s_u(1 + ln\frac{E_u}{2s_u(1+v_u)})]$ where: E_u = 2.5 (MPa); v_u = 0.5; s_u = 30 (kPa)

$$\sigma_{r1\,lim} = 75 + 30(1 + ln\frac{2500}{2(30)(1+0.5)}) = 204(kPa)$$

$$q_{ult,g} = (204)tan^2(68.5) = 1315(kPa)$$

$$q_{bottom} = q_{ult,g}\frac{R_s R_a - R_a + 1}{R_s}$$

* For G_1: $q_{bottom} = (1315)\dfrac{(5)(0.35)-(0.35)+1}{5} = 631(kPa)$

* For G_2: $q_{bottom} = (1315)\dfrac{(10)(0.35)-(0.35)+1}{10} = 546(kPa)$

* Weight of footing/area of footing = (23.5)(0.46) = 10.8 (kPa)

* For G_1 (n_s = 5): $q_{top} = 631 - 10.8 = 620(kPa)$

* For G_2 (n_s = 10): $q_{top} = 546 - 10.8 = 535(kPa)$

Shearing below pier tip:

1) Short pier (P_1): L = 2.79 (m)

$$Q_{top,g} + Q_{weight,g} = Q_{shaft} + Q_{tip,g}$$

$$q_{ult}A_g + W = f_s A_{shaft} + q_{tip,g}A_g$$

$$q_{ult} = (f_s A_{shaft} + q_{tip}A_g - A_g H_{shaft}\gamma_g)/A_g$$

$$= f_s \frac{A_{shaft}}{A_g} + q_{tip} - H_{shaft}\gamma_g$$

$$= 4 f_s d' H_{shaft}/d_{shaft}^2 + q_{tip,g} - H_{shaft}\gamma_g$$

- Undrained Analysis: $q_{tip} = \overline{s_u}N_c$ ($N_c \approx 9$)

$$f_s = \overline{s_u}$$

$$\overline{s_u} = \frac{(150)(0.54)+(30)(1.79)}{2.33} = 58(kPa)$$

$$q_{ult} = (4)(58)(0.84)(2.33)/(0.76)^2 + (9)(30) - (2.33)(20.6) = 1008(kPa)$$

* For G_1 (n_s = 5): $q_{top} = (1008)(0.48) - 10.8 = 473(kPa)$

- Drained Analysis: $f_s' = \sigma_v' \tan \overline{\phi' K_{ps}}$

$$\overline{\sigma_v'} = [\frac{(0.54)(18.87)+(2)(18.87)}{2}(1.54) + \frac{(2)(18.87)+(2.79)(18.87)-(0.79)(9.81)}{2}(0.79)]/2.33$$

$$= 29.85 \approx 30 \text{ (kPa)}$$

$$\overline{\phi'} = \frac{d_1\phi_1 + d_2\phi_2}{d_1 + d_2} \qquad \text{where: } \phi_1 = 35^0; \phi_2 = 24^0; d_1 = 0.54(m); d_2 = 1.79(m)$$

$$= \frac{(0.54)(35)+(1.79)(24)}{2.33} = \underline{\underline{27^0}}$$

$$\overline{K_{ps}} = \frac{K_1 d_1 + K_2 d_2}{d_1 + d_2} = \frac{(3.69)(0.54)+(2.37)(1.79)}{2.33} = \underline{\underline{2.68}}$$

$$\overline{f_s} = (30)(\tan 27)(2.68) = 40.97 \approx 41(kPa)$$

* Tip elevation: $\phi = 24^0$

Meyerhof's method: $\phi = 24^0 : N_q = 9.6 ; N_\gamma = 5.7$

$$s_q = s_\gamma = 1 + 0.1K_p \frac{B}{L} = 1 + (2.37)(1)(0.1) = 1.237$$

$$d_q = d_\gamma = 1 + 0.1\sqrt{K_p}\frac{D}{B} = 1 + (0.1)\sqrt{2.37}\frac{2.79}{0.84} = 1.51$$

$$\sigma'_v = (2)(18.87) + (0.79)(9.06) = 44.9 \approx 45(kPa)$$

$$q_{tip,g} = (0.5)(0.84)(9.06)(5.7)(1.237)(1.51) + (45)(9.6)(1.237)(1.51) = 850(kPa)$$

$$q_{ult} = (4)(41)(0.84)(2.33)/(0.76)^2 + 850 - (2.33)(20.6) = 1358(kPa)$$

* For G_1 ($n_s = 5$): $q_{top} = (1358)(0.48) - 10.8 = 641(kPa)$

Terzaghi's method: $\phi = 24^0 : N_q = 11.39 ; N_\gamma = 9.11 ; s_\gamma = 0.6$

$$\sigma'_v = (2)(18.87) + (0.79)(9.06) = 44.9 \approx 45(kPa)$$

$$q_{tip,g} = (0.5)(0.84)(9.06)(9.11)(0.6) + (45)(11.39) = 513(kPa)$$

$$q_{ult} = (4)(41)(0.84)(2.33)/(0.76)^2 + 513 - (2.33)(20.6) = 1021(kPa)$$

* For G_1 ($n_s = 5$): $q_{top} = (1021)(0.48) - 10.8 = 479(kPa)$

Hansen's method: $\phi = 24^0 : N_q = 9.6 ; N_\gamma = 5.7$

$$s_q = 1 + \frac{B'}{L'} \sin\phi = 1 + \sin 24 = 1.41 ; \; s_\gamma = 1 - 0.4\frac{B'}{L'} = 0.6$$

$$d_q = 1 + 2\tan\phi(1 - \sin\phi)^2 \frac{D}{B} = 2.04 ; \; d_\gamma = 1$$

$$\sigma'_v = (2)(18.87) + (0.79)(9.06) = 44.9 \approx 45(kPa)$$

$$q_{tip,g} = (0.5)(0.84)(9.06)(5.7)(0.6)(1) + (45)(9.6)(1.41)(2.03) = 1256(kPa)$$

$$q_{ult} = (4)(41)(0.84)(2.33)/(0.76)^2 + 1256 - (2.33)(20.6) = 1764(kPa)$$

* For G_1 ($n_s = 5$): $q_{top} = (1764)(0.48) - 10.8 = 836(kPa)$

Vesic's method: $\phi = 24^0 : N_q = 9.6 ; N_\gamma = 9.4$

$$s_q = 1 + \frac{B}{L} \tan\phi = 1 + \tan 24 = 1.45 ; \; s_\gamma = 1 - 0.4\frac{B}{L} = 0.6$$

$$d_q = 1 + 2\tan\phi(1 - \sin\phi)^2 \frac{D}{B} = 2.03 ; \; d_\gamma = 1$$

$$\sigma'_v = (2)(18.87) + (0.79)(9.06) = 44.9 \approx 45(kPa)$$

$$q_{tip,g} = (0.5)(0.84)(9.06)(9.4)(0.6)(1) + (45)(9.6)(1.45)(2.03) = 1293(kPa)$$

$$q_{ult} = (4)(41)(0.84)(2.33)/(0.76)^2 + 1293 - (2.33)(20.6) = 1800(kPa)$$

* For G_1 ($n_s = 5$): $q_{top} = (1800)(0.48) - 10.8 = 853(kPa)$

2) Longer pier: L = 5.10 (m)

- Undrained Analysis: $\overline{s_u} = \frac{(150)(0.54)+(30)(4.10)}{4.64} = 44(kPa)$

$q_{ult} = (4)(44)(0.84)(4.64)/(0.76)^2 + (9)(30) - (4.64)(20.6) = 1362(kPa)$

* For G_2 (n_s = 10): $q_{top} = (1362)(0.42) - 10.8 = 561(kPa)$

- Drained Analysis: $f_s' = \sigma_v' \tan\overline{\phi' K_{ps}}$

$$\overline{\sigma_v'} = [\frac{(0.54)(18.87)+(2)(18.87)}{2}(1.54) + \frac{(2)(18.87)+(5.1)(18.87)-(3.1)(9.06)}{2}(3.1)]/4.64$$

= 43 (kPa)

$$\bar{\phi} = \frac{d_1\phi_1 + d_2\phi_2}{d_1 + d_2} = \frac{(0.54)(35)+(4.1)(24)}{4.64} = \underline{\underline{25^0}}$$

$$\overline{K_{ps}} = \frac{(3.69)(0.54)+(2.37)(4.1)}{4.64} = \underline{\underline{2.52}}$$

$\overline{f_s} = (43)(\tan 25)(2.52) = 50.5(kPa)$; $\sigma'_v = (18.87)(2)+(3.1)(9.06) = 65.8(kPa)$

Meyerhof's method: $\phi = 24^0$; $N_q = 13.2$; $N_\gamma = 5.7$

$$s_q = s_\gamma = 1.237$$

$$d_q = d_\gamma = 1 + 0.1\sqrt{K_p}\frac{D}{B} = 1 + (0.1)\sqrt{2.37}\frac{5.1}{0.84} = 1.93$$

$q_{tip,g} = (0.5)(0.84)(9.06)(5.7)(1.237)(1.93)+(65.8)(13.2)(1.237)(1.93) = 2125(kPa)$

$q_{ult} = (4)(50.5)(0.84)(4.64)/(0.76)^2 + 2125 - (20.6)(4.64) = 3392(kPa)$

* For G_2 (n_s = 10): $q_{top} = (3392)(0.42) - 10.8 = 1414(kPa)$

Terzaghi's method: $\phi = 24^0$: $N_q = 11.39$; $N_\gamma = 9.11$; $s_\gamma = 0.6$

$q_{tip,g} = (0.5)(0.84)(9.06)(6.93)(9.11)(0.6)+(65.8)(11.39) = 923(kPa)$

$$q_{ult} = (4)(50.5)(0.84)(4.64)/(0.76)^2 + 770 - (4.64)(20.6) = 2037(kPa)$$

* For G_2 (n_s = 10): $q_{top} = (2037)(0.42) - 10.8 = 845(kPa)$

Hansen's method: $\phi = 24^0 : N_q = 9.6 ; N_\gamma = 5.7$

$$s_q = 1 + \frac{B'}{L'} sin\phi = 1 + sin24 = 1.41;\ s_\gamma = 1 - 0.4\frac{B'}{L'} = 0.6$$

$$d_q = 1 + 2tan\phi(1 - sin\phi)^2 \frac{D}{B} = 2.9;\ d_\gamma = 1$$

$$q_{tip,g} = (0.5)(0.84)(9.06)(5.7)(0.6)(1) + (65.8)(9.6)(1.41)(2.9) = 2596(kPa)$$

$$q_{ult} = (4)(50.5)(0.84)(4.64)/(0.76)^2 + 2596 - (4.64)(20.6) = 3863(kPa)$$

* For G_2 (n_s = 10): $q_{top} = (3863)(0.42) - 10.8 = 1612(kPa)$

Vesic's method: $\phi = 24^0 : N_q = 9.6 ; N_\gamma = 9.4$

$$s_q = 1 + \frac{B}{L} tan\phi = 1 + tan24 = 1.45;\ s_\gamma = 1 - 0.4\frac{B}{L} = 0.6$$

$$d_q = 1 + 2tan\phi(1 - sin\phi)^2 \frac{D}{B} = 2.9;\ d_\gamma = 1$$

$$\sigma'_v = (2)(18.87) + (0.79)(9.06) = 44.9 \approx 45(kPa)$$

$$q_{tip,g} = (0.5)(0.84)(9.06)(9.4)(0.6)(1) + (65.8)(9.6)(1.45)(2.9) = 2678(kPa)$$

$$q_{ult} = (4)(50.5)(0.84)(4.64)/(0.76)^2 + 2678 - (4.64)(20.6) = 3945(kPa)$$

* For G_2 (n_s = 10): $q_{top} = (3945)(0.42) - 10.8 = 1646(kPa)$

Shearing within pier reinforced zone:

$R_a = 0.35$; n = 2.8 (assumed); $\phi_G = 35^0 ; \phi_S = 24^0 ; c_S = 2(kPa)$

$$\phi_{comp} = tan^{-1}[R_a n \tan\phi_G + (1 - R_a n)\tan\phi_s]$$

$$= tan^{-1}[(0.35)(2.8)\tan 47 + (1-(0.35)(28))\tan 24] = 47^{\circ}$$

$$c_{comp} = (1 - R_a n)c_s = 0(kPa)$$

Meyerhof's method: $\phi = 47^0$: $N_c = 173.62$; $N_q = 187.2$; $N_\gamma = 414.2$

$$s_q = s_\gamma = 1 + 0.1K_p \frac{B}{L} = 1 + (0.1)(3.69)(1) = 1.369$$

$$d_q = d_\gamma = 1 + 0.1\sqrt{K_p}\frac{D}{B} = 1 + (0.1)\sqrt{3.69}\frac{0.46}{2.29} = 1.04$$

$$\sigma'_v = (18.87)(0.46) = 8.7(kPa)$$

$$q_{ult} = (0.5)(18.87)(2.29)(1.369)(1.04)(414.2) + (8.7)(187.2)(1.369)(1.04) = 15060(kPa)$$

$$q_{top} = 15060 - 10.8 = 15049(kPa)$$

Terzaghi's method: $\phi = 47^0$: $N_q = 241.3$; $N_\gamma = 575.9$; $s_\gamma = 0.6$

$$q_{ult} = (0.5)(18.87)(2.29)(575.9)(0.6) + (8.7)(241.3) = 9656(kPa)$$

$$q_{top} = 9656 - 10.8 = 9645(kPa)$$

Hansen's method: $\phi = 47^0$: $N_q = 187.2$; $N_\gamma = 299.5$

$$s_q = 1 + \frac{B'}{L'}\sin\phi = 1 + \sin 47 = 1.73;\ s_\gamma = 1 - 0.4\frac{B'}{L'} = 0.6$$

$$d_q = 1 + 2\tan 47(1 - \sin 47)^2 \frac{D}{B} = 1.03;\ d_\gamma = 1$$

$$q_{ult} = (0.5)(18.87)(2.29)(299.5)(0.6) + (8.7)(187.2)(1.73)(1.03) = 6785(kPa)$$

$$q_{top} = 6785 - 10.8 = 6774(kPa)$$

Vesic's method: $\phi = 47^0$: $N_q = 187.2$; $N_\gamma = 403.6$

$$s_q = 1 + \frac{B'}{L'}\tan\phi = 1 + \tan 47 = 12.01;\ s_\gamma = 1 - 0.4\frac{B'}{L'} = 0.6$$

$$d_q = 1 + 2\tan 47(1 - \sin 47)^2 \frac{D}{B} = 1.03;\ d_\gamma = 1$$

$$q_{ult} = (0.5)(18.87)(2.29)(403.6)(0.6) + (8.7)(187.2)(2.07)(1.03) = 8705(kPa)$$

$$q_{top} = 8705 - 10.8 = 8694(kPa)$$

Shearing below pier-reinforced zone:

1) Shorter pier (P_1)

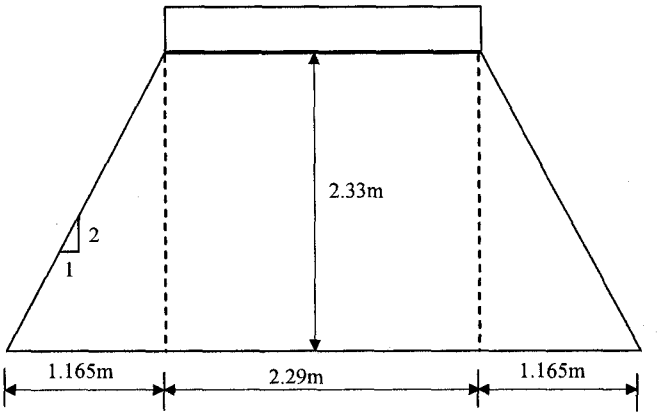

$B'xL' = 4.62x4.62(m)$; $\phi = 24^0$; c = 2 (kPa)

- Undrained Analysis: s_u = 30 (kPa); ϕ_s = 0

$$q_{ult} = 5.14 s_u (1 + s_c + d_c) + \bar{q}$$

Where: $s_c = 0.2\frac{B}{L} = 0.2;\ d_c = 0.2\frac{D}{B} = 0.24$

$$\bar{q} = (18.87)(2) + (9.06)(0.79) = 44.9 \approx 45(kPa)$$

Thus: $q_{ult} = (5.14)(30)(1 + 0.2 + 0.24) + 45 = 267(kPa)$

$$q_{bottom} = \frac{(267)(2.29 + 2.33)^2}{(2.29)^2} = 1087(kPa)$$

$$q_{top} = 1087 - 10.8 = \underline{\underline{1076(kPa)}}$$

- Drained Analysis: $\phi = 24^0$; c = 2 (kPa)

Meyerhof's method: $N_q = 9.6\,; N_\gamma = 5.7$

$$s_q = s_\gamma = 1 + 0.1K_p \frac{B}{L} = 1 + (0.1)(2.37)(1) = 1.237$$

$$d_q = d_\gamma = 1 + 0.1\sqrt{K_p}\,\frac{D}{B} = 1 + (0.1)\sqrt{2.37}\,\frac{2.79}{4.62} = 1.09$$

$$\sigma'_v = (18.87)(2) + (9.06)(0.79) = 45(kPa)$$

$$q_{ult} = (0.5)(4.62)(9.06)(1.237)(1.09)(5.7) + (45)(9.6)(1.237)(1.09) = 744(kPa)$$

$$q_{bottom} = \frac{(744)(2.29 + 2.33)^2}{(2.29)^2} = 3028(kPa)$$

$$q_{top} = 3028 - 10.8 = \underline{\underline{3017(kPa)}}$$

Terzaghi's method: $\phi = 24^0 : N_q = 11.39\,; N_\gamma = 9.11\,;\ s_\gamma = 0.6$

$$q_{ult} = (0.5)(9.06)(4.62)(9.11)(0.6) + (45)(11.39) = 627(kPa)$$

$$q_{bottom} = \frac{(627)(2.29 + 2.33)^2}{(2.29)^2} = 2552(kPa)$$

$$q_{top} = 2552 - 10.8 = 2541(kPa)$$

Hansen's method: $\phi = 24^0 : N_q = 9.6\,; N_\gamma = 5.7$

$$s_q = 1 + \frac{B'}{L'}\sin\phi = 1 + \sin 24 = 1.41\,;\ s_\gamma = 1 - 0.4\frac{B'}{L'} = 0.6$$

$$d_q = 1 + 2\tan 24(1 - \sin 24)^2 \frac{D}{B} = 1.19\,;\ d_\gamma = 1$$

$$q_{ult} = (0.5)(9.06)(4.62)(5.7)(0.6) + (45)(9.6)(1.41)(1.19) = 796(kPa)$$

$$q_{bottom} = \frac{(796)(2.29+2.33)^2}{(2.29)^2} = 3240(kPa)$$

$$q_{top} = 3240 - 10.8 = 3229(kPa)$$

Vesic's method: $\phi = 24^0 : N_q = 9.6 ; N_\gamma = 9.4$

$$s_q = 1 + \frac{B'}{L'}\tan\phi = 1 + \tan 24 = 1.45 ;\ s_\gamma = 1 - 0.4\frac{B'}{L'} = 0.6$$

$$d_q = 1 + 2\tan 24(1 - \sin 24)^2 \frac{D}{B} = 1.19 ;\ d_\gamma = 1$$

$$q_{ult} = (0.5)(9.06)(4.62)(9.4)(0.6) + (45)(9.6)(1.45)(1.19) = 863(kPa)$$

$$q_{bottom} = \frac{(863)(2.29+2.33)^2}{(2.29)^2} = 3513(kPa)$$

$$q_{top} = 3513 - 10.8 = 3502(kPa)$$

2) Longer pier (P_2):

- Undrained Analysis: $s_u = 30$ (kPa); $\phi_u = 0$

$$q_{ult} = 5.14 s_u (1 + s_c + d_c) + \bar{q}$$

Where: $s_c = 0.2\frac{B}{L} = 0.2 ;\ d_c = 0.4\frac{5.10}{6.93} = 0.29$

$$\bar{q} = (18.87)(2) + (9.06)(3.1) = 66(kPa)$$

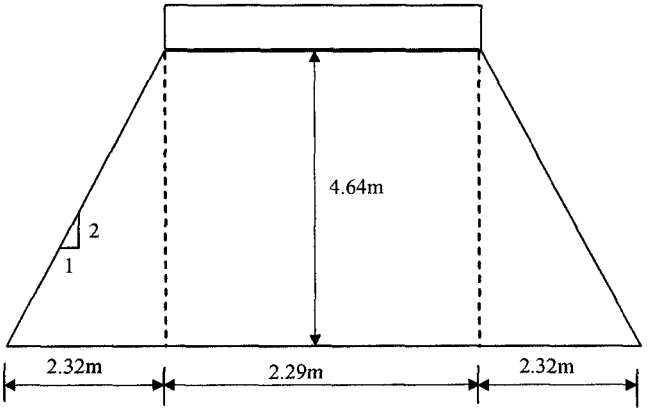

$B'xL' = 6.93x6.93(m)$; $\phi = 0$; c = 17 (kPa)

Thus: $q_{ult} = (5.14)(30)(1+0.2+0.29)+66 = 296(kPa)$

$$q_{bottom} = \frac{(296)(2.29+4.64)^2}{(2.29)^2} = 2711(kPa)$$

$$q_{top} = 2711 - 10.8 = \underline{\underline{2700}}(kPa)$$

- Drained Analysis: $\phi = 24^0$; c = 2 (kPa)

Meyerhof's method: $N_c = 19.32$; $N_q = 9.6$; $N_\gamma = 5.7$

$s_c = 1.47$; $s_q = s_\gamma = 1.237$

$$d_c = 1 + 0.2\sqrt{K_p}\frac{D}{B} = 1 + (0.2)\sqrt{2.37}\frac{5.1}{6.93} = 1.227$$

$$d_q = d_\gamma = 1 + 0.1\sqrt{K_p}\frac{D}{B} = 1 + (0.1)\sqrt{2.37}\frac{5.1}{6.93} = 1.113$$

$\sigma'_v = 65.8(kPa)$

$$q_{ult} = (0.5)(6.93)(9.06)(1.237)(1.113)(5.7)+(65.8)(9.6)(1.237)(1.113) = 1121(kPa)$$

$$q_{bottom} = \frac{(1121)(2.29+4.64)^2}{(2.29)^2} = 10266(kPa)$$

$$q_{top} = 10266 - 10.8 = \underline{\underline{10255}}(kPa)$$

Terzaghi's method: $\phi = 24^0 : N_q = 11.39 ; N_\gamma = 9.11 ; \ s_\gamma = 0.6$

$$q_{ult} = (0.5)(9.06)(6.93)(9.11)(0.6) + (65.8)(11.39) = 923(kPa)$$

$$q_{bottom} = \frac{(627)(2.29 + 4.64)^2}{(2.29)^2} = 8453(kPa)$$

$$q_{top} = 8453 - 10.8 = 8442(kPa)$$

Hansen's method: $\phi = 24^0 : N_q = 9.6 ; N_\gamma = 5.7$

$$s_q = 1 + \frac{B'}{L'} \sin\phi = 1 + \sin 24 = 1.41 ; \ s_\gamma = 1 - 0.4\frac{B'}{L'} = 0.6$$

$$d_q = 1 + 2\tan 24(1 - \sin 24)^2 \frac{D}{B} = 1.1 ; \ d_\gamma = 1$$

$$q_{ult} = (0.5)(9.06)(6.93)(5.7)(0.6) + (65.8)(9.6)(1.41)(1.1) = 1002(kPa)$$

$$q_{bottom} = \frac{(1002)(2.29 + 4.64)^2}{(2.29)^2} = 9176(kPa)$$

$$q_{top} = 9176 - 10.8 = 9165(kPa)$$

Vesic's method: $\phi = 24^0 : N_q = 9.6 ; N_\gamma = 9.4$

$$s_q = 1 + \frac{B'}{L'} \tan\phi = 1 + \tan 24 = 1.46 ; \ s_\gamma = 1 - 0.4\frac{B'}{L'} = 0.6$$

$$d_q = 1 + 2\tan 24(1 - \sin 24)^2 \frac{D}{B} = 1.19 ; \ d_\gamma = 1$$

$$q_{ult} = (0.5)(9.06)(6.93)(9.4)(0.6) + (65.8)(9.6)(1.46)(1.19) = 1195(kPa)$$

$$q_{bottom} = \frac{(1195)(2.29 + 4.64)^2}{(2.29)^2} = 10943(kPa)$$

$$q_{top} = 10943 - 10.8 = 10933(kPa)$$

SETTLEMENT COMPUTATIONS

DESIGN PARAMETERS:		Value	
Parameters	Symb	**Metric**	**English**
Geopier diameter	d	0.76 m	30 in
Footing depth	Df	0.46 m	1.5 ft
Depth to groundwater	H_W	2.00 m	6.6 ft
Total unit weight of soil	γ	1.92 g/cm^3	120 pcf
Soil frictional angle	ϕ	24 deg	24 deg
Soil undrained shear strength	c	2.0 kPa	41.75365 psf
Max. horizontal pressure	P_{MAX}	120 kPa	2500 psf
From Table 4.2:			
Geopier cell capacity	Q_{cell}	230 kN	52 kips
Footing bearing pressure	q_{all}	210 kPa	4.4 ksf
Geopier stiffness modulus	k_g	45.0 MN/m^3	165 pci
Soil stiffness modulus	k_m	4.2 MN/m^3	16 pci

Unit weight of water	γ_W	1.0 g/cm^3	62.4 pcf
GP cross section area	A_g	0.46 m^2	4.91 ft^2

FOOTING UZ SETTLEMENT CALCULATIONS - SQUARE FOOTINGS

		English Units			*Metric Units*			
Parameters	Symb	**Unit**	G_1	G_1	**Unit**	G_1	G_1	Equation
Column load	P	**kips**	184.3525	225	**mtons**	84	102	
					kN	820	1000	
Required footing width	Br	**ft**	6.5	7.2	**m**	1.98	2.18	sqrt(P/qall)
Selected footing width	B	**ft**	7.5	7.5	**m**	2.29	2.29	
Footing bearing pressure	q	**ksf**	3.3	4.0	**kN/m^2**	157	191	P/(B*B)
Required No. Geopier elements	Nr		3.6	4.3		3.6	4.3	P/Q_{cell}
Selected No. Geopier elements	N		4	4		4	4	
Area replacement ratio	Ra		0.35	0.35		0.35	0.35	$N*A_g/(B*B)$
Stiffness ratio	Rs		10.6	10.6		10.6	10.6	k_g/k_m
Stress at top of GP	q_g	**ksf**	8.0	9.7	**kN/m^2**	382	466	q*Rs/(Rs*Ra-Ra+1)
Load at top of GP	Qg	**kips**	39	48	**kN**	174	212	q_g*A_g
Upper zone settlement	s_{uz}	**in**	0.33	0.41	**mm**	9	10	q_g/k_g

SHAFT LENGTH REQUIREMENTS AND LOWER ZONE SETTLEMENT

Trial shaft length	H_S	**ft**	8	15	**m**	2.33	4.64	
Drill depth	H_d	**ft**	9.2	16.7	**m**	2.79	5.10	D_f+H_S
Soil vert. stress at top of GP	$\sigma_{v'top}$	**psf**	181	181	**kN/m^2**	9	9	$\gamma*D_f$
Passive earth pressure coeff.	K_P		2.37	2.37				$\tan^2(45+\phi/2)$
Hori. earth pressure at top of GP	Ptop	**psf**	429	429	**kN/m^2**	21	21	$K_P*\sigma_{v'top}$
Vert. earth pressureat bott of GP	$\sigma_{v'bot}$	**psf**	935	1370	**kN/m^2**	45	66	$\gamma*H_d-\gamma_w*(H_d-H_W)$
Hori. earth pressure at ftg bottom	Pbot	**psf**	2218	2500	**kN/m^2**	106	120	$K_P*\sigma_{v'bot}$ or P_{MAX}
Conservative avg. hori. Stress	Pavg	**psf**	1323	1464	**kN/m^2**	63	70	(Ptop+Pbot)/2
Shaft resistance (drained)	Qs	**kips**	35	78	**kN**	157	347	Pavg*tanϕ*π*d*Hs
Is shaft long enough?			**incr Hs**	**ok**		**incr Hs**	**ok**	is (Qs>Qg)?
Geopier Tip Stress/Load*	Qt	**kips**	4	0	**kN**	17	0	Qg-Qs
Shaft resist. (undrained) Ref. Check		**kips**	3	5	**kN**	11	22	c*π*d*Hs

** If the Geopier tip stress greater than zero, check its effect on lower zone settlement.*

Lower Zone bott. from footing bott.	H_{2b}	**ft**	15.0	15.0	**m**	4.6	4.6	2*B
Upper zone thickness	H_{uz}	**ft**	10.1	17.7	**m**	3.1	5.4	H_S+d
Lower zone thickness	H_{lz}	**ft**	4.9	-2.7	**m**	1.5	-0.8	$H_{2b}-H_{uz}$
Thickness of LZ sublayer 1	H_{lz1}	**ft**	7.4	0.0	**m**	2.3	0.0	
Thickness of LZ sublayer 2	H_{lz2}	**ft**	0.0	0.0	**m**	0.0	0.0	
Total thickness ok?			**check**	**ok**		**check**	**ok**	
E modulus of LZ sublayer 1	E	**ksf**	73	73	**MN/m^2**	3.50	3.50	
E modulus of LZ sublayer 2	E	**ksf**	21	209	**MN/m^2**	1.00	10.00	
Settlement of LZ sublayer 1	s_{lz1}	**in**	0.36	0.00	**mm**	9	0	q*I*Hlz/Elz
Settlement of LZ sublayer 2	s_{lz2}	**in**	0.00	0.00	**mm**	0	0	q*I*Hlz/Elz
Total lower zone settlement	s_{lz}	**in**	0.36	0.00	**mm**	9	0	$s_{lz1}+s_{lz2}$
Total UZ + LZ settlement	**S**	**in**	**0.69**	**0.41**	**mm**	18	10	$s_{uz}+s_{lz}$

APPENDIX D: PRINCIPLES OF THE HARDENING-SOIL CONSTITUTIVE MODEL

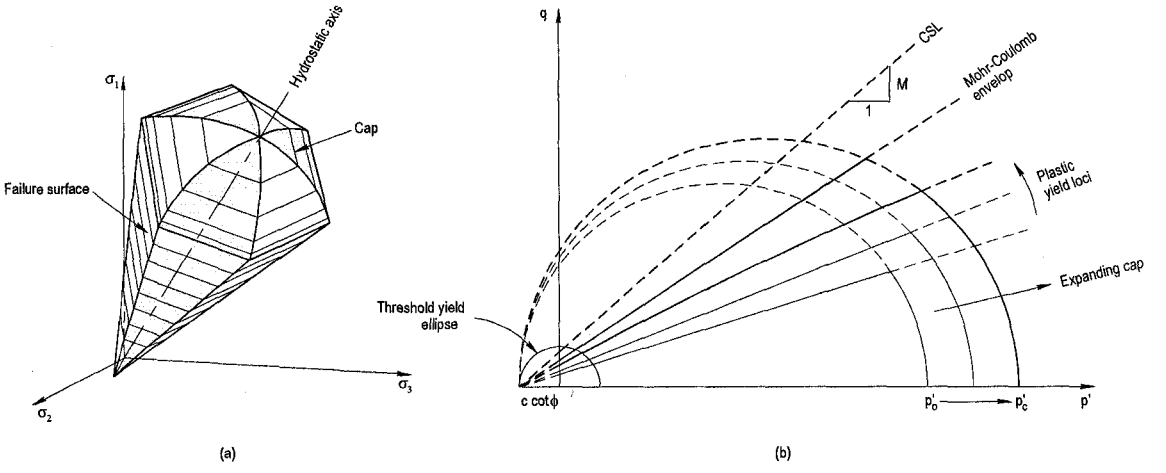

Figure D.1. Failure and cap surfaces of the hardening-soil model in (a) principal stress space and (b) q-p' space

The hardening-soil model is essentially an elasto-plastic model which was developed based on isotropic plastic theory combined with hardening rules. Figure D.1 describes the principles of the hardening-soil model in which the yield curve consists of two distinguishable segments named as the plastic yield curve and the cap. The shape and the location of the plastic yield curve depend upon the stress state (p', q) and plastic strains whereas the size of the cap is controlled by the isotropic preconsolidation pressure, p'_c. Failure state of the material is defined in accordance with Mohr-Coulomb failure criterion. The failure surface of the material due to primary deviatoric loading is, therefore, illustrated by a hexagonal cone in the principal stress space and the failure due to primary hydrostatic compression is defined by a cap (Fig. D.1a). The projection of the failure surface onto q-p' space is shown in Fig. D.1b. The material is assumed to behave elastically when the stress state is within the yield curve and elasto-plastically when the stress state is on the yield curve. The nonassociated flow rule is applied for the deviatoric shear yielding whereas the associated flow rule is used to describe the yielding on the compression cap.

Constitutive parameters of the hardening-soil model can be readily determined from consolidated-drained (CD) triaxial and oedometer tests. Fundamental model parameters include stress-dependent modulus according to power law (m), plastic straining due to primary deviatoric loading (E_{50}), plastic straining due to primary hydrostatic compression (E_{oed}), elastic unloading/reloading (E_{ur}, ν_{ur}), and effective stress shear strength parameters (c', ϕ', ψ).

The basic idea of the hardening-soil model is that the stress-strain relationship in deviatoric loading (i.e., triaxial loading condition) can be formulated as a hyperbola using the following equation:

$$\varepsilon_1 = \frac{q}{2E_{50}(1-\frac{q}{q_a})} \qquad for: q < q_f \qquad [D.1]$$

Ultimate deviatoric stress is defined in accordance with Mohr-Coulomb criterion:

$$q_f = (c\cot\phi + \sigma_3^{'})\frac{2\sin\phi}{1-\sin\phi} \qquad and: q_a = \frac{q_f}{R_f} \qquad [D.2]$$

The parameter E_{50} is the given by following equation:

$$E_{50} = E_{50}^{ref}(\frac{c\cos\phi + \sigma_3^{'}\sin\phi}{c\cos\phi + p^{ref}\sin\phi})^m \qquad [D.3]$$

For isotropic compression loading condition, the stress-strain behavior of the material is controlled by the parameter E_{oed} instead of E_{50}. E_{oed} is also a stress dependent parameter which is given by following equation:

$$E_{oed} = E_{oed}^{ref}(\frac{c\cos\phi + \sigma_3^{'}\sin\phi}{c\cos\phi + p^{ref}\sin\phi})^m \qquad [D.4]$$

For unloading-reloading stress path (i.e., elastic behavior), a stress dependent modulus named E_{ur} is used. The E_{ur} is defined as follows:

$$E_{ur} = E_{ur}^{ref}\left(\frac{c\cos\phi + \sigma_3^{'}\sin\phi}{c\cos\phi + p^{ref}\sin\phi}\right)^m \qquad [D.5]$$

The yield function is proposed in the following form:

$$f = \overline{f} - \gamma^p \qquad where: \overline{f} = \frac{q}{E_{50}\left(1-\frac{q}{q_a}\right)} - \frac{2q}{E_{ur}} \qquad and: \gamma^p = 2\varepsilon_1^p - \varepsilon_v^p \qquad [D.6]$$

The plastic flow rule has the linear form as follows:

$$\begin{aligned} &\varepsilon_v^p = \sin\psi_m \gamma^p \\ &\sin\psi_m \frac{\sin\phi_m - \sin\phi_{cv}}{1-\sin\phi_m\sin\phi_{cv}} \\ &\sin\phi_m = \frac{\sigma_1^{'} - \sigma_3^{'}}{\sigma_1^{'} + \sigma_3^{'} - 2c\cot\phi} \\ &\sin\phi_{cv} = \frac{\sin\phi - \sin\psi}{1-\sin\phi\sin\psi} \end{aligned} \qquad [D.7]$$

APPENDIX E: DISTRIBUTION OF AXIAL STRAIN ALONG PIER SHAFT

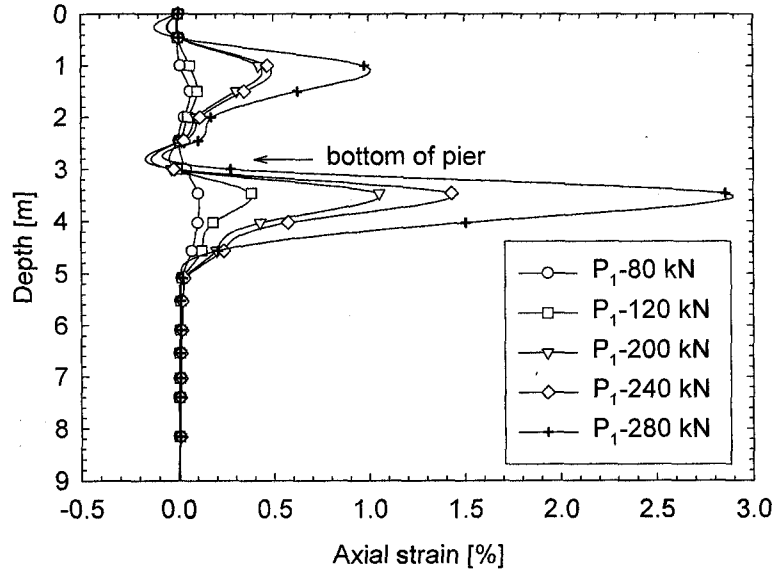

Figure E.1. Distribution of axial strain along P_1 as a function of the compressive load

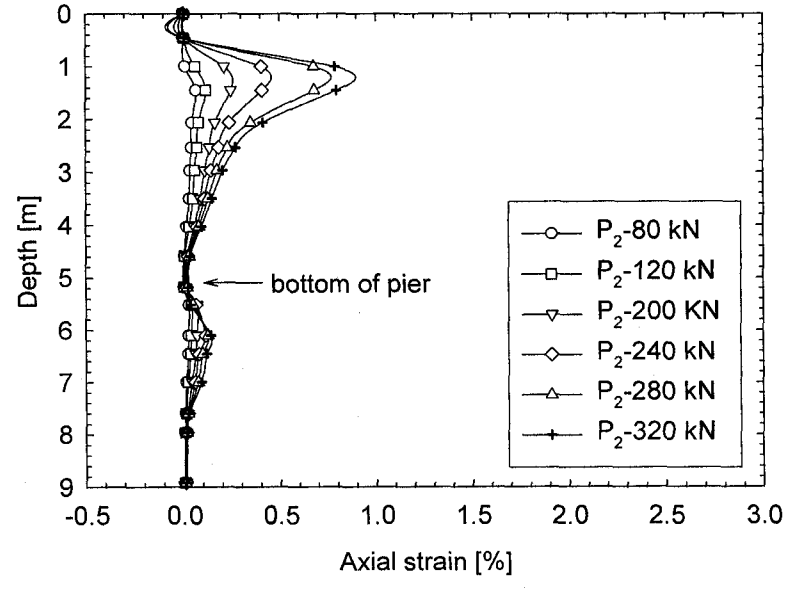

Figure E.2. Distribution of axial strain along P_2 as a function of the compressive load